Developing Mass Spectrometry-Based Analytical Methodologies for Analyzing Complex Protein and Lipid Samples

Weimin Hou

Thesis submitted to the
Faculty of Graduate and Postdoctoral Studies
in partial fulfillment of the requirements for
the degree of Doctor of Philosophy

In the Ottawa-Carleton Chemistry Institute
Department of Chemistry, University of Ottawa
Ottawa, Ontario, Canada
2013

Candidate	Supervisors
Weimin Hou	Dr. Daniel Figeys
	Dr. Natalie Goto

Abstract

Mass spectrometry has increasingly become the method of choice for the analysis of complex biological samples, including proteins and lipids. This thesis describes the development of MS-based analytical methodologies for the analysis of complex proteomic and lipidomic samples.

Chapter 3 describes the development of microfluidic proteomic reactors, in the formats of SCX reactor, SCX 96-well plate reactor, and SAX reactor, for the enzymatic digestion of complex proteomic samples for subsequent LC-MS/MS analysis. These microfluidic proteomic reactors greatly simplified the enzymatic digestion of complex proteomic samples by combining multiple processing steps, such as rapid extraction and enrichment of proteins. Furthermore, chemical and enzymatic treatments of proteins were all performed in a few nanoliters effective volume, resulting in an increased protein digestion efficacy. After the protein digestion process, the resulting peptides were eluted in buffers that were compatible with HPLC-MS/MS analysis.

In chapter 4, a methodology based on nano-HPLC-ESI-MS/MS for the analysis of PAF and LPC lipid species is described. In this method, lipid extracts from biological samples were separated by nano-flow HPLC prior to being introduced into a Q-TRAP 2000 mass spectrometer, where the lipid species of interest were detected using a precursor ion scan at m/z 184. Absolute quantitation of PAF family lipid species were performed with standard addition method, where 5 standard solutions containing 0.2-1 ng each of C16:0, C18:0 PAF and C16:0, C18:0 *lyso*-PAF were used in the experiment. Further, the spiking of identical amount of non-endogenous C13:0 LPC at time of extraction allow the relative comparisons of other LPC lipid species of interest between different samples. The developed methods were employed to analyze the changes of PAF and LPC lipid species in NGF-differentiated PC12 cells, in the posterior/entorhinal cortex of AD patients and TgCRND8 transgenic mice, and over the course of 24 hour exposure of human hNT neurons to $A\beta_{42}$ treatment, respectively, in comparison to controls.

Chapter 5 describes the development of a novel shotgun lipidomic methodology for the determination of stereospecificity of diacyl glycerophospholipids including glycerophosphatidic acids (PA), glycerophosphoserines (PS), glycerophosphoglycerols (PG), glycerophosphoinositols(PI), and glycerophosphoethanolamines (PE), which can be conventionally ionized under negative ion mode. The stereospecificity of diacyl glycerophospholipids was determined based on the relative abundance of the lyso-form fragment ions, attributed to the neutral loss of fatty acyl moieties. The fragmentation patterns of a variety of diacyl glycerophospholipid standards were first fully examined over a wide range of collision energy. We observed that lyso-form fragment ions corresponding to the neutral loss of fatty acyl moieties attached to the *sn2* position as free fatty acids ($[M-Sn2]^-$) and as ketenes ($[M-(Sn2-H_2O)]^-$) exhibited consistently higher intensity than their counter part ions due to the neutral loss of fatty acyl moieties attached to the *sn1* position ($[M-Sn1]^-$ and $[M-(Sn1-H_2O)]^-$). We then examined the product ion spectra of diacyl glycerophospholipids recorded from lipid extracts of rat hepatoma cells, where the stereospecific information of these lipids was conclusively determined.

Acknowledgements

I am deeply grateful to my supervisor Dr. Daniel Figeys for giving me the opportunity to pursue a Ph.D. in his laboratory. I would like to thank him for his time, advice and encouragement over the years. I would also like to thank my thesis co-supervisor Dr. Natalie Goto and CIHR training program in lipidomics co-mentor Dr. Steffany Bennett for their support and suggestions over the years.

Over the years I have worked with many colleagues in Dr. Figeys' lab. I would like to take this opportunity to thank all of them for their kindly help and making the lab an enjoyable place. Specially, I would like to thank Dr. Martin Ether, Dr. Hu Zhou and Dr. Jeff C. Smith.

I would also like to thank NSERC, OGS, University of Ottawa, CIHR lipid training grant and my supervisor Dr. Daniel Figeys for financially assistance.

Finally, I would like to thank my wife, my parents, and my parents-in-law for their support and unconditional love.

Table of Contents

List of Figures

List of Tables

Abbreviations

Aβ	amyloid-β
AD	Alzheimer disease
BSA	bovine serum albumin
CAD	collision-activated dissociation
DAG	diacylglycerol
DNA	deoxyribonucleic acid
DP	declustering potential
DTT	dithiothreitol
ECD	electron capture dissociation
ETD	electron transfer dissociation
EDTA	ethylenediaminetetraacetic acid
ESI	Electrospray ionization
FAS	fatty acyl scans
HPLC	High performance liquid chromatography
IP	Immunoaffinity purification
LC	liquid chromatography
LPC	*lyso*-phosphatidylcholine

LTQ	Linear ion trap quadrupole
MALDI	matrix-assisted laser desorption/ionization
MDMS-SL	multidimensional mass spectrometry-based shotgun lipidomics
MPIS	multiple precursor ion scans
MS	mass spectrometry
MS/MS	Tandem mass spectrometry
m/z	mass to charge ratio
NGF	nerve growth factor
NL	neutral loss
NP-40	nonidet P-40
PA	glycerophosphatidic acid
PAF	platelet activating factor
PC	glycerophosphocholine
PE	glycerophosphoethanolamine
PG	glycerophosphoglycerol
PI	glycerophosphoinositol
PIS	precursor ion scan
PS	glycerophosphoserine
PBS	Phosphate buffered saline
PTM	post-translational modification

QTOF	quadrupole time-of-flight
SAX	strong anion exchange
SCX	strong cation exchange
SDS	sodium dodecyl sulfate
SDS-Page	Sodium dodecyl sulphate polyacrylamide gel electrophoresis
SILAC	Stable isotope labelling of amino acids in cell culture
sn	stereospecific number
TIC	total ion current
TLC	thin-layer chromatography
WT	wild-type
XIC	extracted ion chromatograph

Chapter 1 Introduction

1.1 MS-based Proteomics

1.1.1 The general picture

Proteomics can be understood as the large-scale study of gene and cellular functions at the protein level. Mass spectrometry has become the method of choice for analysis of complex protein samples (*1-2*). MS-based proteomics is a discipline made possible by the availability of gene and genome sequence databases, advances in analytical technologies, notably the discovery and development of 'soft ionization' methods (*3-4*), and the development of database searching algorithms (*5-7*). These technologies have allowed high-throughput characterization and quantification of proteins in a biological sample or system.

Bottom-up or shotgun proteomics is the most common MS-based method for studying proteins (*1-2*). In bottom-up proteomics studies (Figure 1.1.1a), a mixture of proteins is normally enzymatically cleaved into peptides. The resultant complex peptide mixture is separated using high performance liquid chromatography and other methods, prior to being analyzed by MS. In contrast to bottom-up proteomics methods, top-down MS-based proteomics (Figure 1.1.1b) refers to the analysis of intact proteins, which are not enzymatically digested prior to MS analysis (*8-9*). Top-down MS-based proteomic approach is normally applied to relatively simple protein samples. The analysis of intact proteins using MS provides comprehensive information on post-translational modifications (PTMs) through the identification of the intact mass of a given protein. The proteomics part covered in the thesis falls within the scope of bottom-up or shotgun proteomics.

The proteome is not only complex, it is spatially, temporally, and chemically dynamic (*10-11*). The explicit goal of global proteomics is the systematic analysis of a large number of proteins expressed in a cell or an organism (*1*). Complementing global proteome profiling, targeted proteomics focuses on a predefined list of small number of proteins/peptides (*12-13*). These proteins/peptides are often first identified in a global proteome study. Targeted proteomics strategies have the potential for providing greater

sensitivity and allowing for the detection of lower abundance candidate peptides and proteins present (*13*).

It is worth noting that proteomics must deal with a limited amount of starting materials. This is unlike DNA sequencing, where the samples are scalable through the polymerase chain reaction. In addition, proteomics also faces other challenges such as sample degradation, a large dynamic range, various forms of post-translational modifications, and spatial and temporary variations. All of these difficulties make any comprehensive proteomics project a daunting task.

1.1.2 Bottom-up/shotgun proteomic experiments

In a typical bottom-up/shotgun proteomic experiment, protein samples are converted into an even more complex mixture of peptides, normally using trypsin. Trypsin has high activity and is a stable protease, which specifically cleaves proteins on the carboxy-terminal side of arginine and lysine residues (*14-15*). The tryptic peptides, as analyzed by a mass spectrometer, can result in information-rich, and easily interpretable, peptide-fragmentation spectra (*2*).

Another advantage of digesting a protein into a set of peptides is that the physico-chemical properties of the protein become less important. As long as some of the peptides originated from the protein can be sequenced by the mass spectrometer, the protein will likely be identified (*2*). For example, membrane proteins work well with MS-based proteomic approaches whereas they are very difficult to work with using other methods, because of their insolubility in water.

A mass spectrometer consists of an ion source, a mass analyser that separates the charged analytes according to their mass-to-charge ratio (*m/z*), and a detector that registers the number of ions at each *m/z* value. Mass spectrometry measurements are carried out in the gas phase at low pressure to minimize collisions.

Electrospray ionization (ESI) (*4*) and matrix-assisted laser desorption/ionization (MALDI) (*3*) are two 'soft' ionization techniques that allow the transfer of intact analytes such as peptides from the liquid phase (ESI) or solid phase (MALDI) to the gas phase for mass spectrometric analysis. The proteomic experiments covered in the thesis only involve electrospray ionization under positive ion mode. Because ESI transfers the analytes from solution to gas phase, it is readily coupled to high-performance liquid chromatography (HPLC) separation of peptide mixture.

Briefly, as shown in Figure 1.1.2, the peptides are introduced to the electrospray tip (10 μm picotip emitter) as the eluent flow from high performance liquid chromatography (HPLC). Flow rates at the tip are typically around 200 nL/min (*16-17*). About +1.5 kV is applied between the electrospray emitter and the orifice of the mass spectrometer, resulting in the formation of a Taylor cone at the end of the emitter and forcing the ejection of positively charged droplets from the emitter towards the orifice of the mass spectrometer. As the droplets traverse the space between the emitter and the orifice, solvent evaporation occurs. The droplets continue to shrink until they reach the "Rayleigh limit", at which point the surface tension can no longer sustain the charge and a "Coulombic explosion" occurs. The Coulombic explosion results in smaller droplets, which can repeat this process, until peptide ions are in the gas phase (*4*).

These peptide ions can be singly or multiply charged, designated as $(M + nH)^{n+}$, where M refers to the mass of the peptide, H^+ is the mass of a proton, and n is the charge (number of protons). Doubly and triply charged peptide ions typically result in information-rich fragmentation spectra, and are normally used for peptide/protein identification. In proteomics, ESI is often used for the analysis of complex peptide samples, where it is mostly coupled with hybrid instruments such as Orbitrap and QqTOF to perform MS, MS/MS, and MS^n experiments, and with triple quadruple instruments to perform multiple reaction monitoring (MRM) and single reaction monitoring (SRM) experiments.

Typical shotgun proteomics employs a series of MS and MS/MS for peptide identification. A MS spectrum is first acquired to survey the m/z of the analytes present in the sample. Then, a series of MS/MS spectra are generated for selected m/z (precursors) from the MS spectrum. In MS/MS, the precursor ion is first isolated, and then fragmented

into smaller fragments, which are then subjected to mass analysis. For LC-MS/MS, the process is repeated for the duration of the LC separation of the peptide mixture.

In shotgun proteomic experiments, peptide fragmentation is typically achieved using collision-activated dissociation (CAD) (*2*), which involves colliding the peptide ions with neutral atoms or molecules in the gas phase. Alternatively, electron capture dissociation (ECD) (*18-20*), which involves attaching low energy electrons to multiply charged protein/peptide ions, can also be employed for peptide fragmentation. As shown in Figure 1.1.3, CAD and ECD cleave on different sites and therefore result in different type of fragment ions. CAD cleaves the peptide bond and results in b ions when the charge is retained by the amino-terminal fragment, or y ions when it is retained by the carboxy-terminal fragment (*2*). ECD cleaves the N-Cα bond and results in c ions when the charge is retained by the amino-terminal fragment, or z ions when the charge is retained by the carboxy-terminal fragment (*21*). ECD generates more extensive fragmentation than CAD and therefore provides better sequence coverage of larger and highly charged analytes (*18*). As a result, ECD is normally integrated with top-down proteomic experiments. The electron-based fragmentation methods have also shown great promise for improved characterization of labile PTMs such as phosphorylation (*22-23*).

It should be noted that knowing the fragmentation pattern of a peptide in a CAD or ECD process is important for peptide identification. As will be discussed later, protein/peptide identification is a matching process between the observed peptide fragment ions and the theoretical peptide fragment ions. The theoretical peptide fragment ions are predicated based on the known fragmentation pattern of a peptide in a CAD or ECD process.

1.1.3 Protein/peptide separation

In biological samples, such as human blood plasma, the protein concentration range can span 12 orders of magnitude, where albumin and immunoglobulins are present in the magnitude of mg/mL whereas cytokines are at the level of pg/mL (*10*). In order to monitor the expression levels of clinically relevant proteins in plasma, the MS-based proteomic

technologies must be capable of detecting proteins at ng/mL levels or lower. Detecting and quantifying potentially thousands of proteins present in a complex biological sample, spanning over a huge range of relative abundances, poses an enormous analytical challenge.

Single-dimension liquid chromatography does not provide sufficient peak capacity to separate peptide mixtures, which are generated by the proteolysis of complex protein mixtures. The sample complexity can be reduced, and therefore the depth and breadth of proteome coverage can be increased, with fractionation/separation techniques at either the protein or the peptide level, or both.

Protein mixtures are often separated by SDS–PAGE and the whole lane of the gel are excised into slices so that the proteins in each gel slice can be analysed separately by single-dimension HPLC–MS/MS (*24*). If protein samples are separated by two-dimensional gel electrophoresis (2DE), spots of interest are excised, digested and analysed by HPLC–MS/MS. As an alternative to protein fractionation, peptide mixtures can be separated by following two orthogonal separation mechanisms. The most popular peptide separation methodology at present is the so-called multidimensional protein-identification technology (MudPIT) (*25-26*), where the peptide mixtures, generated by tryptic digestion of protein samples, are first separated on the basis of charge (strong cation exchange), and then on the basis of hydrophobicity (reversed phase). In-depth characterization of the proteome of complex proteomic samples, such as biofluids, has also been made possible through the development and application of immunoaffinity depletion chromatography (*27*).

To improve the capability of detecting lower abundant proteins in a complex proteomic samples, various combinations of protein/peptide separation and immunodepletion of high abundant proteins can be explored. In principle, these methods are capable of detecting proteins of very low abundance, although considerable effort is required and a sufficient amount of starting protein sample must be available. The ability of MS-based proteomic technologies to identify low abundance proteins from complex mixtures is a driving force in proteomics.

1.1.4 Protein/peptide identification

It is important to note that *de novo* sequencing of the complete amino acid sequence of a protein using a mass spectrometer is generally not feasible. In shotgun proteomics, only a small portion of peptides can be transferred into a mass spectrometer for analysis. In top-down proteomics, although intact proteins can be transferred into the mass spectrometer for analysis, it is still not possible to elucidate the complete amino acid sequence of a protein.

In shotgun proteomics, protein identification is carried out at the peptide level, i.e., through peptide identification. Further, peptide identification is achieved through a database-matching process, rather than a peptide-sequencing process. The fact that only a finite numbers of the possible peptide amino-acid sequences actually occur in nature renders the database-matching methodology feasible for peptide identification. An observed peptide-fragmentation spectrum might not contain sufficient information to unambiguously derive the complete amino-acid sequence, but it might still have sufficient information to match it uniquely to a peptide sequence, which is theoretically predicated on the basis of the genomic information of the proteome of interest. The current MS-based proteomics would not be possible without the previous achievements of genomics, which provided the 'blueprint' of all the possible protein sequences of a biological system.

There are several different algorithms that are used to search sequence databases with tandem MS spectra data, including PeptideSearch (*6*), Sequest (*5*), and Mascot (*7*). Correspondingly, there are a number of different techniques and strategies for peptide identification.

MALDI-TOF can be used to identify proteins by what is known as peptide-mass mapping or peptide-mass fingerprinting, mostly attributed to the high mass accuracy, high resolution and sensitivity of TOF mass analyser. In this method, proteins are identified by matching a list of experimental peptide masses with the predicated list of all peptides masses of a comprehensive protein database.

Protein identifications using MS/MS spectra are more commonly used in shotgun proteomics. In addition to the peptide mass, the peak pattern in the MS/MS spectrum also

provides valuable information about peptide sequence. Peptide identification is carried out using the precursor ion m/z information and its MS/MS spectrum which are then matched against a comprehensive protein sequence databases using an appropriate algorithm mentioned above. For examples, in the cross-correlation method (e.g. Sequest), the observed m/z of the precursor ion and the specificity of trypsin is used to generate a list of isobaric peptides from the protein database. This information is generally not sufficient to match to a single peptide. Then theoretical MS/MS spectra are generated for all of the isobaric peptide sequences, obtained from the database, on the basis of the known fragmentation patterns of the peptides in CAD or ECD processes (Figure 1.1.3). The overlap or "cross-correlation" of these predicted spectra with the measured mass spectra is calculated and the one with the best cross-correlation coefficient is considered to be the best match. Often, this will identify the best matching peptide sequence; however this might not be sufficient to pinpoint a single protein. Generally, multiple peptides derived from the same proteins will be analyzed and will as a group point to a unique protein. In the "probability based matching" method (e.g. Mascot), the calculated fragments from peptide sequences in the database are compared with the observed peaks. A score is then calculated to indicate the statistical significance of the match between the spectrum and the sequences contained in a database. In each of these methods mentioned above, the identified peptides are then compiled into a protein 'hit list', which is the output of a typical proteomic experiment.

High-throughput MS-based proteomic experiments involve searching large numbers of peptide MS/MS spectra recorded with a mass spectrometer against the protein sequence database to derive a list of identified peptides and their corresponding proteins. It should be acknowledged that challenges exist in distinguishing the correct peptide assignments from false identifications (*28*). Tremendous efforts have been devoted to tackle the issues of false positive (a protein not present in the sample is 'identified') and false negative (a protein present in the sample is not 'identified') results in the current MS-based proteomic experiments (*29-30*). It should also be noted that only a limited number of peptide ions, representing a small percentage of the complete amino acids sequence of a protein, are observed and analyzed in shotgun proteomics (*31*).

1.1.5 Quantitative proteomics

Increasingly, proteomics has evolved into a quantitative science. Quantitative proteomics is a powerful tool to quantify protein changes due to stimuli or to make comparisons between healthy and disease states (*1, 32-33*). Relative quantification of identified proteins allows a wider range of biological questions to be addressed by a proteomics experiment. Currently, relative comparisons of peptide/protein abundance between proteomic samples can be carried out with stable-isotope labeling of proteins or peptides via chemical labeling and metabolic labeling, or label free approaches.

As shown in Figure 1.1.4, several chemical labeling techniques have been developed for quantitative MS-based proteomics. Representative chemical labeling techniques include enzymatic labeling of ^{18}O atoms during protein digestion, isotope-coded affinity tag (ICAT), and isobaric tags for relative and absolute quantification (iTRAQ). In the enzymatic labeling approach (Figure 1.1.4a), protein digestion of one proteomic sample is carried out in ^{18}O water while the control is performed in normal water. ^{18}O atoms are incorporated into the C terminus of every N-terminal peptide produced by proteolysis (*34-35*). Reaction products from ^{18}O-labeled and non-labeled reactions are then mixed together, followed by LC-MS analysis. The relative abundance of the treated and control samples can be measured by comparing the peak intensities of the labeled and unlabeled peptides. Isotope-coded affinity tags (ICAT) (Figure 1.1.4b) can be used to label proteins or peptides *via* a chemical reaction with the sulfhydryl group of cysteine residues (*36*). The relative abundance of proteins in the treated and control samples can be measured by comparing the peak intensities of the labeled and unlabeled peptides. Isobaric tags for relative and absolute quantification (iTRAQ) is one of the most commonly used techniques for peptide labeling (*37-39*) (Figure 1.1.4c). The iTRAQ tags react specifically with primary amine groups of tryptic peptides, e.g. N-termini and the side chains of lysine residues. It is worth noting that all the tagged peptides remain indistinguishable in the MS scan. The relative abundance of the normally multiplexed treated and control samples is measured by comparing the peak intensities of the so-called "reporter ions", which are released in the MS/MS scan.

Recently, a method called 'stable-isotope labelling with amino acids in cell culture', or SILAC, has been described (*40*). In this method (Figure 1.1.5), one or two amino acids

(typically arginine and/or lysine) are labeled with "heavy" isotopes (e.g. ^{13}C and/or ^{15}N atoms) and added to the growth medium, which is arginine and/or lysine deficient. Then, the heavy isotope-labeled amino acids are incorporated into all the proteins after several cell doublings. Potentially all protein/peptides can be labelled and the absence of any *in vitro* reaction steps make the method easy to apply as well as compatible with multistage purification procedures.

The stable-isotope labelling technologies make use of the facts that pairs of chemically identical analytes with different stable-isotope composition can be differentiated in a mass spectrometer owing to their mass difference, and that the ratio of signal intensities for such analyte pairs accurately indicates the abundance ratio for the two analytes in the complex mixture. This is because pairs of chemically identical analytes of different stable-isotope composition have identical sample loss during processing, often co-eluted in HPLC separation, and exhibit nearly identical ionization efficiency.

Relative peptide and protein abundance from LC-MS/MS measurements can also be estimated with label free approaches (Figure 1.1.6). The label free quantitative proteomics can be carried out by comparing peak area of a peptide (*41*) or by counting the number of times the MS/MS spectra of a peptide are recorded and identified (spectral counting) in individual LC-MS runs (*42*). In contrast to quantitative approaches that use labeling, label free does not require multiple samples to be combined prior to analysis. Instead, each sample is separately prepared, and subjected to individual LC-MS/MS runs. As a result, the label free quantitative proteomic approaches require high reproducibility among each individual LC-MS/MS run. Nevertheless, the label free quantitative proteomic approaches have enabled fast and low-cost measurements of protein expression level of complex biological samples.

1.1.6 Thesis objective: Proteomic reactor development

As discussed above, the shotgun proteomic approach requires the processing of proteins into peptides before they are analyzed by mass spectrometry (*1-2, 43-44*). In order to improve detection capabilities for lower abundance proteins in complex proteomic

samples, various combinations of protein/peptide separation have been explored. Improving the ability of MS-based proteomic technologies to identify low abundance proteins from complex mixtures is a driving force in proteomics.

For the past 30 years, gel electrophoresis has been used for protein pre-fractionation (1D & 2D) (*45-46*). As the separated proteins are difficult to extract from the polyacrylamide gel (*47*), they are enzymatically cleaved into peptides in the gel (*48*). Unfortunately, protein/peptide loss and contamination are intrinsic limitations associated with in-gel sample processing techniques (*49*). Notably, the in-gel sample processing techniques provide limited dynamic range and are not ideal for the analysis of proteins in lower abundance (*45*).

Recently, gel free alternatives for the fractionation of proteins and peptides have been proposed. These gel-free approaches rely on either solution based protein separations such as size exclusion (*50*), reverse-phase liquid chromatography (*51*), free-flow electrophoresis (FFE) (*52-53*) and 2D chromatography (*54*), or peptide separations (*55-58*). In these approaches, the proteins are digested in a large volume of solution (in-solution digestion) either before or after separation. Even though these gel-free approaches bypass the need for gels, they do not address the fundamental issue of efficiency of protein processing.

Various approaches to in-solution digestion have been proposed, notably, the approach to process proteins using immobilized trypsin in monolithic columns followed by peptide fractionation (*59-60*), and that to digest proteins by absorbing them on a hydrophobic support, followed by introducing trypsin (*61-62*). However, these approaches have notable limitations. These approaches either do not offer protein preconcentration before enzymatic digestion or require a high amount of starting protein sample. In general, these approaches require further development before being readily amenable to real biological samples.

MS-based proteomics must deal with a limited amount of starting materials. In addition, it also faces other challenges such as a huge dynamic range of protein concentration. As such, the systematic identification and quantification of lower abundance proteins, often with more biological significance, still remains elusive.

We hypothesized that miniaturization of protein processing will improve recovery and reduce sample losses. This will lead to more proteins identified per sample and the improved ability to process minute amounts of samples. This thesis presents the development of a microfluidic device, termed the *proteomic reactor* to simplify and improve the processing of proteomic samples. Compared to other in-gel or gel free protein digestion/separation techniques, proteomic reactor techniques require a significantly smaller amount of starting protein samples but are still capable of identifying a comparable amount of proteins. By minimizing sample loss and improving the protein digestion efficiency during the sample processing processes, the proteomic reactor techniques can increase the depth and breadth of proteome coverage and identification confidence, and therefore increase the possibility of identifying lower abundance proteins. As the total time to process protein samples using the proteomic reactor techniques is relatively short (~2 hours) in comparison to other protein digestion methodologies, the proteomic reactor approaches can also increase the throughput for processing complex biological samples, which is necessary for large scale analysis of proteomes.

In this thesis, we developed SCX proteomic reactor (chapter 3.1), SCX 96-well plate proteomic reactor (chapter 3.2) and SAX proteomic reactor (chapter 3.3).

1.2 MS-based Lipidomics

1.2.1 The general picture

We know that lipids play many important roles in cells such as cellular structural support, energy storage, and signal transduction (*63-64*). Also, recent research points to the vital roles that lipids may have in Alzheimer disease (*65*), cancer (*66-67*), inflammation and cardiovascular diseases (*68*), male infertility (*69*) and other diseases. Glycerophospholipids, for example, form the largest lipid subclass by mass, and they are important components of biological membranes in which they modulate membrane trafficking (*70-71*). Furthermore, some of their metabolites, such as platelet activating factors, are powerful intracellular signalling molecules (*72*). These metabolites can induce a broad range of biological responses (*73*), including the progression of neurodegeneration (*74-75*). Although the study of lipids is not new, their global quantitative study is more recent. The term *lipidomics* was thus coined to define the global study of the lipid components of cells, tissues or organisms.

Certain challenges still remain in lipidomics. First, in contrast to genomics and proteomics, there is no information that can predict the number of individual lipids present in an organism. Second, despite its rapid advancement, current technology still cannot exhaustively map lipidomes; thus an emphasis on developing mapping techniques is needed. Third, the structural identification of lipids by mass spectrometry, via the gas phase fragmentation of lipid ions, is complicated; thus, a means to solve this problem is vital for structural identification. Fourth, given the diversity in lipid classes, it is not possible to accommodate all classes with a common method for extraction, chromatography, and detection. In the following section, we review recent developments in the field of lipidomics with an emphasis on phospholipids.

1.2.2 Structural diversity of lipids

The structural diversity of lipids, and the fact that their structure cannot be predicted *a priori*, is a serious challenge to the field of lipidomics. Eukaryotic cells provide an excellent example of the structural complexity of lipids. Lipid can be broadly classified

under eight classes: Fatty acyls, sterol lipids, prenol lipids, saccharolipids, polyketides sphingolipids, glycerolipids, and glycerophospholipids. Glycerophospholipids and sphingomyelins are two common structural classes of phospholipids (*76*). The research in this thesis involves primarily glycerophospholipids.

Typical glycerophospholipids (Figure 1.2.1) consist of a glycerol backbone, a radyl moiety (acyl ester, alkyl ether, or vinyl ether) at the *sn-1* (stereospecific number) position, an acyl ester at the *sn-2* position, and a polar head group attached to the *sn-3* position through a phosphodiester linkage. The common polar head groups in glycerophospholipids include choline, ethanolamine, inositol, serine, and glycerol. Correspondingly, the glycerophospholipid classes are: the glycerophosphocholines (PC), glycerophosphoethanolamines (PE), glycerophosphoinositols (PI), glycerophosphoserines (PS), and glycerophosphoglycerols (PG), with each class containing a different type of polar head group, while glycerophosphates (PA) have a hydrogen rather than a polar head group attached to the phosphate. Figure 1.2.2 shows the representative structures of glycerophospholipids. Lyso variants of glycerophospholipids can also be formed if a radyl moiety is missing at either the *sn-1* or *sn-2* position. Platelet activating factors (PAF) are a special subclass of phosphatidylcholines (PC), with an ether alkyl at the sn-1 position and an acetyl at sn-2 position (*77*).

In addition to a variety of polar head groups, phospholipids contain fatty acyl moieties with different chain lengths and different numbers of double bonds on different sites. The identification of a glycerophospholipid involves determining its polar head group, its radyl groups at both sn-1 and sn-2 positions, and, ideally, the locations of (possibly multiple) carbon-carbon double bonds on each radyl moiety. Unfortunately, due to the extraordinary structural diversity of phospholipids, the complete identification of all species in lipid extracts obtained from cell or tissue samples has not yet been accomplished. The full identification of species thus remains a challenging task, especially considering the fact that some lipid species are present in low abundance.

1.2.3. Structure elucidation of glycerophospholipids

To delineate lipid structure characteristics, the lipidomics field has benefited from the technical developments established in proteomics. However, as discussed in chapter 1.1.4, protein identification is mostly a "matching" process: the amino acid sequences of some peptide fragments of a protein are determined by mass spectrometry, and the obtained information is used to search against a library that contains all the possible protein sequences predicted by the genomic information of the biological system (*5-7*). Normally the matching of the amino acid sequences of one or two peptides to those of a protein in the library is sufficient to unambiguously "identify" the protein. In contrast, lipid identification is a "*de novo*" process, where the structural elucidation of a lipid species is based on the interpretation of MS-derived structural information. It is also a "top-down" approach, where the identification process is required to be carried out on intact lipid species (*78-79*). As lipids are subject to CAD, structural information on all parts of the lipids (including both the head group and fatty acyl chains) are required for a complete elucidation of the lipid structure. Therefore, it is crucial to have the lipids in their native, unmodified state to allow accurate structure elucidation of the lipids species of interest. However, lipid species are subject to modifications or degradation (*i.e.*, oxidation and hydrolysis) prior to MS analyses (*80*). As a result, lipidomics faces the challenge of decoding as much information as possible about the different lipid moieties to allow a non-biased and true identification of the original structure of lipids.

In the process of glycerophospholipid identification (Figure 1.2.3), a MS scan is first employed to determine the *m/z* of each lipid species. Typically, lipids will only carry one charge. Greater mass accuracy translates into more accurate prediction of the atomic composition of the lipid. In the second stage, individual lipids are subjected to dissociations attributed to ion activation. Although low-energy CAD has been extensively applied for lipid studies, high-energy CAD and electron transfer dissociation (ETD) have also been employed (*81-82*). The fragmentation patterns normally reveal information on the lipid polar head group and its acyl chain moieties. Depending on the polar head group of a lipid species, it can be ionized more efficiently under either positive (protonated) or negative (deprotonated) electrospray ionization. A lipid can also be adducted by a cation (*e.g.*, Na^+) or an anion (*e.g.*,

Cl^-) and then studied under positive or negative ion mode, respectively. As will be discussed later, using a triple quadrupole mass spectrometer, precursor ion scan and neutral loss scan enable the identification of a specific lipid species from a complex mixture by monitoring its specific diagnostic fragments. In a precursor ion scan, while Q1 is scanned, Q3 is fixed to monitor a specific fragment ion; in neutral loss scan, both Q1 and Q3 are scanned in a synchronized manner with a constant mass difference in *m/z* between Q1 and Q3, to monitor the loss of a neutral moiety during fragmentation (*83-84*). The characteristic fragment can be associated with either a polar head group or a fatty acyl moiety.

1.2.3.1 ESI-MS/MS of protonated glycerophospholipids

Glycerophospholipids (*i.e.*, GPCho, GPEtn, GPSer, and their lyso derivatives) have been previously analyzed by positive ESI-MS/MS (*85-86*). The fragmentation of protonated GPCho and lyso-GPCho ions yield a peak at m/z 184, the diagnostic fragment for the phosphocholine head group (*87*). The precursor ion scan of m/z 184 highlights phosphocholine-containing lipids (GPCho and sphingomyelin) out of all the lipids present in a MS scan. Fragmentation of protonated GPEtn ($[M+H]^+$) yields a peak at $[M+H-141]^+$ corresponding to the neutral loss of the phosphoethanolamine head group. Similarly, a peak at $[M+H-185]^+$ in a tandem mass spectrum can be used to confirm the presence of protonated GPSer ($[M+H]^+$), which loses its phosphoserine head group during CAD. Overall, strategies that combine survey scan, precursor ion scans and neutral loss scans can help in the unambiguous determination of the molecular weights and the head group composition of phospholipids. Although positive ESI-MS/MS has been widely used for lipid studies, one of its limitations is that not much information pertaining to the fatty acyl constituents can be revealed from the fragmentation pattern. Alternatively, negative ESI-MS/MS and positive ESI-MS/MS with metal ion adduction have been employed to elucidate lipid structure. This will be discussed in the following sections.

1.2.3.2 ESI-MS/MS of deprotonated glycerophospholipids

GPEtn, GPIns, GPSer, GPGro, GPA, and their lyso variants can all be detected by negative ESI-MS/MS (*86, 88-96*). This approach is very powerful in elucidating the structure of glycerophospholipids. Compared to its positive counterpart, negative ESI-MS/MS yields fragmentation patterns with a wealth of structural information on the polar head groups and the fatty acyl constituents of phospholipids. Fragmentation of GPEtn anions ($[M-H]^-$) generates fragments at m/z 140 and 196, both of which correspond to the polar head group of GPEtn (*92*). As deprotonated GPIns ($[M-H]^-$) are subject to CAD, a peak corresponding to the dehydrated GPIns head group is observed at m/z 241. Similarly, PtdInsP and $PtdInsP_2$ can be identified by precursor ion scans of m/z 321 and 401, respectively, under negative ion mode (*94, 97*). The fragmentation of deprotonated GPGro yields a head group specific fragment at m/z 171 (*96*). GPSer anions ($[M-H]^-$) is identified by a peak at $[M-H-87]^-$, which corresponds to the neutral loss of the serine head group (*95*). A fragment at m/z 153 ($[Glycerophosphate-H_2O]^-$) is detected in the fragmentation spectra of all phospholipid species under negative ion mode.

Low-energy CAD of glycerophospholipids under negative ion mode also yields fragments decoding structural information on the fatty acyl constituents at the *sn*-1/*sn*-2 positions. These fragments include the carboxylate anions ($[R_xCOO]^-$(x=1, 2)), ions arising from the neutral loss of fatty acids ($[M-H-R_xCOOH]^-$(x=1, 2)), and ions due to neutral loss of the fatty moieties as ketene ($[M-H-R'_xCH=C=O]^-$(x=1, 2)) (*92-96*).

It has been found that in a low-energy CAD process, the loss of fatty acyl chains from the *sn*-2 position is sterically more favourable than that from the *sn*-1 position. As a result, the abundances of the $[M-H-R_2COOH]^-$ and $[M-H-R'_2CH=C=O]^-$ ions are greater than those of the $[M-H-R_1COOH]^-$ and $[M-H-R'_1CH=C=O]^-$ ions. However, as the major fragmentation pathways differ among different lipid species, the relative abundance of the carboxylate anion $[R_1COO]^-$ with respect to $[R_2COO]^-$ changes. For GPEtn and GPGro, the abundances of $[R_2COO]^-$ ions are greater than $[R_1COO]^-$ ions (*92, 96*). For GPIns, the carboxylate anions $[R_1COO]^-$ and $[R_2COO]^-$ are generated due to direct dissociation from

the glycerol backbone, and also due to the further dissociation of fragment ions $[M-H-R_xCOOH]^-$, $[M-H-R'_xCH=C=O]^-$ and $[M-H-R_xCOOH-inositol]^-$, which are affected by the collision energy applied. Thus, the relative abundance of the carboxylate anions $[R_1COO]^-$ and $[R_2COO]^-$ for GPIns depends on the collision energy applied (*94*). For GPA, the major pathway that leads to the formation of the carboxylate anions $[R_1COO]^-$ and $[R_2COO]^-$ is the fragmentation of $[M-H-R_2COOH]^-$ and $[M-H-R_1COOH]^-$, respectively. As a result, the higher abundance of $[M-H-R_2COOH]^-$ ions leads to higher abundance of $[R_1COO]^-$ ions (*93*). As GPSer is subjected to low-energy CAD, it first loses the serine head group to generate [M-H-87]$^-$ ions. The fragmentation patterns of [M-H-87]$^-$ ions are virtually identical to those of the corresponding GPA (*95*).

1.2.3.3 ESI-MS/MS of metal ion adducted glycerophospholipids

The fragmentation of lipids can be modified by changing the counter ion present in solution. In particular, alkali metal ions (*e.g.*, Li^+, Na^+ and K^+) have been commonly used for adducting phospholipids (*90, 98-100*). As these metal ions adducted glycerophospholipids are subject to CAD, their fragmentation patterns reveal information on the polar head groups and the fatty acyl constituents. The fragmentation of sodiated GPCho and sphingomyelin both generated a sodiated five-member cyclophosphane at m/z 147, and a product ion at $[M+Na-59]^+$ due to the neutral loss of trimethylamine $N(CH_3)_3$, both of which are diagnostic fragments of the phosphocholine head group. In the tandem mass spectra of lithiated GPCho, abundant product ions can be found at $[M+Li-59]^+$ (neutral loss of trimethylamine $N(CH_3)_3$), $[M+Li-183]^+$ (neutral loss of cyclophosphane), and $[M+Li-189]^+$ (neutral loss of lithium cyclophosphane) (*87*). It has been observed that the most prominent ion is $[M+Li-183]^+$ for lithiated diacyl-GPCho, whereas the most high abundance ion is $[M+Li-59]^+$ for lithiated plasmenyl-, plasmanyl- and lyso-PCs (*101-102*). CAD of lithiated GPEtn yields fragment ions associated with the polar head group, including ions at $[M+Li-43]^+$ (neutral loss of aziridine (CH_2CH_2NH)), $[M+Li-141]^+$ (neutral loss of phosphoethanolamine head group),

$[M+Li-147]^+$ (neutral loss of lithium phosphoethanolamine head group), and m/z 148 (phosphoethanolamine head group) (*100*). The CAD analyses of GPSer as lithiated adducts yield diagnostic fragments of phosphoserine as a lithium salt at m/z 192 (*95*). In addition to structural information on the polar head groups, structural information pertaining to the two fatty acyl moieties can also be revealed from product ions like $[M-H+Met-R_xCOOH]^-$ and $[M-H+Met-R'_xCH=C=O]^-$ (x=1 ,2), arising from the loss of fatty acyl moieties as fatty acids or alkenes, respectively.

Metal ions such as Sr^{2+}, Ba^{2+}, Mn^{2+}, Co^{2+}, Ni^{2+}, Cu^{2+}, and Zn^{2+} have been also used to adduct phospholipids (*99*). The fragmentation spectra of these ions also decode information on the polar head groups of phospholipids, and their fatty acyl chain moieties ($[M-H+Met-R_xCOOH]^-$, $[M-H+Met-R'_xCH=C=O]^-$). Cobalt(II) ion complexes of GPEtn and GPSer yield $[M-H+Met-R_1COOH]^-$ ions with higher abundance than $[M-H+Met-R_2COOH]^-$ ions, whereas cobalt(II) adducted GPGro fragmentation patterns generate $[M-H+Met-R_2COOH]^-$ ions with higher abundance than $[M-H+Met-R_1COOH]^-$ ions. The information on abundance ratios could be used to determine the stereospecific positions of the two fatty acid substituents. Chlorine adduct has also been reported for the identification of the fatty acyl substituents of GPCho in negative ESI-MS/MS (*98, 103*). In conclusion, glycerophospholipids with different adduct formations generate lipid-specific fragmentation signatures that allow unambiguous identification of the lipid species of interest.

1.2.4 Glycerophospholipid identification by multiple precursor ion scans and neutral loss scans

Strategies that combine survey, product ion, precursor ion, and neutral loss scans can be employed for the study of the lipidome. A product ion scan records all fragment ions generated during CAD, including fragment ions relevant to the polar head groups and the fatty acyl moieties. Precursor ion scan and neutral loss scan each monitor a specific fragmentation reaction (*i.e.*, whether a specific diagnostic fragment is generated (charged) or

lost (uncharged)). Compared to product ion scan, precursor ion and neutral loss scans have the capability of identifying a lipid species that contains a specific diagnostic moiety (*e.g.*, a polar head group or a fatty acyl moiety) from a complex mixture. On the other hand, precursor ion and neutral loss scans could not make full use of many other fragment ions that are helpful in lipid structural elucidation. The combination of multiple precursor ion scans and neutral loss scans would enable simultaneous monitoring of multiple fragmentation reactions. This allows the identification of multiple diagnostic fragments from a complex mixture of product ions for lipid structure elucidation (*83-84, 104-107*).

A two-dimensional ESI-MS/MS analysis of lipid extracts has been reported using multiple precursor ion and neutral loss scans under either positive or negative ion mode (*108*). This strategy made possible the identification of isobaric peaks, and the determination of the regiospecificity of individual lipid species. If multiple precursor ion and neutral loss scans are carried out on a triple-quadrupole mass spectrometer, each scan must be performed one at a time, due to the path stability selection adopted by a triple-quadrupole mass spectrometer. However, if the multiple scans are carried out on a hybrid quadrupole time-of-flight (TOF) mass spectrometer with ion trapping capability (*e.g.*, QSTAR Pulsar), all modes may be performed simultaneously due to the non-scanning acquisition of TOF mass analyzers. It has been reported that the hybrid quadrupole time-of-flight (TOF) mass spectrometer allows the simultaneous acquisition of 41 precursor ion spectra, which decode information on specific lipid classes and common fatty acyl chain moieties (*107*). The high mass accuracy and high resolution of TOF analyzers are very helpful in determining the atomic composition and hence the structure of a lipid species.

1.2.5 Glycerophospholipid identification by multiple stage tandem mass spectrometry

Structural information revealed by tandem MS alone could not always provide adequate information to identify a lipid species unambiguously. In many cases, the lipid species of interest are complex and/or the determination of very specific information on a fatty acyl chain is required (*e.g.*, double bond location). Thus, multiple stage tandem MS could be applied to tackle such structural information. Hsu *et al.* characterized the structure

of cardiolipin using negative ion mode with multiple stage quadrupole ion trap MS. The MS^3-spectra of the phosphatidic anions provided critical information on the identity of the fatty acyl substituents and their stereospecific position (*109*). Hsu *et al.* also determined the double bond position along the fatty acyl group of glycerophospholipids using multiple-stage MS (*110*). In another work, Hsu *et al.* employed multiple stage MS to differentiate 1-*O*-alk-1′-enyl-2-acyl-, 1-*O*-alkyl-2-acyl- and diacyl-glycerophospholipid molecules from each other based on the MS^3 or MS^4 spectra of their $[M-H-R_2COOH-headgroup]^-$ ions. These ions arise from the consecutive losses of the fatty acid substituents at the *sn*-2 position, and their respective polar head groups from the $[M-H]^-$ ions (*111*). It has been also reported that isobaric lyso-GPCho and PAF can be effectively identified by MS^3 on a QTRAP mass spectrometer (*112*).

1.2.6 Characterization of the fatty acyl constituents of glycerophospholipids

Under both positive and negative ESI-MS/MS, glycerophospholipid fragments yield product ions allowing relatively easy elucidation of their polar head groups. The characterization of the two fatty acyl moieties at the *sn*-1/*sn*-2 positions, however, poses challenges. The structural information relevant to the fatty acyl chains can only be revealed under negative ion mode ESI or positive ion mode ESI with metal ion adduction. In eukaryotes, the fatty acids at the *sn*-2 position of glycerophospholipids are always linked to the glycerol backbone through an ester bond. The fatty acids at the *sn*-1 position can be attached via an ester linkage (diacyl-GP), an alkyl ether linkage (1-alkyl, 2-acyl-GP), or a vinyl ether linkage (plasmologens). For the complete identification of a glycerophospholipid, the following information pertaining to the fatty acyl chains is needed: (***i***) the chain length of the two fatty acyl moieties, and the total number of carbon double bonds in each chain; (***ii***) the assignment of the two fatty acyl moieties to *sn*-1/*sn*-2 position (for diacyl-GPs); and (***iii***) the location of the polyunsaturated carbon double bonds on each acyl moiety.

The molecular weight of a phospholipid can be determined precisely by a survey scan. The polar head group of a phospholipid can be identified by carrying out a precursor ion scan or a neutral loss scan as discussed above. The sum information of the two fatty acid chains

(*i.e.*, the length of the two fatty acyl chains at the *sn*-1 and *sn*-2 positions, and the total number of double bonds) can thus be decoded. However, a number of combinations of different fatty acyl moieties could all add up to the same molecular weight, leaving the length of each fatty acyl chain, and the number of double bonds on each fatty acyl moiety undetermined. Using negative ESI-MS/MS, a variety of fragment ions relevant to the two fatty acyl moieties can be observed. These include carboxylate anions $[R_xCOO]^-$, as well as $[M-H-R_xCOOH]^-$ and $[M-H-R'_xCH=C=O]^-$ ions. The latter two ions arise from the loss of one of the two fatty acyl moieties. These fragment ions reveal critical structural information relevant to the fatty acyl constituents, and allow the unambiguous determination of the length of each fatty acyl moiety and the total number of double bonds on each acyl chain (*92-96, 113*). Under positive ion mode ESI, the fragmentation of metal adducted glycerophospholipids also yields fragment ions corresponding to their polar head groups and fatty acyl moieties ($[M-H+Met-R_xCOOH]^-$, $[M-H+Met-R'_xCH=C=O]^-$). This permits the unequivocal characterization of the fatty acyl moieties (*98-99*).

The use of MS to determine the regiospecificity of the two fatty acyl substituents of diacyl-glycerophospholipids has been attempted (*113-114*). As discussed earlier, it appears that under low-energy CAD the $[R_1COO]^-/[R_2COO]^-$ abundance ratio follows certain rules for some diacyl-glycerophospholipids, and this information has been used to determine the positions of the two fatty acyl chains (*92-94, 96*). Such attempts have also been made on the basis of fragmentation patterns of glycerophospholipids adducted with certain metal ions, where the relative abundance of ions corresponding to the loss of the fatty acyl moiety at sn-1/sn-2 positions has been used to assign the positions of the two fatty acyl substituents (*98-99, 115*). However, it has been observed that the $[R_1COO]^-/[R_2COO]^-$ abundance ratio recorded from the fragmentation of GPIns under negative ion mode is affected by the collision energy applied (*94*). Detailed studies on the effect of collision energy on the $[R_1COO]^-/[R_2COO]^-$ ratio for phospholipid species have been carried out by Hvattum et al. These results reveal that as the collision energy increases from 15 to 70 ev, the abundance of $[R_1COO]^-$ ions increases from lower to higher than the abundance of $[R_2COO]^-$ ions for GPCho, GPEtn, and GPIns (*116*). It is therefore clear that the collision energy applied plays

an important role during the CAD of glycerophospholipids. Other factors, such as the chain length and the number of double bonds of the fatty acyl moieties should also be taken into consideration. Overall, the assignment of the two fatty acyl chain positions based on the abundance ratio of a specific pair of ions is still under scrutiny.

1.2.7 Glycerophospholipid identification with or without separation

Ideally the identification of a lipid species using ESI-MS/MS should be carried out without interference from other lipid species, as the presence of fragment ions from those impurities could mislead the identification. Lipid extracts from biological samples are complex mixtures. The identification process is, thus, almost always carried out in the presence of other lipid species. As a result, glycerophospholipids can be identified to different extents as discussed above, depending on the complexity of the sample and the separation techniques applied.

Lipid extracts can be directly infused into a mass spectrometer without front-end separation through ESI, followed by lipid identification by tandem MS (*86, 88, 103, 117*). One issue associated with direct infusion is the ionization suppression of lipid species with low ionization efficiency. As a result, the detection of these lipid species becomes extremely difficult, especially if they are present in low concentrations in lipid extracts (*97, 118*). If a complex mixture of lipid species is analyzed using direct infusion, a single peak in a survey scan could represent several isobaric lipid species (*86*). CAD of such precursor ions would generate a mixture of fragmentation patterns from several lipid species, making the identification process extremely difficult/impossible.

A technique called intra-source separation has been introduced to perform total cellular lipidome analyses by direct infusion of crude lipid extracts without front-end chromatographic separation (*83, 106, 108*). By employing both positive and negative ion mode, as well as adjusting the pH of the lipid extract, anionic lipids, weak anionic lipids and neutral polar lipids can be preferentially ionized under different experimental conditions. Therefore, intra-source separation of different lipid classes is achieved. Intra-source

separation in combination with multiple precursor ion scans and neutral loss scans has enabled the unambiguous identification of complex lipid extracts (*83, 108*). However, precaution must be taken in dealing with isobaric lipid species, and in correcting isotopic peak intensities.

The coupling of HPLC with ESI-MS/MS is the most frequently used technique for lipidomic analysis, and the majority of reports on MS-based lipidomics rely on online or offline separation of lipids (*63, 85, 113, 119-120*). Normal-phase HPLC generally separates phospholipids based on the polarity of their head groups; whereas reverse-phase HPLC separates phospholipids based on the hydrophobicity of their fatty acyl chains (*113*). In RP-HPLC separation, the order of elution in a class of lipid is related to the length of the fatty acyl chain. Lipids containing shorter fatty acyl chains elute faster than those with longer ones. Furthermore, the higher the degree of unsaturation, the faster the lipid elutes (*113*). Direct infusion ESI-MS/MS is incapable of resolving isobaric glycerophospholipids with different fatty acyl chain composition. However, these isobaric glycerophospholipid species can be resolved and identified with the application of reversed-phase HPLC (*113*). Despite the concerns of potential sample loss during liquid chromatography separations, ESI-MS/MS integrated with front-end separation has become the method of choice in MS-based lipidomics.

1.2.8. Lipid quantification

In the lipidomics field, MS is employed not only for qualitative analyses (*i.e.*, lipid structure elucidation) but also for quantitative purposes (*i.e.*, measuring the absolute concentration of lipid species or the relative abundance of a group (class) of lipid species in complex mixtures) (*86, 90, 103, 121-122*). Unlike the field of quantitative proteomics where several quantitative techniques have been well established and broadly accepted, a general consensus is yet to be reached for the most appropriate lipid quantification approach. However, adding lipid standards prior to MS analysis is a general practice (Figure 1.2.4). The quantitative analysis of a lipidome is generally divided into global and targeted lipidomics. Global lipidomics allows the identification and relative quantification of

numerous molecular lipid species across multiple structural classes in total lipid extracts. This strategy includes shotgun lipidomics, which utilizes direct infusion of lipid extracts into a mass spectrometer (*83, 123*), and LC-MS/MS (*113, 124*). In global lipidomics, normally a variety of lipid standards are spiked in to cover a relatively broad spectrum of lipid species. Precursor ion scan and neutral loss scan are widely adopted MS techniques for global quantitative lipidomics. Targeted lipidomics, on the other hand, permits the quantitative analysis of a single lipid species or several lipids within a specific lipid class (*125-126*). In comparison to precursor ion scan and neutral loss scan, selected reaction monitoring (SRM) can provide exclusive sensitivity and accuracy for targeted quantitative analysis of lipid species of interest.

It should be noted that the instrument response varies between different classes of lipids (*118*). In addition, identical lipid species exhibit different behaviours when analyzed using different types of mass spectrometers or when analyzed using the same mass spectrometer under different experimental parameters (*80, 127*). Therefore, the relative intensities of signals corresponding to different lipid species in a mass spectrum do not directly reflect their molar abundances and concentrations. It has been documented that as glycerophospholipids are analyzed by ESI-MS, the instrument response decreases with increasing fatty acyl chain length, and increases with increasing degrees of acyl chain unsaturation (*86, 118*). It is also impractical to use mass spectrometry to directly estimate the relative abundance of different phospholipid subclasses due to the difference in the ionization efficiency of their polar head groups (*118*). The gross estimation of the relative abundance of lipid species within a specific phospholipid subclass is less problematic, provided the responses of all the lipid species are normalized with appropriate internal standards (*128-129*). Specifically, when using direct infusion ESI-MS (including intra-source separation), the peak intensity is proportional to the concentration of a lipid species in a mixture. However, when front-end separation is applied (*e.g.*, GC or LC), the integrated peak area of a lipid species is generally considered to be proportional to its quantity present in a complex mixture.

1.2.8.1 Absolute lipid quantification

The absolute quantification of specific lipid species relies on the availability of their synthetic lipid standards in non-labelled or isotopically-labelled forms. This strategy is applicable to a limited number of lipids in complex mixtures (*77, 121*). The absolute concentration of lipids can be determined by standard addition methods. In brief, known amounts of standards of the target lipid are sequentially spiked in the complex mixture. The respective MS responses are used to determine the original concentration of the lipid species of interest (*77, 121*). The absolute concentration of a lipid species can also be determined by spiking in known amounts of lipid standards labelled with stable isotopes (stable-isotope dilution) (*130*). The isotopically-labelled lipid standard and its normal counterpart exhibit identical responses in mass spectrometers as they have identical physiochemical properties. Therefore the original concentration of the target lipid species can be determined by comparing the peak heights or peak areas of the paired heavy and normal lipids.

1.2.8.2 Relative lipid quantification

In many cases, comprehensive lipid profiling between wild and mutant, basal and stimulated, and normal and disease samples is required (*84, 88, 129*). Mass spectrometry is the method of choice to tackle this daunting task. This approach requires comparison of multiple MS analyses using different scan modes. Fluctuations in signal intensity due to variations in lipid extraction, sample preparation and sample analysis can be an issue, as each sample is individually processed. Fortunately, non-naturally occurring lipid standards can be spiked into the samples at different stages of sample processing, which facilitates the correction of signal intensity. As the ionization efficiency of different glycerophospholipids differs significantly, normally at least one lipid standard belonging to each phospholipid subclass is spiked into samples to serve as internal standards for its respective subclass. When the analytical strategy includes both positive and negative ESI-MS, lipid species that can be detected in both positive and negative modes (*i.e.*, GPEtn and GPSer) are chosen as internal standards for normalization (*88*).

1.2.8.3 Stable isotope labelling through metabolism

Isotopic labelling is also employed for the relative quantitation of a lipidome, and for tracking the fate of lipids via different metabolic pathways (*72*). Appropriate chemicals labelled with stable isotopes are introduced into the growth medium during cell culture, and depending on the target metabolic pathway, either all or a fraction of the lipids are labelled. For instance, Ekroos *et al.* cultured cells with ^{13}C labelled glucose for 24 hours; the lipid extracts from these cells contained a mixture of isotopically labelled endogenous lipids, providing a comprehensive internal standard for quantitative profiling of phospholipids (*84*). Delong *et al.* introduced ethanol-1,1,2,2-d_4-amine (D4-ethanolamine) and choline chloride-(*trimethyl*-d_9) (D9-choline chloride) into the cell culture medium to distinguish the metabolic product GPCho from different metabolic pathways (*128*). Wenk *et al.* metabolically labelled mouse neuronal cells with [^3H]inositol to profile lipids involved in intracellular signalling (*97*). Hence, stable isotopic labelling through metabolism is a promising approach for the relative quantitation of lipidome.

1.2.9 Thesis objectives in lipidomics

1.2.9.1 Development of a nanoflow rate HPLC-ESI-MS/MS methodology for the analysis of Platelet Activating Factor (PAF) family and *lyso*-glycerophosphocholine (LPC) lipids

The PAF subclass of glycerophospholipids are purported to be key mediators of neuronal differentiation and neuronal cell death *in vitro* and *in vivo* (*74, 131-138*). Signaling is isoform-specific. Differences in the *sn*-1 carbon chain length and degree of saturation determine whether activation of the PAF G-protein coupled receptor (PAFR) is cytotoxic or cytoprotective (*139-142*). However, it is not known whether specific PAF subspecies are preferentially generated over the course of neuronal differentiation or neurodegenerative disease.

Even though direct infusion approaches (without front-end LC separation) have been employed to study Platelet Activating Factor (PAF) family and *lyso*-glycerophosphocholine (LPC) lipids, lipid species having low ionization efficiencies are difficult to analyze by this method. As a result, the direct infusion approaches are not ideal for studying the PAF and LPC lipid species, both of which are present in low concentrations (*97, 118*). Coupling of reversed-phase HPLC (*113*) with ESI-MS/MS has been used for lipidomic analysis. However, to the best of our knowledge, the liquid chromatographic separations of lipid species for the published studies were performed at a higher flow rate (e.g., μL/min), and therefore these methods required relatively larger starting materials.

We hypothesized that the nanoflow HPLC-ESI-MS/MS technology, which is commonly used in proteomics, could be adapted for quantitative lipidomic profiling of PAF and LPC lipid species. We expect that the nanoflow HPLC-ESI-MS/MS could be used to improve the sensitivity and deepen the range of detection for the PAF/LPC family lipids.

In this thesis, we developed a nanoflow rate HPLC-ESI-MS/MS method for the analysis of Platelet Activating Factor (PAF) family and *lyso*-glycerophosphocholine (LPC) lipids. This method was applied to the undifferentiated and differentiated PC12 cells. The PC12 cell has been widely used as model for neural differentiation, where the PAF subclass of glycerophospholipids is implicated. This method was further applied to the posterior-entorhinal cortex of individuals with Alzheimer's disease, TgCRND8 transgenic mice expressing mutant human amyloid precursor protein, and human hNT neurons directly exposed to soluble $A\beta_{42}$ oligomers, to study whether specific PAF/LPC subspecies are preferentially generated over the course of neurodegenerative disease.

1.2.9.2 Development of MS-based methodology for determining the stereospecificity of diacyl glycerophospholipids

For the complete identification of a glycerophospholipid, the information pertaining to the fatty acyl chains, such as the chain length of the two fatty acyl moieties and the total number of carbon double bonds in each fatty acyl chain is needed, in addition to information

about the polar head group. For diacyl glycerophospholipids, the assignment of the two fatty acyl moieties to *sn*-1/*sn*-2 position is required.

Previous studies on a limited number of standard diacyl glycerophospholipids revealed that the relative abundance of the fatty acyl anions and the lyso-form fragment ions, which resulted from the neural loss of the two fatty acyl moieties, is associated with their stereospecific position when they are subjected to fragmentation (*87, 92-96, 98-100, 102*). Using MS to determine the regiospecificity of diacyl-glycerophospholipids under negative ion mode has been demonstrated with a number of lipid standards (*113-114*). Of note, for diacyl glycerophosphoinositols (PI), however, the relative abundance of the two fatty acyl anions recorded under negative ion mode depends on collision energy and the characteristics (e.g. length and number of double bonds) of the fatty acyl moieties (*94*). As such, it is still not feasible to use MS-based approaches to determine the stereospecificity of diacyl glycerophospholipids in real biological samples.

Shotgun lipidomic approaches usually analyze lipid extracts with very little, if any, pre-purification (*83, 106, 108*). Consequently, interference can arise from the presence of other isobaric species, or from lipid species with a molecular ion mass that is encompassed by the isolation window preceding fragmentation. As a result, the peak intensities of some fatty acyl anions of interest can be the sum of contributions from more than one lipid species. It is therefore almost impossible to make correct positional assignments using MS techniques that look only at fatty acyl anions while neglecting lyso-form fragment ions, especially when dealing with complex mixtures. In order to exclusively identify glycerophospholipids, it is desirable to include the fragment ions that can provide connections between the fatty acyl moieties and their respective molecular ions. However, to date the structural information pertaining to the lyso-form fragment ions has not been fully exploited for the purpose of determining the stereospecificity of diacyl glycerophospholipids.

In this thesis, we developed a novel methodology to fully determine the stereospecificity of diacyl PA, PS, PG, PI, and PE. This methodology is based on the structural information derived from both the acyl anions and the lyso-form fragment ions from MS/MS spectra obtained using a hybrid quadrupole time-of-flight (QqTOF) mass spectrometer. We first examined a variety of diacyl glycerophospholipid standards with

different fatty acyl chain compositions, including PA, PS, PG, PI, and PE, over a wide range of collision energy. Using the developed novel methodology, we then further analyzed the fatty acyl compositions of glycerophospholipids in lipid extract from a real biological sample.

Figure Captions

Figure 1.1.1 Bottom-up and top-down proteomic approaches. (a) Bottom-up proteomic approach. A mixture of proteins is normally enzymatically cleaved into peptides, which are then separated using high performance liquid chromatography, prior to being analyzed by MS. **(b) Top-down approach.** Proteins are not enzymatically digested prior to MS analysis.

Figure 1.1.2 Electrospray ionization (ESI). Peptides are introduced to the electrospray tip as the eluent flow from HPLC. A high voltage is applied between the electrospray emitter and the orifice of the mass spectrometer, resulting in the formation of a Taylor cone at the end of the emitter and forcing the ejection of positively charged droplets from the emitter towards the orifice of the mass spectrometer. As the droplets traverse the space between the emitter and the orifice, solvent evaporation occurs. The droplet continues to shrink until it reaches the "Rayleigh limit", at which point the surface tension can no longer sustain the charge and a "Coulombic explosion" occurs. As a result, the droplet is ripped apart. The Coulombic explosion results in smaller droplets, which can repeat this process, as well as isolated peptide ions. (The figure is modified based on http://www.chm.bris.ac.uk/ms/theory/esi-ionisation.html).

Figure 1.1.3 CAD and ECD cleave on different bonds. CAD cleaves the peptide bond and results in b ions when the charge is retained by the amino-terminal fragment, or y ions when it is retained by the carboxy-terminal fragment. ECD cleaves the N-Cα bond and results in c ions when the charge is retained by the amino-terminal fragment, or z ions when the charge is retained by the carboxy-terminal fragment. (This figures only indicates the bonds cleaved by CAD and ECD, but not represent the real structures of the fragments ions)

Figure 1.1.4 Quantitative proteomics: stable-isotope labeling of protein/peptide via chemical labeling. (a) Enzymatic labeling. Enzymatic digestion of one proteomic sample is carried out in ^{18}O water while the control is performed in normal water. ^{18}O atoms are incorporated into the C terminus of every N-terminal peptide produced by proteolysis. The relative abundance of the labeled and unlabeled peptides in the treated and control samples

can be measured by comparing the peak intensities in the MS scan. **(b) Isotope-coded affinity tags (ICAT).** ICAT tags are used to label proteins or peptides *via* a chemical reaction with the sulfhydryl group of cysteine. The relative abundance of the labeled and unlabeled peptides in the treated and control samples can be measured by comparing the peak intensities in the MS scan. **(c) Isobaric tags for relative and absolute quantification (iTRAQ).** The iTRAQ tags react specifically with primary amine groups of tryptic peptides (e.g. N-termini and the side chains of lysine residues). The relative abundance of the multiplexed treated and control samples is measured by comparing the peak intensities of the so-called "reporter ions" in the MS/MS scan.

Figure 1.1.5 Quantitative proteomics: stable-isotope labelling with amino acids in cell culture (SILAC). For the treatment samples, amino acids (typically arginine and/or lysine) that are labeled with "heavy" isotopes (e.g. ^{13}C and/or ^{15}N atoms) are added to arginine and/or lysine deficient cell culture medium. The heavy isotope-labeled amino acids are then incorporated into all the proteins after several cell doublings. For the control samples, the cells are cultured in the conventional cell culture medium, which does not contain stable-isotope labelled amino acids. The relative abundance of the labeled and unlabeled peptides in the treated and control samples can be measured by comparing the peak intensities in the MS scan.

Figure 1.1.6 Quantitative proteomics: label free approaches. In label free quantitative approach, each sample is separately prepared, and subjected to individual LC-MS/MS run. Label free quantitative proteomics can be carried out by comparing peak area of a peptide in MS scan or by counting the number of times the MS/MS spectra of a peptide are recorded and identified (spectral counting) in individual LC-MS runs. Label free does not require multiple samples to be combined prior to MS analysis.

Figure 1.2.1 Diagram of the structure of glycerophospholipids, a sub-class of lipids. Typical glycerophospholipids consist of a glycerol backbone, a radyl moiety (acyl ester, alkyl ether, or vinyl ether) at the *sn-1* (stereospecific number) position, an acyl ester at the *sn-2* position, and a polar head group attached to the *sn-3* position through a phosphodiester

linkage. The common polar head groups in glycerophospholipids include choline, ethanolamine, inositol, serine, and glycerol. Adapted with permission from Briefings in Functional Genomics. Copyright © 2008 Oxford University Press.

Figure 1.2.2 Representative lipid structures of glycerophospholipids. (a) Glycerophosphocholines. (b) Glycerophosphoethanolamines. (c) Glycerophosphoserines. (d) Glycerophosphoglycerols. (e) Glycerophosphates. (f) Glycerophosphoinositols. Adapted with permission from Mass Spectrometry Reviews. Copyright © 2010 Wiley Periodicals, Inc.

Figure 1.2.3 The MS-based method for the identification of glycerophospholipids. The identification of glycerophospholipids can be performed by direct infusion of lipid extracts through ESI to a mass spectrometer or by integrating front-end LC separation with a mass spectrometer. Depending on the polar head group of the lipid species of interest, they can be studied under positive ion mode or negative ion mode. A MS scan is first employed to determine the information on the intact molecular weight of each lipid species. In the second stage, individual lipids are subjected to CAD and information on polar head group and fatty acyl moieties are obtained. As there is no genomic information can predicate the structure of a lipid species, lipid structural elucidation is performed on the intact lipid species ("top-down") and is totally based on fragment ions recorded in the MS/MS spectra ("*de novo*").

Figure 1.2.4 The MS-based method for quantitative analysis of glycerophospholipids. The quantitative analysis of a lipidome generally involves the addition of lipid standards at the time of lipid extraction. The lipid extracts can be introduced into a mass spectrometer directly through ESI (direct infusion) or by integrating a front-end LC separation. Depending on the polar head group of the lipid species of interest, quantitative analysis can be performed under positive ion mode or negative ion mode. Precursor ion scan (PIS) and neutral loss scan (NLS) are used for the quantitative analysis of a large number of lipid species across multiple structural classes in total lipid extracts (global quantitative lipidomics). Selected reaction monitoring (SRM) is used for the quantitative analysis of a

single lipid species or several lipids within a specific lipid class (targeted quantitative lipidomics).

Figure 1.1.1

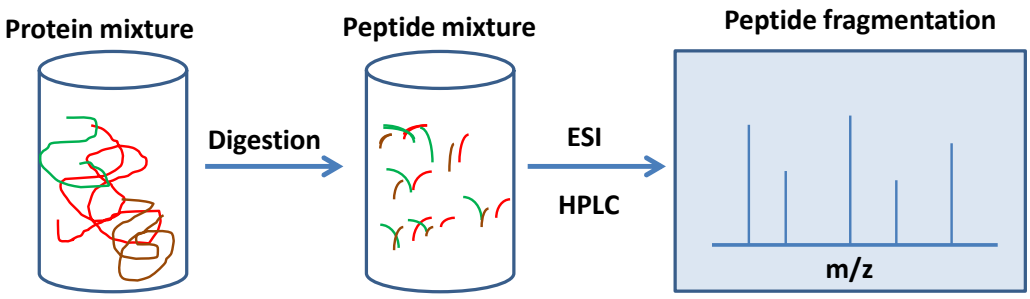

(a) Bottom-up approach

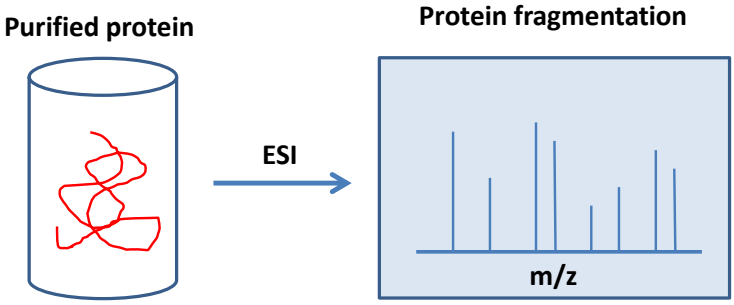

(b)Top-down approach

Figure 1.1.2

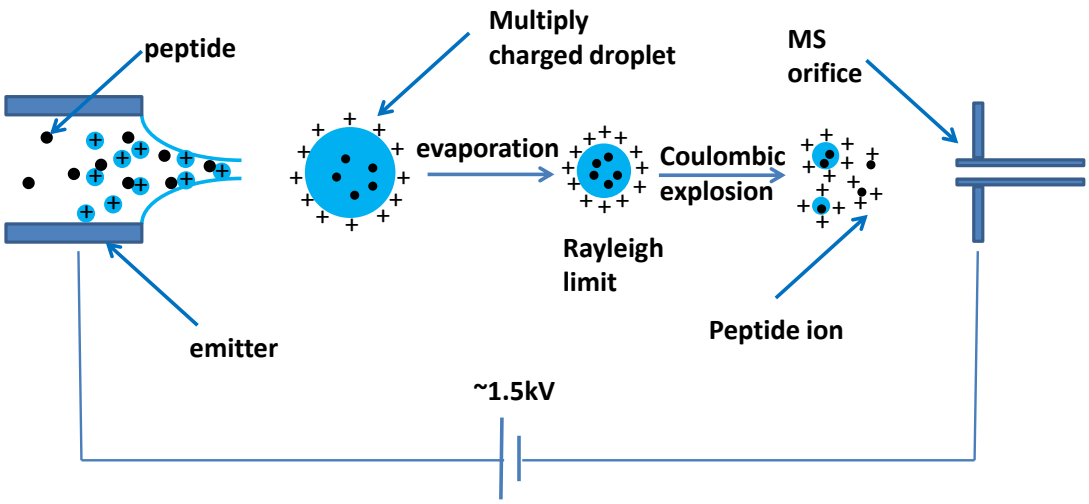
peptide
Multiply
charged droplet
MS
orifice
evaporation
Coulombic
explosion
Rayleigh
limit
emitter
Peptide ion
~1.5kV

Figure 1.1.3

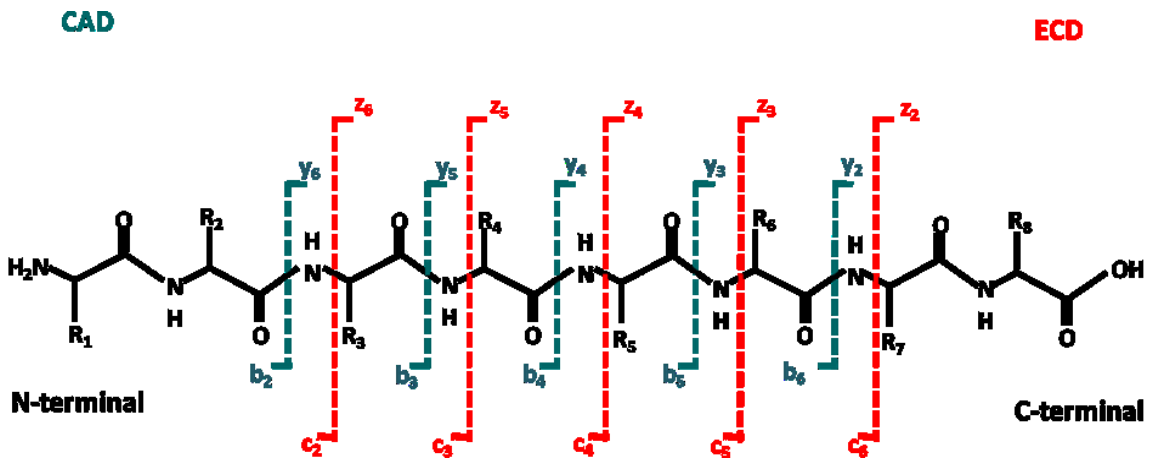

Figure 1.1.4

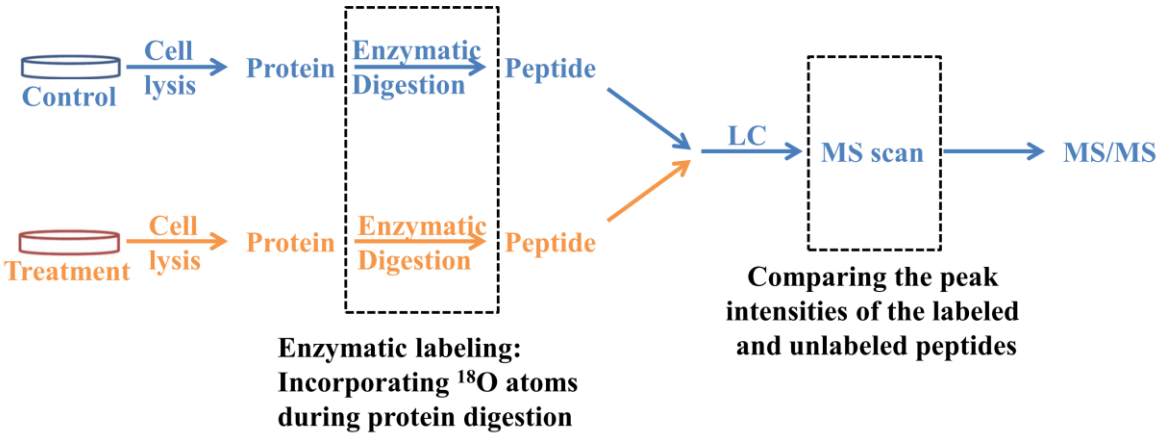

(a)

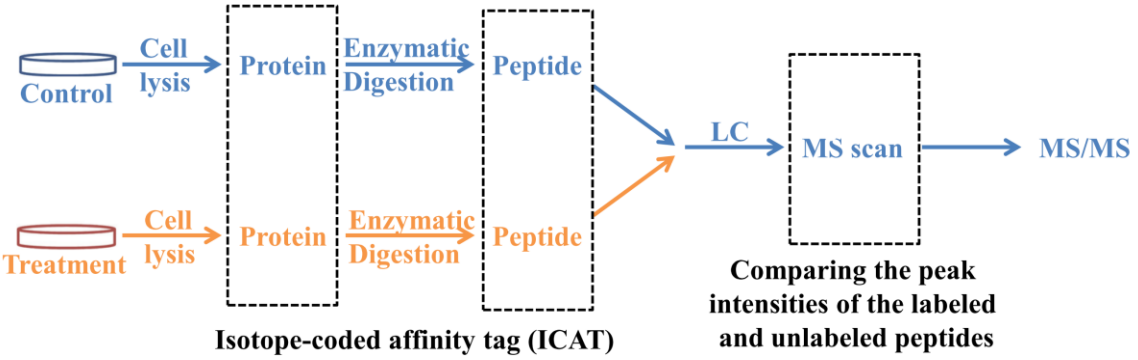

(b)

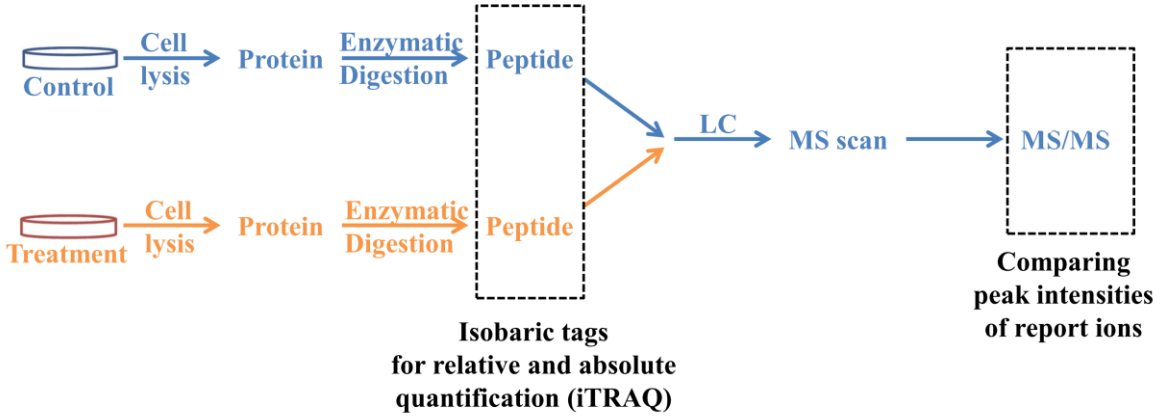

(c)

Figure 1.1.5

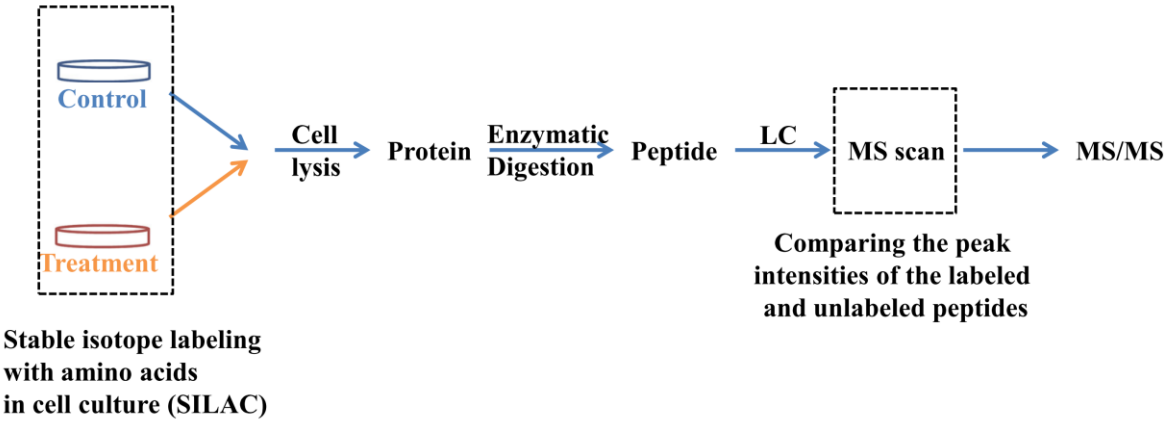
Control
Treatment
Cell lysis
Protein
Enzymatic Digestion
Peptide
LC
MS scan
MS/MS
Comparing the peak intensities of the labeled and unlabeled peptides
Stable isotope labeling with amino acids in cell culture (SILAC)

Figure 1.1.6

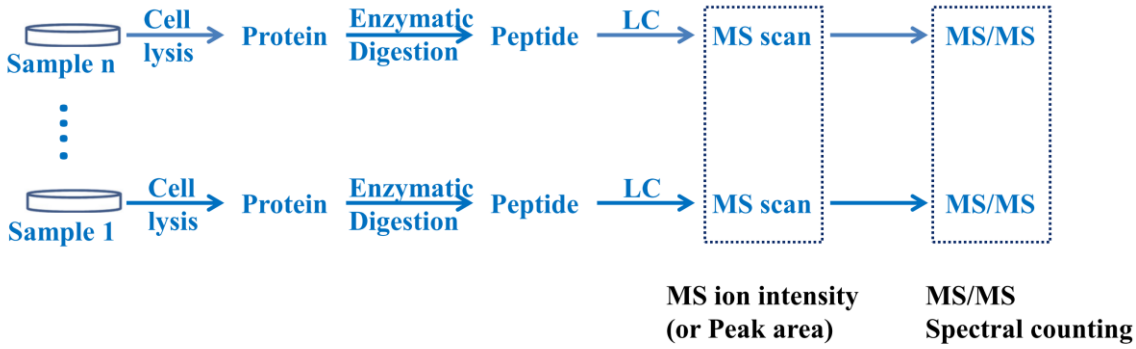
Sample n
Cell lysis
Protein
Enzymatic Digestion
Peptide
LC
MS scan
MS/MS
Sample 1
Cell lysis
Protein
Enzymatic Digestion
Peptide
LC
MS scan
MS/MS
MS ion intensity (or Peak area)
MS/MS Spectral counting

Figure 1.2.1

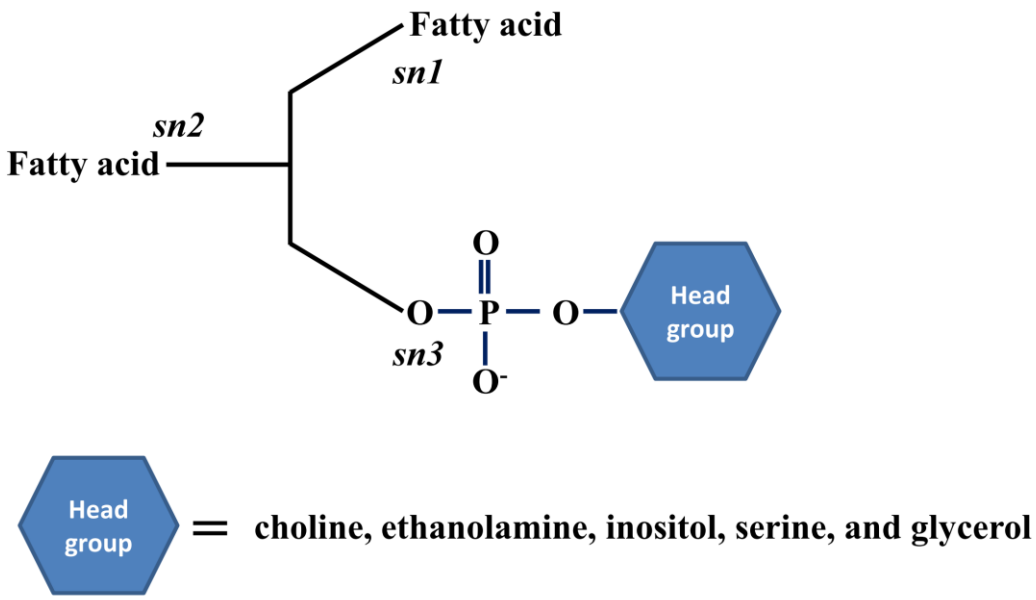
Fatty acid
sn1
sn2
Fatty acid
O
O
P
O
O
sn3
O-
Head group
Head group
= choline, ethanolamine, inositol, serine, and glycerol

Figure 1.2.2

A. Glycerophosphocholines

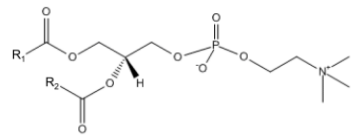

1,2-diacyl-*sn*-glycero-3-phosphocholine

B. Glycerophosphoethanolamines

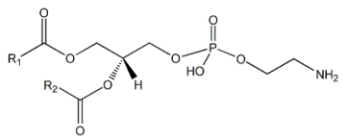

1,2-diacyl-*sn*-glycero-3-phosphoethanolamine

C. Glycerophosphoserines

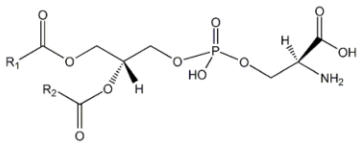

1,2-diacyl-*sn*-glycero-3-phosphoserine

D. Glycerophosphoglycerols

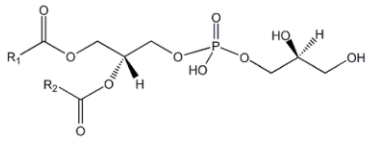

1,2-diacyl-*sn*-glycero-3-phospho-(1'-*sn*-glycerol)

E. Glycerophosphates

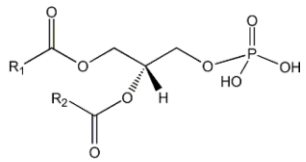

1,2-diacyl-*sn*-glycero-3-phosphate

F. Glycerophosphoinositols

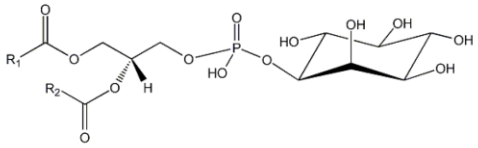

1,2-diacyl-*sn*-glycero-3-phospho-(1'-myo-inositol)

Figure 1.2.3

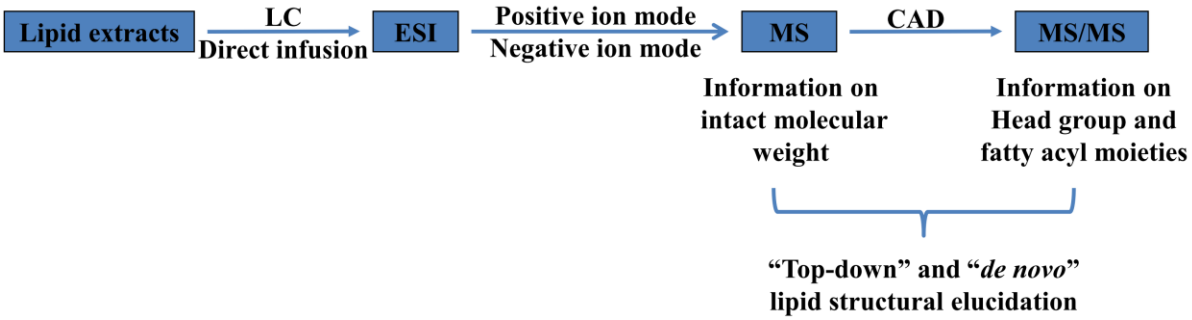
Lipid extracts
LC
Direct infusion
ESI
Positive ion mode
Negative ion mode
MS
CAD
MS/MS
Information on intact molecular weight
Information on Head group and fatty acyl moieties
"Top-down" and "de novo" lipid structural elucidation

Figure 1.2.4

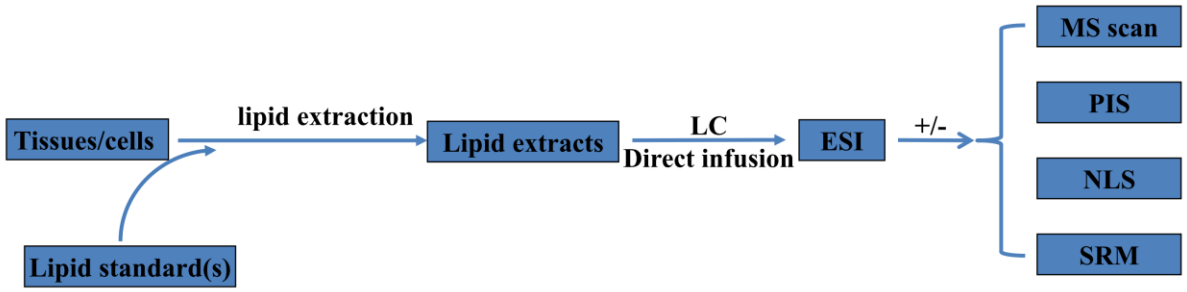
Tissues/cells
lipid extraction
Lipid extracts
LC
Direct infusion
ESI
+/-
MS scan
PIS
NLS
SRM
Lipid standard(s)

References:

1. Aebersold, R., and Mann, M. (2003) Mass spectrometry-based proteomics, *Nature 422*, 198-207.
2. Steen, H., and Mann, M. (2004) The ABC's (and XYZ's) of peptide sequencing, *Nat Rev Mol Cell Biol 5*, 699-711.
3. Karas, M., and Hillenkamp, F. (1988) Laser desorption ionization of proteins with molecular masses exceeding 10,000 daltons, *Anal Chem 60*, 2299-2301.
4. Fenn, J. B., Mann, M., Meng, C. K., Wong, S. F., and Whitehouse, C. M. (1989) Electrospray ionization for mass spectrometry of large biomolecules, *Science 246*, 64-71.
5. Eng, McCormack, and Yates. (1994) An approach to correlatetandem mass spectral data of peptides with amino acid sequences in a protein database, *Journal of the American Society for Mass Spectrometry 5*.
6. Mann, M., and Wilm, M. (1994) Error-tolerant identification of peptides in sequence databases by peptide sequence tags, *Anal Chem 66*, 4390-4399.
7. Perkins, D. N., Pappin, D. J., Creasy, D. M., and Cottrell, J. S. (1999) Probability-based protein identification by searching sequence databases using mass spectrometry data, *Electrophoresis 20*, 3551-3567.
8. Ge, Y., Lawhorn, B. G., ElNaggar, M., Strauss, E., Park, J. H., Begley, T. P., and McLafferty, F. W. (2002) Top down characterization of larger proteins (45 kDa) by electron capture dissociation mass spectrometry, *J Am Chem Soc 124*, 672-678.
9. Zabrouskov, V., and Whitelegge, J. P. (2007) Increased coverage in the transmembrane domain with activated-ion electron capture dissociation for top-down Fourier-transform mass spectrometry of integral membrane proteins, *J Proteome Res 6*, 2205-2210.
10. Anderson, N. L., and Anderson, N. G. (2002) The human plasma proteome: history, character, and diagnostic prospects, *Mol Cell Proteomics 1*, 845-867.
11. Beck, M., Topf, M., Frazier, Z., Tjong, H., Xu, M., Zhang, S., and Alber, F. (2011) Exploring the spatial and temporal organization of a cell's proteome, *J Struct Biol 173*, 483-496.

12. Schiess, R., Wollscheid, B., and Aebersold, R. (2009) Targeted proteomic strategy for clinical biomarker discovery, *Mol Oncol 3*, 33-44.
13. Picotti, P., Rinner, O., Stallmach, R., Dautel, F., Farrah, T., Domon, B., Wenschuh, H., and Aebersold, R. (2010) High-throughput generation of selected reaction-monitoring assays for proteins and proteomes, *Nat Methods 7*, 43-46.
14. Olsen, J. V., Ong, S. E., and Mann, M. (2004) Trypsin cleaves exclusively C-terminal to arginine and lysine residues, *Mol Cell Proteomics 3*, 608-614.
15. Wierenga, S. K., Zocher, M. J., Mirus, M. M., Conrads, T. P., Goshe, M. B., and Veenstra, T. D. (2002) A method to evaluate tryptic digestion efficiency for high-throughput proteome analyses, *Rapid Commun Mass Spectrom 16*, 1404-1408.
16. Hou, W., Ethier, M., Smith, J. C., Sheng, Y., and Figeys, D. (2007) Multiplexed proteomic reactor for the processing of proteomic samples, *Anal Chem 79*, 39-44.
17. Zhou, H., Hou, W., Lambert, J. P., and Figeys, D. (2010) New ammunition for the proteomic reactor: strong anion exchange beads and multiple enzymes enhance protein identification and sequence coverage, *Anal Bioanal Chem 397*, 3421-3430.
18. Bakhtiar, R., and Guan, Z. (2006) Electron capture dissociation mass spectrometry in characterization of peptides and proteins, *Biotechnol Lett 28*, 1047-1059.
19. Horn, D. M., Ge, Y., and McLafferty, F. W. (2000) Activated ion electron capture dissociation for mass spectral sequencing of larger (42 kDa) proteins, *Anal Chem 72*, 4778-4784.
20. Zubarev, R. A., Horn, D. M., Fridriksson, E. K., Kelleher, N. L., Kruger, N. A., Lewis, M. A., Carpenter, B. K., and McLafferty, F. W. (2000) Electron capture dissociation for structural characterization of multiply charged protein cations, *Anal Chem 72*, 563-573.
21. Anusiewicz, I., Jasionowski, M., Skurski, P., and Simons, J. (2005) Backbone and side-chain cleavages in electron detachment dissociation (EDD), *J Phys Chem A 109*, 11332-11337.
22. Palumbo, A. M., Smith, S. A., Kalcic, C. L., Dantus, M., Stemmer, P. M., and Reid, G. E. (2011) Tandem mass spectrometry strategies for phosphoproteome analysis, *Mass Spectrom Rev 30*, 600-625.

23. Siuti, N., and Kelleher, N. L. (2007) Decoding protein modifications using top-down mass spectrometry, *Nat Methods 4*, 817-821.
24. Lasonder, E., Ishihama, Y., Andersen, J. S., Vermunt, A. M., Pain, A., Sauerwein, R. W., Eling, W. M., Hall, N., Waters, A. P., Stunnenberg, H. G., and Mann, M. (2002) Analysis of the Plasmodium falciparum proteome by high-accuracy mass spectrometry, *Nature 419*, 537-542.
25. Washburn, M. P., Wolters, D., and Yates, J. R., 3rd. (2001) Large-scale analysis of the yeast proteome by multidimensional protein identification technology, *Nat Biotechnol 19*, 242-247.
26. Wolters, D. A., Washburn, M. P., and Yates, J. R., 3rd. (2001) An automated multidimensional protein identification technology for shotgun proteomics, *Anal Chem 73*, 5683-5690.
27. Schutzer, S. E., Liu, T., Natelson, B. H., Angel, T. E., Schepmoes, A. A., Purvine, S. O., Hixson, K. K., Lipton, M. S., Camp, D. G., Coyle, P. K., Smith, R. D., and Bergquist, J. (2010) Establishing the proteome of normal human cerebrospinal fluid, *PLoS One 5*, e10980.
28. Cargile, B. J., Bundy, J. L., and Stephenson, J. L., Jr. (2004) Potential for false positive identifications from large databases through tandem mass spectrometry, *J Proteome Res 3*, 1082-1085.
29. Keller, A., Nesvizhskii, A. I., Kolker, E., and Aebersold, R. (2002) Empirical statistical model to estimate the accuracy of peptide identifications made by MS/MS and database search, *Anal Chem 74*, 5383-5392.
30. Nesvizhskii, A. I., Keller, A., Kolker, E., and Aebersold, R. (2003) A statistical model for identifying proteins by tandem mass spectrometry, *Anal Chem 75*, 4646-4658.
31. Duncan, M. W., Aebersold, R., and Caprioli, R. M. (2010) The pros and cons of peptide-centric proteomics, *Nat Biotechnol 28*, 659-664.
32. Ong, S. E., and Mann, M. (2005) Mass spectrometry-based proteomics turns quantitative, *Nat Chem Biol 1*, 252-262.
33. MacCoss, M. J., and Matthews, D. E. (2005) Quantitative MS for proteomics: teaching a new dog old tricks, *Anal Chem 77*, 294A-302A.

34. Yao, X., Freas, A., Ramirez, J., Demirev, P. A., and Fenselau, C. (2001) Proteolytic 18O labeling for comparative proteomics: model studies with two serotypes of adenovirus, *Anal Chem 73*, 2836-2842.

35. Stewart, II, Thomson, T., and Figeys, D. (2001) 18O labeling: a tool for proteomics, *Rapid Commun Mass Spectrom 15*, 2456-2465.

36. Gygi, S. P., Rist, B., Gerber, S. A., Turecek, F., Gelb, M. H., and Aebersold, R. (1999) Quantitative analysis of complex protein mixtures using isotope-coded affinity tags, *Nat Biotechnol 17*, 994-999.

37. Choe, L., D'Ascenzo, M., Relkin, N. R., Pappin, D., Ross, P., Williamson, B., Guertin, S., Pribil, P., and Lee, K. H. (2007) 8-plex quantitation of changes in cerebrospinal fluid protein expression in subjects undergoing intravenous immunoglobulin treatment for Alzheimer's disease, *Proteomics 7*, 3651-3660.

38. Pierce, A., Unwin, R. D., Evans, C. A., Griffiths, S., Carney, L., Zhang, L., Jaworska, E., Lee, C. F., Blinco, D., Okoniewski, M. J., Miller, C. J., Bitton, D. A., Spooncer, E., and Whetton, A. D. (2008) Eight-channel iTRAQ enables comparison of the activity of six leukemogenic tyrosine kinases, *Mol Cell Proteomics 7*, 853-863.

39. Ross, P. L., Huang, Y. N., Marchese, J. N., Williamson, B., Parker, K., Hattan, S., Khainovski, N., Pillai, S., Dey, S., Daniels, S., Purkayastha, S., Juhasz, P., Martin, S., Bartlet-Jones, M., He, F., Jacobson, A., and Pappin, D. J. (2004) Multiplexed protein quantitation in Saccharomyces cerevisiae using amine-reactive isobaric tagging reagents, *Mol Cell Proteomics 3*, 1154-1169.

40. Ong, S. E., Blagoev, B., Kratchmarova, I., Kristensen, D. B., Steen, H., Pandey, A., and Mann, M. (2002) Stable isotope labeling by amino acids in cell culture, SILAC, as a simple and accurate approach to expression proteomics, *Mol Cell Proteomics 1*, 376-386.

41. Chelius, D., and Bondarenko, P. V. (2002) Quantitative profiling of proteins in complex mixtures using liquid chromatography and mass spectrometry, *J Proteome Res 1*, 317-323.

42. Lundgren, D. H., Hwang, S. I., Wu, L., and Han, D. K. (2010) Role of spectral counting in quantitative proteomics, *Expert Rev Proteomics 7*, 39-53.

43. Lambert, J. P., Ethier, M., Smith, J. C., and Figeys, D. (2005) Proteomics: from gel based to gel free, *Anal Chem 77*, 3771-3787.

44. Romijn, E. P., Krijgsveld, J., and Heck, A. J. (2003) Recent liquid chromatographic-(tandem) mass spectrometric applications in proteomics, *J Chromatogr A 1000*, 589-608.

45. Gygi, S. P., Corthals, G. L., Zhang, Y., Rochon, Y., and Aebersold, R. (2000) Evaluation of two-dimensional gel electrophoresis-based proteome analysis technology, *Proc Natl Acad Sci U S A 97*, 9390-9395.

46. Beausoleil, S. A., Jedrychowski, M., Schwartz, D., Elias, J. E., Villen, J., Li, J., Cohn, M. A., Cantley, L. C., and Gygi, S. P. (2004) Large-scale characterization of HeLa cell nuclear phosphoproteins, *Proc Natl Acad Sci U S A 101*, 12130-12135.

47. Aebersold, R. H., Leavitt, J., Saavedra, R. A., Hood, L. E., and Kent, S. B. (1987) Internal amino acid sequence analysis of proteins separated by one- or two-dimensional gel electrophoresis after in situ protease digestion on nitrocellulose, *Proc Natl Acad Sci U S A 84*, 6970-6974.

48. Wilm, M., Shevchenko, A., Houthaeve, T., Breit, S., Schweigerer, L., Fotsis, T., and Mann, M. (1996) Femtomole sequencing of proteins from polyacrylamide gels by nano-electrospray mass spectrometry., *Nature 379*, 466-469.

49. Havlis, J., and Shevchenko, A. (2004) Absolute quantification of proteins in solutions and in polyacrylamide gels by mass spectrometry, *Anal Chem 76*, 3029-3036.

50. Ihling, C., and Sinz, A. (2005) Proteome analysis of Escherichia coli using high-performance liquid chromatography and Fourier transform ion cyclotron resonance mass spectrometry, *Proteomics 5*, 2029-2042.

51. Martosella, J., Zolotarjova, N., Liu, H., Nicol, G., and Boyes, B. E. (2005) Reversed-phase high-performance liquid chromatographic prefractionation of immunodepleted human serum proteins to enhance mass spectrometry identification of lower-abundant proteins, *J Proteome Res 4*, 1522-1537.

52. Moritz, R. L., Clippingdale, A. B., Kapp, E. A., Eddes, J. S., Ji, H., Gilbert, S., Connolly, L. M., and Simpson, R. J. (2005) Application of 2-D free-flow electrophoresis/RP-HPLC for proteomic analysis of human plasma depleted of multi high-abundance proteins, *Proteomics 5*, 3402-3413.

53. Burggraf, D., Weber, G., and Lottspeich, F. (1995) Free flow-isoelectric focusing of human cellular lysates as sample preparation for protein analysis, *Electrophoresis 16*, 1010-1015.

54. Linke, T., Ross, A. C., and Harrison, E. H. (2006) Proteomic analysis of rat plasma by two-dimensional liquid chromatography and matrix-assisted laser desorption ionization time-of-flight mass spectrometry, *J Chromatogr A*.

55. Dai, J., Shieh, C. H., Sheng, Q. H., Zhou, H., and Zeng, R. (2005) Proteomic analysis with integrated multiple dimensional liquid chromatography/mass spectrometry based on elution of ion exchange column using pH steps, *Anal Chem 77*, 5793-5799.

56. Jessani, N., Niessen, S., Wei, B. Q., Nicolau, M., Humphrey, M., Ji, Y., Han, W., Noh, D. Y., Yates, J. R., 3rd, Jeffrey, S. S., and Cravatt, B. F. (2005) A streamlined platform for high-content functional proteomics of primary human specimens, *Nat Methods 2*, 691-697.

57. Washburn, M. P., Wolters, D., and Yates, J. R. r. (2001) Large-scale analysis of the yeast proteome by multidimensional protein identification technology.

, *Nat Biotechnol. 19*, 242-247.

58. Wu, C. C., MacCoss, M. J., Howell, K. E., and Yates, J. R., 3rd. (2003) A method for the comprehensive proteomic analysis of membrane proteins, *Nat Biotechnol 21*, 532-538.

59. Duan, J., Sun, L., Liang, Z., Zhang, J., Wang, H., Zhang, L., Zhang, W., and Zhang, Y. (2006) Rapid protein digestion and identification using monolithic enzymatic microreactor coupled with nano-liquid chromatography-electrospray ionization mass spectrometry, *J Chromatogr A 1106*, 165-174.

60. Lim, L. W., Tomatsu, M., and Takeuchi, T. (2006) Development of an on-line immobilized-enzyme reversed-phase HPLC method for protein digestion and peptide separation, *Anal Bioanal Chem*.

61. Craft, D., Doucette, A., and Li, L. (2002) Microcolumn capture and digestion of proteins combined with mass spectrometry for protein identification, *J Proteome Res 1*, 537-547.

62. Craft, D., and Li, L. (2005) Integrated sample processing system involving on-column protein adsorption, sample washing, and enzyme digestion for protein identification by LC-ESI MS/MS, *Anal Chem 77*, 2649-2655.
63. Wenk, M. R. (2005) The emerging field of lipidomics, *Nat Rev Drug Discov 4*, 594-610.
64. van Meer, G., Voelker, D. R., and Feigenson, G. W. (2008) Membrane lipids: where they are and how they behave, *Nat Rev Mol Cell Biol 9*, 112-124.
65. Sagin, F. G., and Sozmen, E. Y. (2008) Lipids as key players in Alzheimer disease: alterations in metabolism and genetics, *Curr Alzheimer Res 5*, 4-14.
66. Denizot, Y., Desplat, V., Drouet, M., Bertin, F., and Melloni, B. (2001) Is there a role of platelet-activating factor in human lung cancer?, *Lung Cancer 33*, 195-202.
67. Montrucchio, G., Sapino, A., Bussolati, B., Ghisolfi, G., Rizea-Savu, S., Silvestro, L., Lupia, E., and Camussi, G. (1998) Potential angiogenic role of platelet-activating factor in human breast cancer, *Am J Pathol 153*, 1589-1596.
68. Tselepis, A. D., and John Chapman, M. (2002) Inflammation, bioactive lipids and atherosclerosis: potential roles of a lipoprotein-associated phospholipase A2, platelet activating factor-acetylhydrolase, *Atheroscler Suppl 3*, 57-68.
69. Roudebush, W. E., Massey, J. B., Elsner, C. W., Shapiro, D. B., Mitchell-Leef, D., and Kort, H. I. (2005) The significance of platelet-activating factor and fertility in the male primate: a review, *J Med Primatol 34*, 20-24.
70. Pereto, J., Lopez-Garcia, P., and Moreira, D. (2004) Ancestral lipid biosynthesis and early membrane evolution, *Trends Biochem Sci 29*, 469-477.
71. Cronan, J. E. (2003) Bacterial membrane lipids: where do we stand?, *Annu Rev Microbiol 57*, 203-224.
72. Bleijerveld, O. B., Houweling, M., Thomas, M. J., and Cui, Z. (2006) Metabolipidomics: profiling metabolism of glycerophospholipid species by stable isotopic precursors and tandem mass spectrometry, *Anal Biochem 352*, 1-14.
73. Wykle, R. L., O'Flaherty, J. T., and Thomas, M. J. (1988) Platelet-activating factor, *Methods Enzymol 163*, 44-54.
74. Bazan, N. G. (1998) The neuromessenger platelet-activating factor in plasticity and neurodegeneration, *Prog Brain Res 118*, 281-291.

75. Farooqui, A. A., Horrocks, L. A., and Farooqui, T. (2007) Modulation of inflammation in brain: a matter of fat, *J Neurochem 101*, 577-599.

76. Fahy, E., Subramaniam, S., Brown, H. A., Glass, C. K., Merrill, A. H., Jr., Murphy, R. C., Raetz, C. R., Russell, D. W., Seyama, Y., Shaw, W., Shimizu, T., Spener, F., van Meer, G., VanNieuwenhze, M. S., White, S. H., Witztum, J. L., and Dennis, E. A. (2005) A comprehensive classification system for lipids, *J Lipid Res 46*, 839-861.

77. Whitehead, S. N., Hou, W., Ethier, M., Smith, J. C., Bourgeois, A., Denis, R., Bennett, S. A., and Figeys, D. (2007) Identification and quantitation of changes in the platelet activating factor family of glycerophospholipids over the course of neuronal differentiation by high-performance liquid chromatography electrospray ionization tandem mass spectrometry, *Analytical chemistry 79*, 8539-8548.

78. Bou Khalil, M., Hou, W., Zhou, H., Elisma, F., Swayne, L. A., Blanchard, A. P., Yao, Z., Bennett, S. A., and Figeys, D. (2010) Lipidomics era: accomplishments and challenges, *Mass Spectrom Rev 29*, 877-929.

79. Hou, W., Zhou, H., Elisma, F., Bennett, S. A., and Figeys, D. (2008) Technological developments in lipidomics, *Brief Funct Genomic Proteomic 7*, 395-409.

80. DeLong, C. J., Baker, P. R., Samuel, M., Cui, Z., and Thomas, M. J. (2001) Molecular species composition of rat liver phospholipids by ESI-MS/MS: the effect of chromatography, *J Lipid Res 42*, 1959-1968.

81. Liang, X., Liu, J., LeBlanc, Y., Covey, T., Ptak, A. C., Brenna, J. T., and McLuckey, S. A. (2007) Electron transfer dissociation of doubly sodiated glycerophosphocholine lipids, *J Am Soc Mass Spectrom 18*, 1783-1788.

82. Harvey, D. J. (2005) A new charge-associated mechanism to account for the production of fragment ions in the high-energy CID spectra of fatty acids, *J Am Soc Mass Spectrom 16*, 280-290.

83. Han, X., and Gross, R. W. (2005) Shotgun lipidomics: electrospray ionization mass spectrometric analysis and quantitation of cellular lipidomes directly from crude extracts of biological samples, *Mass Spectrom Rev 24*, 367-412.

84. Ekroos, K., Chernushevich, I. V., Simons, K., and Shevchenko, A. (2002) Quantitative profiling of phospholipids by multiple precursor ion scanning on a hybrid quadrupole time-of-flight mass spectrometer, *Anal Chem 74*, 941-949.

85. Retra, K., Bleijerveld, O. B., van Gestel, R. A., Tielens, A. G., van Hellemond, J. J., and Brouwers, J. F. (2008) A simple and universal method for the separation and identification of phospholipid molecular species, *Rapid Commun Mass Spectrom 22*, 1853-1862.

86. Brugger, B., Erben, G., Sandhoff, R., Wieland, F. T., and Lehmann, W. D. (1997) Quantitative analysis of biological membrane lipids at the low picomole level by nano-electrospray ionization tandem mass spectrometry, *Proc Natl Acad Sci U S A 94*, 2339-2344.

87. Hsu, F. F., and Turk, J. (2003) Electrospray ionization/tandem quadrupole mass spectrometric studies on phosphatidylcholines: the fragmentation processes, *J Am Soc Mass Spectrom 14*, 352-363.

88. Ivanova, P. T., Cerda, B. A., Horn, D. M., Cohen, J. S., McLafferty, F. W., and Brown, H. A. (2001) Electrospray ionization mass spectrometry analysis of changes in phospholipids in RBL-2H3 mastocytoma cells during degranulation, *Proc Natl Acad Sci U S A 98*, 7152-7157.

89. Taguchi, R., Hayakawa, J., Takeuchi, Y., and Ishida, M. (2000) Two-dimensional analysis of phospholipids by capillary liquid chromatography/electrospray ionization mass spectrometry, *J Mass Spectrom 35*, 953-966.

90. Kerwin, J. L., Tuininga, A. R., and Ericsson, L. H. (1994) Identification of molecular species of glycerophospholipids and sphingomyelin using electrospray mass spectrometry, *J Lipid Res 35*, 1102-1114.

91. Smith, P. B., Snyder, A. P., and Harden, C. S. (1995) Characterization of bacterial phospholipids by electrospray ionization tandem mass spectrometry, *Anal Chem 67*, 1824-1830.

92. Hsu, F. F., and Turk, J. (2000) Charge-remote and charge-driven fragmentation processes in diacyl glycerophosphoethanolamine upon low-energy collisional activation: a mechanistic proposal, *J Am Soc Mass Spectrom 11*, 892-899.

93. Hsu, F. F., and Turk, J. (2000) Charge-driven fragmentation processes in diacyl glycerophosphatidic acids upon low-energy collisional activation. A mechanistic proposal, *J Am Soc Mass Spectrom 11*, 797-803.

94. Hsu, F. F., and Turk, J. (2000) Characterization of phosphatidylinositol, phosphatidylinositol-4-phosphate, and phosphatidylinositol-4,5-bisphosphate by electrospray ionization tandem mass spectrometry: a mechanistic study, *J Am Soc Mass Spectrom 11*, 986-999.

95. Hsu, F. F., and Turk, J. (2005) Studies on phosphatidylserine by tandem quadrupole and multiple stage quadrupole ion-trap mass spectrometry with electrospray ionization: structural characterization and the fragmentation processes, *J Am Soc Mass Spectrom 16*, 1510-1522.

96. Hsu, F. F., and Turk, J. (2001) Studies on phosphatidylglycerol with triple quadrupole tandem mass spectrometry with electrospray ionization: fragmentation processes and structural characterization, *J Am Soc Mass Spectrom 12*, 1036-1043.

97. Wenk, M. R., Lucast, L., Di Paolo, G., Romanelli, A. J., Suchy, S. F., Nussbaum, R. L., Cline, G. W., Shulman, G. I., McMurray, W., and De Camilli, P. (2003) Phosphoinositide profiling in complex lipid mixtures using electrospray ionization mass spectrometry, *Nat Biotechnol 21*, 813-817.

98. Han, X., and Gross, R. W. (1995) Structural Determination of Picomole Amounts of Phospholipids Via Electrospray Ionization Tandem Mass Spectrometry, *J Am Soc Mass Spectrom 6*, 1202-1210.

99. Ho, Y. P., Huang, P. C., and Deng, K. H. (2003) Metal ion complexes in the structural analysis of phospholipids by electrospray ionization tandem mass spectrometry, *Rapid Commun Mass Spectrom 17*, 114-121.

100. Hsu, F. F., and Turk, J. (2000) Characterization of phosphatidylethanolamine as a lithiated adduct by triple quadrupole tandem mass spectrometry with electrospray ionization, *J Mass Spectrom 35*, 595-606.

101. Hsu, F. F., Turk, J., Thukkani, A. K., Messner, M. C., Wildsmith, K. R., and Ford, D. A. (2003) Characterization of alkylacyl, alk-1-enylacyl and lyso subclasses of glycerophosphocholine by tandem quadrupole mass spectrometry with electrospray ionization, *J Mass Spectrom 38*, 752-763.

102. Hsu, F. F., Bohrer, A., and Turk, J. (1998) Formation of lithiated adducts of glycerophosphocholine lipids facilitates their identification by electrospray ionization tandem mass spectrometry, *J Am Soc Mass Spectrom 9*, 516-526.

103. Lehmann, W. D., Koester, M., Erben, G., and Keppler, D. (1997) Characterization and quantification of rat bile phosphatidylcholine by electrospray-tandem mass spectrometry, *Anal Biochem 246*, 102-110.

104. Schwudke, D., Oegema, J., Burton, L., Entchev, E., Hannich, J. T., Ejsing, C. S., Kurzchalia, T., and Shevchenko, A. (2006) Lipid profiling by multiple precursor and neutral loss scanning driven by the data-dependent acquisition, *Anal Chem 78*, 585-595.

105. Han, X., Yang, K., Yang, J., Cheng, H., and Gross, R. W. (2006) Shotgun lipidomics of cardiolipin molecular species in lipid extracts of biological samples, *J Lipid Res 47*, 864-879.

106. Han, X., and Gross, R. W. (2003) Global analyses of cellular lipidomes directly from crude extracts of biological samples by ESI mass spectrometry: a bridge to lipidomics, *J Lipid Res 44*, 1071-1079.

107. Ejsing, C. S., Duchoslav, E., Sampaio, J., Simons, K., Bonner, R., Thiele, C., Ekroos, K., and Shevchenko, A. (2006) Automated identification and quantification of glycerophospholipid molecular species by multiple precursor ion scanning, *Anal Chem 78*, 6202-6214.

108. Han, X., Yang, J., Cheng, H., Ye, H., and Gross, R. W. (2004) Toward fingerprinting cellular lipidomes directly from biological samples by two-dimensional electrospray ionization mass spectrometry, *Anal Biochem 330*, 317-331.

109. Hsu, F. F., Turk, J., Rhoades, E. R., Russell, D. G., Shi, Y., and Groisman, E. A. (2005) Structural characterization of cardiolipin by tandem quadrupole and multiple-stage quadrupole ion-trap mass spectrometry with electrospray ionization, *J Am Soc Mass Spectrom 16*, 491-504.

110. Hsu, F. F., and Turk, J. (2008) Structural characterization of unsaturated glycerophospholipids by multiple-stage linear ion-trap mass spectrometry with electrospray ionization, *J Am Soc Mass Spectrom 19*, 1681-1691.

111. Hsu, F. F., and Turk, J. (2007) Differentiation of 1-O-alk-1'-enyl-2-acyl and 1-O-alkyl-2-acyl glycerophospholipids by multiple-stage linear ion-trap mass spectrometry with electrospray ionization, *J Am Soc Mass Spectrom 18*, 2065-2073.

112. Smith, J. C., Hou, W., Whitehead, S. N., Ethier, M., Bennett, S. A., and Figeys, D. (2008) Identification of lysophosphatidylcholine (LPC) and platelet activating factor (PAF) from PC12 cells and mouse cortex using liquid chromatography/multi-stage mass spectrometry (LC/MS(3)), *Rapid Commun Mass Spectrom 22*, 3579-3587.

113. Houjou, T., Yamatani, K., Imagawa, M., Shimizu, T., and Taguchi, R. (2005) A shotgun tandem mass spectrometric analysis of phospholipids with normal-phase and/or reverse-phase liquid chromatography/electrospray ionization mass spectrometry, *Rapid Commun Mass Spectrom 19*, 654-666.

114. Vernooij, E., Brouwers, J., Kettenes-van den Bosch, J., and Crommelin, D. (2002) RP-HPLC/ESI MS determination of acyl chain positions in phospholipids, *J. Sep. Sci. 25*, 285-289.

115. Ho, Y. P., and Huang, P. C. (2002) A novel structural analysis of glycerophosphocholines as TFA/K(+) adducts by electrospray ionization ion trap tandem mass spectrometry, *Rapid Commun Mass Spectrom 16*, 1582-1589.

116. Hvattum, E., Hagelin, G., and Larsen, A. (1998) Study of mechanisms involved in the collision-induced dissociation of carboxylate anions from glycerophospholipids using negative ion electrospray tandem quadrupole mass spectrometry, *Rapid Commun Mass Spectrom 12*, 1405-1409.

117. Han, X., and Gross, R. W. (1994) Electrospray ionization mass spectroscopic analysis of human erythrocyte plasma membrane phospholipids, *Proc Natl Acad Sci U S A 91*, 10635-10639.

118. Koivusalo, M., Haimi, P., Heikinheimo, L., Kostiainen, R., and Somerharju, P. (2001) Quantitative determination of phospholipid compositions by ESI-MS: effects of acyl chain length, unsaturation, and lipid concentration on instrument response, *J Lipid Res 42*, 663-672.

119. Pulfer, M., and Murphy, R. C. (2003) Electrospray mass spectrometry of phospholipids, *Mass Spectrom Rev 22*, 332-364.

120. Milne, S., Ivanova, P., Forrester, J., and Alex Brown, H. (2006) Lipidomics: an analysis of cellular lipids by ESI-MS, *Methods 39*, 92-103.

121. Liebisch, G., Drobnik, W., Lieser, B., and Schmitz, G. (2002) High-throughput quantification of lysophosphatidylcholine by electrospray ionization tandem mass spectrometry, *Clin Chem 48*, 2217-2224.

122. Zacarias, A., Bolanowski, D., and Bhatnagar, A. (2002) Comparative measurements of multicomponent phospholipid mixtures by electrospray mass spectroscopy: relating ion intensity to concentration, *Anal Biochem 308*, 152-159.

123. Schwudke, D., Liebisch, G., Herzog, R., Schmitz, G., and Shevchenko, A. (2007) Shotgun lipidomics by tandem mass spectrometry under data-dependent acquisition control, *Methods Enzymol 433*, 175-191.

124. Laaksonen, R., Katajamaa, M., Paiva, H., Sysi-Aho, M., Saarinen, L., Junni, P., Lutjohann, D., Smet, J., Van Coster, R., Seppanen-Laakso, T., Lehtimaki, T., Soini, J., and Oresic, M. (2006) A systems biology strategy reveals biological pathways and plasma biomarker candidates for potentially toxic statin-induced changes in muscle, *PLoS ONE 1*, e97.

125. Krank, J., Murphy, R. C., Barkley, R. M., Duchoslav, E., and McAnoy, A. (2007) Qualitative analysis and quantitative assessment of changes in neutral glycerol lipid molecular species within cells, *Methods Enzymol 432*, 1-20.

126. Murphy, R. C., Barkley, R. M., Zemski Berry, K., Hankin, J., Harrison, K., Johnson, C., Krank, J., McAnoy, A., Uhlson, C., and Zarini, S. (2005) Electrospray ionization and tandem mass spectrometry of eicosanoids, *Anal Biochem 346*, 1-42.

127. Larsen, A., Uran, S., Jacobsen, P. B., and Skotland, T. (2001) Collision-induced dissociation of glycero phospholipids using electrospray ion-trap mass spectrometry, *Rapid Commun Mass Spectrom 15*, 2393-2398.

128. DeLong, C. J., Shen, Y. J., Thomas, M. J., and Cui, Z. (1999) Molecular distinction of phosphatidylcholine synthesis between the CDP-choline pathway and phosphatidylethanolamine methylation pathway, *J Biol Chem 274*, 29683-29688.

129. Rouzer, C. A., Ivanova, P. T., Byrne, M. O., Milne, S. B., Marnett, L. J., and Brown, H. A. (2006) Lipid profiling reveals arachidonate deficiency in RAW264.7 cells: Structural and functional implications, *Biochemistry 45*, 14795-14808.

130. Haroldsen, P. E., Clay, K. L., and Murphy, R. C. (1987) Quantitation of lyso-platelet activating factor molecular species from human neutrophils by mass spectrometry, *J Lipid Res 28*, 42-49.
131. Bate, C., Salmona, M., and Williams, A. (2004) The role of platelet activating factor in prion and amyloid-beta neurotoxicity, *Neuroreport 15*, 509-513.
132. Bellizzi, M. J., Lu, S. M., Masliah, E., and Gelbard, H. A. (2005) Synaptic activity becomes excitotoxic in neurons exposed to elevated levels of platelet-activating factor, *J Clin Invest 115*, 3185-3192.
133. Xu, Y., Zhang, B., Hua, Z., Johns, R. A., Bredt, D. S., and Tao, Y. X. (2004) Targeted disruption of PSD-93 gene reduces platelet-activating factor-induced neurotoxicity in cultured cortical neurons, *Exp Neurol 189*, 16-24.
134. Francescangeli, E., Domanska-Janik, K., and Goracci, G. (1996) Relative contribution of the de novo and remodelling pathways to the synthesis of platelet-activating factor in brain areas and during ischemia, *J Lipid Mediat Cell Signal 14*, 89-98.
135. Francescangeli, E., Freysz, L., and Goracci, G. (1996) PAF-synthesizing enzymes in neural cells during differentiation and in gerbil brain during ischemia, *Adv Exp Med Biol 416*, 21-27.
136. Francescangeli, E., Grassi, S., Pettorossi, V. E., and Goracci, G. (2002) Activation of PAF-synthesizing enzymes in rat brain stem slices after LTP induction in the medial vestibular nuclei, *Neurochem Res 27*, 1465-1471.
137. Francescangeli, E., Lang, D., Dreyfus, H., Boila, A., Freysz, L., and Goracci, G. (1997) Activities of enzymes involved in the metabolism of platelet-activating factor in neural cell cultures during proliferation and differentiation, *Neurochem Res 22*, 1299-1307.
138. Kornecki, E., and Ehrlich, Y. H. (1988) Neuroregulatory and neuropathological actions of the ether-phospholipid platelet-activating factor, *Science 240*, 1792-1794.
139. Southall, M. D., Isenberg, J. S., Nakshatri, H., Yi, Q., Pei, Y., Spandau, D. F., and Travers, J. B. (2001) The platelet-activating factor receptor protects epidermal cells from tumor necrosis factor (TNF) alpha and TNF-related apoptosis-inducing ligand-

induced apoptosis through an NF-kappa B-dependent process, *J Biol Chem 276*, 45548-45554.

140. Li, T., Southall, M. D., Yi, Q., Pei, Y., Lewis, D., Al-Hassani, M., Spandau, D., and Travers, J. B. (2003) The epidermal platelet-activating factor receptor augments chemotherapy-induced apoptosis in human carcinoma cell lines, *J Biol Chem 278*, 16614-16621.

141. Brewer, C., Bonin, F., Bullock, B., Nault, M.-C., Morin, J., Imbeault, S., Shen, T. Y., Franks, D. J., and Bennett, S. A. L. (2002) Platelet activating factor-induced apoptosis is inhibited by ectopic expression of the platelet activating factor G-protein coupled receptor, *J Neurochem 82*, 1502-1511.

142. Ryan, S. D., Harris, C. S., Carswell, C. L., Baenziger, J. E., and Bennett, S. A. (2008) Heterogeneity in the sn-1 carbon chain of platelet-activating factor glycerophospholipids determines pro- or anti-apoptotic signaling in primary neurons, *Journal of lipid research 49*, 2250-2258.

Chapter 2 Experiments

2.1 Proteomic Experiments

2.1.1 Materials

Ammonium bicarbonate, dithiothreitol (DTT) and sodium carbonate were purchased from EMD Chemicals, Inc. (Darmstadt, Germany); N-2-Hydroxyethylpiperazine-N-2-Ethane Sulfonic Acid (HEPES), Magnesium acetate, ethylene glycol tetraacetic acid (EGTA), ethylenediaminetetraacetic acid (EDTA) and nonidet P-40 (NP-40) were obtained from Sigma-Aldrich (Saint Louis, MO). Glycerol was purchased from MP Biomedicals.

Standard proteins ovalbumin (catalogue number A7641), fetuin A (F3004), serum albumin (A9056), carbonic anhydrase 2 (C3934), serotransferrin (T1408) and lysozyme C (L7651) were obtained from Sigma-Aldrich (Saint Louis, MO); sequencing grade trypsin was purchased from Promega (Madison, WI); chymotrypsin and Glu-C were obtained from Roche Applied Science (Indianapolis, IN); DMEM medium was from GIBCO-BRL (Burlington, ON); protease inhibitor cocktail was from Sigma-Aldrich (Saint Louis, MO); Bradford protein assay kit was from Bio-Rad (Hercules, CA).

Strong cation exchange (SCX) beads were obtained from the Nest Group (Southboro, MA) or Polymer Laboratories, Varian, Inc.; Strong anion exchange beads were obtained from Polymer Laboratories, Varian, Inc; prototypical SCX Plates (reactor plate) were graciously provided by Millipore (Billerica, MA); the MultiScreen HTS Vacuum Manifold was obtained from Millipore (Billerica, MA).

The 5 μm C18 beads were from Waters (Milford, MA); 10 μm picotip emitters were purchased from New Objective (Woburn, MA); Acetonitrile with 0.1% formic acid and water with 0.1% formic acid were purchased from J.T. Baker (Phillipsburg, NJ).

2.1.2 Cell culture and cell lysis

Mouse P19 testicular cancer cells were cultured at 37°C in 5% CO_2 in DMEM medium (GIBCO-BRL, Burlington, ON) supplemented with 10%(v/v) fetal calf serum (*1-2*). Cells were harvested and washed twice with phosphate buffered saline (PBS). Cell lysis was performed using a modified RIPA lysis buffer (50 mM Tris-HCl pH 7.4, 150 mM NaCl, 1%(w/v) NP-40, 0.25%(w/v) Na deoxycholate, 1 mM EDTA, protease inhibitor cocktail). Collected cells were placed on ice with RIPA buffer for 10 minutes, and cell lysates were centrifuged for 10 min at 14,000 rpm to pellet cell debris. Supernatants were collected and protein concentration was assessed using a Bradford protein assay kit (Bio-Rad, Hercules, CA) with bovine serum albumin as the standard (Sigma, St. Louis, MO).

Human MCF-7 breast epithelial cancer cells were cultured at 37 °C in 5% CO_2 in a DMEM medium (GIBCOBRL, Burlington, ON) supplemented with 10% (v/v) fetal bovine serum (*2*). The cells were harvested following treatment with trypsin, washed with phosphate buffered saline (PBS), and re-suspended in a 2 mL hypotonic buffer (50 mM Tris pH 7.5, 1 mM DTT, 1 mM EDTA, 5 mM $CaCl_2$, 5 mM $MgCl_2$, protease inhibitor cocktail) on ice for 10 min. Crude cell homogenate was then centrifuged at 3000 g for 15 minutes. Supernatants were collected and aliquots were stored at -80°C. The protein concentration was assessed using Bio-Rad DC protein assay (Bio-Rad, Hercules, CA) with bovine serum albumin as the standard (Sigma, St. Louis, MO).

Saccharomyces cerevisiae yeast cells were grown on a 200 mL plate to an OD_{600} of 0.8 at which point the cell pellets were harvested by centrifugation and washed with water (*3*). The cell pellets were then frozen at -80°C until ready to be used. The cell pellets were re-suspended in an equivalent volume of lysis buffer (100 mM HEPES pH 8.0, 20 mM magnesium acetate, 10% glycerol (v/v), 10 mM EGTA, 0.1 mM EDTA, protease inhibitors cocktail) and frozen in liquid nitrogen in small droplets and lysed using a coffee grinder half-filled with dry ice for 1 minute. The dry ice was allowed to evaporate, and the resulted whole cell extract was sonicated three times for 30 seconds with at least 1 minute on ice between each pulse. Nonidet P-40 (NP-40) was added to a final concentration of 0.4% (w/v), and the sample was manually mixed for 30 seconds. The extract was clarified by centrifugation at

14000 rpm for 15 minutes (4ºC) and the supernatant was transferred to a fresh tube. The final protein concentration was determined using a Bradford protein assay kit (Bio-Rad).

2.1.3 Protein sample preparation/digestion

2.1.3.1 Protein digestion using proteomic reactor

As described in publications (*1-3*), protein samples were processed using the SCX proteomic reactor, SCX plate reactor, and SAX proteomic reactor described in this thesis. Detailed protocols to process protein samples using the SCX proteomic reactor will be described in chapter 3.1.2; the protocol to process protein samples using the SCX plate reactor will be described in chapter 3.2.4; and the protocol to process protein samples using SAX proteomic reactor will be described in chapter 3.3.4.

2.1.3.2 In-solution protein digestion

The in-solution digestion of P19 cell lysate was performed as described previously (*1, 3*). The RIPA buffer from the protein extract was exchanged using a centricon YM-3 filter (Millipore, Billerica, MA) washed three times with 20 mM TRIS, 150 mM NaCl pH 7.4 buffer. The protein concentration was then determined by Bradford assay. Three aliquots of P19 lysate each corresponding to 10 µg of total protein were then dissolved in 100 µL of 100 mM NH_4HCO_3 buffer containing 10 mM dithiothreitol (pH 8.0). After incubation at 37 °C for 2 h, the protein solution was added with 2 µL of 1 M iodoacetamide and incubated in the dark for additional 30 min at room temperature. 1.5 µL of 1 M dithiothreitol was then added to react with the remaining iodoacetamide. Digestion was performed with 2.5 µg of trypsin at 37 °C overnight. The solvent was then evaporated and the sample was reconstituted in a final volume of 40 µL of 200 mM ammonium bicarbonate and 4 µL of 50% (v/v) formic acid, which is the same solvent used for the reactor samples prior to HPLC-MS analysis.

For the standard protein mixture, a total of 10 µg of standard protein sample was dissolved in 50 µL 100 mM NH_4HCO_3 buffer containing 10 mM dithiothreitol (pH 8.0) (*1,*

3). After incubation at 37 °C for 2 h, 2 µL of 1 M iodoacetamide was added and the solution was incubated in the dark for an additional 30 min at room temperature. 1.5 µL of 1 M DTT was then added to react with the remaining iodoacetamide. An in-solution digestion was performed with trypsin (1/4 amount of the protein) at 37 °C overnight. The tryptic digestion was quenched by adding formic acid to a final concentration of 2% (v/v).

2.1.4 HPLC-MS/MS experiments

The 40 µL peptide mixture obtained from the P19 cell lysate digested with SCX reactor were acidified with 4 µL of 50% (v/v) formic acid (*1*). The resulting peptides were then analyzed with a HPLC-ESI-MS/MS system, where a LCQ DecaXP instrument (Thermo-Finnigan, San Jose, CA) was integrated with a micro flow HPLC 1100 system (Agilent, Palo Alto, CA). 5 µL of each sample was first loaded onto a 4 cm X 75 µm ID pre-column packed with 5 µm C18 beads (Waters, Milford, MA) using a micro flow HPLC 1100 system (Agilent, Palo Alto, CA). The peptides were then separated with a 5 cm X 75 µm ID C18 column integrated with a 10 µm picotip emitter (New Objective, Woburn, MA) using a 5-80% (v/v) linear gradient of acetonitrile with 0.1% (v/v) formic acid over 2 hours. The analytical column was also packed with 5 µm C18 beads. The flow rate through the column was approximately 200 nL/min. Data dependant MS scans were performed, where the three most intense ions in each MS spectrum were subjected to MS/MS analysis using collision induced dissociation. The experiments were performed in dynamic exclusion mode, where a peak could be sequenced a maximum of three times before being excluded for 3 minutes.

The peptides obtained from the P19 cell lysate digested with the SCX plate reactor were analyzed using a QSTAR Pulsar quadrupole-TOF mass spectrometer (ABI/MDS Sciex, Concord, ON) (*2*). 8 µL out of 25 µL total elution volume were loaded onto a 75 µm× 50 mm pre-column (5 µm YMC ODS-A C18 beads, Waters, Milford, MA) at 1.5-2 µL/min using an Agilent 1100 series HPLC system (Agilent Technologies, Palo Alto, CA). Following a 12 minutes desalting step, the flow was split and peptides were eluted through a second 75 µm × 50 mm column (5 µm YMC ODS-A C18 beads) at approximately 200 nL/min using a 5-80% (v/v) gradient of acetonitrile with 0.1% (v/v) formic acid over 1.5 hrs.

The LC effluent was interfaced with the QSTAR Pulsar quadrupole-TOF mass spectrometer via a 10 μm picotip emitter (New Objective, Woburn, MA) by electrospray ionization. Data dependant MS scans were performed, where the four most intense ions in each MS spectrum were subjected to MS/MS analysis using CAD. A peak could be sequenced a maximum of three times before being excluded for 3 minutes.

The peptides derived from the MCF-7 fractions digested with the SCX plate reactor were analyzed using a LCQ Deca XP mass spectrometer (ThermoFinnigan, San Jose, CA) (*2*). 8 μL of the total 30 μL of resulting peptides were loaded onto a LC setup as described above. Again, data dependant MS scans were performed, where the three most intense ions in each MS spectrum were subjected to MS/MS analysis using CAD. The experiments were performed in dynamic exclusion mode. A peak could be sequenced a maximum of three times before being excluded for 3 minutes.

The peptides of yeast samples and protein standard mixtures that were eluted from the SAX or SCX reactors were acidified with formic acid and loaded onto a 200 μm × 50 mm fused silica precolumn that was packed in-house with 5 cm of 5-μm YMC ODS-A C18 beads (Waters Co., Milford, MA) using an 1100 micro-HPLC system (Agilent Technologies, Santa Clara, CA) (*3*). Following a desalting step, the flow was split, and peptides were eluted through a second 75 μm × 50 mm column packed with the same beads at approximately 200 nL/min. The peptides were eluted using a 2-h gradient (5-80% acetonitrile(v/v) with 0.1% formic acid (v/v)) into an ESI LTQ linear ion trap mass spectrometer (Thermo Electron, Waltham, MA). MS/MS spectra were acquired in a data-dependent acquisition mode that automatically selected and fragmented the ten most intense peaks from each of the MS spectrum generated.

2.1.5 Data analysis

In this thesis, all the MS/MS spectra recorded were analyzed using Mascot (Matrix Science, Boston, MA). The MS/MS spectra recorded for peptides from P19 cell lysate, digested with SCX reactor and in-solution digestion, were analyzed using Mascot using the

following parameters: oxidation (M) as an optional modification, a maximum of 2 tryptic miscleavages, a peptide tolerance of 2 Da and a MS/MS tolerance of 0.8 Da, *mus* taxonomy and 2+ and 3+ precursor ions only (*1*). Only the proteins with at least one new peptide were kept (Require Bold Red option in Mascot). A Mascot peptide score threshold of 15 was used for the peptide scores on the LCQ, which is above the significance level indicating identity or extensive homology (*4*). It should be noted that the efficacy of digesting proteins using the SCX proteomic reactors was assessed by comparing the total number of proteins identified to those identified using the in-solution protein digestion method, where the same criteria for protein/peptide identification were applied.

The MS/MS spectra recorded for peptides from P19 cell lysate, digested with the SCX plate reactor, were searched against the mouse taxonomy in the NCBI non-redundant database using Mascot; data files from all the 35 fractions of MCF7 cell lysates, digested with SCX plate reactor, were searched against the human taxonomy in the NCBI nr database using Mascot (*2*). The Mascot peptide and MS/MS tolerances for the experiment performed on a QSTAR mass spectrometer were set to ±100 ppm and 0.2 Daltons, respectively. The Mascot peptide and MS/MS tolerances were set for the LCQ Deca XP experiments at 2 and 0.8 Daltons, respectively. For all experiments, 1 missed cleavage was allowed and the ion score threshold was set at 20. In addition, the protein cut-off score was set at 39 (*5*).

The MS/MS spectra from the yeast samples, digested with SAX and SCX reactors and in-solution approach, were searched against a database consisting of the Saccharomyces Genome Database (http://www.yeastgenome.org/, 6716 protein entries, released December 2, 2008) and the reverse sequence of all protein entries (*3*). Mascot 2.2.02 (Matrix Science) was used to search the protein sequence database using the following parameters: carbamidomethyl (C) was set as a fixed modification, and oxidation (M, +15.99492 Da) was set as a variable modification. The precursor and fragment mass tolerances for the LTQ data were set at 2.0 and 0.8 Da, respectively. Mascot ion cut off scores were set to 30. Furthermore, only the peptides that ranked first with a probability-based Mowse (expect) P-value smaller than 0.05 were accepted (*6*).

2.2 Lipidomic Experiments

2.2.1 Materials:

1-*O*-hexadecyl-2-acetyl-*sn*-glycero-3-phosphocholine (C16:0 PAF), 1-*O*-hexadecyl-2-hydroxy-*sn*-glycero-3-phosphocholine (C16:0 *lyso*-PAF), 1-*O*-octadecyl-2-acetyl-*sn*-glycero-3-phosphocholine (C18:0 PAF), and 1-*O*-octadecyl-2-hydroxy-*sn*-glycero-3-phosphocholine (C18:0 *lyso*-PAF) were purchased from Biomol Research Laboratories (Plymouth Meeting, PA). The C13:0 lyso-phosphatidylcholine (C13:0 LPC) and diacyl glycerophospholipid standards PA (12:0/13:0), PA (17:0/14:1), PA (17:0/20:4), PS (12:0/13:0), PS (17:0/14:1), PS (17:0/20:4), PG (12:0/13:0), PG (17:0/14:1), PG (17:0/20:4), PI (12:0/13:0), PI (17:0/14:1), PI (17:0/20:4), PE (12:0/13:0), PE (17:0/14:1), and PE (17:0/20:4) were quantitative standards from Avanti Polar Lipids, Inc. (Alabaster, AL).

Chloroform and methanol were liquid chromatography grade from Fisher Scientific (Waltham, MA). Ammonium acetate was purchased from Sigma Chemical Co. (St. Louis, MO). Cell media and fetal bovine serum (FBS) was from Invitrogen (Carlsbad, California). Bovine serum albumin was from Sigma (St Louis, MO).

The 5 μm C18 beads were from Waters (Milford, MA); 10 μm picotip emitters were purchased from New Objective (Woburn, MA); Acetonitrile with 0.1% formic acid(v/v) and water with 0.1% formic acid(v/v) were purchased from J.T. Baker (Phillipsburg, NJ).

2.2.2 Cell culture, tissue samples and lipid extraction

Rat pheochromocytoma PC12 cells originally obtained from the American Type Tissue Collection were cultured in RPMI containing 10% (v/v) horse serum and 5% (v/v) newborn calf serum (complete media) at 37°C in a 5% CO_2/95% air atmosphere (*7*). PC12 cells were differentiated to a neuronal phenotype by seeding at a density of $5x10^4$ cells/dish on 10 cm diameter tissue culture plates coated with 2 μg/ml rat tail collagen (Roche, Mississauga, ON). Twenty-four hours after plating, cells were cultured in differentiation media (RPMI containing 0.5% (v/v) heat-inactivated horse serum and 50 ng/ml 7S nerve

growth factor (NGF, Sigma)). Cells were fed every second day for 7 days. Untreated controls were seeded at a density of $1x10^5$ cells/dish and lipids extracted 72 h after plating. Plating controls seeded and cultured at the same time were counted immediately prior to lipid extraction to establish final cell number (PC12 cells – 1.79e7, NGF-differentiated PC12 cells – 2.34e6). All culture reagents were obtained from Invitrogen (Burlington, ON) except where indicated.

Glycerophospholipids were extracted according to a modified Bligh/Dyer procedure (*8-9*). Briefly, media was removed from each plate and cells were washed extensively with 10 mM phosphate buffered saline. Cultures of undifferentiated PC12 and NGF-differentiated PC12 cells were placed on ice and 1 ml of ice-cold methanol acidified with 2% (v/v) acetic acid was added to each plate. Cells were then scraped and collected in acidified methanol. Four plates per condition were harvested and pooled. Lipids were extracted using a volumetric ratio of 0.95 of chloroform and 0.8 of 0.1 M sodium acetate (aq) per volume of methanol in acid-washed borosilicate glass tubes (Fisher, Ottawa, ON). Phospholipids were collected from the organic phase after layer separation by centrifugation. The aqueous phase was then back-extracted three times in the organic phase of a wash solution prepared by combining RPMI+ 0.025% BSA, methanol, chloroform, and sodium acetate in the volumetric ratio of 1:2.5:3.75:1. The organic fractions were combined, evaporated under a stream of nitrogen gas, and dissolved in 300 µl EtOH.

Alzheimer brain from deceased patients (74$\pm$8 yrs) was obtained from the Douglas Hospital Research Centre Brain Bank (Montreal, Canada). Control patients (78$\pm$16 yrs) suffered sudden death due to non-neurological complications. At autopsy, parahippocampal gyri were removed and flash-frozen in liquid nitrogen without fixation for lipid extraction. Post-mortem delay was between 5 and 25 h.

TgCRND8 mice, expressing a double mutant (M146L and L286V) form of the human amyloid precursor protein under the control of the PrP gene promoter (*10*), and NonTg littermate controls were sacrificed between 10-12 weeks of age via lethal injection of euthanol. Cerebral cortices (posterior cortex, temporal lobe) were removed on ice. All manipulations were performed in compliance with approved institutional protocols and

according to the strict ethical guidelines for animal experimentation established by the Canadian Council for Animal Care.

Human hNT neurons were generated from NT2/D1 precursor cells (*11*). Cultures were treated with $A\beta_{42}$ (25 μM) prepared as soluble oligomers (*12*) for 6 and 24 hours, respectively. All treatments were carried out in serum-free media containing 0.025% bovine serum albumin to ensure neurons were not exposed to the secreted PAF acetylhydrolase (PAF-AH) isoform present in serum supplements. No degradation of exogenous PAF in media was detected under these conditions confirming the absence of PAF-AH activity in treatment media.

Glycerophospholipids were extracted according to a modified Bligh/Dyer procedure (*8-9*). Briefly, tissue and cell pellets were weighed and placed in 1 ml of ice-cold methanol acidified with 2% acetic acid. Human samples were spiked with 187.5 ng C13:0 LPC at time of extraction (*13*). Lipids were extracted using a volumetric ratio of 0.95 of chloroform and 0.8 of 0.1 M Na acetate (aq) per volume of MeOH in acid-washed borosilicate glass tubes (Fisher, Ottawa, ON). Phospholipids were collected from the organic phase after layer separation by centrifugation (1500 rpm, 15 min, 4ºC). The aqueous phase was then back-extracted three times in the organic phase of a wash solution prepared by combining RPMI+ 0.025% BSA, methanol, chloroform, and sodium acetate in the volumetric ratio of 1:2.5:3.75:1. The organic fractions were combined, evaporated under a stream of nitrogen gas, and dissolved in 300 μl EtOH.

The expression plasmid pcDNA3.1/V5-His-TOPO containing mouse lipin-1α coding sequences (*14*) was transfected into rat hepatoma McA-RH7777 cells using the calcium phosphate precipitation method, and stable transformants were obtained following selection with G418(*15*). The cells were maintained at 37ºC in a 5% CO_2 humidified incubator in Dulbecco's Modified Eagle Medium (DMEM) supplemented with 10% fetal bovine serum (v/v), 10% horse serum(v/v), 1% antibiotyc-antimycotic solution(v/v) (Invitrogen) and 200 μg/ml G418. Lipids were extracted from rat hepatoma cells over expressing lipin-1α (~$4X10^7$) with chloroform/methanol/acetic acid/saturated $NaCl/H_2O$ (4:2:0.1:1:2, v/v) (*16*). After phase separation by centrifugation (1500 rpm, 15 min, 4ºC), the organic phase fraction

was collected and evaporated under a stream of nitrogen gas, followed by dissolving in 300 µl methanol (*17*).

2.2.3 HPLC-ESI-MS/MS experiments

2.2.3.1 HPLC-ESI-MS/MS system

A micro flow 1100 HPLC system (Agilent, Palo Alto, CA) was used to introduce the analytes into a 2000 Q TRAP mass spectrometer (*7, 13*). The solvents used were water and acetonitrile each with 0.1% formic acid (J.T.Baker, Phillipsburg, NJ). Samples were loaded successively onto an Agilent 96-well sampling plate, which was then covered with a pre-slit well cap and thermostated at 4^{o}C. An Agilent 1100 autosampler was employed to introduce the analytes onto a 200 um x 50 mm pre-column packed with 5 µm YMC ODS-A C18 beads (Waters, Milford, MA) at a flow rate of 10 µl/min. Following the completion of loading 40 µL of analyte, the HPLC flow was split and the analyte was eluted through a 75 um x 50 mm picotip emitter (New Objective, Woburn, MA), which was interfaced with the mass spectrometer via electrospray ionization, at ~200 nL/min. The emitter was packed with the same beads as those of the pre-column. A linear gradient was used to separate the glycerophospholipid species. The gradient of the HPLC was increased from 5% to 60% acetonitrile(v/v) in 1.5 minutes, from 60% to 80% acetonitrile(v/v) over the next 35 minutes, and from 80% to 95% acetonitrile(v/v) over the next 4 minutes. Most of the lipid species were eluted from the columns between 60% to 80% acetonitrile(v/v). The column was then washed with 95% acetonitrile (v/v) for ~ 40 minutes, followed by regeneration at 95% H_2O for 15 minutes (*7, 13*).

Data were collected on a Q-TRAP 2000 mass spectrometer operated with Analyst 1.4.1 (Applied Biosystems/MDS Sciex, Concord, ON). In the detection process, total lipid extract were analyzed by Enhanced MS scan over the range of m/z from 450 to 600. The glycerophosphocholine species were further analysed in positive ion mode using precursor ion scan for an MS/MS fragment with a mass to charge ratio (m/z) of 184.0, a diagnostic fragment of phosphocholine (*18*). The resolution for both Q1 and Q3 were set at low to

maximize the sensitivity for ion detection. Capillary voltage was 3.5 kV. Nitrogen served as the collision gas and the collision energy was 40 eV (*7, 13*).

2.2.3.2 Lipid sample preparation

Lipid extract was normally diluted appropriately to avoid overloading the LC-MS system. Lipid extract from differentiated PC12 cells was diluted by a factor of 8 prior to MS analysis. For absolute quantitation of the four PAF family species, 8 μL of lipid extract, 5 μL of a standard solution containing known amount of C16:0, C18:0 PAF and C16:0, C18:0 *lyso*-PAF, and 27 μL of H_2O with 0.1% (v/v) formic acid were mixed together to bring the final volume to 40 μL. Five standard solutions containing 200, 400, 600, 800, and 1000 pg each of C16:0, C18:0 PAF and C16:0, C18:0 *lyso*-PAF were used in the experiment. At each standard addition concentration, samples were analyzed in triplicate (*7*).

For relative quantification of PAF family species and other glycerophosphocholine species, 46 μL, consisting of 10 μl of lipid extract, 5 μL of deuterated standards (d_4-C16:0 PAF/d_4-C_{16}-*lyso*-PAF) at final concentration of 2.5 ng/species, and 31 μl of 0.1% (v/v) formic acid in H_2O, was analyzed per MS run (*13*).

2.2.3.3 Data analysis

Analyst 1.4.1 (Applied Biosystems/MDS Sciex) was used to measure the peak areas of the lipid species of interest from their respective extracted ion chromatograph (XIC), which was extracted from the precursor ion scan of m/z 184 (*7, 13*). For absolute quantification, concentrations of the native PAF species were calculated using the regression curve when y=0 and expressed as the mean of the triplicate samples ± 95% confidence interval (*7*). The 95% confidence interval was determined using the Student's *t*-test. PAF species data were then standardized to total cell number and expressed as pg per 10^6 cells. Tissue wet weight in grams was divided by the specific gravity of brain tissue (1.050) to obtain the volume in ml for molar calculations (*19*).

For relative quantification, lipid samples were spiked with identical amount (e.g. 187.5 ng for human tissue samples) of C13:0 LPC at time of extraction (*13*). Peak areas of the lipid species of interest were normalized with respect to that of the internal standard C13:0 lyso-phosphatidylcholine (C13:0 LPC). Deuterated standards (d_4-C16:0 PAF/d_4-C_{16}-*lyso*-PAF) were used to identify C16:0 PAF and/or C_{16}-*lyso*-PAF from other isobaric lipid species, as the deuterated and normal C16:0 PAF and C_{16}-*lyso*-PAF had the same elution time.

2.2.4 Shotgun lipidomics (ESI-MS/MS)

The mixture of lipid standards was prepared by taking equal volumes of each lipid standard solution (*17*). The final concentration of each lipid standard was around 1 μM. After vortexing, the mixture of lipid standards was transferred to a QSTAR Pulsar QqTOF mass spectrometer (MDS Sciex, Concord, ON, Canada) using a syringe pump at a flow rate of 250 nL/min, controlled by Analyst software. For the lipid extract from rat hepatoma cells over expressing lipin-1α, 50 μL of lipid samples were diluted with an equal volume of methanol, followed by spiking with 3 μL of ammonium acetate at a concentration of 250 mM so that the final concentration of ammonium acetate in the lipid sample was around 7.5 mM. The sample was then introduced into the mass spectrometer with the syringe pump at 250 nL/min.

The nano-spray needle potential was set at -1,200 V and the declustering potential (DP) was set at -30 eV (*17*). The mixture of lipid standards was first monitored by TOF MS until the total ion current (TIC) became stable. Product ion spectra of each lipid standard were then recorded sequentially at collision energies from 20 to 70 eV for PA, PS, PG, and PE, and from 20 to 80 eV for PI. Each product ion spectrum was recorded for 2 minutes to minimize the influence of signal intensity fluctuation. Quadrupole Q1 was operated at unit resolution.

For the analyses of the lipid extract from the lipin 1α cell line, precursor ion scans of *m/z* -153 and -196 were first performed to highlight molecular ions of PA/PS/PG/PI and PE, respectively (*17*). Quadrupole Q1 was operated at unit resolution and ~20 ms dwell time with

step size of 0.3 Da. Product ion scans were then carried out for the lipid species of interest, each spectrum recorded for up to 2 minutes. For PI species, the collision energy was set at 55 eV. For all the other glycerophospholipids, the product ion scans were performed at 40 eV.

References

1. Ethier, M., Hou, W., Duewel, H. S., and Figeys, D. (2006) The proteomic reactor: a microfluidic device for processing minute amounts of protein prior to mass spectrometry analysis, *J Proteome Res 5*, 2754-2759.
2. Hou, W., Ethier, M., Smith, J. C., Sheng, Y., and Figeys, D. (2007) Multiplexed proteomic reactor for the processing of proteomic samples, *Anal Chem 79*, 39-44.
3. Zhou, H., Hou, W., Lambert, J. P., and Figeys, D. (2010) New ammunition for the proteomic reactor: strong anion exchange beads and multiple enzymes enhance protein identification and sequence coverage, *Anal Bioanal Chem 397*, 3421-3430.
4. Mawuenyega, K. G., Kaji, H., Yamuchi, Y., Shinkawa, T., Saito, H., Taoka, M., Takahashi, N., and Isobe, T. (2003) Large-scale identification of Caenorhabditis elegans proteins by multidimensional liquid chromatography-tandem mass spectrometry, *J Proteome Res 2*, 23-35.
5. Kapp, E. A., Schutz, F., Connolly, L. M., Chakel, J. A., Meza, J. E., Miller, C. A., Fenyo, D., Eng, J. K., Adkins, J. N., Omenn, G. S., and Simpson, R. J. (2005) An evaluation, comparison, and accurate benchmarking of several publicly available MS/MS search algorithms: sensitivity and specificity analysis, *Proteomics 5*, 3475-3490.
6. Elias, J. E., Haas, W., Faherty, B. K., and Gygi, S. P. (2005) Comparative evaluation of mass spectrometry platforms used in large-scale proteomics investigations, *Nat Methods 2*, 667-675.
7. Whitehead, S. N., Hou, W., Ethier, M., Smith, J. C., Bourgeois, A., Denis, R., Bennett, S. A., and Figeys, D. (2007) Identification and quantitation of changes in the platelet activating factor family of glycerophospholipids over the course of neuronal differentiation by high-performance liquid chromatography electrospray ionization tandem mass spectrometry, *Anal Chem 79*, 8539-8548.
8. Bonin, F., Ryan, S. D., Migahed, L., Mo, F., Lallier, J., Franks, D. J., Arai, H., and Bennett, S. A. L. (2004) Anti-apoptotic actions of the platelet activating factor acetylhydrolase I alpha 2 catalytic subunit, *J Biol Chem 279*, 52425-52436.

9. Bligh, E. G., and Dyer, W. J. (1959) A rapid method of total lipid extraction and purification, *Can J Biochem Physiol 37*, 911-917.
10. Chishti, M. A., Yang, D. S., Janus, C., Phinney, A. L., Horne, P., Pearson, J., Strome, R., Zuker, N., Loukides, J., French, J., Turner, S., Lozza, G., Grilli, M., Kunicki, S., Morissette, C., Paquette, J., Gervais, F., Bergeron, C., Fraser, P. E., Carlson, G. A., George-Hyslop, P. S., and Westaway, D. (2001) Early-onset amyloid deposition and cognitive deficits in transgenic mice expressing a double mutant form of amyloid precursor protein 695, *J Biol Chem 276*, 21562-21570.
11. Pleasure, S. J., Page, C., and Lee, V. M.-Y. (1992) Pure, postmitotic, polarized human neurons derived from NTera 2 cells provide a system for expressing exogenous proteins in terminally differentiated neurons, *J. Neurosci. 12*, 1802-1815.
12. Klein, W. L. (2002) Abeta toxicity in Alzheimer's disease: globular oligomers (ADDLs) as new vaccine and drug targets, *Neurochem Int 41*, 345-352.
13. Ryan, S. D., Whitehead, S. N., Swayne, L. A., Moffat, T. C., Hou, W., Ethier, M., Bourgeois, A. J., Rashidian, J., Blanchard, A. P., Fraser, P. E., Park, D. S., Figeys, D., and Bennett, S. A. (2009) Amyloid-beta42 signals tau hyperphosphorylation and compromises neuronal viability by disrupting alkylacylglycerophosphocholine metabolism, *Proc Natl Acad Sci U S A 106*, 20936-20941.
14. Peterfy, M., Phan, J., and Reue, K. (2005) Alternatively spliced lipin isoforms exhibit distinct expression pattern, subcellular localization, and role in adipogenesis, *J Biol Chem 280*, 32883-32889.
15. Chen, C., and Okayama, H. (1987) High-efficiency transformation of mammalian cells by plasmid DNA, *Mol Cell Biol 7*, 2745-2752.
16. Tran, K., Thorne-Tjomsland, G., DeLong, C. J., Cui, Z., Shan, J., Burton, L., Jamieson, J. C., and Yao, Z. (2002) Intracellular assembly of very low density lipoproteins containing apolipoprotein B100 in rat hepatoma McA-RH7777 cells, *J Biol Chem 277*, 31187-31200.
17. Hou, W., Zhou, H., Bou Khalil, M., Seebun, D., Bennett, S. A., and Figeys, D. (2011) Lyso-form fragment ions facilitate the determination of stereospecificity of diacyl glycerophospholipids, *Rapid Commun Mass Spectrom 25*, 205-217.

18. Brugger, B., Erben, G., Sandhoff, R., Wieland, F. T., and Lehmann, W. D. (1997) Quantitative analysis of biological membrane lipids at the low picomole level by nano-electrospray ionization tandem mass spectrometry, *Proc Natl Acad Sci U S A 94*, 2339-2344.
19. Nelson, S. R., Mantz, M. L., and Maxwell, J. A. (1971) Use of specific gravity in the measurement of cerebral edema, *J Appl Physiol 30*, 268-271.

Chapter 3 Developing proteomic reactor techniques for processing complex protein samples

3.1 Developing a SCX Proteomic Reactor

3.1.1 Introduction

Different proteomic approaches have been developed over the years which commonly require the processing of proteins into peptides before they are analyzed by mass spectrometry (*1-4*). In gel-based experiments, such as the well established 2D gel electrophoresis approach (*5*), the separated proteins are difficult to extract from the polyacrylamide gel (*6*). Instead, proteins are enzymatically cleaved into peptides in the gel (*7*) before they can be extracted and analyzed. Unfortunately, protein/peptide loss and contamination are hard to avoid with 2D gel electrophoresis (*8*) and the proteins are digested in a large volume of solution (typically 25 µl).

Gel-free proteomics has been proposed as a complementary approach to 2D gel electrophoresis (*9*). These gel-free approaches rely on either solution based protein separations such as size exclusion (*10*), reverse-phase liquid chromatography (*11*), free-flow electrophoresis (FFE) (*12-13*) and 2D chromatography (*14*), or peptide separations (*15-18*). In these approaches, the proteins are digested in a large volume of solution either before or after separation. Even though gel-free approaches bypass the need for gels, they do not address the fundamental issue of efficiency of protein processing.

Various approaches to in-solution digestion have been proposed, but they have notable limitations. For example, two groups have reported approaches for processing proteins using immobilized trypsin in monolithic columns followed by peptide fractionation (*19-20*). Unfortunately, no protein preconcentration is associated with these approaches. This means that the samples must have low amounts of contaminants and high levels of

proteins. Another group reported protein separation coupled to immobilized trypsin (*21-22*) In these studies, protein separation is performed at the same time as the digestion followed by mass spectrometry. However, peptide fractionation is not performed in this approach, which drastically limits the number of proteins that can be handled by the systems. Craft *et al.* (*23-24*) digested proteins by absorbing them on a hydrophobic support, introducing trypsin, gradually eluting them, and then analysing the resulting peptides by mass spectrometry. Unfortunately, this technique required a high amount of sample (200 ng per protein) and was only successful for standard protein solutions which were contaminant free. In general, these approaches require further development before being readily amenable to real biological samples.

This section presents the development of a single microfluidic device, termed the *proteomic reactor* to simplify and improve the processing of proteomic samples. We postulated that microfluidic volume could be used to decrease sample loss during proteomic analysis, while a small bed of extraction material incorporated within the microfluidic path could be used to more efficiently perform extractions and reactions on proteins and peptides.

At the core of the proteomic reactor is the ability to use multiple ionic interactions between proteins and the bed of the reactor to extract proteins from solution. The first generation of the proteomic reactor contains a small bed of packed strong cation exchange material (SCX). The proteomics samples are resuspended in a low pH buffer, spiked with trypsin and loaded onto the reactor (Figure 3.1.1b). The vast majority of proteins in proteomics samples will be multiply charged due to the protonation of lysine, arginine, histidine, and N-termini at pH lower than 3. As well, the majority of proteins will also be deprotonated (or carrying very few charges) at pH=8. This means that at low pH most proteins can have multiple ionic interactions with charge surfaces whereas at physiological pH these interactions will be much fewer. As well, at low pH trypsin remains stable but is inactivated. Therefore, at low pH a strong cation exchanger bed incorporated within the reactor can readily extract most proteins without issues of isocratic elution. This is often an issue disregarded in microfluidics. However, real biological samples are present in relatively large volumes (10-100 μl) which are a few orders of magnitude larger than the microfluidic dead volume. In conventional chromatography, in which the analytes exchange between the

stationary and mobile phase, this large difference in volume would cause isocratic elution of many analytes. Fortunately, the presence of multiple charges on the proteins favours the formation of multiple weak interactions with the strong cation exchanger which overall greatly favours the extraction of the proteins onto the SCX. No isocratic elution is observable within the limits of the volumes used in these experiments. Therefore, the proteomic reactor can pre-concentrate protein samples on a small bed. As importantly, at low pH many other biomolecules will either be neutral or negatively charged and therefore will not interact with the SCX and will readily flow through the reactor. The non-ionic detergents, DNA, RNA, lipids and other neutral or negatively charged biomolecules are readily washed away while the proteins are retained by the SCX material. Therefore, the proteomic reactor is also useful to clean-up samples. Finally, chemical and biochemical reactions can be performed on the proteins extracted in the reactors such as derivatization and digestion of protein samples. Proteins can then be derivatized by adding the reagents to the reactors. As well, proteins are digested by increasing the pH to 8.0, which in turn, will activate the trypsin loaded onto the reactor with the protein sample (Figure 3.1.1c). Although the proteomic reactor can be used as a standalone device, the resulting peptides are eluted using a buffer readily compatible with HPLC-ESI-MS/MS (Figure 3.1.1d).

Another advantage of the proteomic reactor is that it concentrates proteins from complex mixtures onto approximately 1 μL of packed SCX material. The strong affinity of positively charged proteins towards the SCX material at low pH enables minute amounts of proteins to be easily extracted from mid to high μL solution volumes. Furthermore, the protein samples' affinity for the SCX material can be modulated by introducing solutions with different pH and salt concentrations, which is advantageous for capturing and processing proteins on the reactor. While the pH is low during sample loading, the protein samples will bind to the SCX material on the reactor. During digestion/alkylation, the higher pH and salt contents render the protein samples mostly in a free solution phase. The interstitial volume within the proteomic reactor is limited to approximately 50 nL, suggesting that the overall pre-concentration effect ranges from 20 to 2000 fold if 1 μL to 100 μL of starting material is used.

We first use BSA to characterize the SCX proteomic reactor. Briefly, we established the maximum loading capacity of the proteomic reactor, as well as assessed the capability of the reactor to retain proteins on the SCX bed and elute retained proteins from the reactor using a MS compatible elution buffer. We then used a protein extract from P19 cells to assess the impact of cysteine reduction and alkylation on the efficacy of protein digestion on the SCX proteomic reactor. Briefly, two aliquots of P19 protein samples were processed on the SCX reactors under two conditions: one protein aliquot underwent a reduction/alkylation reaction prior to its tryptic digestion while another protein aliquot was directly digested without the reduction/alkylation step. Finally, we assessed the efficacy of digesting protein samples on the SCX reactor in comparison to that of conventional in-solution protein digestion approach. This was performed with five different amounts of proteins (0.1, 0.5, 1, 5, and 10 μg) from P19 cell lysate in triplicate. These different amounts of proteins correspond to the total proteins that would be obtained from 300 to 30,000 cells, based on the results of Bradford assay and cell counts.

3.1.2 Experimental

3.1.2.1 Protein samples preparation and LC-MS/MS data analysis

P19 cell lysates and standard protein BSA were employed in the study. Five different amounts of proteins (0.1, 0.5, 1, 5, and 10 μg) from P19 cell lysates were digested in triplicate with both the SCX reactor and the conventional in-solution protein digestion approach. 5 μL of the resulting peptides from each sample were analyzed with a LC-MS/MS system, where a micro flow HPLC 1100 system (Agilent, Palo Alto, CA) was integrated with a LCQ DecaXP instrument (Thermo-Finnigan, San Jose, CA). Details were described in chapter 2. The MS/MS spectra were analyzed using Mascot (Matrix Science, Boston, MA) using *mus* taxonomy. The details regarding P19 cell culture and protein extraction, in-solution digestion of P19 protein samples, LC-MS/MS system, and parameters used in Mascot search were described in chapter 2.

3.1.2.2 Proteomic reactor assembly and protein processing on reactor

The reactor was assembled by connecting a 200 μm inner diameter capillary tubing (~30 cm) into an inline micro-filter (UpChurch Scientific, Oak Harbor, WA), which was used as a frit. All tubing was washed with 500 μL of 10 mM potassium phosphate buffer (pH 3) prior to loading of SCX material. A slurry of SCX material (12 μm beads; The Nest Group, Southboro, MA) was then introduced from the other end of the capillary tubing by applying 200 psi of nitrogen. Unless specified otherwise, 4 centimeters of capillary tubing was packed with SCX material, enabling a protein binding capacity of 12 μg. Each packed reactor was then equilibrated by passing 50 μL of 10 mM potassium phosphate buffer (pH 3).

3.1.2.3 Digesting protein samples on the SCX proteomic reactor

The digestion of protein samples on the SCX proteomic reactor was validated with both protein standards and protein samples directly obtained through cell lysate. The steps are summarized below.

Protein samples were acidified prior to the proteomic reactor digestion by diluting them with 50 mM H_3PO_4 (pH~1.8) in a ratio of 1:9 (v/v). Trypsin (Promega, Madison, WI) (0.5 μg/μL in 10 mM potassium phosphate buffer (pH 3)) was added to the protein sample in a ratio of 1:5 (w/w). The acidified protein samples with trypsin were then loaded onto the reactor through continuous flow mode of operation, where a pressure of 200 psi was maintained until all sample solution was driven through the reactor bed. The flow rate remained at approximately 10 μL/min. Next, the reactor was washed three times with 20 μL of wash buffer (8 mM potassium phosphate buffer, 20% (v/v) acetonitrile), and then further washed with 25 μL of deionized water to remove the wash buffer. After washing steps, the reactor was dried with nitrogen gas for 30-60 seconds.

The proteins that were retained by the reactor were then reduced using a solution of 100 mM DTT (dithiothreitol) and 10 mM ammonium bicarbonate for 30 minutes. The reducing step was conducted through infusion operation mode, where the flow was halted by

dropping the nitrogen pressure to atmospheric pressure, as soon as the solvent front reached the outlet of the reactor column. The reactor remained hydrated while the reduction reaction was allowed to proceed for 30 minutes. The reactor was then dried and washed with 4 µL of 10 mM potassium phosphate buffer to decrease the pH to 3 and thus quench the reaction.

The alkylation and the activation of trypsin were carried out concomitantly by introducing a digestion/alkylation solution (100 mM Tris-HCl, pH 8, 10 mM iodoacetamide) through infusion operation mode. The reactions proceeded at atmospheric pressure and at room temperature for 2 hours. The resulting peptides were then eluted using 40 µL of 200 mM ammonium bicarbonate.

3.1.3 Results and discussion

3.1.3.1 Characterization of the SCX proteomic reactor

I first established the maximum loading capacity of the proteomic reactor (Figure 3.1.2). Briefly, the maximum protein binding capacity of the proteomic reactor was determined by sequentially loading 4 aliquots of acidified bovine serum albumin (BSA) onto the same proteomic reactor. Each aliquot containing 5µg of BSA and was acidified by diluting them with 50 mM H_3PO_4 (pH~1.8) in a ratio of 1:9 (v/v). The flow-through solutions (Load1/Load2/Load3/Load4) for each aliquot were collected after each loading, and the presence of protein was assessed by SDS-PAGE followed by coomassie-blue staining. The presence of protein in the flow-through solutions was only observed from the third aliquot onwards (Load3/Load4). Therefore, the protein binding capacity of the reactor in the present format (4 cm SCX bed) is between 10-15 µg.

Using this proteomic reactor saturated with BSA, I assessed whether the retention of the protein onto the SCX bed was affected by washing steps. Briefly, the reactor was washed three times with 20 µL of wash buffer (8 mM potassium phosphate buffer, pH 3.0, 20% (v/v) acetonitrile) (Wash1), and then further washed with 25 µL of deionized water (Wash2) to remove the wash buffer. No noticeable proteins were observed in the flow-through solutions of Wash1 and Wash2 as assessed by SDS-PAGE followed by coomassie-blue staining. This

indicates that even when the reactor bed is saturated with proteins, the retention of the proteins by the SCX material is not affected by the various washing conditions when proper pH and salt contents are maintained.

I then tested whether the protein could be eluted from the reactor using our MS compatible elution buffer. Briefly, two subsequent elution steps (40 µL of 200 mM ammonium bicarbonate, pH 9.0) were performed to verify the efficacy of eluting the retained protein samples from the reactor (Elute1/Elute2). The eluent collected for each elution step, along with the unpacked SCX beads (Beads) were monitored for BSA by SDS-PAGE. It was observed that most proteins were eluted in the first elution (Elute1), but some were present in the second elution (Elute2). Analysis of the unpacked SCX beads (Beads) from the reactor by SDS-PAGE indicated that small portion of proteins remained on the beads. Incomplete elution of protein from the reactor is considered acceptable as the solutions employed to elute the resulting peptides from the reactor are intended to be compatible with the HPLC-MS analysis. Moreover, in the full protocol trypsin is used to generate peptides that are less likely to be strongly retained by the SCX bed. To avoid cross-contamination, a new proteomic reactor was used for each analysis. The cost of a reactor is estimated to be around $0.02 each.

3.1.3.2 The impact of reduction/alkylation reaction on the performance of the SCX proteomic reactor

One advantage of the proteomic reactor is that chemical reactions can be performed directly on the proteins retained on the reactor. Here we tested the performance of protein reduction and alkylation of cysteines using a complex protein sample loaded on the reactor.

We used a protein extract from P19 cells to demonstrate the impact of cysteine reduction and alkylation on the efficacy of protein digestion on the SCX proteomic reactor. Briefly, protein processing was tested under two conditions: first, one protein aliquot underwent a reduction/alkylation reaction on the reactor prior to its digestion while another protein aliquot was directly digested on another reactor. The resulting peptides were

analyzed using the LCQ mass spectrometer as described in the experimental section. The experiments were repeated twice. The resulting data were compared for sequence coverage of the identified proteins. Furthermore, in-house software was used to track individual peptides and to verify their protein annotation from sample to sample.

Ninety four proteins were identified in all of the samples with varying sequence coverage. The difference in the number of peptides identified between the two conditions tested for each protein was calculated (Figure 3.1.3). Overall, 57% of the identified proteins had increased sequence coverage when reduction/alkylation was performed on the proteomic reactor. In other words, there was an increase in the number of identified peptides per protein. Twenty eight% of the identified proteins had the same sequence coverage and 15% had a decrease in sequence coverage. The vast majority of proteins with a decrease in sequence coverage had only one less peptide identified; while a significant portion of the proteins with an increase in sequence coverage had two or more peptides identified. This clearly indicates that the DDT reduction and iodoacetamide alkylation performed on the reactor can significantly improve the sequence coverage for the proteins identified.

3.1.3.3 Comparing the performance of the SCX proteomic reactor to in-solution digestion approach

Another advantage of the proteomic reactor is that enzymatic catalysis can be performed on the reactor and benefit from an enhanced concentration effect. This was demonstrated using different amounts of protein lysate loaded onto the reactor, for which the resulting peptides were analyzed by HPLC-ESI-MS/MS. Briefly, five different amounts of proteins (0.1, 0.5, 1, 5, and 10 μg) from P19 cell lysate were processed in triplicate on the reactor and the resulting peptides were analyzed by HPLC-ESI-MS/MS. These different amounts correspond to the total proteins that would be obtained from 300 to 30,000 cells, based on the results of Bradford assay and cell counts.

Figure 3.1.4 shows the average number of proteins identified in each run and the total number of unique proteins identified after combining the triplicate runs versus the different

amount of proteins digested. Proteins were detected in all the samples, including an average of 25 proteins identified in samples containing only 0.1 μg of P19 cell lysate. No significant gain was observed when more than 0.5 μg of protein was loaded.

In practice only 11% of the total volume of protein digest for each sample was analyzed by the HPLC-ESI-MS/MS, considering that only 5 μL of the 40 μL collected from the reactor were loaded onto the HPLC-ESI-MS/MS. For example, this means that for the 0.1 μg of proteins loaded and processed on the reactor only 11 ng were actually analyzed with the HPLC-ESI-MS/MS, with an average of 25 proteins identified. In other words, an average of 440 pg of total protein lysate is required for every protein identified.

Figure 3.1.4 shows that the reactor works better when the saturation point of the binding capacity is attained (10 μg); however, even at 0.5 μg, 75% of the identifiable proteins can still be detected. Although we did not change the size of the proteomic reactor according to protein content, it is possible to make shorter or longer proteomic reactors to accommodate different levels of proteins.

The reactor's performance for digesting proteins was compared to an in-solution digestion using the same amount of protein (10 μg), as described in experimental section. Briefly, 10 μg of P19 cell lysate was digested in-solution and on the reactor, respectively, to obtain 44 μL of peptide solution in both cases. The resulting peptides for each method were then analyzed by HPLC-ESI-MS/MS as described in the experimental section. The in-solution digestions were performed three times and 22 unique proteins were identified. In comparison, 205 unique proteins were identified using the reactor digestions when performed three times. Of the 22 proteins identified in the in-solution digestion, 21 were also identified from the proteomic reactor digestion. The significantly improved performance of the reactor than the in-solution approach, i.e., ~10 times more protein identification and a ~5 fold reduction in processing time, is likely due to 1) the efficient concentration of the protein samples and the buffer exchange prior to digestion, and 2) the efficient digestion of protein samples in the volumes of nanoliters.

3.1.4 Conclusions

The microfluidic proteomic reactor provides an integrated platform to efficiently and reliably purify and concentrate down to nL volumes complex proteomic samples. Furthermore, we have demonstrated that chemical reactions, such as cysteine reduction and alkylation, can be performed on the reactor. The reactor digestion also led to approximately 10 times more protein identifications than in-solution digestions. We expect that the performance of the reactor will be further enhanced by coupling it to protein fractionation approaches and to more efficient mass spectrometers.

Figure Captions

Figure 3.1.1 Schematic representation of sample treatment steps using SCX proteomic reactor. a) Sample treatment steps done using the proteomic reactor. b) Schematic representation of the proteomic reactor. Pressurized nitrogen is used to push the liquid into the reactor. The protein and trypsin are bound to the SCX. c) Trypsin is activated by adjusting the pH to 8; the flow is stopped to let the digestion proceed without losing peptides. d) Peptides are eluted by using an ammonium bicarbonate solution. Reprinted with permission from Journal of Proteome Research. Copyright © 2006, American Chemical Society.

Figure 3.1.2 Characterization of the SCX proteomic reactor. The Standard represents 20 µg of BSA standard solution. For Load1/Load2/Load3/Load4, 5 µg of acidified BSA standard solution was introduced into a SCX proteomic reactor sequentially and the eluent was collected separately. The reactor was then washed three times with 20 µL of wash buffer (8 mM potassium phosphate buffer, pH 3.0, 20% (v/v) acetonitrile) (Wash1), and then further washed with 25 µL of deionized water (Wash2) to remove the wash buffer. Two subsequent elution steps (40 µL of 200 mM ammonium bicarbonate, pH 9.0) were performed to verify the efficacy of eluting the retained protein samples from the SCX reactor (Elute1/Elute2). The eluent was collected for each elution step, along with the unpacked SCX beads (Beads).

Figure 3.1.3 Effect of DDT reduction and iodoacetamide alkylation on the identification of peptides from mouse P19 total cell lysate. The same amount of protein samples were processed on the reactor either with a reduction/alkylation step (treatment) or without this step (control). The experiments were repeated twice for each condition. The resulting peptides were then subjected to LC-MS/MS analysis and protein/peptide identification. The list of protein identified and the number of peptides identified for each protein were then recorded for each sample. The change in the number of peptides identified for the same protein was compared between the two experiment conditions (2 treatments vs. 2 controls).

This comparison was performed for all individual proteins identified. The total number of times that such changes observed (in 4 comparisons) was grouped in terms of the number of peptide differences. A positive difference indicates an increase in the number of peptides identified when both reduction and alkylation are performed. The percentages represent the proportion of proteins having, respectively, an increase, the same, or a decrease in number of peptides identified. Reprinted with permission from Journal of Proteome Research.

Figure 3.1.4 Evaluation of the performance of the proteomic reactors for processing complex proteomic samples. The sample used is total cell lysate from mouse P19 cells. The circles represent the average of triplicate digestion for each protein quantities on reactor of 40 mm X 200 μm packed with 12 μm SCX beads. Error bars correspond to one standard deviation. The different X axes represent respectively the number of cells corresponding to the protein content used in the digestion, (determined by Bradford assay) and the quantity used for mass spectrometry. The diamonds represent the results when the peak lists from the three replicates were merged prior to the Mascot search. Reprinted with permission from Journal of Proteome Research.

Figure 3.1.1

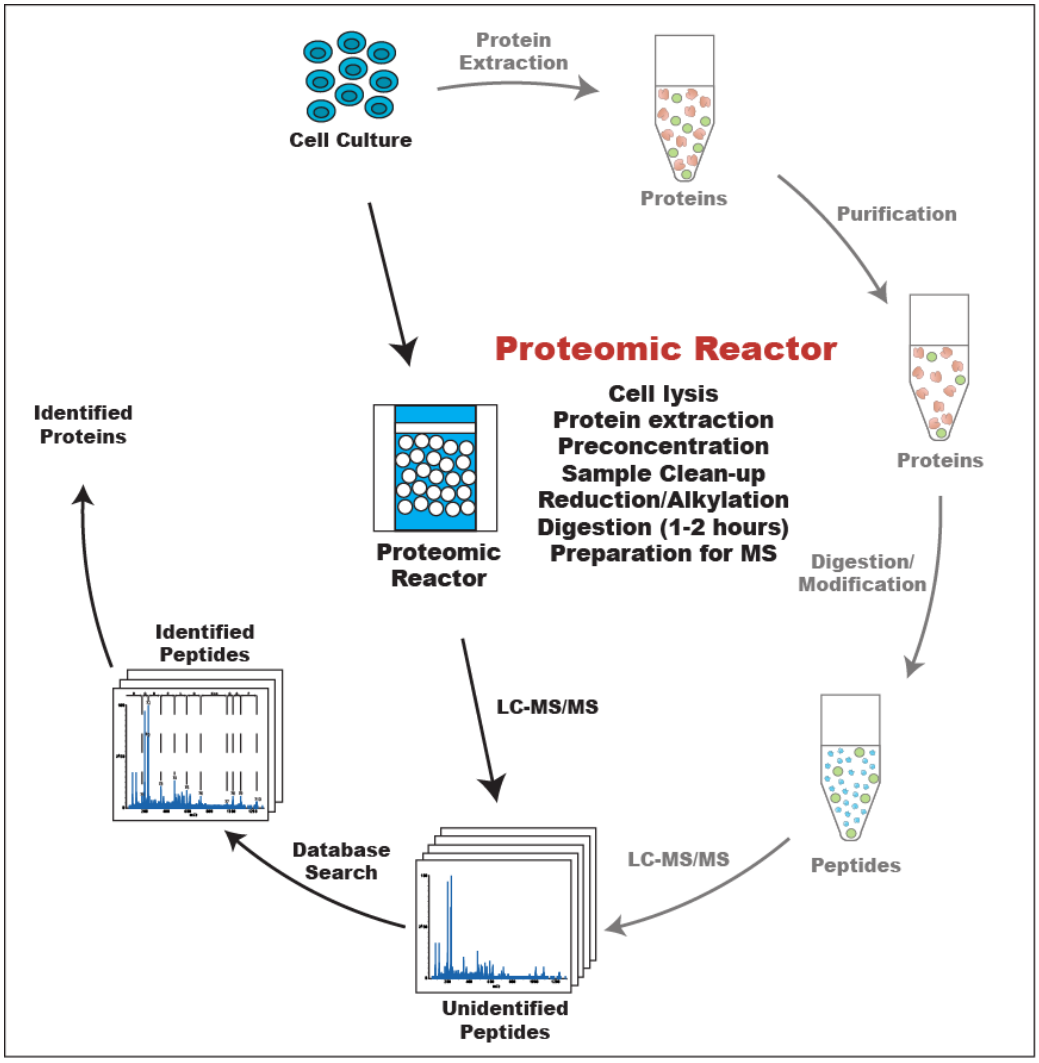

(a)

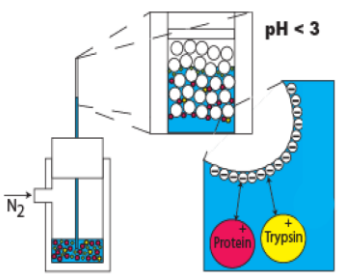

(b)

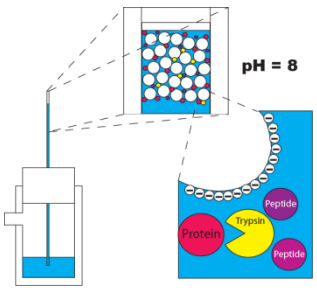

(c)

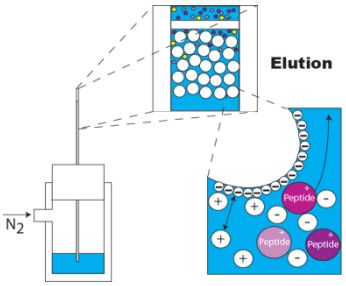

(d)

Figure 3.1.2

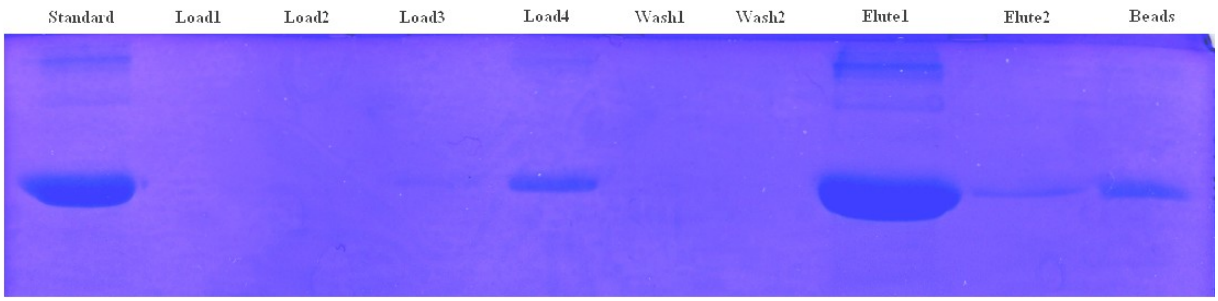
Standard
Load1
Load2
Load3
Load4
Wash1
Wash2
Elute1
Elute2
Beads

Figure 3.1.3

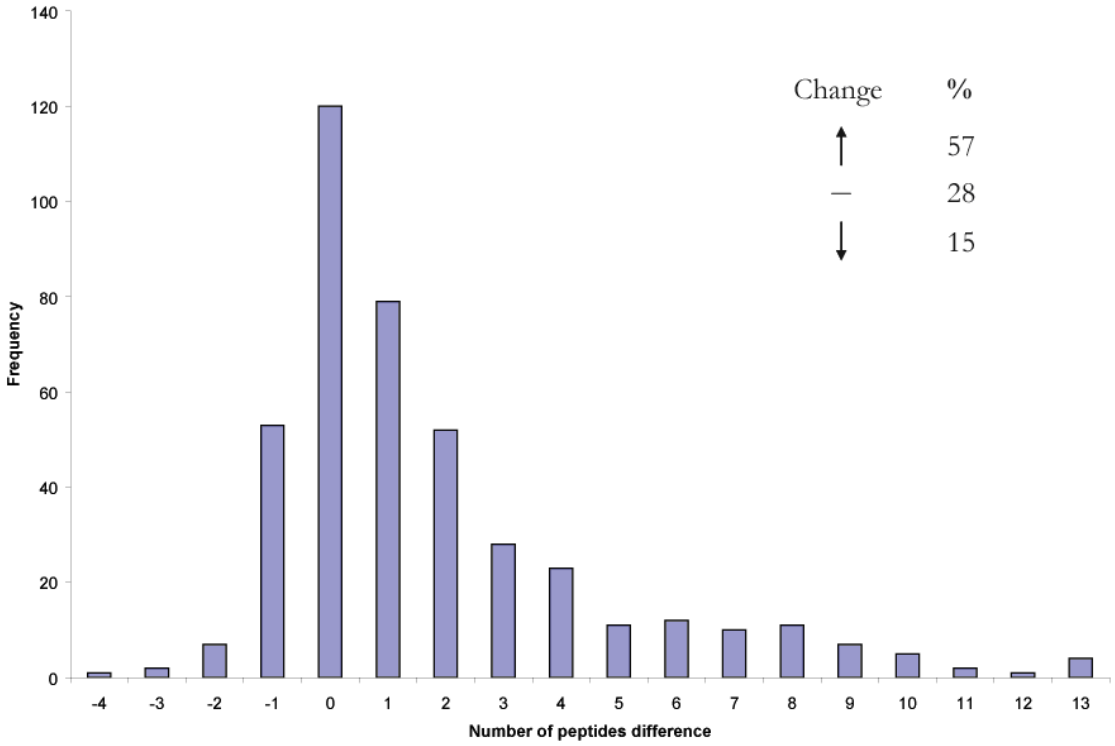
Change
%
57
28
15
Frequency
140
120
100
80
60
40
20
0
-4
-3
-2
-1
0
1
2
3
4
5
6
7
8
9
10
11
12
13
Number of peptides difference

Figure 3.1.4

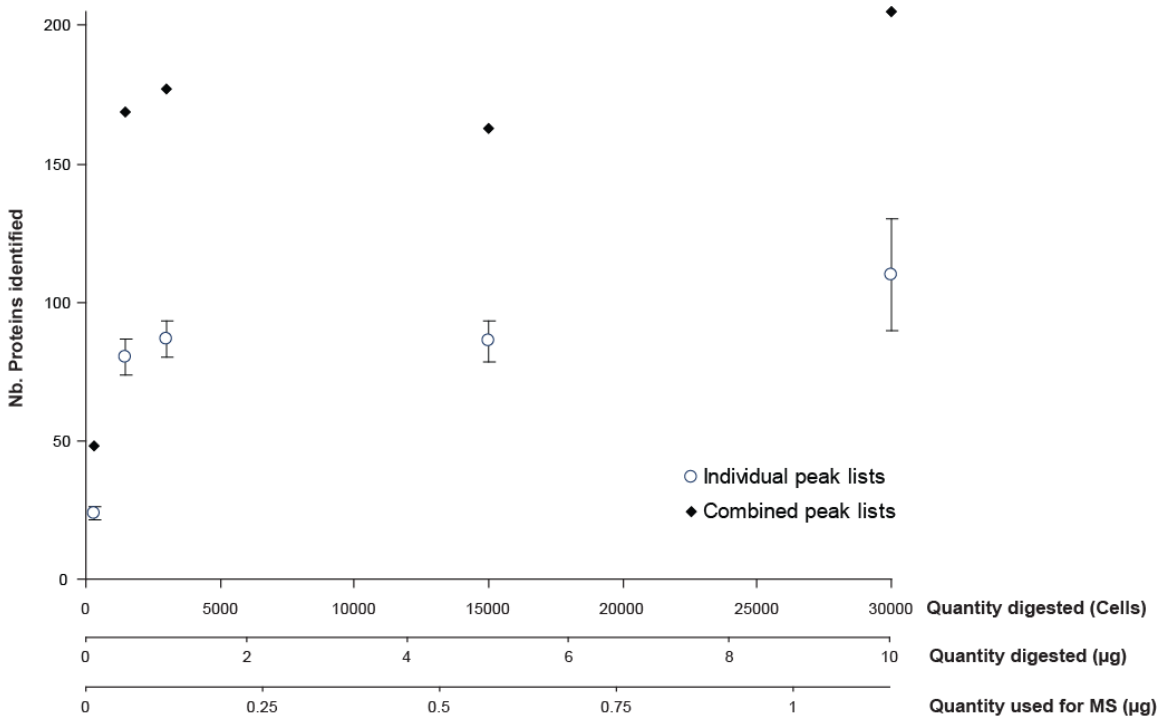
Nb. Proteins identified
200
150
100
50
0
Individual peak lists
Combined peak lists
0
5000
10000
15000
20000
25000
30000
Quantity digested (Cells)
0
2
4
6
8
10
Quantity digested (µg)
0
0.25
0.5
0.75
1
Quantity used for MS (µg)

3.2 SCX Plate Proteomic Reactor

3.2.1 Introduction:

In section 3.1, we have described a proteomic reactor technique that processes minute amounts of protein samples on SCX resins. Although the reactor can process minute amounts of protein, the serial nature of the associated protocols limits the number of samples that can be processed concomitantly.

In this section we describe the development of a 96-well plate version of the proteomic reactor which allows multiplexed processing of minute amount of protein samples. The prototypical SCX 96-well plates were graciously provided by Millipore (Billerica, MA). All of the protein processing abilities of the SCX proteomic reactor may also be carried out in the 96-well reactor plate. Ten to 200 μL of protein solution can be readily processed in each well. The protein mixtures retained in each well can then be desalted, washed, and digested; digestion is complete in about 2 hours. Afterwards, the resulting peptides are eluted from the reactor plate, collected, and analyzed by HPLC-ESI-MS/MS. Full processing of the proteins is routinely performed on the reactor plate in less than three hours, including two hours for the enzymatic digestion.

In this thesis, the performance of this 96-well plate reactor for protein binding and elution was demonstrated using the standard protein BSA. The protein digestion process on the plate reactor was tested with different amounts of protein extracts from P19 whole cell lysates. Furthermore, the 96-well plate reactor was coupled with size exclusion chromatography (SEC) fractionation to obtain a broader coverage of the proteome. The performance of the plate reactor with SEC fractionation was demonstrated using MCF7 whole cell lysate.

3.2.2 Protein sample preparation and LC-MS/MS data analysis

Cell lysates of mouse P19 testicular cancer cells and MCF-7 breast epithelial cancer cells were employed in the study. The peptides from different amounts P19 cell lysates (0.2,

0.5, 1.0, 1.5 and 2.0 μg) derived from the reactor plate were analyzed using a QSTAR Pulsar quadrupole-TOF mass spectrometer (ABI/MDS Sciex, Concord, ON). The peptides from the fractions of MCF7 cell lysates were analyzed using a LCQ Deca XP mass spectrometer (ThermoFinnigan, San Jose, CA). The MS/MS spectra were analyzed using Mascot (Matrix Science, Boston, MA), where for P19 mouse taxonomy was used and for MCF7 human taxonomy was used. The details regarding cell culture and protein extraction, LC-MS/MS system, and parameters used in Mascot search were described in chapter 2.

3.2.3 Characterization of the 96 well plate reactor

The 96 well plate reactor has a capillary (~1 mm x 1 mm (OD)) attached to the bottom of each well and ~300 nL of SCX media was immobilized inside the capillary as well as at the bottom of each well. The protein binding capacity and the reproducibility of each well were measured and examined through wells located at different positions across a 96 well reactor plate.

As shown in Figure 3.2.1, 1 ug of acidified BSA standard in 20 uL solution was introduced into the same well sequentially and the eluent (L1/L2/L3/L4) was collected separately. The retained BSA standard was eluted from the well (E1/E2) using 25 uL elution buffer (200 mM ammonium bicarbonate). The eluent collected for each step (E1/E2), along with 2 ug of BSA standard (STD) were monitored for BSA by SDS-PAGE followed by silver stain. The amount of BSA standard in each gel band was quantified using software Image J. For gel band L1, the amount of BSA standard is below the sensitivity of the software. Based on the total amount of BSA eluted in E1/E2, we found that the protein binding capacity of a well was ~ 2 μg. We further found that the protein binding capacity was consistent from well to well and protein samples can be fully recovered using 25 μL elution buffer (200 mM Ammonium bicarbonate).

3.2.4 Processing protein samples using the 96-well plate

The work-flow of sample processing through the plate reactor is shown in Figure 3.2.2 (a). The wells on the 96-well plate were first conditioned by flowing 200 µL of wash buffer (8 mM potassium phosphate buffer, 20% (v/v) acetonitrile) through them. Once the wells were conditioned, 10 to 200 µL of protein samples at pH ~ 2.0 (acidified by 5% (v/v) of 1 M H_3PO_4) were mixed with ~ 0.5 µg of trypsin (inactive at pH 2.0). The samples were applied to the wells and proteins retained by the SCX resin at the bottom of each well. The retained protein samples were then washed with 30 µL of 10 mM potassium phosphate buffer (pH 3.0) and 30 µL of deionized water successively. The wells were then dried. Cysteine reduction occurred in the wells by adding 5 µL of 100 mM dithiothreitol and 10 mM ammonium bicarbonate (Reducing Buffer) for 30 minutes, after which the wells were washed with 5 µL of 10 mM potassium phosphate buffer (pH 3.0) and dried. The digestion of the protein was achieved by introducing 5 µL of digestion/alkylation solution (10 mM iodoacetamide, 100 mM Tris-HCl, pH 8) in each well. The digestion was allowed to proceed for 2 hours, after which the resulting peptides were eluted into a collection plate using a volume of 25~30 µL of 200 mM ammonium bicarbonate (Elution Buffer). All the above processes were carried out using a MultiScreen HTS vacuum manifold.

We used a P19 cell lysate to test the analytical performance of the 96-well reactor for identifying proteins. Different amounts of protein extracts from P19 whole cell lysate (0.2, 0.5, 1.0, 1.5 and 2.0 µg) were processed on the reactor plate as described above, and the resulting peptides were eluted in 25 µL of elution buffer. Eight µL were analyzed by HPLC-ESI-MS/MS, and the resulting MS/MS were searched against the mouse taxonomy in the NCBI nr database using Mascot.

It follows that 7, 11, 19, 35, and 68 proteins were successfully identified from the different levels of the P19 cell lysate, respectively. This clearly demonstrates that the reactor plate can efficiently processes complex protein mixtures from as little as 200 ng of total protein lysate. It is worth noting that nearly 70 unique proteins were identified with high confidence from less than 2 µg of untreated P19 whole cell lysate. Considering that only 8 µL of the final elution (25 µL) was analyzed, one protein was virtually identified per less than 10 ng of total protein lysate introduced on the reactor well.

3.2.5 Coupling of the Reactor Plate with SEC

We then coupled the reactor plate with size exclusion chromatography fractionation of protein mixtures, as shown in Figure 3.2.2 (b), to create a completely gel-free technique for protein sample processing. MCF7 cell lysate was fractionated and then the 96-well plate reactor was used to process the fractions simultaneously.

The separation of 400 μg of MCF7 whole cell lysate was carried out using a 300×7.80 mm (5 μm) BioSep-SEC-S 3000 analytical column (Phenomenex, Torrance, USA). Samples were directly injected into the analytical column using a manual injection valve (Valco, Houston, TX) equipped with a 100-μL sample loop. The isocratic mobile phase (50 mM NaH_2PO_4) was delivered at 1 mL/min using an Agilent 1100 series micro-bore HPLC system (Agilent Technologies, Palo Alto, CA). The protein elution chromatography was monitored at 220 nm using a variable wavelength UV detector, and 40 fractions were collected based on the elution time. About 200 μL of eluent was collected for each fraction. 100 μL of eluent from each of the 35 selected fractions were introduced into a well on the plate reactor and processed as described before.

The chromatographic traces and the regions in which fractions were collected are illustrated in Figure 3.2.3 (a). Eight μL of the 30 μL resulting peptide solution (27% of the sample) were analyzed by HPLC-ESI-MS/MS using an LCQ Deca XP mass spectrometer. During the course of 35 LC-MS runs, multiple columns and pre-columns have been used to avoid issues associated with column aging.

The distribution of the number of proteins identified per fraction is illustrated in Figure 3.2.3(b). A total of 1,917 proteins were identified across the 35 fractions with an average of 55 proteins per fraction. From fractions B6 to C3, an average of 94 proteins per fraction was identified. Once redundancy was removed, we obtained 875 unique proteins based on a Mascot peptide threshold score of 20 and a protein score of 39. These results clearly demonstrate that protein fractionation coupled to the reactor plate greatly enhances the total number of proteins identified. Furthermore, as little as 10 ng of total protein lysate

processed in the reactor was needed for each protein identification, which represents an exquisite level of sensitivity.

3.2.6 Discussion

3.2.6.1 High Confidence in Protein Identification

The thresholds that were used for protein identification were stringent (an ion score cut off of 20 for peptides and a protein score cut off of 39 for proteins) which led to the identification of 875 unique proteins. As a result of the stringent searching criteria, 771 proteins were identified by at least two distinct peptides (with peptide ion scores higher than or equal to 20), as shown in Figure 3.2.4. For those 104 proteins identified by a single peptide, the lowest peptide score was 39. This stringent filtering is likely leading to a high false negative level. A recent bioinformatic study of search engine ion score cut-offs reported that a Mascot peptide score threshold of 20 provides a false positive rate below 1% (*25*). Using these criteria (i.e. no protein score cut-off), we identified a total of 2,683 non redundant proteins, the majority of which were single peptide identifications (1912) (Figure 3.2.4).

3.2.6.2 Efficacy of protein fractionation with SEC chromatography

Higher abundance proteins (i.e. proteins that have a higher Mascot score) tended to spread over multiple fractions, while, as expected, proteins with a smaller number of hits were found in a narrower range of fractions. Interestingly, of the 875 unique proteins identified from the combined data file, nearly 300 proteins were identified only through the combination of peptides identified in multiple fractions. This is probably related to the limited duty cycle of the HPLC-ESI-MS/MS over a 2 hour total experiment, preventing a significant number of peptides from being fragmented in each run.

3.2.6.3 Factors Limiting the Performance of the Plate Reactor

The overall performance of the plate reactor can be further improved. First, the binding capacity of each well on the plate is 2 μg or less of protein. Even though 400 μg of MCF7 protein lysate were separated by size exclusion chromatography, no more than 70 μg of the protein samples were loaded on the reactor plate for the 35 fractions. Hence, increasing the well capacity or the number of fractions would increase the total sample load. Second, to avoid saturating the pre-column, only 8 μL out of the 30 μL resulting peptides from each reactor plate well were injected on the HPLC-ESI-MS/MS for protein identification. Increasing the HPLC capacity or performing multiple runs from the same sample would further enhance the performance (*26-27*). Third, rapid 2 hour gradients were performed on the HPLC; increasing the duration of the gradient will increase the number of MS/MS generated. Finally, more sensitive mass spectrometers with faster duty cycles should also improve the performance of this approach (*28*). We recently demonstrated that changing the mass spectrometer from an LCQ to an LTQ ion trap mass spectrometer can double the number of proteins identified from one fraction, all other processing methods being the same (data not shown).

3.2.7 Conclusions

In summary, we established a completely gel free approach for large scale protein identification using a 96-well plate reactor to process 35 fractions of a size exclusion chromatographic separation of MCF7 lysate. Under stringent criteria, a total of 875 unique proteins were identified. A more relaxed ion score cutoff level associated with a 1% false positive rate resulted in the identification of 2,683 unique proteins. This novel approach proves to be very efficient and sensitive in processing minute amounts of protein samples, demonstrated by one protein being identified per 3-10 ng of total protein lysate loaded on the reactor plate.

Figure Captions

Figure 3.2.1. Characterization of the 96-well SCX plate reactor. For L1/L2/L3/L4, 1 μg of acidified BSA standard in 20 μL solution was introduced into a well sequentially and the eluent was collected separately. For E1/E2, the retained BSA standard was eluted from the well using 25 μL elution buffer (200 mM ammonium bicarbonate). The eluent collected for each step, along with 2 μg of BSA standard (STD) were monitored for BSA by SDS-PAGE followed by silver stain. The amount of BSA standard in each gel band was quantified using software ImageJ. For L1, the amount of BSA standard is below the sensitivity of the software.

Figure 3.2.2 (a). The work flow of sample processing through the plate reactor. Details are provided in the experimental section. **(b). The coupling of the reactor plate with size exclusion chromatographic fractionation of proteins.** Four hundred μg of MCF7 whole cell lysate was separated through size exclusion chromatography. Thirty five fractions were collected and half of each fraction was introduced into a well on the reactor plate and processed as described in the experimental section. The resulting peptides were eluted in a volume of 30 μL, from which 8 μL was introduced into a LC-ESI-MS/MS system.

Figure 3.2.3 (a). The size exclusion chromatographic separation of MCF7 whole cell lysate recorded at 220 nm using a variable wavelength detector. For each fraction, around 200 μL was collected for a time interval of 12 seconds (0.20 min). **(b) The corresponding total number of proteins identified in each of these 35 fractions.** From fractions B6 to C2, an average of 94 proteins per fraction was identified.

Figure 3.2.4. The distribution of proteins identified as a function of numbers of unique peptides. Eight hundred seventy five unique proteins were identified; 104 proteins were identified with a single peptide, and 771 proteins were identified with at least two unique peptides when the Mascot protein and peptide score thresholds were 39 and 20, respectively. When the protein score threshold was removed, 2683 unique proteins were identified; 1912 of these were identified with a single peptide. Reprinted with permission from Analytical Chemistry. Copyright © 2007, American Chemical Society.

Figure 3.2.1

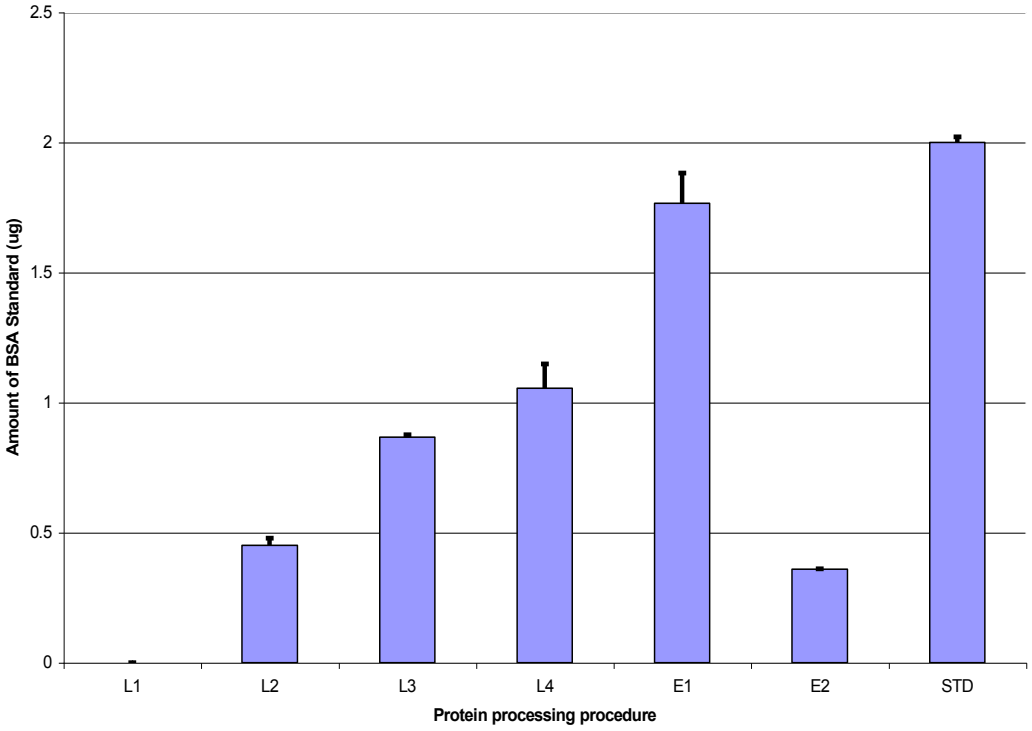
2.5
2
1.5
1
0.5
0
Amount of BSA Standard (ug)
L1
L2
L3
L4
E1
E2
STD
Protein processing procedure

Figure 3.2.2

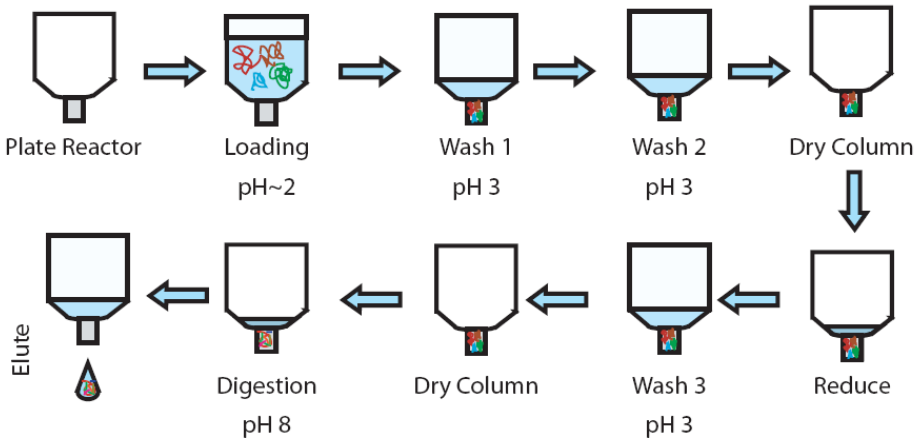

(a)

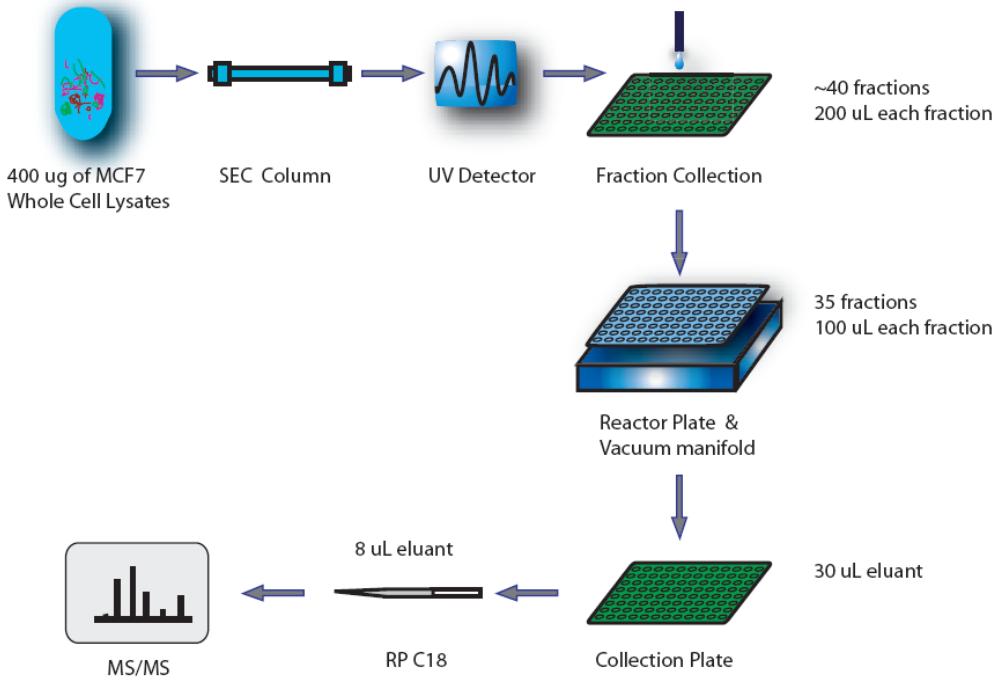

(b)

Figure 3.2.3

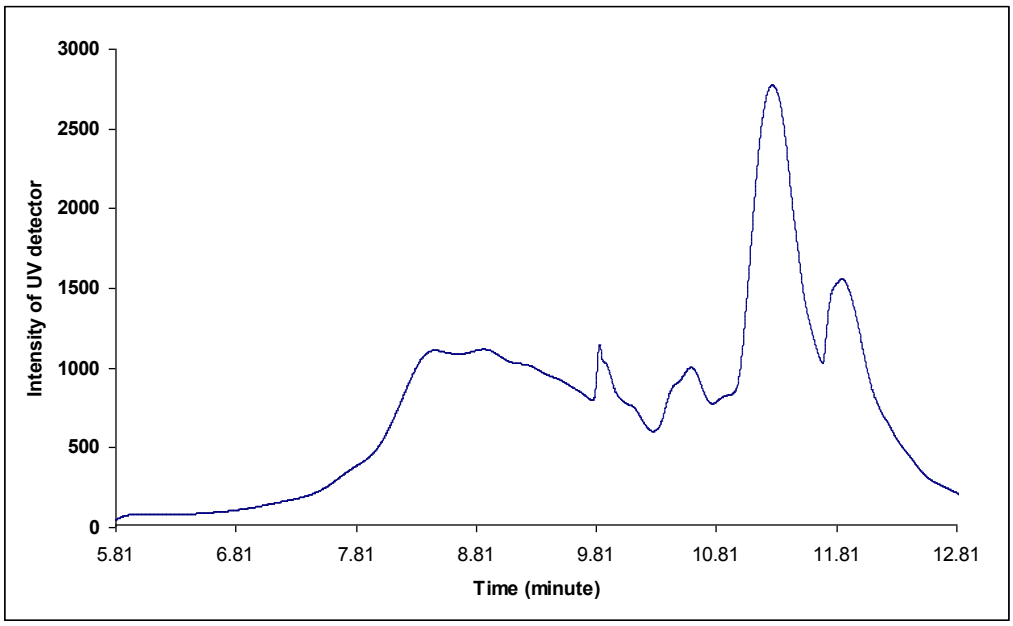

(a)

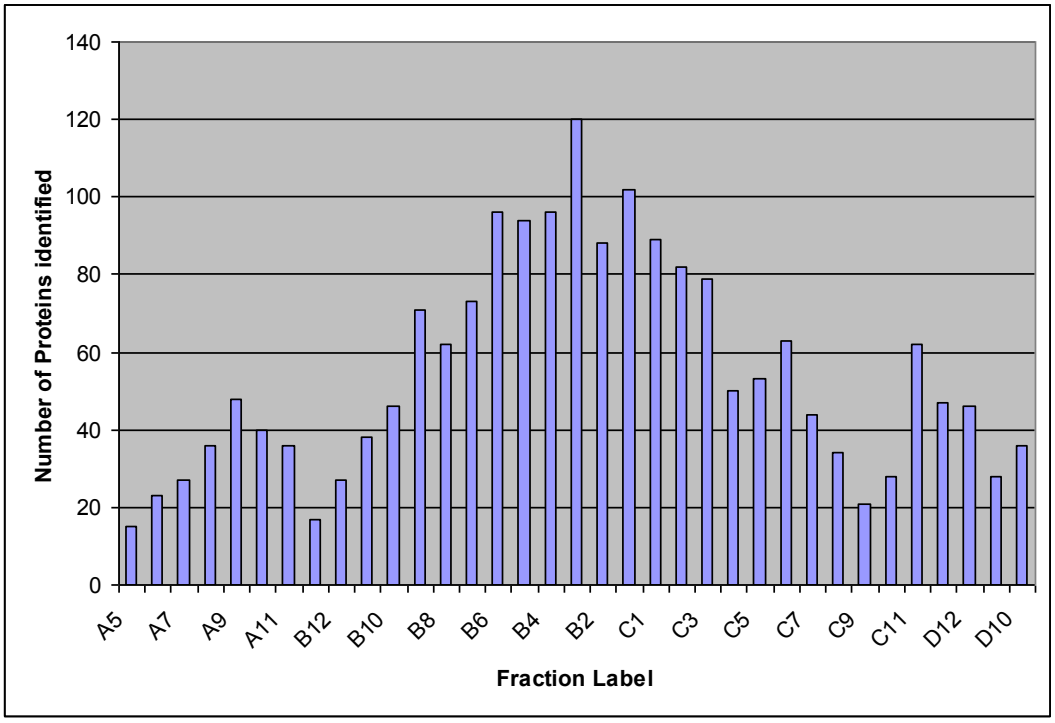

(b)

Figure 3.2.4

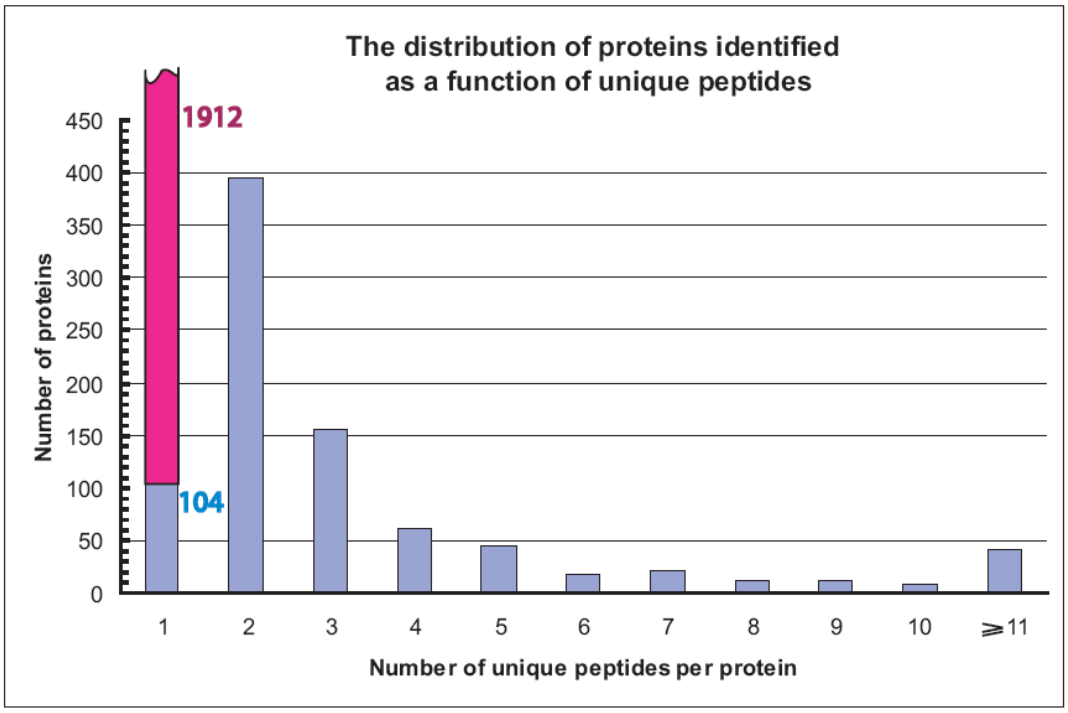
The distribution of proteins identified
as a function of unique peptides
1912
104
Number of proteins
450
400
350
300
250
200
150
100
50
0
1
2
3
4
5
6
7
8
9
10
⩾11
Number of unique peptides per protein

3.3 Developing a SAX Proteomic Reactor

3.3.1 Introduction

Anion exchangers can also be used to capture proteins. For example, in the literature, strong anion exchange (SAX) has been reported in phosphopeptide studies; whereas, weak cation exchange (WCX) and weak anion exchange (WAX) have been used in few proteomic experiments (*29-36*).

Important features of a proteomic reactor include an ability to modulate the affinity of proteins and peptides for ion exchange material, and to modulate the activity of enzymes while keeping the volume as small as possible. Changing the pH and ionic strength of buffers modulates the affinity of proteins for the ion exchange material and activity of enzymes; whereas, the volume of the sample can be minimized using microfluidic designs.

Outside their isoelectric points, proteins and peptides are charged and can form ionic bonds with cation or anion exchange materials. Fortunately, the theoretical pI distribution of the proteome shows that more than 99% of proteins are in the pI range of 2.5~12 (99.8% in Saccharomyces Genome Database; 99.4% in IPI human 3.53 database; 99.6% in IPI mouse 3.53 database). Furthermore, over 96% of the predicted peptides resulting from the *in silico* proteome digestion either by trypsin, chymotrypsin or Glu-C have a pI within the range of 2.5~12. This means that the complete proteome can be captured on the SCX proteomic reactor as the pH is below 2.5, or retained on the SAX proteomic reactor when the pH is above 12.

The selection of SCX and SAX material for the proteomic reactor needs to take into account the extreme pH (2.5 and 12) used in the processes. For example, the routinely used silica-based SAX and SCX beads cannot tolerate a high pH. Instead, therefore, we used the rigid macroporous polystyrene-divinylbenzene (PS/DVB) polymer matrix derivatized with chemically stable quaternized poly (ethylenimine) PEI ($N(CH_3)_3^+$) groups to fabricate the SAX reactor and sulfate groups (SO_3^-) for the SCX reactor. These materials are stable at extreme pH (pH range from 1 to 14).

Although our initial design of the proteomic reactor focused solely on the use of trypsin to digest proteins, other proteolytic enzymes have been used in proteomics as well. We are particularly interested in proteolytic enzymes that are active at physiological pH and are inactive but stable at lower or higher pH. Some enzymes that are used in proteomics such as Proteinase K (*18*) and pepsin (*37*) only function at high or low pH. Other enzymes such as Lys-C, Arg-C, and Asp-N (*38-39*) may also be suitable. One disadvantage of using these enzymes is the relatively high costs. Chymotrypsin and Glu-C are suitable enzymes because of their optimal pH for protein digestion (pH 8.0) and their low prices.

In this section, we demonstrate the development of the SAX proteomic reactor using a standard protein mixture, where trypsin was used as the enzyme. We then demonstrated the performance of the SAX proteomic reactors using yeast lysates in comparison to SCX-based proteomic reactors. The data revealed that the SAX proteomic reactors enrich different peptides than SCX-based proteomic reactors. Therefore, the combination of SCX and SAX proteomic reactors increased the number of identified peptides and proteins by 50%.

3.3.2 Protein samples preparation and LC-MS/MS data analysis

Protein extract from yeast and standard proteins ovalbumin (A7641), fetuin A (F3004), serum albumin (A9056), carbonic anhydrase 2 (C3934), serotransferrin (T1408) and lysozyme C (L7651) were used in the study. Yeast samples and the standard protein mixture were processed with both SAX and SCX proteomic reactor, where trypsin was used for protein digestions. The resulting peptides were analyzed with a LTQ linear ion trap mass spectrometer (Thermo Electron, Waltham, MA). The MS/MS spectra from the yeast sample were searched against a database consisting of the Saccharomyces Genome Database (http://www.yeastgenome.org/, 6716 protein entries, released December 2, 2008) and the reverse sequence of all protein entries. Details were described in chapter 2.

3.3.3 Construction and characterization of SAX proteomic reactor

A capillary tubing (200-μm i.d.) was used to construct the proteomic reactor. Briefly, a frit was formed at one end of fused silica tubing using a mixture of potassium silicate (KASIL 1, PQ Corporation, Valley Forge, PA) and formamide with a volume ratio of 11:2. After leaving the fritted tubing at ambient condition for at least 24 hours, a 5 cm long reactor was constructed by pressure packing (400 psi) a slurry of SAX beads (10 μm, Polymer Laboratories, Varian, Inc.) from the open end of the capillary tubing.

The capability of the novel SAX proteomic reactor to retain proteins was evaluated using a mixture of protein standards, including ovalbumin (pI: 5.19), fetuin A (pI: 5.26), serum albumin (pI: 5.82, carbonic anhydrase 2 (pI: 6.41), serotransferrin (pI: 6.75) and Lysozyme C (pI: 9.36). These protein standards were present at equimolar concentration.

Two and 10 μg of the protein standard mixture, alkalified with ammonium hydroxide (pH 12), was loaded onto a SAX reactor, respectively. The SAX reactor was then washed with an alkaline buffer (3 N ammonium hydroxide, pH 12, 20 μL) and dried. The retained proteins were then eluted with acidic buffer (0.5% formic acid (v/v), pH 2.5). The flow-through solutions of each step were collected for SDS-PAGE analysis. There are no protein bands detected by SDS-PAGE and colloidal blue staining (nanogram-level sensitivity) in the flow through and wash fractions at 10 μg and 2 μg sample amounts (Figure 3.3.1). The observation indicates that the protein samples are retained by the SAX reactor at pH 12 and are not affected by the washing step. The pattern of elute fraction collected from SAX reactor is the same with that of the control, suggesting that all the protein standards with different pIs can be effectively eluted with the acidic buffer at pH 2.5, with almost 100% recovery.

3.3.4 Development of a SAX reactor using a mixture of standard proteins

The performance of the novel SAX proteomic reactor was first evaluated using a mixture of protein standards, as described in the previous section.

As shown in Figure 3.3.2, 10 μg of protein samples and trypsin (4:1, w/w) were alkalified with ammonium hydroxide (pH 12) prior to being loaded at 150 psi onto the SAX reactors. The SAX reactor was then washed with an alkaline buffer (20 μL of 3N ammonium hydroxide, pH 12,) and dried. The proteins retained on the reactors were then subjected to disulfide bond reduction by introducing the reduction buffer (50 mM dithiothreitol, 20 mM ammonium bicarbonate, pH 8.0) into the reactor, which lasts for 30 min at room temperature. The reactors were then washed with 5 μL of 20 mM ammonium bicarbonate buffer (pH 8.0) and dried. The reduced proteins were then subjected to simultaneous alkylation and enzymatic digestions by introducing the digestion buffer (10 mM iodoacetamide, 20 mM ammonium bicarbonate, pH 8.0) into the reactors for 2 h at 37 °C. The resulting peptides were eluted with acidic buffer (0.5% formic acid (v/v), pH 2.5).

The mixture of protein standards was also processed with SCX proteomic reactors and the conventional in-solution digestion, as described in the experimental section. Tryptic digestions of 10 μg of protein samples were repeated 2 times for each of the 3 protein digestion methods and an equivalence of 1 μg of initial protein sample was used for each LC-MS/MS analysis. The proteins and peptides identified were compared.

All six proteins were identified following digestion on the SAX reactor using as little as 1 μg of the protein mixture (Table 3.3.1). The SAX reactor showed a slight improvement in the number of identified peptides compared to the SCX reactor and in-solution digestion, but overall the SAX and SCX reactors had similar identification capabilities at the unique peptide level. The SAX reactor also showed higher sequence coverage of two standard proteins (ovalbumin and serotransferrin) than SCX reactor. For the SAX and SCX reactors, the overlap between unique peptides found in the two repeated runs was up to 90%. This supports the reproducibility of the performance of SAX and SCX reactors. Overall, these results show that the SAX reactor is suitable for in-reactor digestions using the procedures mentioned above.

3.3.5 A comparison of the performance of SAX and SCX reactors using trypsin for processing yeast samples

The performance of the SAX and SCX proteomic reactors were further compared for analysis of the yeast proteome. 2 μg of yeast lysates were processed with SAX and SCX proteomic reactors in triplicate, respectively. The data obtained was shown in Table 3.3.2. The number of identified unique peptides using either SAX or SCX reactor is similar, suggesting SAX is also suitable for processing complex proteomic samples. It is interesting to notice that 24% more unique proteins (286 vs. 230) were identified on the SAX reactor compared to the SCX reactor, although they identified an almost equal amount of unique peptides.

We further compared the unique peptides and proteins that were identified on the SCX and SAX proteomic reactors (Figure 3.3.3A and B). Both SAX and SCX reactors showed high reproducibility in yeast peptide/protein identifications, where more than 60% unique peptides and 65% proteins overlapped between different runs for each approach. Although the total number of unique peptides observed from SCX and SAX are similar, only around 40% of the identified peptides overlapped (Figure 3.3.3A). In addition, the overlap in proteins identified with SCX and SAX reactors is also low (Figure 3.3.3B).

Figure 3.3.4a shows the overlap in unique peptides and proteins between the combined data of three LC-MS/MS runs using SAX and SCX reactors. It can be seen that the unique peptides and proteins only identified by SAX reactor are 51% (376/733) and 49% (113/230) of the total unique peptides and proteins identified by SCX reactor. This suggests that combining the SAX and SCX reactor increases the number of unique peptides and proteins identified by 50%. Zooming on two proteins (YGR009C, YHR174W) identified from both SAX and SCX reactors (Figure 3.3.4b), it is clear that the unique peptides identified from SAX and SCX reactor were normally mapped to different sequence locations in these proteins. Therefore, extensive sequence coverage can be obtained by using both the SAX and SCX proteomic reactors in combination.

Figure 3.3.5 further delineated the theoretical pI distributions of the identified unique peptides from both the SAX and SCX reactors. The unique peptides were grouped according to their theoretical pI that was calculated by Compute pI (http://web.expasy.org/compute_pi/). It can be seen that the majority of the peptides obtained from both the SAX and SCX reactors have pIs lower than 7. Differences in the pI distribution were observed between the SAX and SCX proteomic reactor approaches, where the SAX reactor approach identified more acidic peptides (~9%), although the total number of unique peptides identified was similar (Table 3.3.2). At the protein level, among the 286 proteins identified with the SAX reactor approach, around 70% exhibited pIs below 7; while among the 230 proteins identified with the SCX reactor approach, around 56% had pIs below 7. In other words, the SAX reactor identified 14% more acidic proteins than the SCX reactor. These data indicated that the SAX reactor was biased for relatively acidic proteins/peptides and the SCX reactor for relatively basic protein/peptides.

3.3.6 Conclusions

Our new version of the proteomic reactor, the SAX reactor, is capable of identifying a greater number of acidic peptides and proteins compared to SCX proteomic reactor. The data also demonstrated that the SAX reactor was complementary to the SCX proteomic reactor for peptide and protein identification. The SAX reactor was biased for relatively acidic proteins/peptides and the SCX reactor for relatively basic protein/peptides. The combination of the two proteomic reactors leads to an overall increase in the number of unique peptides and proteins identified.

3.4 Chapter Summary

In summary, we developed different versions of microfluidic proteomic reactors, namely, the SCX proteomic reactor, the 96-well SCX plate reactor, and the SAX proteomic reactor, for processing complex protein samples. These microfluidic proteomic reactors provided an integrated platform for efficiently and reliably processing minute amounts of

protein samples. The reactor digestion technique led to approximately 10 times more protein identifications than the in-solution digestion technique. In addition, the 96-well SCX plate reactor was suitable for simultaneously processing multiplexed protein samples in parallel, and the SAX reactor was found to be complementary to the SCX proteomic reactor for peptide and protein identification. The combination of the SCX and SAX proteomic reactors would lead to an overall increase of unique peptides and proteins identified.

Table 3.3.1 Protein/peptide identification and protein sequence coverage obtained as using SAX and SCX reactors to process standard protein mixture

	Results			Protein sequence coverage					
Digestion methods	Peptides	Unique Peptides	Proteins	Ovalbumin (pI: 5.19) (42.9 kDa)	Fetuin A (pI: 5.26) (38.4 kDa)	Serum albumin (pI: 5.82) (69.3 kDa)	Carbonic anhydrase 2 (pI:6.41) (29.1 kDa)	Serotransferrin (pI: 6.75) (77.8 kDa)	Lysozyme C (pI: 9.36) (16.2 kDa)
SAX 1	293	105	6	63.7%	30.6%	50.9%	69.6%	60.8%	44.9%
SAX 2	305	107	6	68.7%	35.4%	51.6%	60.0%	59.5%	40.8%
SCX 1	246	111	6	58.0%	28.1%	47.0%	67.3%	54.3%	34.7%
SCX 2	225	113	6	46.4%	34.3%	52.1%	64.2%	54.7%	42.9%
Solution1	229	94	6	41.2%	38.4%	54.0%	63.1%	42.8%	59.9%
Solution2	194	98	6	48.5%	38.4%	51.7%	71.2%	48.0%	59.2%

Table 3.3.2 Summary of the number of unique peptides and proteins identified from yeast sample using the SAX and SCX reactors.

	SAX Reactor				SCX Reactor			
	1st run	2nd run	3rd run	combined	1st run	2nd run	3rd run	combined
Peptides	1397	1431	1542	4370	1694	1516	1539	4749
Unique Peptides	514	533	539	727	550	523	521	733
Proteins	210	230	220	286	189	178	174	230

Figure Captions

Figure 3.3.1 SDS-PAGE analysis of flow-through, wash and elute fractions of SAX reactor using standard proteins. Total is the total standard protein mixture as a control; FT is the flow-through fraction (at pH 12); Wash is the wash fraction (at pH 12); Elute is the elute fraction (at pH 2.5). Adapted with permission from Analytical and Bioanalytical Chemistry. Copyright © 2010, Springer.

Figure 3.3.2 Flowchart of protein processing steps using SAX proteomic reactor. (a) Protein sample preparation. (b) SAX reactor: (1) Protein sample was mixed with trypsin (4/1, w/w), alkalified by adding ammonium hydroxide and loaded onto the SAX reactor; (2) after washing and drying, the reduction buffer (50 mM dithiothreitol, 20 mM ammonium bicarbonate, pH 8.0) was introduced onto the reactor, and the proteins present on the reactor were subjected to disulfide bond reduction; after another washing (5 μL of 20 mM ammonium bicarbonate, pH 8.0) and drying, the digestion buffer (10 mM iodoacetamide, 20 mM ammonium bicarbonate, pH 8.0) was introduced onto the reactor to perform alkylation and tryptic digestion; (3) the resulting peptides were then eluted with acid buffers (0.5% formic acid, pH 2.5). (c) The resulting peptides from the SAX reactor were analyzed by LC-MS/MS. Adapted with permission from Analytical and Bioanalytical Chemistry. Copyright © 2010, Springer.

Figure 3.3.3. Reproducibility of unique peptide (a) and protein (b) identified using SAX and SCX reactors. The unique peptides and proteins identified were compared between experiments using the same type of proteomic reactor technique (SCX or SAX) or different types of proteomic reactor techniques (SCX or SAX). Both SAX and SCX reactors showed high reproducibility in peptide/protein identification between different runs using the same type of proteomic reactor technique (SCX or SAX). The overlap in peptide/proteins

identification using different types of proteomic reactor techniques (SCX or SAX) was low. Adapted with permission from Analytical and Bioanalytical Chemistry. Copyright © 2010, Springer.

Figure 3.3.4. (a) Overlap between unique peptides and proteins identified with SAX and SCX reactors. (b) Differences in sequence coverage for protein YJR009C and YHR174W identified with SAX reactor (blue) and SCX reactor (red). Adapted with permission from Analytical and Bioanalytical Chemistry. Copyright © 2010, Springer.

Figure 3.3.5. Theoretical p*I* distributions of unique peptides and proteins identified by SAX and SCX reactors. *X*-axis: theoretical p*I* regions; *Y*-axis: percentage of identified unique peptides in a given p*I* region. Using the combined data from three LC-MS/MS runs. Adapted with permission from Analytical and Bioanalytical Chemistry. Copyright © 2010, Springer.

Figure 3.3.1

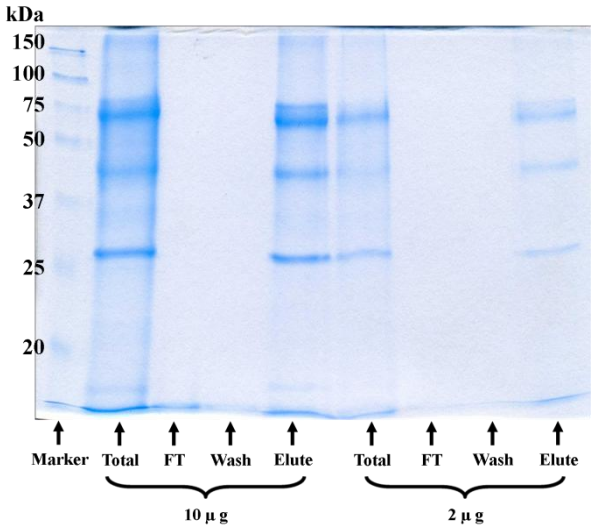
kDa
150
100
75
50
37
25
20
Marker
Total
FT
Wash
Elute
Total
FT
Wash
Elute
10 µg
2 µg

Figure 3.3.2

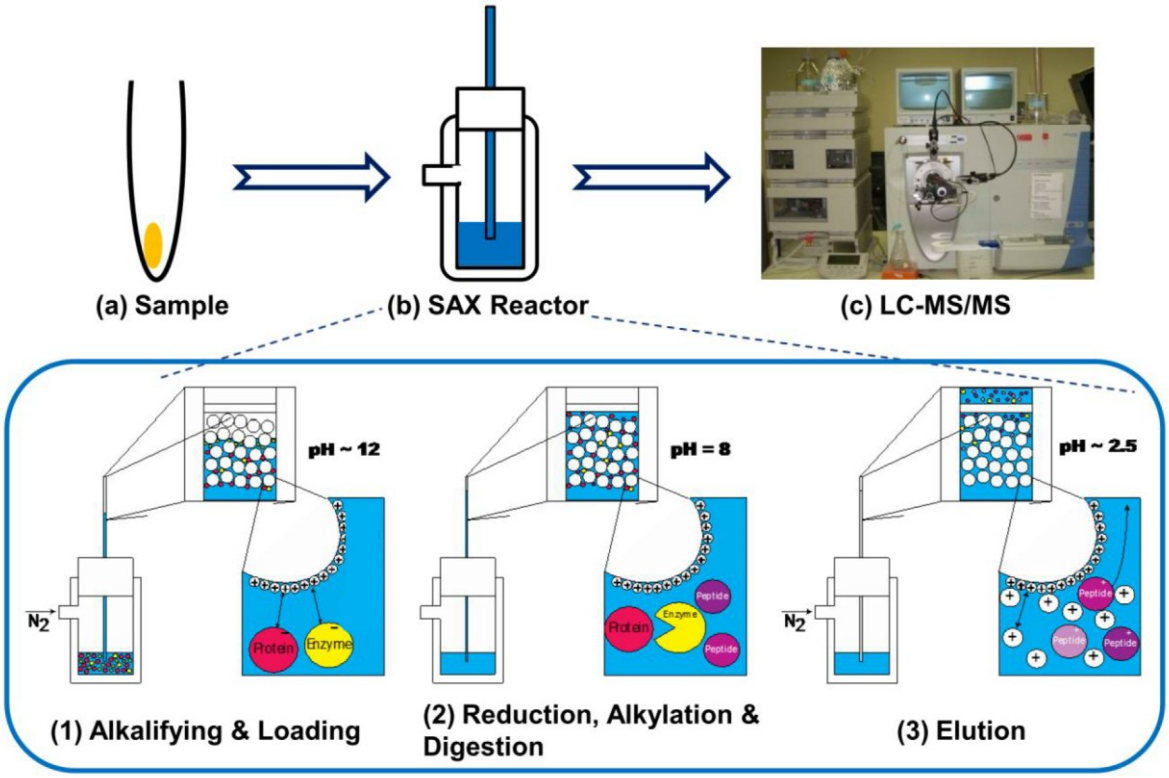
(a) Sample
(b) SAX Reactor
(c) LC-MS/MS
pH ~ 12
pH = 8
pH ~ 2.5
N2
Protein
Enzyme
Peptide
(1) Alkalifying & Loading
(2) Reduction, Alkylation & Digestion
(3) Elution

Figure 3.3.3

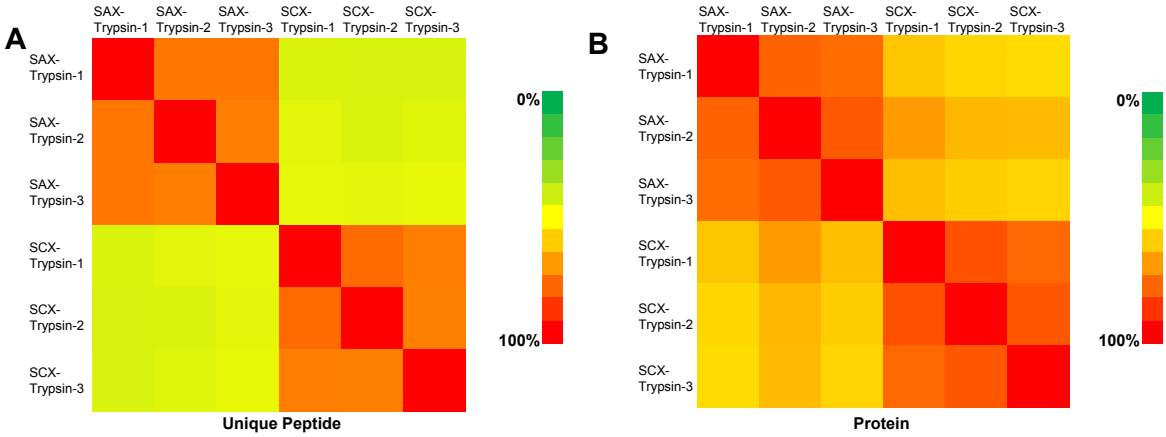
A
SAX-Trypsin-1
SAX-Trypsin-2
SAX-Trypsin-3
SCX-Trypsin-1
SCX-Trypsin-2
SCX-Trypsin-3
0%
100%
Unique Peptide
B
SAX-Trypsin-1
SAX-Trypsin-2
SAX-Trypsin-3
SCX-Trypsin-1
SCX-Trypsin-2
SCX-Trypsin-3
0%
100%
Protein

Figure 3.3.4

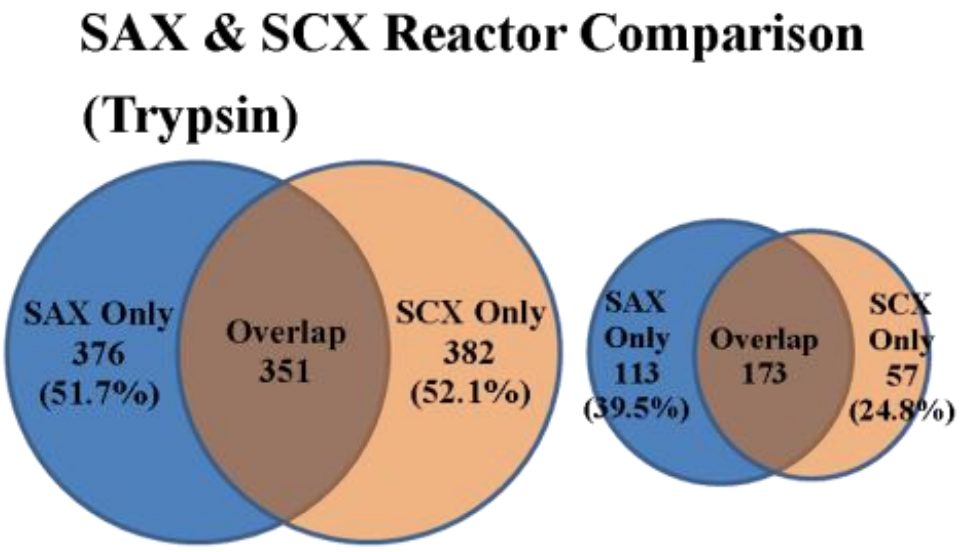

(a)

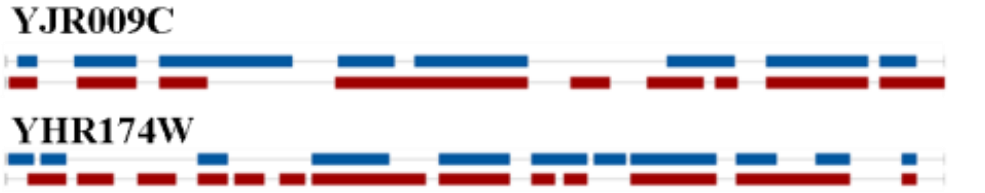

(b)

Figure 3.3.5

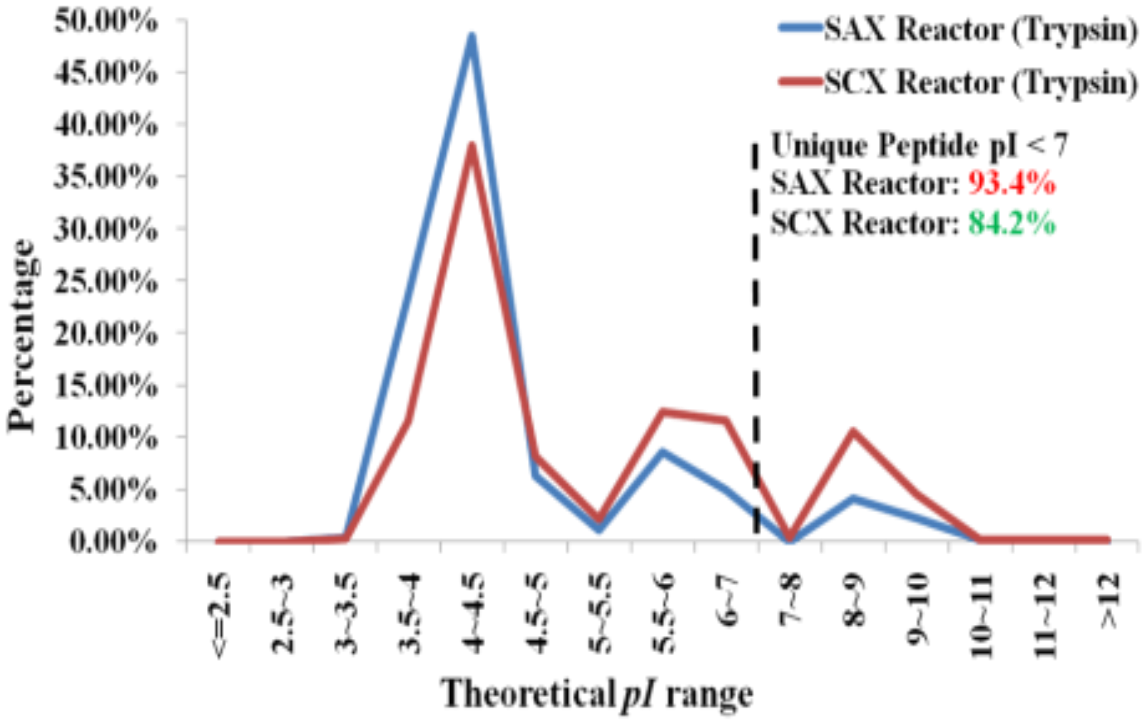
SAX Reactor (Trypsin)
SCX Reactor (Trypsin)
Unique Peptide pI < 7
SAX Reactor: 93.4%
SCX Reactor: 84.2%
Percentage
50.00%
45.00%
40.00%
35.00%
30.00%
25.00%
20.00%
15.00%
10.00%
5.00%
0.00%
<=2.5
2.5~3
3~3.5
3.5~4
4~4.5
4.5~5
5~5.5
5.5~6
6~7
7~8
8~9
9~10
10~11
11~12
>12
Theoretical pI range

References

1. Aebersold, R., and Mann, M. (2003) Mass spectrometry-based proteomics, *Nature 422*, 198-207.
2. Lambert, J. P., Ethier, M., Smith, J. C., and Figeys, D. (2005) Proteomics: from gel based to gel free, *Anal Chem 77*, 3771-3787.
3. Steen, H., and Mann, M. (2004) The ABC's (and XYZ's) of peptide sequencing, *Nat Rev Mol Cell Biol 5*, 699-711.
4. Romijn, E. P., Krijgsveld, J., and Heck, A. J. (2003) Recent liquid chromatographic-(tandem) mass spectrometric applications in proteomics, *J Chromatogr A 1000*, 589-608.
5. Hamdan, M., and Righetti, P. G. (2003) Assessment of protein expression by means of 2-D gel electrophoresis with and without mass spectrometry, *Mass Spectrom Rev 22*, 272-284.
6. Aebersold, R. H., Leavitt, J., Saavedra, R. A., Hood, L. E., and Kent, S. B. (1987) Internal amino acid sequence analysis of proteins separated by one- or two-dimensional gel electrophoresis after in situ protease digestion on nitrocellulose, *Proc Natl Acad Sci U S A 84*, 6970-6974.
7. Wilm, M., Shevchenko, A., Houthaeve, T., Breit, S., Schweigerer, L., Fotsis, T., and Mann, M. (1996) Femtomole sequencing of proteins from polyacrylamide gels by nano-electrospray mass spectrometry., *Nature 379*, 466-469.
8. Havlis, J., and Shevchenko, A. (2004) Absolute quantification of proteins in solutions and in polyacrylamide gels by mass spectrometry, *Anal Chem 76*, 3029-3036.
9. Lambert, J. P., Ethier, M., Smith, J. C., and Figeys, D. (2005) Proteomics: from gel based to gel free., *Anal Chem. 15*, 3771-3787.
10. Ihling, C., and Sinz, A. (2005) Proteome analysis of Escherichia coli using high-performance liquid chromatography and Fourier transform ion cyclotron resonance mass spectrometry, *Proteomics 5*, 2029-2042.
11. Martosella, J., Zolotarjova, N., Liu, H., Nicol, G., and Boyes, B. E. (2005) Reversed-phase high-performance liquid chromatographic prefractionation of immunodepleted human serum proteins to enhance mass spectrometry identification of lower-abundant proteins, *J Proteome Res 4*, 1522-1537.

12. Moritz, R. L., Clippingdale, A. B., Kapp, E. A., Eddes, J. S., Ji, H., Gilbert, S., Connolly, L. M., and Simpson, R. J. (2005) Application of 2-D free-flow electrophoresis/RP-HPLC for proteomic analysis of human plasma depleted of multi high-abundance proteins, *Proteomics 5*, 3402-3413.
13. Burggraf, D., Weber, G., and Lottspeich, F. (1995) Free flow-isoelectric focusing of human cellular lysates as sample preparation for protein analysis, *Electrophoresis 16*, 1010-1015.
14. Linke, T., Ross, A. C., and Harrison, E. H. (2006) Proteomic analysis of rat plasma by two-dimensional liquid chromatography and matrix-assisted laser desorption ionization time-of-flight mass spectrometry, *J Chromatogr A*.
15. Dai, J., Shieh, C. H., Sheng, Q. H., Zhou, H., and Zeng, R. (2005) Proteomic analysis with integrated multiple dimensional liquid chromatography/mass spectrometry based on elution of ion exchange column using pH steps, *Anal Chem 77*, 5793-5799.
16. Jessani, N., Niessen, S., Wei, B. Q., Nicolau, M., Humphrey, M., Ji, Y., Han, W., Noh, D. Y., Yates, J. R., 3rd, Jeffrey, S. S., and Cravatt, B. F. (2005) A streamlined platform for high-content functional proteomics of primary human specimens, *Nat Methods 2*, 691-697.
17. Washburn, M. P., Wolters, D., and Yates, J. R. r. (2001) Large-scale analysis of the yeast proteome by multidimensional protein identification technology, *Nat Biotechnol. 19*, 242-247.
18. Wu, C. C., MacCoss, M. J., Howell, K. E., and Yates, J. R., 3rd. (2003) A method for the comprehensive proteomic analysis of membrane proteins, *Nat Biotechnol 21*, 532-538.
19. Duan, J., Sun, L., Liang, Z., Zhang, J., Wang, H., Zhang, L., Zhang, W., and Zhang, Y. (2006) Rapid protein digestion and identification using monolithic enzymatic microreactor coupled with nano-liquid chromatography-electrospray ionization mass spectrometry, *J Chromatogr A 1106*, 165-174.
20. Lim, L. W., Tomatsu, M., and Takeuchi, T. (2006) Development of an on-line immobilized-enzyme reversed-phase HPLC method for protein digestion and peptide separation, *Anal Bioanal Chem*.

21. Slysz, G. W., and Schriemer, D. C. (2003) On-column digestion of proteins in aqueous-organic solvents, *Rapid Commun Mass Spectrom 17*, 1044-1050.
22. Slysz, G. W., and Schriemer, D. C. (2005) Blending protein separation and peptide analysis through real-time proteolytic digestion, *Anal Chem 77*, 1572-1579.
23. Craft, D., Doucette, A., and Li, L. (2002) Microcolumn capture and digestion of proteins combined with mass spectrometry for protein identification, *J Proteome Res 1*, 537-547.
24. Craft, D., and Li, L. (2005) Integrated sample processing system involving on-column protein adsorption, sample washing, and enzyme digestion for protein identification by LC-ESI MS/MS, *Anal Chem 77*, 2649-2655.
25. Kapp, E. A., Schutz, F., Connolly, L. M., Chakel, J. A., Meza, J. E., Miller, C. A., Fenyo, D., Eng, J. K., Adkins, J. N., Omenn, G. S., and Simpson, R. J. (2005) An evaluation, comparison, and accurate benchmarking of several publicly available MS/MS search algorithms: sensitivity and specificity analysis, *Proteomics 5*, 3475-3490.
26. Durr, E., Yu, J., Krasinska, K. M., Carver, L. A., Yates, J. R., Testa, J. E., Oh, P., and Schnitzer, J. E. (2004) Direct proteomic mapping of the lung microvascular endothelial cell surface in vivo and in cell culture, *Nat Biotechnol 22*, 985-992.
27. Liu, H., Sadygov, R. G., and Yates, J. R., 3rd. (2004) A model for random sampling and estimation of relative protein abundance in shotgun proteomics, *Anal Chem 76*, 4193-4201.
28. Riter, L. S., Gooding, K. M., Hodge, B. D., and Julian, R. K., Jr. (2006) Comparison of the Paul ion trap to the linear ion trap for use in global proteomics, *Proteomics 6*, 1735-1740.
29. Gan, C. S., Reardon, K. F., and Wright, P. C. (2005) Comparison of protein and peptide prefractionation methods for the shotgun proteomic analysis of Synechocystis sp. PCC 6803, *Proteomics 5*, 2468-2478.
30. Motoyama, A., Xu, T., Ruse, C. I., Wohlschlegel, J. A., and Yates, J. R., 3rd. (2007) Anion and cation mixed-bed ion exchange for enhanced multidimensional separations of peptides and phosphopeptides, *Anal Chem 79*, 3623-3634.

31. Navare, A., Zhou, M., McDonald, J., Noriega, F. G., Sullards, M. C., and Fernandez, F. M. (2008) Serum biomarker profiling by solid-phase extraction with particle-embedded micro tips and matrix-assisted laser desorption/ionization mass spectrometry, *Rapid Commun Mass Spectrom 22*, 997-1008.

32. Dai, J., Wang, L. S., Wu, Y. B., Sheng, Q. H., Wu, J. R., Shieh, C. H., and Zeng, R. (2008) Fully Automatic Separation and Identification of Phosphopeptides by Continuous pH-Gradient Anion Exchange Online Coupled with Reversed-Phase Liquid Chromatography Mass Spectrometry, *J Proteome Res*.

33. Han, G., Ye, M., Zhou, H., Jiang, X., Feng, S., Tian, R., Wan, D., Zou, H., and Gu, J. (2008) Large-scale phosphoproteome analysis of human liver tissue by enrichment and fractionation of phosphopeptides with strong anion exchange chromatography, *Proteomics 8*, 1346-1361.

34. Li, X., Gong, Y., Wang, Y., Wu, S., Cai, Y., He, P., Lu, Z., Ying, W., Zhang, Y., Jiao, L., He, H., Zhang, Z., He, F., Zhao, X., and Qian, X. (2005) Comparison of alternative analytical techniques for the characterisation of the human serum proteome in HUPO Plasma Proteome Project, *Proteomics 5*, 3423-3441.

35. Mange, A., Bellet, V., Tuaillon, E., Van de Perre, P., and Solassol, J. (2008) Comprehensive proteomic analysis of the human milk proteome: Contribution of protein fractionation, *J Chromatogr B Analyt Technol Biomed Life Sci 876*, 252-256.

36. Oh, C., Zak, S. H., Mirzaei, H., Buck, C., Regnier, F. E., and Zhang, X. (2007) Neural network prediction of peptide separation in strong anion exchange chromatography, *Bioinformatics 23*, 114-118.

37. Simo, C., Gonzalez, R., Barbas, C., and Cifuentes, A. (2005) Combining peptide modeling and capillary electrophoresis-mass spectrometry for characterization of enzymes cleavage patterns: recombinant versus natural bovine pepsin A, *Anal Chem 77*, 7709-7716.

38. Choudhary, G., Wu, S. L., Shieh, P., and Hancock, W. S. (2003) Multiple enzymatic digestion for enhanced sequence coverage of proteins in complex proteomic mixtures using capillary LC with ion trap MS/MS, *J Proteome Res 2*, 59-67.

39. Mohammed, S., Lorenzen, K., Kerkhoven, R., van Breukelen, B., Vannini, A., Cramer, P., and Heck, A. J. (2008) Multiplexed proteomics mapping of yeast RNA

polymerase II and III allows near-complete sequence coverage and reveals several novel phosphorylation sites, *Anal Chem 80*, 3584-3592.

Chapter 4 Developing a nano-flow HPLC-ESI-MS/MS methodology for the analysis of Platelet Activating Factor (PAF) family and *lyso*-glycerophosphocholine (LPC) lipids

4.1 Developing a nano-flow HPLC-ESI-MS/MS methodology for the analysis of Platelet Activating Factor (PAF) family of lipids over the course of neuronal differentiation

4.1.1 Introduction

Glycerophospholipids are important structural lipids in neuronal membranes (*1*). Both enzymatic modification by phospholipase A_1, A_2, C, and D and non-enzymatic oxidation produces key cellular second messengers including arachidonic acid, eicosanoids, diacylglycerols, and platelet activating factors (PAF) and PAF-like lipids (*2-3*). Enhanced synthesis of bioactive glycerophospholipids during brain development is implicated in control of proliferation of neural precursor cells and differentiation of neuronal and glial lineages (*4*). In adult tissue, increased glycerophosphocholine and glycerophosphoethanolamine concentrations in brain and cerebrospinal fluid are associated with a more rapid cognitive decline in Alzheimer disease (*5*). Changes in the relative ratio of glycerophospholipid subclasses are also believed to both promote neural cell survival and participate in neuronal death in Parkinson's disease, stroke, and spinal cord injury depending upon which subspecies are generated within the injured microenvironment (*2, 4, 6*). Mechanistic insight, however, has been complicated by the difficulties associated with

identifying and quantifying changes in individual molecular species within complex biological samples composed of several thousand lipids.

The PAF subclass of glycerophospholipids are purported to be key mediators of neuronal differentiation and neuronal cell death *in vitro* and *in vivo* (*7-15*). PAF synthesis occurs through two enzymatic pathways: *de novo* and remodeling (Figure 4.1.1). Canonical PAF lipids are defined by alkyl ether linkage at the *sn*-1 position, a short chain acyl group at the *sn*-2 position, and a phosphocholine, phosphoethanolamine, or phosphatidic acid at the *sn*-3 position, however 1-acyl-2-acetyl-sn-glycero-3-phosphocholine species are also produced at significant levels in brain (*16-19*). Moreover, PAF-like lipids with 4-8 carbon side-chains at the *sn*-2 position can be generated by non-enzymatic oxidation of *sn*-2 acyl fatty acids chains in structural membrane glycerophospholipids (*20*). It is not known whether specific PAF subspecies are preferentially generated over the course of neuronal differentiation or neurodegenerative disease.

To date, LC-ESI-MS has proven the most successful in simultaneous detection of multiple glycerophospholipid subspecies at the molecular level. Application of 2-dimensional (2-D) maps of elution time and mass provides a useful means of profiling subclasses within complex samples (*21*). New tandem mass spectrometry (MS/MS) advances in combination with multiple linear regression modelling has significantly enhanced the capacity to subsequently resolve and quantify molecular subspecies (*22*). However, these techniques have yet to be applied to a comparison of lipid species in lipid-enriched neural samples extracted over the course of differentiation or disease. Here, we describe a method to screen, identify, and quantify changes in glycerophospholipid family members that can be used to compare multiple bioactive subspecies generated over the course of neuronal differentiation.

In our approach, nanoflow rate HPLC is combined with positive ion mode ESI-MS to generate 2D profiles of the glycerophospholipid contents of undifferentiated and differentiated PC12 cells. The utilization of precursor ion scans for fragments characteristic of PAF family members and the standard additions of PAF subspecies allows for the

absolute quantitation of PAF molecules during cell differentiation. We show, for the first time, that the combination of nanoflow rate HPLC with different MS techniques allows the analysis of lipid extract and the specific quantitation of PAF family members from as little as 70,000 PC12 cells.

4.1.2 Experiments

Glycerophospholipids were extracted from undifferentiated rat pheochromocytoma PC12 and NGF (nerve growth factor)-differentiated PC12 cells according to a modified Bligh/Dyer procedure (*23*). Lipid extracts were analyzed with a 2000 Q TRAP mass spectrometer (Applied Biosystems/MDS Sciex, Concord, ON) integrated with a micro flow 1100 HPLC system (Agilent, Palo Alto, CA). Enhanced MS scan, precursor ion scan and extracted ion chromatogram (XIC) was applied for detecting and highlighting the lipid species of interest. Absolute quantification of C16:0, C18:0 PAF and C16:0, C18:0 *lyso*-PAF were performed using standard addition approach, where 5 standard solutions containing 200, 400, 600, 800, and 1000 pg each of C16:0, C18:0 PAF and C16:0, C18:0 *lyso*-PAF were used in the experiment. At each standard addition concentration, samples were analyzed in triplicate. Therefore a total of 15 LC/MS runs were required for the quantification of the 4 PAF species of interest in each sample. Other details of these experiments were described in chapter 2.

4.1.3 Profiling glycerophospholipid changes by 2-D mapping

Glycerophospholipid extracts from PC12 cells (non-differentiated vs. NGF-differentiated) were first screened over the range of m/z from 450 to 600 with enhanced MS scan in positive ion mode. The range of m/z from 450 to 600 covers the PAF family members. Typical spectra are presented as 2-D maps of m/z versus elution time with relative glycerophospholipid abundance indicated in colour (Figure 4.1.2). Figure 4.1.2 shows that

the reversed-phase C18 nanoflow liquid chromatography has provided adequate peak capacity for separating the lipid species of interest.

Glycerophosphocholine subclasses, where the PAF family members belong to, were further assessed using precursor ion scan of m/z of 184.0, representing the ionized phosphocholine polar head group. Typical spectra of precursor ion scans are presented in figure 4.1.3, also as 2-D maps of m/z versus elution time with relative abundance indicated in colour. The candidate species of the glycerophosphocholine subclasses can then be estimated on the basis of theoretical mass and elution time. The list of these candidate lipid species are not included in the thesis, as the primary focus of the chapter is the development of a HPLC-MS/MS based analytical approach for the identification and quantification of the PAF family species in non-differentiated and NGF-differentiated PC12 cells.

The recorded 2D maps were reproducible over multiple runs. As well, the lipid species of interest recorded on the 2D maps of PC12 and differentiated PC12 could be readily assigned based on the elution time and the m/z. Variation on the m/z axis was on average 0.13 Da and 0.4 minutes on the elution time axis and did not vary between conditions (non-differentiated vs. NGF-differentiated). Secondly, an increase in the number of glycerophosphocholine species were detected in NGF-treated PC12 cells (Figure 4.1.3b) compared to undifferentiated precursors (Figure 4.1.3a) despite an overall decrease in glycerophospholipids observed following differentiation (Figure 4.1.2). Third, the number of glycerophosphocholine species detected within the scan range of 450 to 600 Da is higher than that previously observed over the same m/z range for mouse B-cell NS-1 cells (*21*). This may reflect the cell-specific differences in lipid metabolism. However, this is also likely attributed to the high sensitivity of the analytical methodology we have developed, where nanoflow rate HPLC was integrated with a more sensitive mass spectrometer.

4.1.4 Differentiation of PAF species from other isobaric lipid species

We intend to identify and quantify the absolute amount of the PAF family species in the complex lipid extracts of non-differentiated and NFG-differentiated PC12 cells. As there is no stable isotope labelled standards available for the PAF family species at the time of the experiment, we use the synthetic standards of the PAF family species, namely, PAF C16, lyso-C16, PAF C18, and lyso-C18, for identification and quantification of endogenous PAF family species in lipid extracts of non-differentiated and NFG-differentiated PC12 cells. The identification was carried out by the standard addition approach.

First, we needed to clearly identify the PAF family species and distinguish these species from any isobaric lipid species. Figure 4.1.4a shows the 2D spectra of the 4 synthetic standards of the PAF family species, where m/z of these protonated lipid standards and the corresponding elution time were recorded. During the process of standard addition, we spiked lipid extracts from PC12 and NGF-differentiated PC12 cells with 200-1000 pg of the synthetic standards (Figure 4.1.4 b, c). The PAF family species (C16:0, C18:0 PAF and C16:0, C18:0 *lyso*-PAF) in the lipid extracts from PC12 cells can be clearly identified by comparing the elution times recorded in 2D spectra of "neat" lipid standards (Figure 4.1.4a) and "spiked" samples (Figure 4.1.4b, c).

Figure 4.1.4 shows the appearance of considerable tailing on the 2D maps, even with pure standards (Figure 4.1.4a). This is mostly contributed to the colour coding of relative abundance used by the Analyst software. To validate our identification of the four PAF family species and ensure that inclusion of molar excesses of lipid standards would not mask detection of endogenous glycerophosphocholine species in biological samples, extracted ion chromatographs (XIC) were performed for the four PAF family species, as shown in Figure 4.1.5a-d respectively. The precursor ion scan at m/z 184 highlighted any glycerophosphocholine species, which contains a phosphocholine polar head group. As results, isobaric glycerophosphocholine species are identified in the 2D maps. However, these multiple isobaric glycerophospholipids can be clearly differentiated by closer examination of the extracted ion chromatographs (XIC) (Figure 4.1.5a-d). For example, 1-

hexadecanoyl-2-formyl-glycerophosphocholine (PFPC), which is isobaric with C16:0 PAF in positive ion mode (*24*), elutes earlier than C16:0 PAF as previously reported (*25*). This can be clearly separated and identified in the XICs (Figure 4.1.5c).

4.1.5 Quantitation of PAF family species based on the standard addition approach

Further mechanistic insight into the role of these changes in glycerophosphocholine families in developing neurons requires an efficient and sensitive means of identifying and quantifying individual molecular species. To this end, we focused on developing a quantitative analysis of changes in the phosphocholine-PAF species (C16:0, C18:0 PAF and C16:0, C18:0 *lyso*-PAF), which are of interest over the course of neuronal differentiation. To develop standard curves, four synthetic PAF standards with defined *sn*-1 and *sn*-2 chains and a phosphocholine *sn*-3 head group were used; namely C16:0, C18:0 PAF and C16:0, C18:0 *lyso*-PAF. We included C18:0 PAF as a negative control as our analysis predicted that the octadecyl-PAF species was present at concentrations below detectable levels in both PC12 and NGF-differentiated PC12 cells.

The standard addition method was used to quantify the absolute levels of the PAF subspecies present in the sample (Figure 4.1.6). Each standard addition, containing 200, 400, 600, 800, and 1000 pg of C16:0, C18:0 PAF and C16:0, C18:0 *lyso*-PAF, was repeated in triplicate. Peaks of interest were identified (m/z 482.4, 524.3, 510.4, 552.4) based on eluting time and their areas were calculated using the Analyst software. The endogenous PAF species C16:0 LPC (m/z 496.3, elution time 9.60 min) was used to correct the variation in intensity between the multiple MS runs for lipid extracts from non-differentiated and NGF-differentiated PC12 cells, respectively. This allowed for the correction in intensity variation within a standard addition experiments related to one sample due to changes in alignment and MS performances. Native PAF subspecies concentrations were then determined from the x-intercept using linear regression analysis (Figure 4.1.6a-f). Cook's distance analysis of residuals was performed to identify sample outliers that aberrantly influenced regression outcome (*26*). The absolute level of PAF species were then calculated according to the

number of cells utilized. Data were expressed as ng per 10^6 cells (Table 4.1.1). Results indicate a 16-fold increase in C16:0 *lyso*-PAF, an 8-fold increase in C16:0 PAF, and a 3-fold increase in C18:0 *lyso*-PAF. C18:0 PAF levels remained below level of detection and were not identified in either PC12 cells or NGF-differentiated PC12 cells.

Further, we used a synthetic internal standard C13:0 LPC not naturally produced by mammalian cells (*27*) to validate the range of linearity of the standard addition approach developed in this work. First, equal amounts (2 ng) of a synthetic internal standard C13:0 LPC were added to serially-diluted PC12 lipid analytes. The integrated peak intensities of endogenous C16:0 LPC (m/z 496.3, elution time 9.6 min) in each sample were normalized to that of the spiked internal standard C13:0 LPC (Figure 4.1.7a). A linear response was established with normalized peak intensities corresponding to C16:0 LPC falling within the linear range between analyte dilution factors 1-16. The second experiment, (Figure 4.1.7b) reverses the conditions. We maintained the same sample concentration but added increasing amounts of C13:0 LPC from 2 to 10 ng, which exceeded the maximum amount of lipid standards spiked in the testing samples for quantification. The expected linear response was observed when integrated peak intensities of C13:0 LPC were normalized to the endogenous standard C16:0 LPC (Figure 4.1.7b). These data indicates that quantification of the 4 PAF family species was performed within the range of linearity of the standard addition method developed in the work.

4.1.5 Conclusions

Here, we describe a rapid means of profiling changes in glycerophospholipids with identification and quantitation of glycerophosphocholine species following induction of neuronal differentiation. The combination of nanoflow rate HPLC with ESI-MS in different scan modes facilitated comparison of multiple species in total lipid 2D maps. In this study, we show that the standard addition of synthetic PAF subspecies allows for absolute quantitation of the changes in PAF family members following neuronal differentiation. Surprisingly, a marked asymmetry was detected in the two predominant PAF species (C16:0,

C18:0) produced by NGF-treated PC12 cells. Differentiation to a peripheral neuronal phenotype was associated with increases in C16:0 PAF and, more dramatically, with production of its immediate precursor and metabolite C16:0 *lyso*-PAF. C18:0 PAF was below limits of detection in both PC12 precursors and differentiated neurons. Interestingly, C18:0 *lyso*-PAF levels were elevated albeit at much lower concentrations than C16:0 *lyso*-PAF. When placed in context with evidence that C18:0 PAF increases in neural fluids following neuropathological challenge, these data point to a quantifiable difference between PAF molecular species produced by differentiating and damaged neurons. The methodology described here will enable a means of screening and comparing changes in glycerophospholipids, specifically PAF species, by neurons and glia during central and peripheral nervous system development and over the course of progressive neurodegenerative disease. This quantitation is critical to pursuing mechanistic insight in the role of glycerophospholipids in neuronal differentiation and death.

Table 4.1.1. LC-MS/MS quantitation of PAF in PC12 cells and NGF-differentiated PC12 cells.

PAF species	*WT-PC12 (ng/10^6 cells)*	*NGF-driven diffentiated PC12 (ng/10^6 cells)*
C16:0 *Lyso*-PAF	1.8 ± 0.3	29.0 ± 1.8
C18:0 *Lyso*-PAF	0.5 ± 0.1	4.3 ± 1.0
C16:0 PAF	1.8 ± 0.3	5.7 ± 1.0
C18:0 PAF	0.5 ± 0.5	0.0 ± 3.5

Figure Captions

Figure 4.1.1. Enzymatic and non-enzymatic generation of PAF family members. PAF species are synthesized through the PAF remodeling pathway (red), *de novo* synthesis (blue), or direct oxidation of membrane lipids (green, enzyme-independent). Predominant molecular species generated by enzymatic synthesis in brain are the C16:0 and C18:0 PAF family members. Oxidation generates PAF-like family members with longer chain fatty acids (up to 8 carbons) at the *sn*-2 position (hatched green box). Reprinted with permission from Analytical Chemistry. Copyright © 2007, American Chemical Society.

Figure 4.1.2. Glycerophospholipid profiles of PC12 cells over the course of differentiation to a neuronal phenotype. 2-D spectra of mass versus elution time with relative lipid abundance from (a) PC12 glycerophospholipid extracts spiked with 1000 ng of C18:0 PAF and (b) glycerophospholipids extracted from PC12 cells differentiated to a neuronal phenotype spiked with 1000 ng of C18:0 PAF. Relative lipid expression between conditions was corrected based on the intensity of the exogenous C18:0 PAF. This standard could be applied as endogenous C18:0 PAF was below limits of detection in both conditions. The experimental conditions of the LC/MS-MS are described in the text. Reprinted with permission from Analytical Chemistry. Copyright © 2007, American Chemical Society.

Figure 4.1.3. Glycerophosphocholine profiles of PC12 cells over the course of differentiation to a neuronal phenotype. 2-D maps of mass versus elution time with relative lipid abundance from (a) PC12 cells and (b) PC12 cells differentiated to a neuronal phenotype. Spectra were obtained for glycerophospholipids and analysed in positive ion mode using a precursor ion scan for an MS/MS fragment with a m/z of 184.0 to detect phosphocholine-containing subspecies. The experimental conditions of the LC/MS-MS are described in the text. Reprinted with permission from Analytical Chemistry. Copyright © 2007, American Chemical Society.

Figure 4.1.4. Identification of key PAF species from PC12 cells and PC12 cells differentiated to a neuronal phenotype. 2-D spectra of mass versus elution time with relative lipid abundance from (a) 1000 ng of C16:0, C18:0 PAF and C16:0, C18:0 *lyso*-PAF standards, (b) PC12 glycerophospholipid extracts spiked with 1000 ng of C16:0, C18:0 PAF and C16:0, C18:0 *lyso*-PAF and (c) glycerophospholipids extracted from PC12 cells differentiated to a neuronal phenotype spiked with 1000 ng of C16:0, C18:0 PAF and C16:0, C18:0 *lyso*-PAF. The experimental conditions of the LC/MS-MS are described in the text. Reprinted with permission from Analytical Chemistry. Copyright © 2007, American Chemical Society.

Figure 4.1.5. Identification of PAF family species from the isobaric lipid species using extracted ion chromatography. Extracted ion chromatographs are shown for identifying (a) C16:0 *lyso*-PAF, (b) C18:0 *lyso*-PAF, (c) C16:0 PAF, and (d) C18:0 PAF from PC12 cell lipid extracts spiked with 200 ng of each standard used in standard addition. In (c), the peak eluting at 11.42 min is consistent with previous reports of PFPC separation, a glycerophospholipid isobaric with C16:0 PAF. Peak retention times were calculated by the instrument software (Analyst 1.4.1). Reprinted with permission from Analytical Chemistry. Copyright © 2007, American Chemical Society.

Figure 4.1.6. Quantitation of PAF species from PC12 cells and PC12 cells differentiated to a neuronal phenotype. Lipid extracts from PC12 cells and PC12 cells differentiated to a neuronal phenotype were spiked with 200, 400, 600, 800, or 1000 ng of C16:0, C18:0 PAF and C16:0, C18:0 *lyso*-PAF and analyzed in positive ion mode followed by a precursor ion scan for masses having a *m/z* 184.0 MS/MS fragment. Each standard addition was repeated in triplicate. Corresponding peaks of interest were identified (*m/z* 482.4, 524.3, 510.4, 552.4) and were normalized against the endogenous C16:0 LPC standard to account for any trial variability within each standard addition point. Native PAF species from the cell samples were calculated from the x-intercept using linear regression. Data points depict mean of triplicate measurements ± standard deviation. Reprinted with permission from Analytical Chemistry. Copyright © 2007, American Chemical Society.

Figure 4.1.7. Validation of range of linearity of the developed standard addition method for PAF species quantitation using an internal standard (C13:0 LPC) and an endogenous standard (C16:0 LPC). (a) PC12 lipid extract was serially diluted and integrated peak intensity for C16:0 LPC (m/z 496.3, elution time 9.60 min) normalized against 2 ng of internal standard C13:0 LPC was plotted. A linear relationship was observed following normalization of C16:0 LPC to C13:0 LPC. (b) To further establish the linear range of response, 2-10 ng of the synthetic internal standard (C13:0 LPC) was added to the same PC12 lipid extract. Variations in the integrated peak area of C16:0 LPC between quadruplicate MS runs are indicated by the red boxes. To correct peak intensity for variations across MS runs, the integrated peak areas of C13:0 LPC was standardized against C16:0 LPC (yellow/black diamonds) demonstrating a linear range of response ($y=0.087x-0.045$, $R^2=0.995$). Reprinted with permission from Analytical Chemistry. Copyright © 2007, American Chemical Society.

Figure 4.1.1

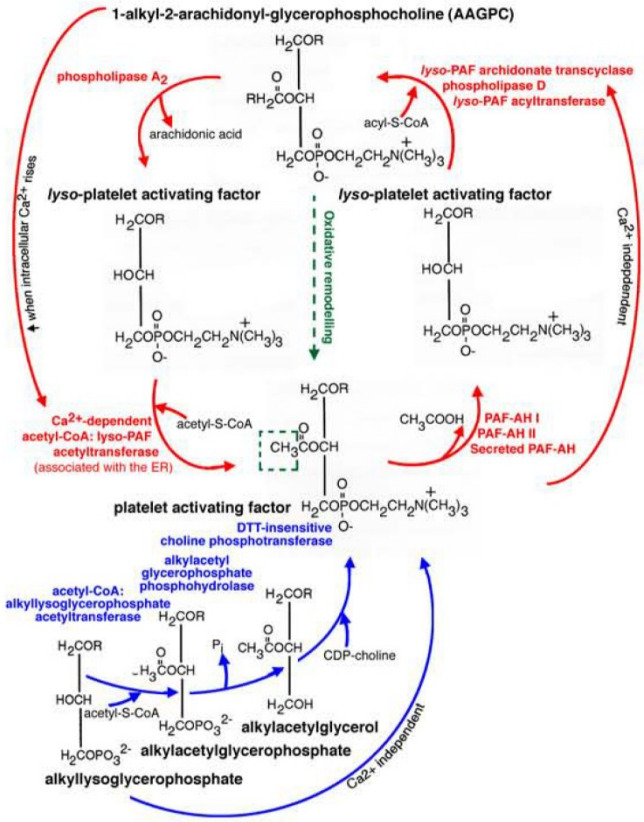
1-alkyl-2-arachidonyl-glycerophosphocholine (AAGPC)
phospholipase A2
arachidonic acid
lyso-PAF archidonate transcyclase
phospholipase D
lyso-PAF acyltransferase
acyl-S-CoA
lyso-platelet activating factor
lyso-platelet activating factor
Oxidative remodelling
when intracellular Ca2+ rises
Ca2+ independent
Ca2+-dependent
acetyl-CoA: lyso-PAF
acetyltransferase
(associated with the ER)
acetyl-S-CoA
CH3COOH
PAF-AH I
PAF-AH II
Secreted PAF-AH
platelet activating factor
DTT-insensitive
choline phosphotransferase
alkylacetyl
glycerophosphate
phosphohydrolase
acetyl-CoA:
alkyllysoglycerophosphate
acetyltransferase
CDP-choline
alkylacetylglycerol
alkylacetylglycerophosphate
alkyllysoglycerophosphate
Ca2+ independent

Figure 4.1.2

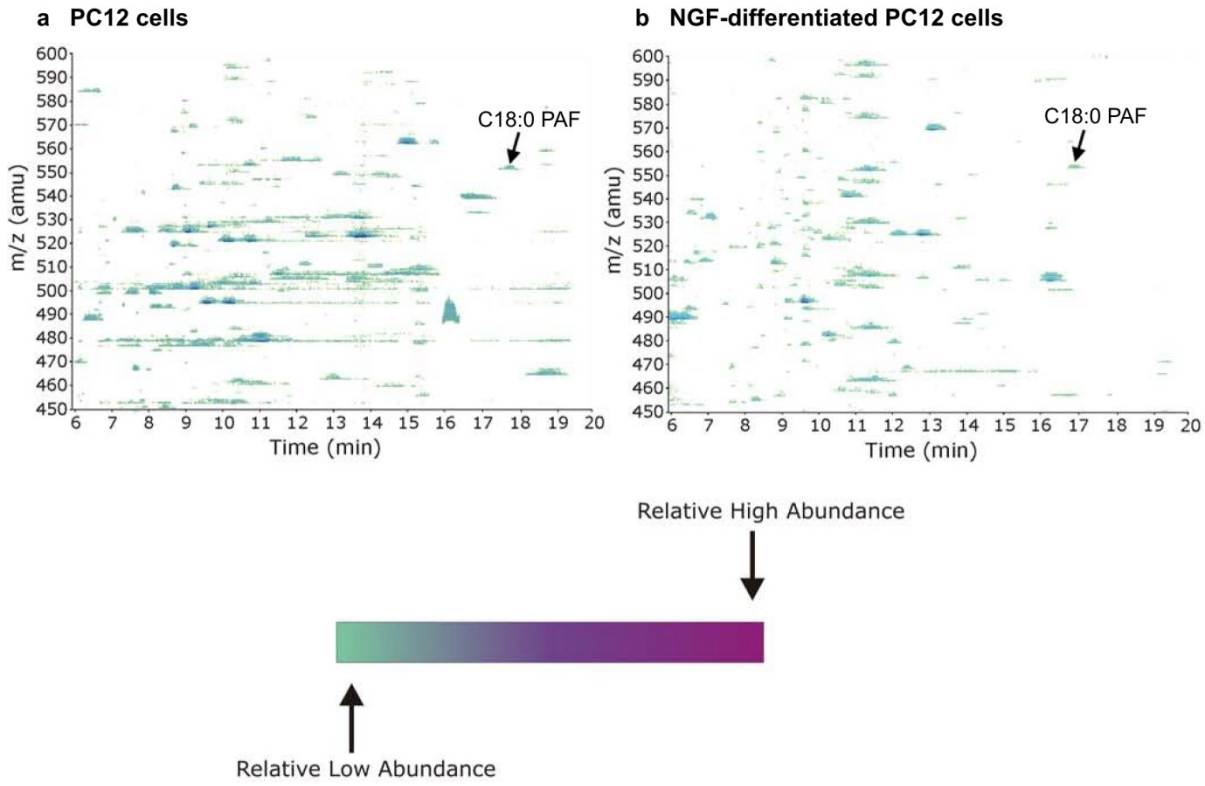
a PC12 cells
b NGF-differentiated PC12 cells
C18:0 PAF
C18:0 PAF
m/z (amu)
Time (min)
Relative High Abundance
Relative Low Abundance

Figure 4.1.3

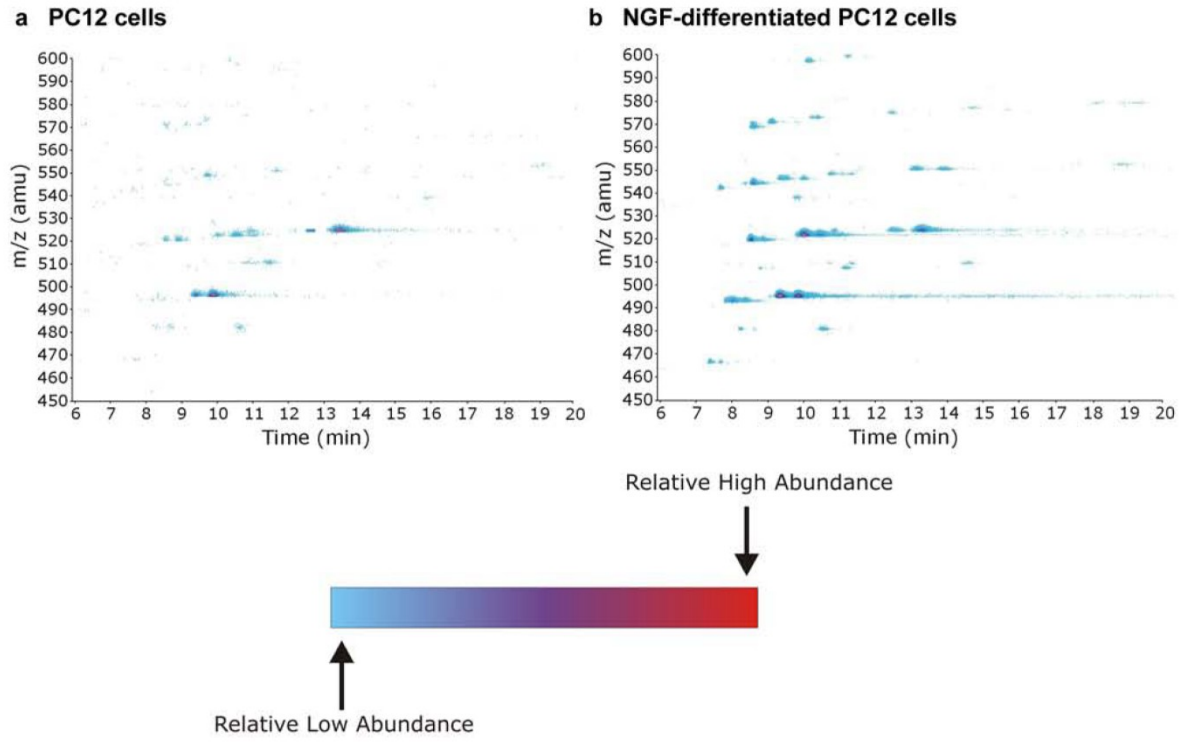
a PC12 cells
b NGF-differentiated PC12 cells
m/z (amu)
Time (min)
Relative High Abundance
Relative Low Abundance

Figure 4.1.4

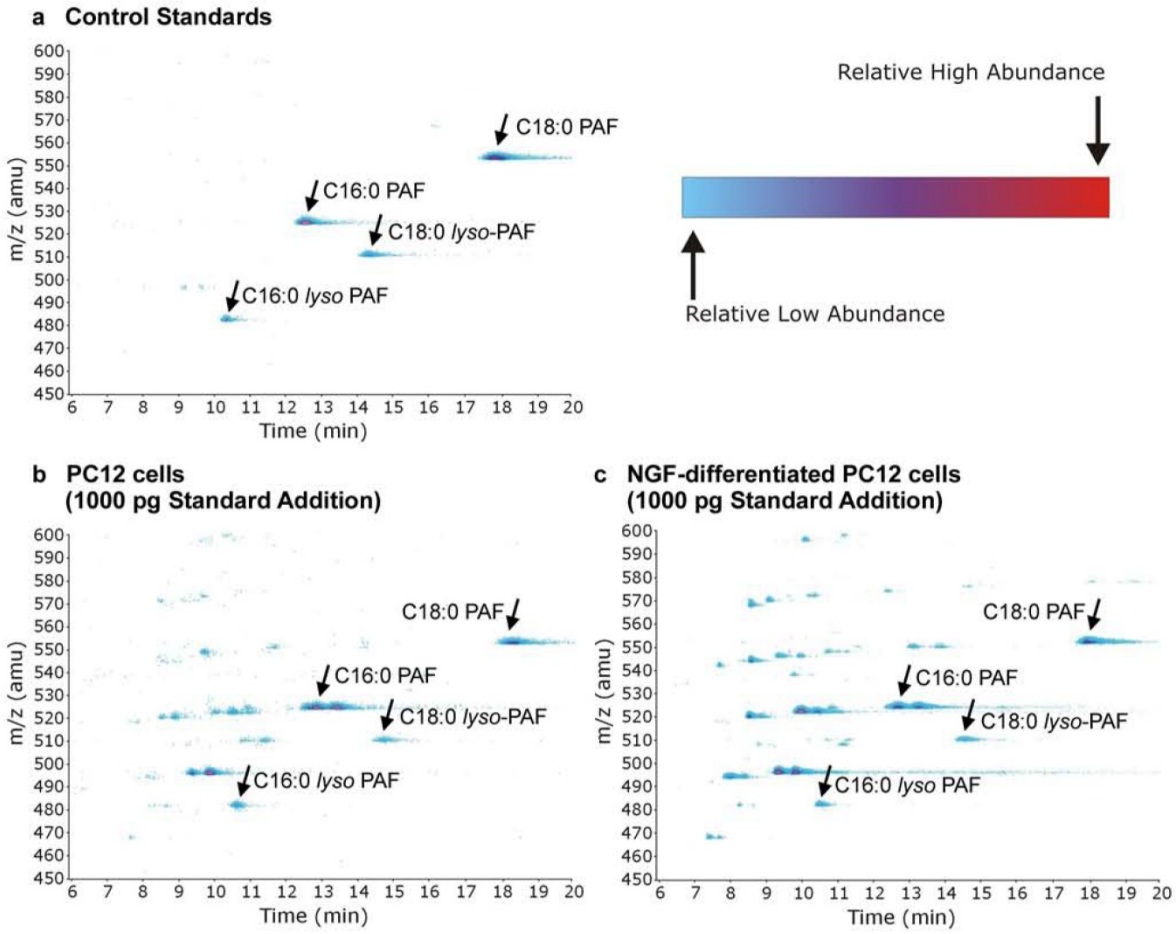
a Control Standards
C18:0 PAF
C16:0 PAF
C18:0 lyso-PAF
C16:0 lyso PAF
m/z (amu)
Time (min)
Relative High Abundance
Relative Low Abundance
b PC12 cells
(1000 pg Standard Addition)
c NGF-differentiated PC12 cells
(1000 pg Standard Addition)

Figure 4.1.5

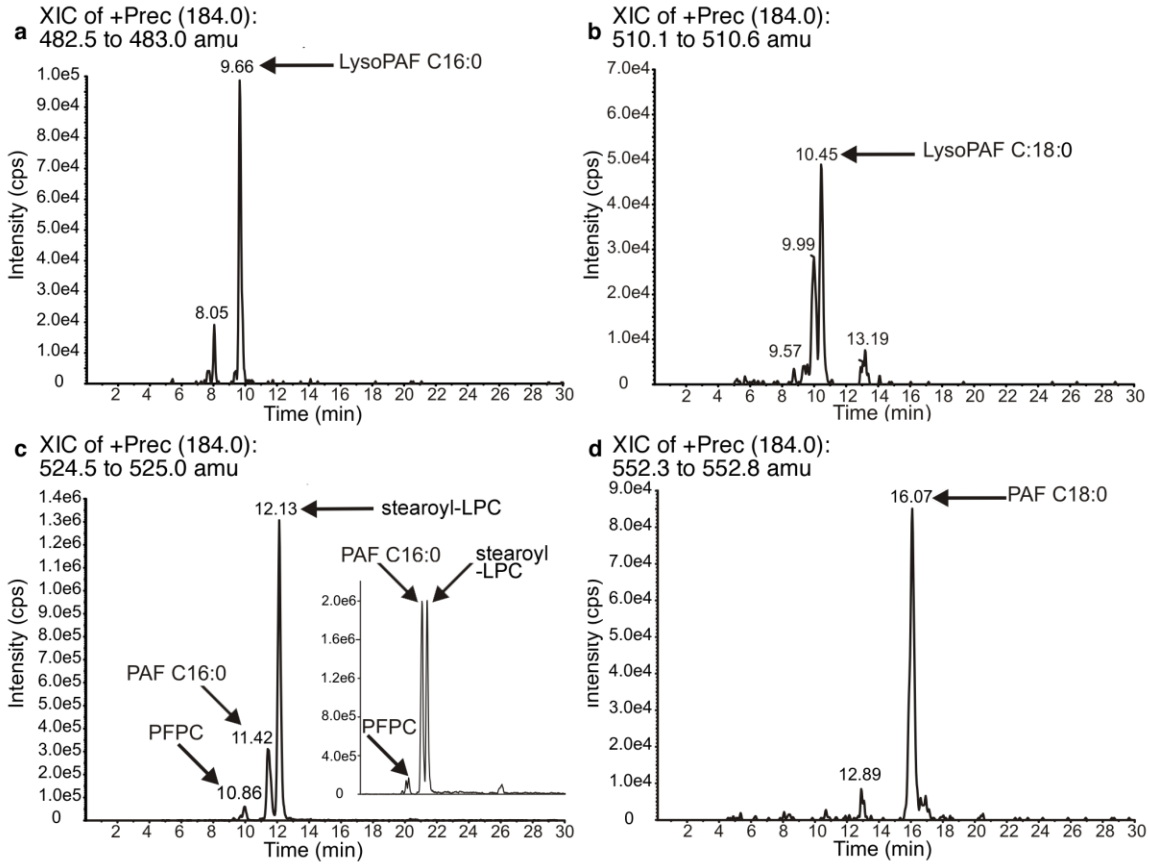
a
XIC of +Prec (184.0):
482.5 to 483.0 amu
9.66
LysoPAF C16:0
8.05
Intensity (cps)
Time (min)
b
XIC of +Prec (184.0):
510.1 to 510.6 amu
10.45
LysoPAF C:18:0
9.99
9.57
13.19
Intensity (cps)
Time (min)
c
XIC of +Prec (184.0):
524.5 to 525.0 amu
12.13
stearoyl-LPC
PAF C16:0
stearoyl
-LPC
PAF C16:0
PFPC
11.42
10.86
PFPC
Intensity (cps)
Time (min)
d
XIC of +Prec (184.0):
552.3 to 552.8 amu
16.07
PAF C18:0
12.89
Intensity (cps)
Time (min)

Figure 4.1.6

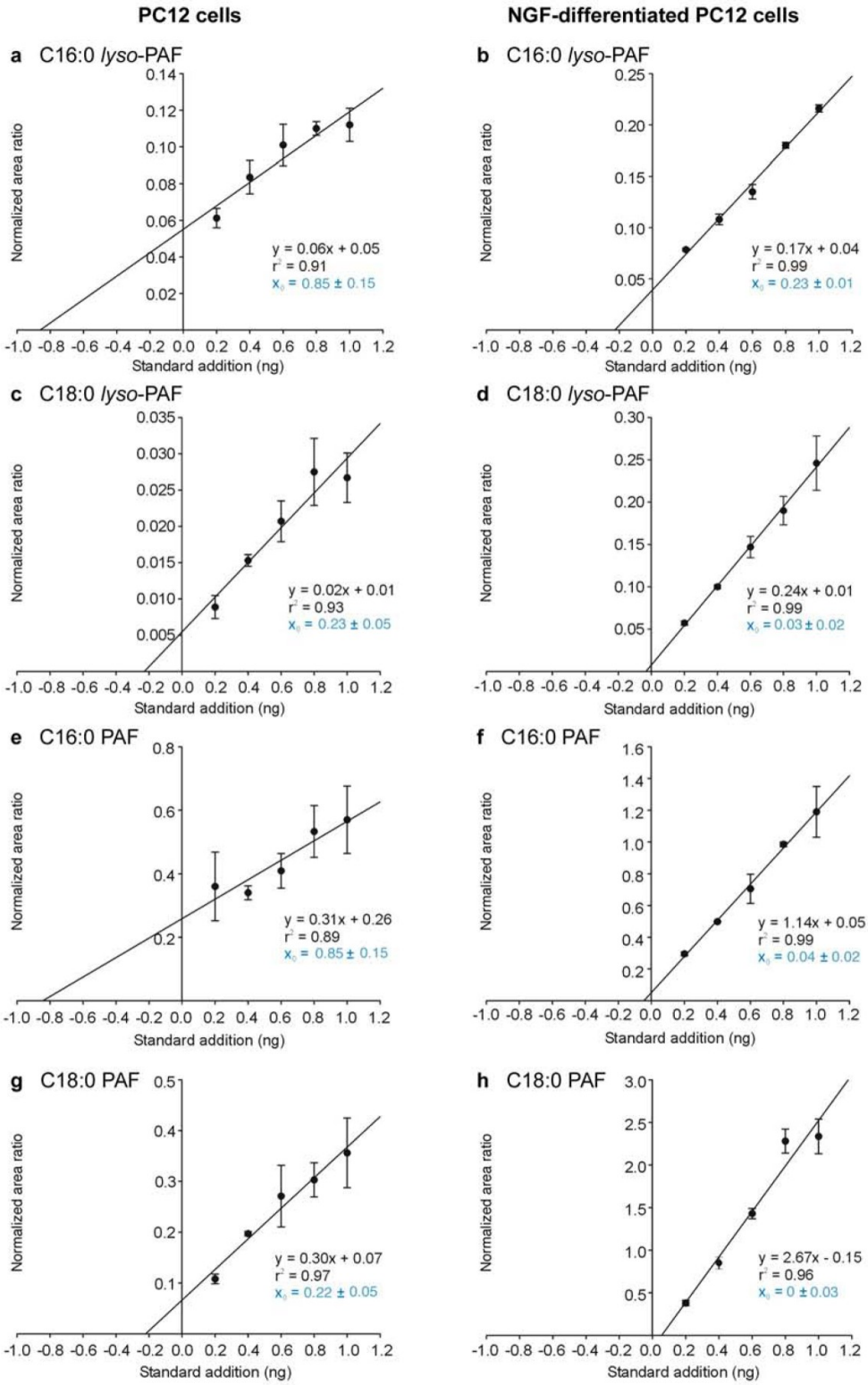
PC12 cells
NGF-differentiated PC12 cells
a C16:0 lyso-PAF
y = 0.06x + 0.05
r² = 0.91
x₀ = 0.85 ± 0.15
b C16:0 lyso-PAF
y = 0.17x + 0.04
r² = 0.99
x₀ = 0.23 ± 0.01
c C18:0 lyso-PAF
y = 0.02x + 0.01
r² = 0.93
x₀ = 0.23 ± 0.05
d C18:0 lyso-PAF
y = 0.24x + 0.01
r² = 0.99
x₀ = 0.03 ± 0.02
e C16:0 PAF
y = 0.31x + 0.26
r² = 0.89
x₀ = 0.85 ± 0.15
f C16:0 PAF
y = 1.14x + 0.05
r² = 0.99
x₀ = 0.04 ± 0.02
g C18:0 PAF
y = 0.30x + 0.07
r² = 0.97
x₀ = 0.22 ± 0.05
h C18:0 PAF
y = 2.67x - 0.15
r² = 0.96
x₀ = 0 ± 0.03
Normalized area ratio
Standard addition (ng)

Figure 4.1.7

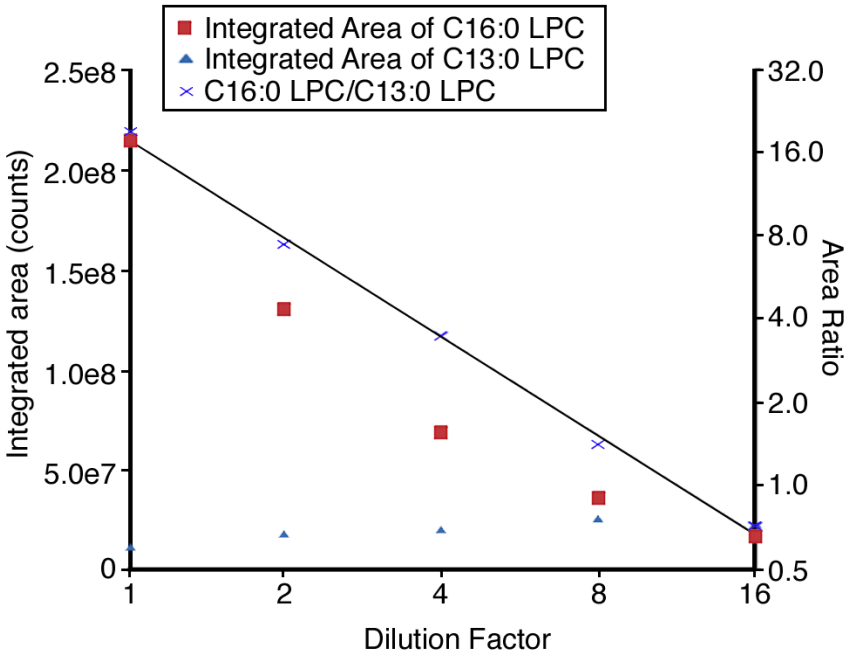

(a)

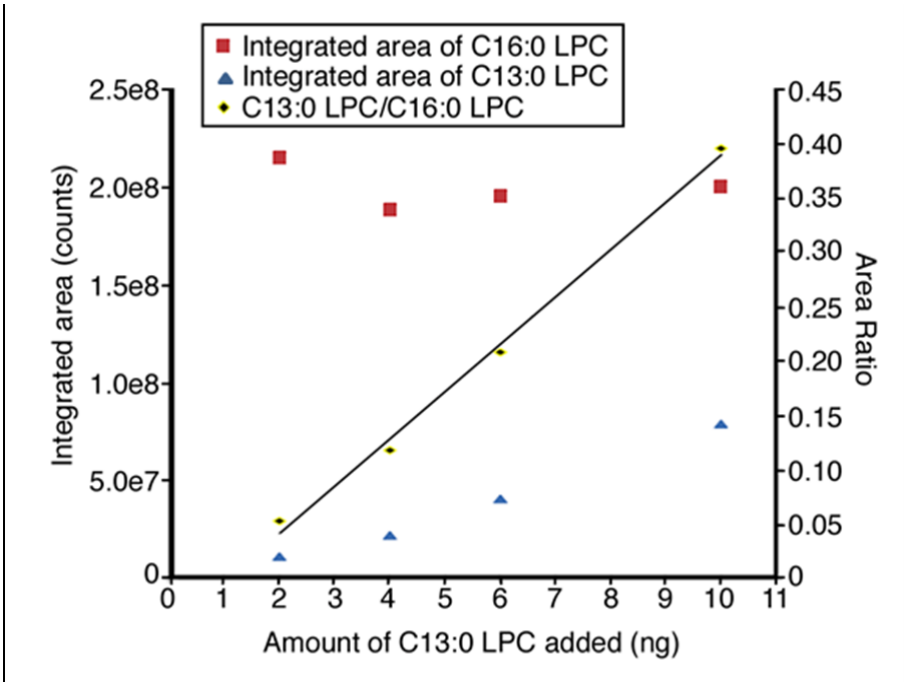

(b)

4.2 Applying nano-flow HPLC-ESI-MS/MS methodology for the analysis of Platelet Activating Factor (PAF) family and lyso-glycerophosphocholine (LPC) lipid species in complex biological samples

4.2.1 Introduction

The aberrant processing of the amyloid precursor protein to different assemblies of amyloid β (Aβ) peptides ranging from 37 and 42 amino acids is an early and necessary prerequisite for the development of Alzheimer Disease (AD) (*28*). The "amyloid cascade hypothesis" defines generation of these smaller, toxic Aβ fragments, specifically soluble $A\beta_{42}$ oligomers, as the root cause of AD (*29*). The severity of AD progression, however, is highly correlated with the rate of abnormal tau processing, the other signature AD pathology(*30*). Underlying molecular mechanisms linking $A\beta_{42}$ biogenesis to the aggregation of normally soluble tau proteins into hyperphosphorylated oligomers, paired helical filaments, and finally neurofibrillary tangles remain elusive. Indeed, whether $A\beta_{42}$ signals the post-translational modification of tau in human neurons is a matter of intense debate with important therapeutic implications (*31*).

$A\beta_{42}$ can activate cytosolic phospholipase A_2 ($cPLA_2$) (*32-33*), a Group IVa PLA_2 that preferentially hydrolyzes arachidonic acid from the *sn*-2 position of 1-*O*-alkyl-2-arachidonoyl- and 1-*O*-acyl-2-arachidonoyl-glycerophospholipids (*34*). Inhibiting $cPLA_2$ activation completely attenuates $A\beta_{42}$ neurotoxicity; however blocking the different metabolic arms of the arachidonic acid cascade confers only partial protection (*32-33, 35*). Little is known about the fate of the glycerophospholipid backbone following the release of arachidonic acid by $cPLA_2$. The alkyl-*lyso*-glycerophosphocholines and *lyso*-phosphatidylcholines (LPCs) are of particular interest. These metabolites are biologically active in their own right and can be further modified by lyso-phosphatidylcholine acyltransferases (LPCATs). LPCAT activity also increases in AD(*36*), notably in the posterior-temporal entorhinal cortex, a region characterized by the earliest tau pathology (*37*). Transfer of a long-chain acyl group to the *sn*-2 position by LPCAT1 and 2 will regenerate structural membrane lipids whereas addition of a small acetyl group produces a

powerful family of lipid second messengers known as platelet activating factors (PAFs) (*38*). PAF lipids signal neuronal death in ischemia, seizure, and AIDS dementia *in vivo* and have been implicated in both $A\beta_{42}$ toxicity and the activation of tau kinases *in vitro* (*7, 39-41*). Signaling is isoform-specific. Differences in the *sn*-1 carbon chain length and degree of saturation determine whether activation of the PAF G-protein coupled receptor (PAFR) is cytotoxic or cytoprotective (*42-45*).

In this section, we used an unbiased lipidomics approach to profile the alkylacylglycerophosphocholine second messengers altered in AD. We found a selective elevation in PAF species defined by a palmitic acid (16:0) at the *sn*-1 position in the posterior-entorhinal cortex of individuals with AD, in TgCRND8 transgenic mice expressing mutant human amyloid precursor protein, and in human neurons directly exposed to soluble $A\beta_{42}$ oligomers.

4.2.2 Experiments

Glycerophospholipids were extracted post-mortem from the posterior/entorhinal cortex of AD patients and control subjects. Glycerophospholipids were also extracted from posterior temporal/entorhinal cortex of TgCRND8 transgenic mice. Human samples were spiked with 187.5 ng C13:0 LPC at time of extraction. Human hNT neurons, generated from NT2/D1 precursor cells(*46*), were treated with $A\beta_{42}$ (25 μM) to test whether $A\beta_{42}$ selectively impairs neuronal C16:0 PAF metabolism. Glycerophospholipids were extracted according to a modified Bligh and Dyer procedure.

Relative quantification of PAF family and LPC lipid species in lipid extracts from AD patients and control subjects were carried out by normalizing the peak area of the lipid species of interest against that of the C13:0 LPC internal standard. The synthetic lipid standards d_4-C16:0 PAF or d_4-C16:0-*lyso*-PAF were spiked at the time of MS analysis for facilitating the identification and quantification of endogenous C16:0 PAF or C16:0-*lyso*-PAF.

4.2.3 Results

4.2.3.1 Metabolism of C16:0 PAF is elevated in the posterior/entorhinal cortex of AD patients

Glycerophospholipids were extracted post-mortem from the posterior/entorhinal cortex of AD patients and control subjects. PAF isoforms were profiled by high performance liquid chromatography electrospray ionization mass spectrometry (LC-ESI-MS) (*47*). Lipids with mass to charge ratios (m/z) of 450-600 were analyzed in positive ion mode by MS scan for a protonated molecule at expected m/z followed by precursor ion scan for a diagnostic phosphocholine product ion at m/z 184. Peak intensities were standardized against C13:0 LPC, a synthetic internal standard added at the time of lipid extraction. Sixteen PAF species and three *lyso*-PAF species were identified in human posterior/entorhinal cortex on the basis of mass and retention time (Figure 4.2.1). Three of these species were significantly elevated in AD cortex: 1-O-hexadecyl-2-acetyl-*sn*-glycero-3-phosphocholine (C16:0-PAF), its immediate metabolite/precursor 1-O-hexadecyl-2-*lyso*-*sn*-glycero-3-phosphocholine (C16-*lyso*-PAF), and 1-O-oleyl-2-*lyso*-*sn*-glycero-3-phosphocholine (C18:1 *lyso*-PAF).

As the elevations in C16:0 PAF and C16:0 *lyso*-PAF suggested a specific disruption in the remodeling of palmitic acid containing-PAF through the Land's cycle, we used deuterated standards to verify the identity. Clear separation was obtained between C16:0 PAF and isobaric C18:0 LPC with the isoform altered in AD co-eluting with d_4-C16:0 PAF (Figure 4.2.2).

The analysis of glycerophospholipids extracted post-mortem from the posterior/entorhinal cortex of AD patients and control subjects revealed that, expressed as pg/mg of tissue (Figure 4.2.3), a significant increase from 258$\pm$30 pM in control to 639$\pm$205 pM in AD cortex and from 316$\pm$25 pM in control to 1035$\pm$455 pM in AD cortex in C16:0 PAF and C16:0 *lyso*-PAF concentrations respectively.

4.2.3.2 Disruption of C16:0 PAF metabolism is an early event in TgCRND8 mice

Aberrations in lipid metabolism in AD etiology that occur early and remain elevated are predicted to have the greatest impact on neuronal function in diseased tissue. To determine whether disruption of C16:0 PAF metabolism is an early event in AD, we analyzed the posterior temporal/entorhinal cortex of TgCRND8 transgenic mice (*48*) (Figure 4.2.4 a). The TgCRND8 line expresses a double mutant form (M146L and L286V) of the human amyloid precursor protein gene under the control of the prion protein promoter. Pathogenic increases in cortical $A\beta_{42}$ / $A\beta_{40}$ ratios are first observed at 10 weeks of age coincident with the onset of learning and memory impairment (*48*). Here, we found that tissue concentrations of C16:0 PAF (Figure 4.2.4b) and C16:0 *lyso*-PAF (Figure 4.2.4c) of 10-12 week old TgCRND mice were already four-fold and two-fold greater than non-transgenic (NonTg) littermates respectively. Tissue concentrations, expressed as pg/mg in Figure 4.2.4, represent molar concentrations of 104$\pm$25 pM and 407$\pm$105 pM for C16:0 PAF in NonTg and TgCRND8 and 268$\pm$135 pM and 597$\pm$320 pM for C16:0 *lyso*-PAF in NonTg and TgCRND8 cortex respectively.

4.2.3.3 C16:0 PAF accumulates in human neurons treated with soluble $A\beta_{42}$ oligomers

Accumulation in C16:0 PAF may simply reflect a change in cell distribution, as seen in experimental allergic encephalomyelitis wherein local tissue levels of total PAF lipids are elevated by the influx of activated microglia actively metabolizing PAFs (*49*). To test whether $A\beta_{42}$ selectively impairs neuronal C16:0 PAF metabolism, human hNT neurons were generated from NT2/D1 precursor cells (*46*). Cultures were treated with $A\beta_{42}$ (25 μM) prepared as soluble oligomers (*50*). All treatments were carried out in serum-free media containing 0.025% bovine serum albumin (w/v) to ensure neurons were not exposed to the secreted PAF acetylhydrolase (PAF-AH) isoform present in serum supplements. No degradation of exogenous PAF in media was detected under these conditions.

A 24 h exposure to $A\beta_{42}$ caused significant neuronal death (Figure 4.2.5 a). Over the course of treatment, C16:0 *lyso*-PAF concentrations increased steadily rising to 15-fold that of control cultures (12±0.1 pM to 180±8 pM, Figure 4.2.5 b). Endogenous C16:0 PAF levels initially dropped from 127±27 pM to 28±4 pM over the first 6 h of treatment and then increased to 5-fold that of control levels within 24 h (619±115 pM, Figure 4.2.5 c). Taken together, these data are consistent with a specific increase in $cPLA_2$/LPCAT remodeling of alkylacylglycerophosphocholines in response to oligomeric $A\beta_{42}$. Also intriguing was the initial drop in endogenous C16:0 PAF levels suggesting a compensatory increase in intracellular catabolism following acute exposure to $A\beta_{42}$ that was insufficient to prevent intracellular accumulation of both C16:0 PAF and C16:0 *lyso*-PAF in human neurons chronically exposed to $A\beta_{42}$.

4.2.4 Discussion

In this study, we elucidate a new pathway of neuronal dysfunction triggered by aberrant alkylacylglycerophosphocholine metabolism in response to oligomeric $A\beta_{42}$. Our lipidomics approach revealed a selective disruption in C16:0 PAF and C16:0 *lyso*-PAF metabolism in the posterior/entorhinal cortex of AD patients, a region noted for the earliest indication of tau pathology (*37*). We found that this disruption occurred early in disease progression in TgCRND8 transgenic mice overexpressing mutant human amyloid precursor protein, coincident with pathogenic increases in cortical $A\beta_{42}$ / $A\beta_{40}$ ratios (*48*). In human neurons, aberrant C16:0 PAF metabolism was elicited by direct exposure to soluble $A\beta_{42}$ oligomers.

The specificity of this metabolic disruption for hexadecyl-PAF was surprising. While consistent with an upregulation in $cPLA_2$ and LPCAT activities observed in AD and in response to $A\beta_{42}$ (*32-33, 36*), structural lipids with a C16:0 *sn*-1 carbon-chain are not normally preferentially modified. Moreover, LPCAT1 and 2 utilize 18:2- and 18:3-CoA (LPCAT1) or 20:4-CoA (LPCAT2) as preferred acyl substrates (*38*) and thus are more likely to regenerate structural membrane lipids over PAF second messengers. Thus, our lipidomics

profile may indicate a shift in substrate availability and/or specificity in diseased tissue. The selective impairment in C16:0 PAF metabolism in response to oligomeric $A\beta_{42}$ may represent a new potential target for therapeutic intervention in AD.

4.3 Chapter Summary

In summary, we developed a nano-HPLC-ESI-MS/MS-based analytical methodology for the analysis of PAF and LPC lipid species in lipid extracts from cells and tissue samples of mice and human. Absolute quantitation of PAF lipid species was performed with standard addition approach, where the PAF subspecies standards of known amount were spiked into lipid samples prior to MS analysis. The relative comparisons of other LPC lipid species of interest between test samples and controls were carried out by spiking in identical amount of non-endogenous C13:0 LPC standard at the time of lipid extraction.

We found a 16-fold increase in C16:0 *lyso*-PAF, an 8-fold increase in C16:0 PAF, and a 3-fold increase in C18:0 *lyso*-PAF in lipid extracts from the NGF-differentiated PC12 cells as compared to the non-differentiated PC12 cells. An elevation of C16 PAF was further identified in the posterior/entorhinal cortex of AD patients and TgCRND8 transgenic mice in comparison to the respective human and mice controls. The methodology described here will enable a means of screening and comparing changes in glycerophospholipids, specifically PAF species, by neurons and glia during central and peripheral nervous system development and over the course of progressive neurodegenerative disease. This quantitation is critical to pursuing mechanistic insight in the role of glycerophospholipids in neuronal differentiation and death.

Figure Captions

Figure 4.2.1 Specific PAF metabolites accumulate in AD tissue. (**a-p)** Thirteen PAF species and (**q-s**) three *lyso*-PAF species were detected in human posterior/entorhinal cortex (by LC-ESI-MS. Species were identified on the basis of mass and retention time. Significant changes in **(h)** C16:0 PAF, **(q)** C16:0 *lyso*-PAF, and (**r**) C18:1 *lyso*-PAF levels were detected in AD tissue (n=4 individuals/condition). Data are expressed as fold change relative to controls ± SEM. (* indicates $p<0.05$, Student's *t* test). Reprinted with permission from Proceedings of the National Academy of Sciences, USA. Copyright © 2009, National Academy of Sciences, USA.

Figure 4.2.2 The identity of C16:0 PAF and C16:0 *lyso*-PAF were verified by co-elution with deuterated standards. As PAF species can be isobaric with other phosphatidylcholines, analytes were re-analyzed following spike with deuterated d_4-C16:0 PAF or d_4-C16:0 *lyso*-PAF. Representative extracted ion chromatographs at m/z 524 (upper panel) or 528 (lower panel) with a phosphocholine product ion at m/z 184.0 detected by precursor ion scan in positive ion mode are presented. C16:0 PAF clearly separates from isobaric C18:0 LPC (upper inset) and coelutes with d_4-C16:0 PAF. Reprinted with permission from Proceedings of the National Academy of Sciences, USA. Copyright © 2009, National Academy of Sciences, USA.

Figure 4.2.3 C16:0-PAF and its immediate precursor and metabolite C16:0-*lyso*-PAF accumulate in AD cortex. (**a)** PAF lipid species were identified in post-mortem human posterior-entorhinal cortex by LC-ESI-MS. A significant increase in **(b)** C16:0 PAF and **(c)** C16:0 *lyso*-PAF levels were detected in AD tissue (n=4 individuals/condition). Data are expressed as fold change relative to controls ± standard error of measurement (SEM). Tissue concentrations, expressed as pg/mg tissue wet weight, were calculated for C16:0 *lyso*-PAF (**c**) and C16:0 PAF **(d**) in comparison to deuterated samples spiked at the time of analysis

(see Fig. 4.2.2). Each square represents an individual patient. (* indicates $p<0.05$, Student's *t* test). Reprinted with permission from Proceedings of the National Academy of Sciences, USA. Copyright © 2009, National Academy of Sciences, USA.

Figure 4.2.4 C16:0 PAF and *lyso*-PAF concentrations are elevated in the entorhinal cortex of TgCNRD8 mice expressing mutant human amyloid precursor protein. (**a**) Dissection coordinates of regions analyzed by LC-ESI-MS are indicated in blue. (**b**) Absolute quantitation of C16:0 PAF and C16:0 *lyso*-PAF species was performed by standard addition method (n=15 measurements/sample). Tissue concentrations of C16:0 PAF and *lyso*-PAF concentrations were elevated in 10-12 week old TgCRND8 mice with the increase in C16:0 PAF reaching statistically significance (*$p<0.05$, Student's *t* test, n=3 mice/condition). Reprinted with permission from Proceedings of the National Academy of Sciences, USA. Copyright © 2009, National Academy of Sciences, USA.

Figure 4.2.5 C16:0 *lyso*-PAF and C16:0 PAF accumulate in human neurons treated with soluble $A\beta_{42}$ oligomers. (**a)** Treatment of hNT neurons for 24 h with 25 μM $A\beta_{42}$ prepared as soluble oligomers elicits significant death as assessed by TUNEL (left panel, *$p<0.05$, Student's *t*-test). Morphology of single hNT neurons (arrowhead) or aggregated in bundles (arrows) on a feeder layer of non-neuronal cells (asterisk) after 24 h treatment with vehicle (serum-free media + 0.025% BSA) (top right panel). Following $A\beta_{42}$ treatment (bottom right panel), marked cell loss was evident with a reduction in the size of neuronal bundles (arrows) and vacuolization of remaining neurons (arrowheads) without significant impact upon feeder layer cells (asterisk). Scale bar 50 μm. Intracellular (**b)** C16:0 *lyso*-PAF and **(c)** C16:0 PAF levels were assessed in vehicle and $A\beta_{42}$-treated cultures over a 24 h period by LC-ESI-MS. Data are expressed as fold change relative to untreated hNT control cultures grown in complete media $\pm$ SEM. Exposure of cultures to serum-free treatment media (vehicle) did not impact upon PAF metabolism. (**b**) Treatment with $A\beta_{42}$ prepared as soluble oligomers steadily increased C16:0 *lyso*-PAF levels. (**c**) A transient decrease in

C16:0 PAF was detected within 6 h of exposure followed by a progressive increase in lipid levels. (*$p<0.05$, **$p<0.01$, ANOVA, *post-hoc* Dunnett's *t* test). Reprinted with permission from Proceedings of the National Academy of Sciences, USA. Copyright © 2009, National Academy of Sciences, USA.

Figure 4.2.1

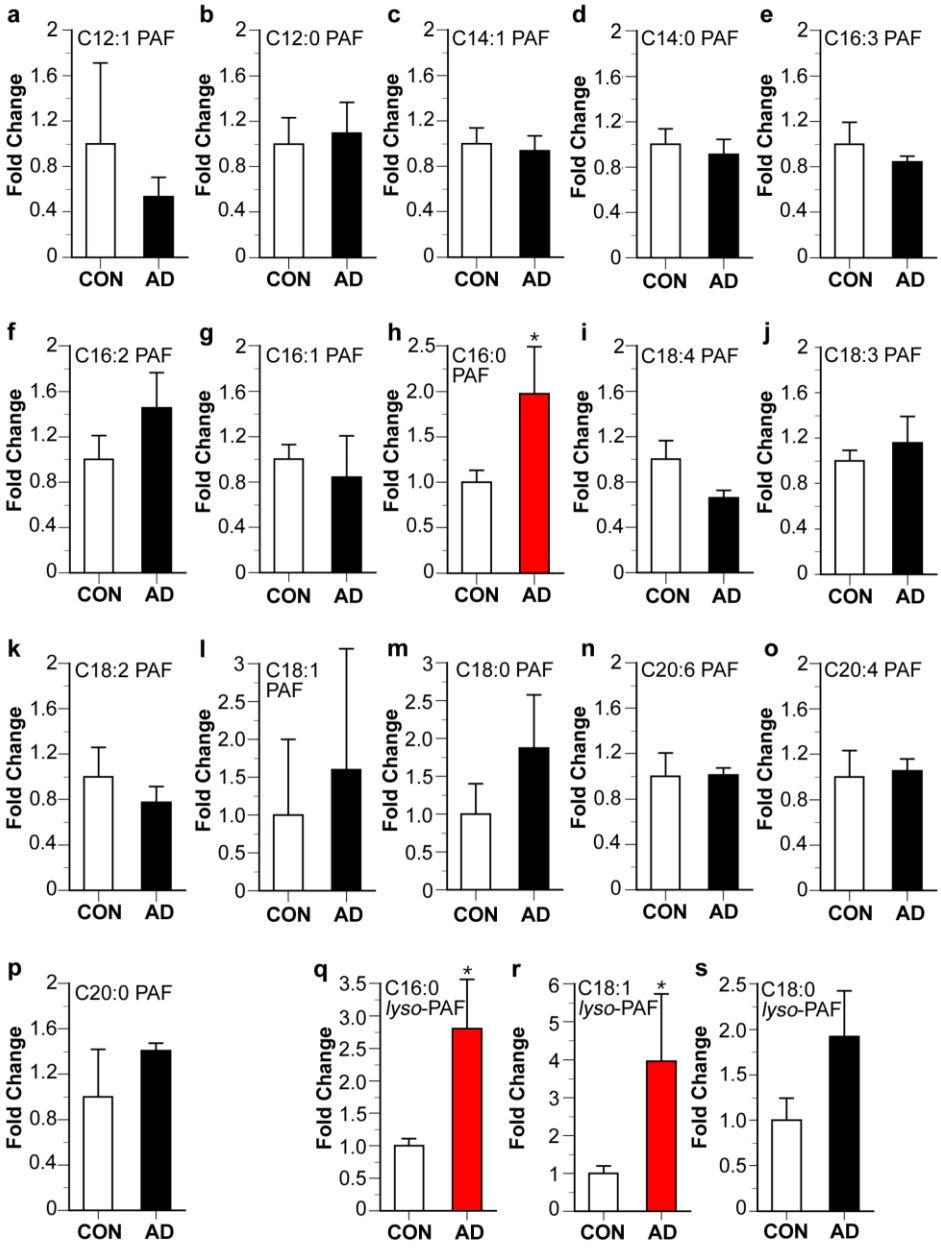
a
C12:1 PAF
b
C12:0 PAF
c
C14:1 PAF
d
C14:0 PAF
e
C16:3 PAF
f
C16:2 PAF
g
C16:1 PAF
h
C16:0 PAF
*
i
C18:4 PAF
j
C18:3 PAF
k
C18:2 PAF
l
C18:1 PAF
m
C18:0 PAF
n
C20:6 PAF
o
C20:4 PAF
p
C20:0 PAF
q
C16:0 lyso-PAF
*
r
C18:1 lyso-PAF
*
s
C18:0 lyso-PAF
Fold Change
CON
AD

Figure 4.2.2

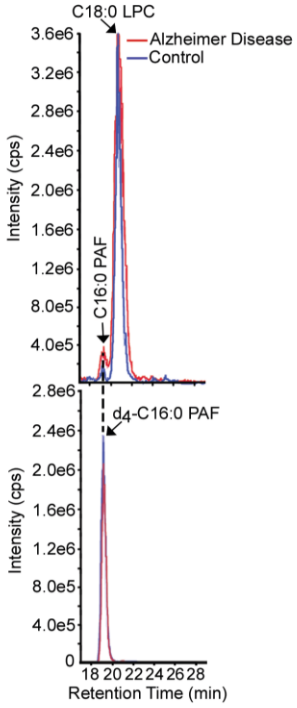
C18:0 LPC
Alzheimer Disease
Control
Intensity (cps)
3.6e6
3.2e6
2.8e6
2.4e6
2.0e6
1.6e6
1.2e6
8.0e5
4.0e5
C16:0 PAF
d4-C16:0 PAF
0
18 20 22 24 26 28
Retention Time (min)

Figure 4.2.3

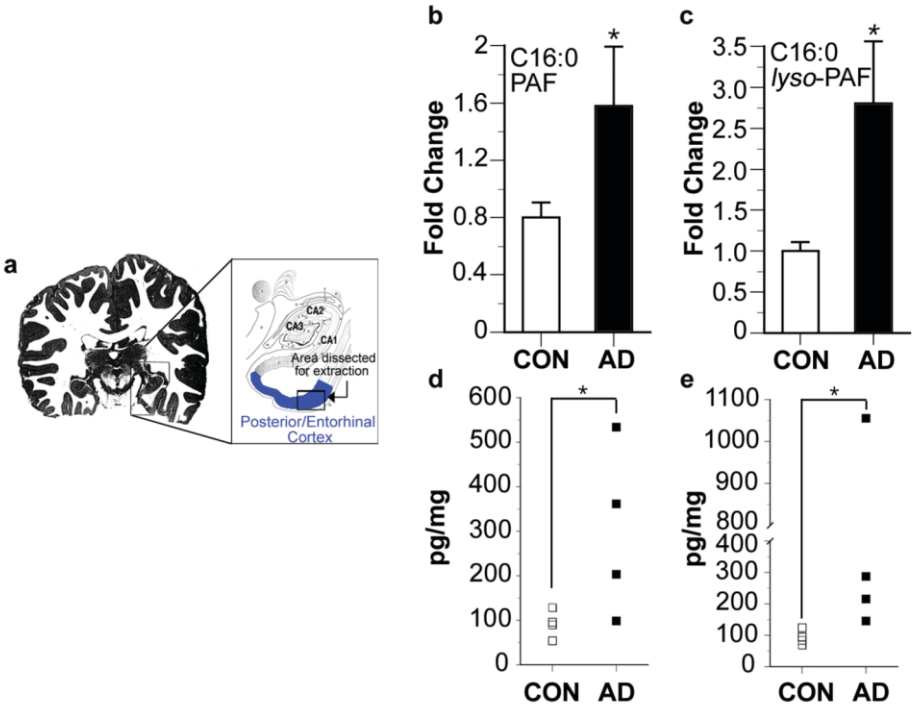
a
CA2
CA3
CA1
Area dissected for extraction
Posterior/Entorhinal Cortex
b
C16:0 PAF
Fold Change
2
1.6
1.2
0.8
0.4
0
*
CON
AD
c
C16:0 lyso-PAF
Fold Change
3.5
3.0
2.5
2.0
1.5
1.0
0.5
0
*
CON
AD
d
pg/mg
600
500
400
300
200
100
0
*
CON
AD
e
pg/mg
1100
1000
900
800
400
300
200
100
0
*
CON
AD

Figure 4.2.4

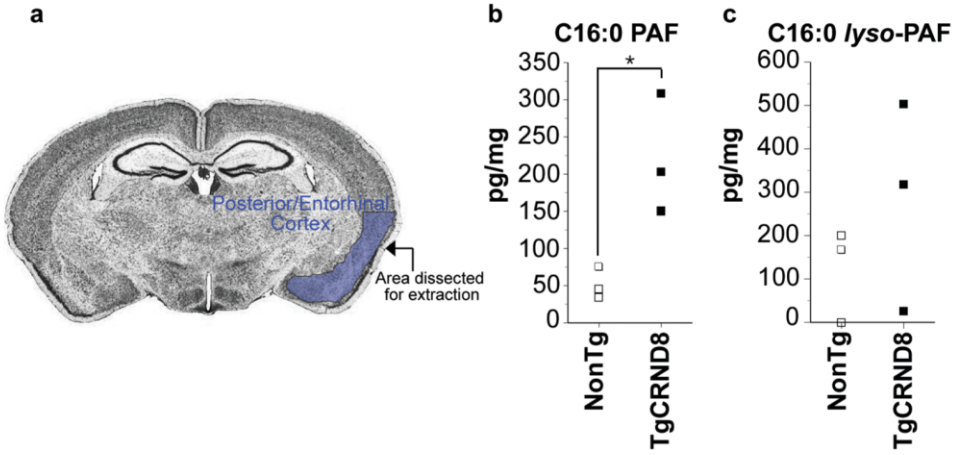
a
Posterior/Entorhinal Cortex
Area dissected for extraction
b
C16:0 PAF
pg/mg
350
300
250
200
150
100
50
0
*
NonTg
TgCRND8
c
C16:0 lyso-PAF
pg/mg
600
500
400
300
200
100
0
NonTg
TgCRND8

Figure 4.2.5

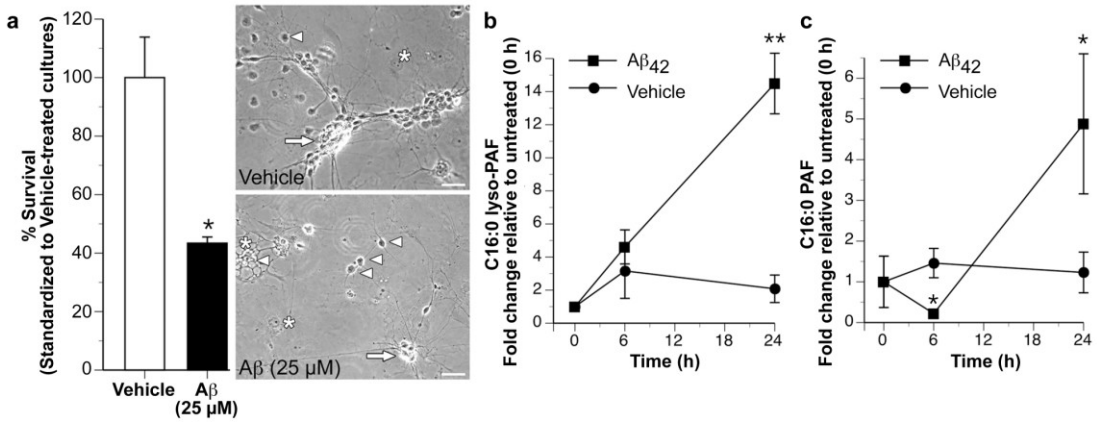
a
% Survival
(Standardized to Vehicle-treated cultures)
120
100
80
60
40
20
0
*
Vehicle
Aβ
(25 μM)
Vehicle
Aβ (25 μM)
b
C16:0 lyso-PAF
Fold change relative to untreated (0 h)
16
14
12
10
8
6
4
2
0
Aβ42
Vehicle
**
0
6
12
18
24
Time (h)
c
C16:0 PAF
Fold change relative to untreated (0 h)
6
5
4
3
2
1
0
Aβ42
Vehicle
*
*
0
6
12
18
24
Time (h)

References

1. Farooqui, A. A., Horrocks, L. A., and Farooqui, T. (2000) Glycerophospholipids in brain: their metabolism, incorporation into membranes, functions, and involvement in neurological disorders, *Chem Phys Lipids 106*, 1-29.
2. Farooqui, A. A., Ong, W. Y., and Horrocks, L. A. (2006) Inhibitors of brain phospholipase A2 activity: their neuropharmacological effects and therapeutic importance for the treatment of neurologic disorders, *Pharmacol Rev 58*, 591-620.
3. Maeba, R., Yusufu, Y., Shimasaki, H., and Ueta, N. (2002) Comparison of the oxidizability of various glycerophospholipids in bilayers by the oxygen uptake method, *Lipids 37*, 893-900.
4. Farooqui, A. A., Horrocks, L. A., and Farooqui, T. (2007) Interactions between neural membrane glycerophospholipid and sphingolipid mediators: a recipe for neural cell survival or suicide, *J Neurosci Res 85*, 1834-1850.
5. Sweet, R. A., Panchalingam, K., Pettegrew, J. W., McClure, R. J., Hamilton, R. L., Lopez, O. L., Kaufer, D. I., DeKosky, S. T., and Klunk, W. E. (2002) Psychosis in Alzheimer disease: postmortem magnetic resonance spectroscopy evidence of excess neuronal and membrane phospholipid pathology, *Neurobiol Aging 23*, 547-553.
6. Bazan, N. G. (2006) The onset of brain injury and neurodegeneration triggers the synthesis of docosanoid neuroprotective signaling, *Cell Mol Neurobiol 26*, 901-913.
7. Bate, C., Salmona, M., and Williams, A. (2004) The role of platelet activating factor in prion and amyloid-beta neurotoxicity, *Neuroreport 15*, 509-513.

8. Bazan, N. G. (1998) The neuromessenger platelet-activating factor in plasticity and neurodegeneration, *Prog Brain Res 118*, 281-291.

9. Bellizzi, M. J., Lu, S. M., Masliah, E., and Gelbard, H. A. (2005) Synaptic activity becomes excitotoxic in neurons exposed to elevated levels of platelet-activating factor, *J Clin Invest 115*, 3185-3192.

10. Xu, Y., Zhang, B., Hua, Z., Johns, R. A., Bredt, D. S., and Tao, Y. X. (2004) Targeted disruption of PSD-93 gene reduces platelet-activating factor-induced neurotoxicity in cultured cortical neurons, *Exp Neurol 189*, 16-24.

11. Francescangeli, E., Domanska-Janik, K., and Goracci, G. (1996) Relative contribution of the de novo and remodelling pathways to the synthesis of platelet-activating factor in brain areas and during ischemia, *J Lipid Mediat Cell Signal 14*, 89-98.

12. Francescangeli, E., Freysz, L., and Goracci, G. (1996) PAF-synthesizing enzymes in neural cells during differentiation and in gerbil brain during ischemia, *Adv Exp Med Biol 416*, 21-27.

13. Francescangeli, E., Grassi, S., Pettorossi, V. E., and Goracci, G. (2002) Activation of PAF-synthesizing enzymes in rat brain stem slices after LTP induction in the medial vestibular nuclei, *Neurochem Res 27*, 1465-1471.

14. Francescangeli, E., Lang, D., Dreyfus, H., Boila, A., Freysz, L., and Goracci, G. (1997) Activities of enzymes involved in the metabolism of platelet-activating factor in neural cell cultures during proliferation and differentiation, *Neurochem Res 22*, 1299-1307.

15. Kornecki, E., and Ehrlich, Y. H. (1988) Neuroregulatory and neuropathological actions of the ether-phospholipid platelet-activating factor, *Science 240*, 1792-1794.

16. Farooqui, A. A., and Horrocks, L. A. (2006) Phospholipase A2-generated lipid mediators in the brain: the good, the bad, and the ugly, *Neuroscientist 12*, 245-260.

17. Tokumura, A., Takauchi, K., Asai, T., Kamiyasu, K., Ogawa, T., and Tsukatani, H. (1989) Novel molecular analogues of phosphatidylcholines in a lipid extract from bovine brain: 1-long-chain acyl-2-short-chain acyl-sn-glycero-3-phosphocholines, *Journal of lipid research 30*, 219-224.

18. Yue, T. L., and Feuerstein, G. Z. (1994) Platelet-activating factor: a putative neuromodulator and mediator in the pathophysiology of brain injury, *Crit Rev Neurobiol 8*, 11-24.

19. Balestrieri, M. L., and Lee, T. (2000) Regulation of the biosynthesis of acyl analogs of platelet-activating factor by purinergic agonist in endothlial cells, *FEBS Lett 479*, 63-66.

20. Marathe, G. K., Harrison, K. A., Murphy, R. C., Prescott, S. M., Zimmerman, G. A., and McIntyre, T. M. (2000) Bioactive phospholipid oxidation products, *Free Radic Biol Med 28*, 1762-1770.

21. Taguchi, R., Hayakawa, J., Takeuchi, Y., and Ishida, M. (2000) Two-dimensional analysis of phospholipids by capillary liquid chromatography/electrospray ionization mass spectrometry, *J Mass Spectrom 35*, 953-966.

22. Callender, H. L., Forrester, J. S., Ivanova, P., Preininger, A., Milne, S., and Brown, H. A. (2007) Quantification of diacylglycerol species from cellular extracts by

electrospray ionization mass spectrometry using a linear regression algorithm, *Anal Chem 79*, 263-272.

23. Bligh, E. G., and Dyer, W. J. (1959) A rapid method of total lipid extraction and purification, *Can J Biochem Physiol 37*, 911-917.

24. Harrison, K. A., Clay, K. L., and Murphy, R. C. (1999) Negative ion electrospray and tandem mass spectrometric analysis of platelet activating factor (PAF) (1-hexadecyl-2-acetyl-glycerophosphocholine), *J Mass Spectrom 34*, 330-335.

25. Owen, J. S., Wykle, R. L., Samuel, M. P., and Thomas, M. J. (2005) An improved assay for platelet-activating factor using HPLC-tandem mass spectrometry, *Journal of lipid research 46*, 373-382.

26. Demidenko, E., and Stukel, T. A. (2005) Influence analysis for linear mixed-effects models, *Statistics in medicine 24*, 893-909.

27. Drobnik, W., Liebisch, G., Audebert, F. X., Frohlich, D., Gluck, T., Vogel, P., Rothe, G., and Schmitz, G. (2003) Plasma ceramide and lysophosphatidylcholine inversely correlate with mortality in sepsis patients, *Journal of lipid research 44*, 754-761.

28. Hardy, J., and Selkoe, D. J. (2002) The amyloid hypothesis of Alzheimer's disease: progress and problems on the road to therapeutics, *Science 297*, 353-356.

29. Haass, C., and Selkoe, D. J. (2007) Soluble protein oligomers in neurodegeneration: lessons from the Alzheimer's amyloid beta-peptide, *Nat Rev Mol Cell Biol 8*, 101-112.

30. Bierer, L. M., Hof, P. R., Purohit, D. P., Carlin, L., Schmeidler, J., Davis, K. L., and Perl, D. P. (1995) Neocortical neurofibrillary tangles correlate with dementia severity in Alzheimer's disease, *Arch Neurol 52*, 81-88.

31. Small, S. A., and Duff, K. (2008) Linking Abeta and tau in late-onset Alzheimer's disease: a dual pathway hypothesis, *Neuron 60*, 534-542.

32. Sanchez-Mejia, R. O., Newman, J. W., Toh, S., Yu, G. Q., Zhou, Y., Halabisky, B., Cisse, M., Scearce-Levie, K., Cheng, I. H., Gan, L., Palop, J. J., Bonventre, J. V., and Mucke, L. (2008) Phospholipase A(2) reduction ameliorates cognitive deficits in a mouse model of Alzheimer's disease, *Nat Neurosci 11*, 1311-1318.

33. Kriem, B., Sponne, I., Fifre, A., Malaplate-Armand, C., Lozac'h-Pillot, K., Koziel, V., Yen-Potin, F. T., Bihain, B., Oster, T., Olivier, J. L., and Pillot, T. (2005) Cytosolic phospholipase A2 mediates neuronal apoptosis induced by soluble oligomers of the amyloid-beta peptide, *Faseb J 19*, 85-87.

34. Kita, Y., Ohto, T., Uozumi, N., and Shimizu, T. (2006) Biochemical properties and pathophysiological roles of cytosolic phospholipase A2s, *Biochim Biophys Acta 1761*, 1317-1322.

35. Firuzi, O., Zhuo, J., Chinnici, C. M., Wisniewski, T., and Pratico, D. (2008) 5-Lipoxygenase gene disruption reduces amyloid-beta pathology in a mouse model of Alzheimer's disease, *FASEB J 22*, 1169-1178.

36. Ross, B. M., Moszczynska, A., Erlich, J., and Kish, S. J. (1998) Phospholipid-metabolizing enzymes in Alzheimer's disease: increased lysophospholipid acyltransferase activity and decreased phospholipase A2 activity, *J Neurochem 70*, 786-793.

37. Thangavel, R., Sahu, S. K., Van Hoesen, G. W., and Zaheer, A. (2008) Modular and laminar pathology of Brodmann's area 37 in Alzheimer's disease, *Neuroscience 152*, 50-55.

38. Shindou, H., and Shimizu, T. (2009) Acyl-CoA: lysophospholipid acyltransferases, *J Biol Chem 284*, 1-5.

39. Tong, N., Sanchez, J. F., Maggirwar, S. B., Ramierez, S. H., Guo, H., Dewhurst, S., and Gelbard, H. A. (2001) Activation of glycogen synthase kinase 3 beta (GSK-3beta) by platelet activating factor mediates migration and cell death in cerebellar granule neurons, *Eur. J. Neurosci. 13*, 1913-1922.

40. Bazan, N. G., Tu, B., and Rodriguez de Turco, E. B. (2002) What synaptic lipid signaling tells us about seizure-induced damage and epileptogenesis, *Prog Brain Res 135*, 175-185.

41. Perry, S. W., Hamilton, J. A., Tjoelker, L. W., Dbaibo, G., Dzenko, K. A., Epstein, L. G., Hannun, Y., Whittaker, J. S., Dewhurst, S., and Gelbard, H. A. (1998) Platelet activating factor receptor activation. An initiator step in HIV-1 neuropathogenesis, *J. Biol. Chem. 273*, 17660-17664.

42. Southall, M. D., Isenberg, J. S., Nakshatri, H., Yi, Q., Pei, Y., Spandau, D. F., and Travers, J. B. (2001) The platelet-activating factor receptor protects epidermal cells from tumor necrosis factor (TNF) alpha and TNF-related apoptosis-inducing ligand-induced apoptosis through an NF-kappa B-dependent process, *J Biol Chem 276*, 45548-45554.

43. Li, T., Southall, M. D., Yi, Q., Pei, Y., Lewis, D., Al-Hassani, M., Spandau, D., and Travers, J. B. (2003) The epidermal platelet-activating factor receptor augments chemotherapy-induced apoptosis in human carcinoma cell lines, *J Biol Chem 278*, 16614-16621.

44. Brewer, C., Bonin, F., Bullock, B., Nault, M.-C., Morin, J., Imbeault, S., Shen, T. Y., Franks, D. J., and Bennett, S. A. L. (2002) Platelet activating factor-induced apoptosis is inhibited by ectopic expression of the platelet activating factor G-protein coupled receptor, *J Neurochem 82*, 1502-1511.

45. Ryan, S. D., Harris, C. S., Carswell, C. L., Baenziger, J. E., and Bennett, S. A. (2008) Heterogeneity in the sn-1 carbon chain of platelet-activating factor glycerophospholipids determines pro- or anti-apoptotic signaling in primary neurons, *J Lipid Res 49*, 2250-2258.

46. Pleasure, S. J., Page, C., and Lee, V. M.-Y. (1992) Pure, postmitotic, polarized human neurons derived from NTera 2 cells provide a system for expressing exogenous proteins in terminally differentiated neurons, *J. Neurosci. 12*, 1802-1815.

47. Whitehead, S. N., Hou, W., Ethier, M., Smith, J. C., Bourgeois, A., Denis, R., Bennett, S. A. L., and Figeys, D. (2007) Rapid identification and quantitation of changes in the platelet activating factor family of glycerophospholipids over the course of neuronal differentiation by high performance liquid chromatography electrospray ionization tandem mass spectrometry, *Anal Chem 79*, 8359-8548.

48. Chishti, M. A., Yang, D. S., Janus, C., Phinney, A. L., Horne, P., Pearson, J., Strome, R., Zuker, N., Loukides, J., French, J., Turner, S., Lozza, G., Grilli, M., Kunicki, S., Morissette, C., Paquette, J., Gervais, F., Bergeron, C., Fraser, P. E., Carlson, G. A., George-Hyslop, P. S., and Westaway, D. (2001) Early-onset amyloid deposition and cognitive deficits in transgenic mice expressing a double mutant form of amyloid precursor protein 695, *J Biol Chem 276*, 21562-21570.

49. Kihara, Y., Yanagida, K., Masago, K., Kita, Y., Hishikawa, D., Shindou, H., Ishii, S., and Shimizu, T. (2008) Platelet-activating factor production in the spinal cord of experimental allergic encephalomyelitis mice via the group IVA cytosolic phospholipase A2-Lyso-PAFAT axis, *J Immunol 181*, 5008-5014.

50. Klein, W. L. (2002) Abeta toxicity in Alzheimer's disease: globular oligomers (ADDLs) as new vaccine and drug targets, *Neurochem Int 41*, 345-352.

Chapter 5 Developing a novel MS-based approach for structural elucidation of diacyl glycerophospholipids

5.1 Introduction

Mass spectrometry has become the method of choice for lipid identification and quantification (*1-7*). Unlike protein analysis where the identification is a "matching" process between the peptide fragments of a protein and its genomic prediction (*8*), lipid identification is inherently a "*de novo*" process where the structural elucidation of a lipid species is based on the interpretation of mass spectrometry-derived structural information. In addition, due to the great structural diversity of lipid species (*9-10*), there is no single platform capable of identifying all lipid species. Therefore, comprehensive lipid profiling of a biological system poses important technical challenges.

Glycerophospholipids play a wide variety of cellular roles in many eukaryotic cells and their fatty acyl compositions are important parameters in regard to the functions they played in a biological system. To date a diversity of mass spectrometric techniques have been successfully employed in elucidating structures of glycerophospholipids, where structural information pertaining to the polar head groups and fatty acyl moieties attached to the glycerol backbone can be obtained either under negative ion mode or under positive ion mode with metal ion adduction (*11-20*). In eukaryotic cells, the linkages of the fatty acyl moieties to *sn2* position are always through esterification; while the bonding to s*n1* position could be acyl ester, alkyl ether, or vinyl ether linkages (*4*).

For diacyl glycerophospholipids, it is well documented that the relative abundance of the fragment ions pertaining to the two fatty acyl moieties is associated with their stereospecific position when they are subjected to fragmentation (*11-20*). For diacyl glycerophosphoinositols (PI), however, the relative abundance of the two fatty acyl anions recorded under negative ion mode depends on collision energy and the characteristics (e.g.

length and number of double bonds) of the fatty acyl moieties (*15*). Therefore the stereospecific position number of the two fatty acyl chains cannot be determined using their relative abundance. Instead, it has been suggested that the stereospecificity of diacyl glycerophosphoinositols could be determined based on the relative abundance of their lyso-form fragments, which correspond to the neutral loss of free fatty acids ($[M-Sn1]^-$/ $[M-Sn2]^-$) and the neutral loss of fatty acids as ketene ($[M-(Sn1-H_2O)]^-$/ $[M-(Sn2-H_2O)]^-$), respectively (*15*). Under low collision energy, it has also been observed for PA, PS, PG, and PE that the lyso-form fragment ions corresponding to the neutral loss of fatty acyl moieties from the *sn2* position ($[M-Sn2]^-$/ $[M-(Sn2-H_2O)]^-$) normally exhibit higher intensities than their counterparts ($[M-Sn1]^-$/ $[M-(Sn1-H_2O)]^-$), which are associated with the neutral loss from *sn1* position (*11-14*).

However, to date the structural information pertaining to the lyso-form fragment ions has not been fully exploited for the purpose of determining the stereospecificity of diacyl glycerophospholipids. One possible reason is that lyso-form fragment ions can only be recorded using either neutral loss scans or product ion scans. Unfortunately, monitoring large numbers of fragment ions for all the lipid species of interest using these approaches would require significant effort. However, large numbers of fatty acyl anions can be readily highlighted using multiple precursor ion scans (MPIS), fatty acyl scans (FAS), and multidimensional mass spectrometry-based shotgun lipidomics (MDMS-SL) (*7, 21-24*).

Shotgun lipidomic approaches usually analyze lipid extracts without or with very little pre-purification (*1, 25-26*). Most lipid species are thus analyzed under conditions subject to interferences from other isobaric species (or lipid species with molecular ion mass included within the isolation window for fragmentation) of the same class or other classes. As a result, the peak intensities of some fatty acyl anions of interest can be the sum of contributions from more than one lipid species. It is therefore very difficult to make correct positional assignments using MS techniques that look only at fatty acyl anions and neglect lyso-form fragment ions (e.g. FAS, MPIS, and MDMS-SL), especially when dealing with complex mixtures. In addition, lipid species that are not present in the mixture can also be wrongfully "identified" (false-positives) by associating two fatty acyl anions that are actually from two different lipid species.

In order to exclusively identify glycerophospholipids, it is desirable to include the fragment ions that can provide connections between the fatty acyl moieties and their respective molecular ions. There are reports that the fatty acyl chain positions of diacyl phosphatidylcholines (PC) can be determined based on the relative abundance of their lyso-form fragment ions, which were recorded in MS^3 mass spectra on an ion trap mass spectrometer (*27*).

In this work, we report a novel methodology to fully determine the stereospecificity of diacyl PA, PS, PG, PI, and PE. This methodology is based on the structural information derived from both the acyl anions and the lyso-form fragment ions from MS^2 obtained using a hybrid quadrupole time-of-flight (QqTOF) mass spectrometer. Unfortunately, previously published works (*11-15*) cannot provide all the information to develop this new methodology because factors such as type of mass spectrometer and collision energy can significantly affect fragmentation patterns (*28-29*). Therefore we examined a variety of diacyl glycerophospholipid standards, including PA, PS, PG, PI, and PE, over a wide range of collision energy. We found that the abundance of the lyso-form ions due to the neutral loss of free fatty acids and fatty acids as ketene from *sn2* position remained consistently higher than the respective ions due to the neutral loss from the *sn1* position. The optimization of the collision energy for each lipid species allowed relatively abundant lyso-form fragment ions to be recorded in MS^2 mass spectra in negative ion mode. It is therefore feasible to assign the fatty acyl positions primarily based on the relative abundance of the lyso-form fragment ions for PA, PS, PG, PI, and PE. Using this methodology, we then analyzed fatty acyl compositions of glycerophospholipids in lipid extract from rat hepatoma cell line over expressing lipin-1α, a protein involved in lipid metabolism (*30-31*). It was demonstrated that the present novel approach is capable of accurately determining the stereospecific information of diacyl glycerophospholipids even under interference from other isobaric lipid species. In addition, this approach is capable of charting the fatty acyl moieties of diacyl glycerophosphoinositols, which is impossible for methodologies that monitor only fatty acyl anions.

5.2 Experiments

The lipid standards and lipid extracts from rat hepatoma cells over expressing lipin-1α were introduced via direct infusion under negative ion mode to QSTAR Pulsar QqTOF mass spectrometer (MDS Sciex, Concord, ON, Canada) for structure elucidation. The diacyl glycerophospholipid standards PA (12:0/13:0), PA (17:0/14:1), PA (17:0/20:4), PS (12:0/13:0), PS (17:0/14:1), PS (17:0/20:4), PG (12:0/13:0), PG (17:0/14:1), PG (17:0/20:4), PI (12:0/13:0), PI (17:0/14:1), PI (17:0/20:4), PE (12:0/13:0), PE (17:0/14:1), and PE (17:0/20:4) were used to reveal the fragmentation patterns of various diacylglycerophospholipids with different combinations of fatty acyl chains attached at sn1 and sn2 positions and polar head groups, as they are fragmented with different collision energy (20 to 70ev). The relative abundance of fragment ions, including the fatty acyl anions $[FA1]^-$ and $[FA2]^-$, lyso-form fragment ions $[M-(Sn1-H_2O)]^-$, $[M-(Sn2-H_2O)]^-$, $[M-Sn1]^-$, and $[M-Sn2]^-$, and polar head group ions, were monitored. The study has revealed that the relative abundance of lyso-form fragment ions ($[M-(Sn2-H_2O)]^-$ / $[M-(Sn1-H_2O)]^-$, and $[M-Sn2]^-$ / $[M-Sn1]^-$) was associated with the stereospecific positions of the two fatty acyl moieties, and can be used to assign the fatty acyl chain positions of a unknown diacylglycerophospholipid. This was demonstrated with lipid extracts from rat hepatoma cells over expressing lipin-1α, where the fatty acyl moiety position were determined based on the relative abundance of lyso-form fragment ions ($[M-(Sn2-H_2O)]^-$ / $[M-(Sn1-H_2O)]^-$, and $[M-Sn2]^-$ / $[M-Sn1]^-$). Details of sample preparation and MS parameters are described in chapter 2.

5.3 Fragmentation patterns of diacyl glycerophospholipid standards under different collision energies

5.3.1 Overview

The fragmentation patterns of each individual glycerophospholipid class using negative ion mode have been studied previously (*11-15*). However, because factors such as the type of mass spectrometer and collision energy can significantly affect fragmentation

patterns (*28-29*), those studies did not provide all the information required to develop the methodology reported in this work. Therefore, we first comprehensively analyzed tandem mass spectra of a range of diacyl glycerophospholipid standards in negative ion mode over a wide range of collision energy using a hybrid quadrupole time-of-flight mass spectrometer, in order to examine the feasibility of using the relative abundances of acyl anions and lyso-form ions to determine the stereospecificity of diacyl glycerophospholipids. Also the optimum collision energy, permitting the recording of measurable abundances of product ions suitable for structure elucidation, was determined for the different lipid standards.

This work was designed to examine all the diacyl glycerophospholipid species (PA, PS, PG, PI, and PE) that are conventionally analyzed under negative ion mode as a whole lipid class. The fragmentation patterns of PA standards are presented first, followed by comparisons of fragmentation patterns of PS, PG, PI, and PE standards with respect to that of PA. The similarities and differences in their fragmentation patterns can then be employed for comprehensive structure elucidation.

5.3.2 Fragmentation patterns of molecular anions diacyl PA as a function of collision energy

As described in the experimental section, PA (17:0/14:1) was studied over a wide range of collision energy from 20 to 70 eV. Figure 5.1 shows representative tandem mass spectra of the molecular anion of PA (17:0/14:1), recorded at selected collision energies. The molecular ions were dominant in the spectrum recorded using a collision energy of 20 eV. Increasing the collision energy to 30 and 40 eV led to observation of abundant fragment ions corresponding to the two fatty acyl anions, polar head group, and 4 lyso-form fragment ions. Further increase of collision energy beyond 50 eV led to observation of only the two fatty acyl anions and the polar head group in high abundance.

Figure 5.2(a) shows that the acyl anions $[FA1]^-$ were more abundant than $[FA2]^-$ over the range of collision energy applied. Figure 5.2(b) summarizes the data for the lyso-form fragment ions corresponding to the neutral loss of free fatty acids ($[M-Sn1]^-$ and $[M-Sn2]^-$)

and also for the fragment ions resulting from neutral loss of fatty acids as ketenes ([M-(Sn1-H_2O)]$^-$ and [M-(Sn2-H_2O)]$^-$). The signal intensities of [M-Sn2]$^-$ and [M-(Sn2-H_2O)]$^-$ were consistently higher than their counterpart ions [M-Sn1]$^-$ and [M-(Sn1-H_2O)]$^-$, respectively, over the range of collision energy examined, in agreement with the previous study by Hsu *et al.* that used a triple-quadrupole mass spectrometer over a smaller collision energy range (25 to 35 eV) (*11*). Figure 5.2(c) shows the ratios of the signal intensities of [FA2]$^-$ vs. [FA1]$^-$, [M-(Sn2-H_2O)]$^-$ vs. [M-(Sn1-H_2O)]$^-$, and [M-Sn2]$^-$ vs. [M-Sn1]$^-$. It can be clearly seen that the ratios of [M-(Sn2-H_2O)]$^-$/[M-(Sn1-H_2O)]$^-$ and [M-Sn2]$^-$/[M-Sn1]$^-$ are always higher than unity while the ratio of [FA2]$^-$/[FA1]$^-$ is always lower than unity. In this case, the length of fatty acyl chains attached to the *sn1* position is longer than that bound to the *sn2* position.

In order to ensure that the observed preferential loss of fatty acyl moieties at the *sn2* position is not attributable to the lengths of the fatty acyl moieties, two other standards PA (12:0/13:0) and PA (17:0/20:4), representing cases in which the length of fatty acyl chains attached to *sn1* is close to and shorter than that bound to *sn2*, respectively, were studied following identical procedures. Figure 5.3 shows that the signal intensities of [M-Sn2]$^-$ and [M-(Sn2-H_2O)]$^-$ were always higher than those of [M-Sn1]$^-$ and [M-(Sn1-H_2O)]$^-$, respectively, over the range of collision energy examined. This result indicated that the preferred relative stereospecific abundances of lyso-form fragment ions and acyl anions of diacyl PA are independent of the lengths of their fatty acyl moieties. It follows that, in the absence of interferences from other lipid species, the relative abundance of both the acyl anions and the lyso-form fragment ions can facilitate the determination of the regiospecificity of diacyl PA.

5.3.3 Fragmentation patterns of molecular anions of diacyl PS, PG, PI, and PE as a function of collision energy

As described in the Experimental section, fragmentation patterns of PS (17:0/14:1), PG (17:0/14:1), PI (17:0/14:1), and PE (17:0/14:1) at different collision energies were also examined and analyzed following a protocol virtually identical to that used for PA (17:0/14:1). Fragmentation patterns of molecular anions of PA (17:0/14:1), PS (17:0/14:1),

PG (17:0/14:1), PI (17:0/14:1), and PE (17:0/14:1), each recorded at the respective optimum collision energy, are shown in Figure 5.4. Except for PI (17:0/14:1), for which the fragmentation spectrum was recorded at 50 eV, all the other spectra were recorded at 40 eV.

It is interesting to note the similarities and differences in the fragmentation patterns among different diacyl glycerophospholipids. PS (17:0/14:1), PG (17:0/14:1), and PI (17:0/14:1) all exhibited sets of lyso-form fragment ions ([M-polar head group-Sn1/2]$^-$ and [M-polar head group-(Sn1/2-H_2O)]$^-$) identical to those for PA (17:0/14:1), corresponding to fragmentation pathways resulting in neutral loss of both fatty acyl moieties and their respective polar head groups (*12-13, 15*). In contrast, PG (17:0/14:1) and PI (17:0/14:1) each exhibited its own set of lyso-form fragment ions, corresponding to neutral loss of fatty acyl moieties as free fatty acids ([M-Sn1/2]$^-$) or as ketenes ([M-(Sn1/2-H_2O)]$^-$). PS (17:0/14:1) exhibited only the [M-polar head group-Sn1/2]$^-$ and [M-polar head group-Sn1/2 – H_2O]$^-$ sets of lyso-form fragment ions, identical to the ([M-Sn1/2]$^-$ and ([M-Sn1/2 – H_2O]$^-$ fragment ions of PA (17:0/14:1) that has no head group. During fragmentation glycerophosphoserines will first shed the serine polar head group and fragment as glycerophosphatidic acids afterwards (*12*). The lyso-form fragment ions of PE (17:0/14:1) were of relatively low abundance with significant values at collision energies around 40 eV, suggesting stronger bonding of the ethanolamine phosphate head group to the glycerol backbone.

Figure 5.5 shows the data for the lyso-form fragment ions of PS (17:0/14:1), PG (17:0/14:1), PI (17:0/14:1), and PE (17:0/14:1) over the range of collision energy applied. It can be seen from Figure 5.5(a) that the lyso-form fragment ions [M- Serine-Sn2]$^-$ and [M-Serine-(Sn2-H_2O)]$^-$ of PS (17:0/14:1) are more abundant than [M-Serine-Sn1]$^-$ and [M-Serine-(Sn1-H_2O)]$^-$, respectively. For PG(17:0/14:1) the lyso-form ions [M-Sn2]$^-$, [M-(Sn2-H_2O)]$^-$, and [M-Glycerol-Sn2]$^-$ are more abundant than their respective counterpart ions [M-Sn1]$^-$, [M-(Sn1-H_2O)]$^-$, and [M-Glycerol-Sn1]$^-$. The observed abundances of the lyso-form fragment ions [M-Glycerol-(Sn2-H_2O)]$^-$ and [M-Glycerol-(Sn1-H_2O)]$^-$ were too low to be visualized in the figures (Figure 5.5(b) and (c)). Similarly for PI(17:0/14:1) the lyso-form ions [M-Sn2]$^-$, [M- (Sn2-H_2O)]$^-$, [M-Inositol-Sn2]$^-$, and [M-Inositol-(Sn2-H_2O)]$^-$ are more abundant than their respective counterpart ions. The signal for the lyso-form fragment ion [M-Inositol-(Sn2-H_2O)]$^-$ was too weak to be visualized in the figures (Figure 5.5(d), (e)).

Lyso-form fragment ions for PE(17:0/14:1) are of relatively low abundance, but at a collision energy of 40 eV, $[M\text{-}Sn2]^-$ and $[M\text{-}(Sn2\text{-}H_2O)]^-$ ions exhibited higher abundance than $[M\text{-}Sn1]^-$ and $[M\text{-}(Sn1\text{-}H_2O)]^-$ ions (Figure 4(f)).

These trends were also confirmed in identical experiments performed on PS(12:0/13:0), PS(17:0/20:4), PG(12:0/13:0), PG(17:0/20:4), PI(12:0/13:0), PI(17:0/20:4), PE(12:0/13:0), and PE(17:0/20:4) (Figures 4.2.6 (a-h)). It is therefore concluded that the relative abundances of the lyso-form fragment ions of diacyl glycerophospholipids provided reliable structural information to determine the stereospecific information of diacyl glycerophospholipids. For diacyl PA, PS, and PI the lyso-form fragment ions $[M\text{-}Sn2]^-$ and $[M\text{-polar head group-}Sn2]^-$ are more abundant than their respective $[M\text{-}(Sn2\text{-}H_2O)]^-$ and $[M\text{-polar head group-}(Sn2\text{-}H_2O)]^-$, suggesting a more facile process for the neutral loss of free fatty acid than the corresponding neutral loss of ketene; whereas the reverse is observed for diacyl PE (Figure 5.5 and Figure 5.6). For diacyl PG the trend is not clear. It was also observed that the optimum collision energy required to record abundant lyso-form fragment ions increases with the length of the fatty acyl chains. The optimum collision energy for PI species is estimated to be above 50 eV whereas it is around 40 eV for other glycerophospholipids.

It is also worth noting that the relative abundance of the two fatty acyl anions of glycerophosphoinositols depended on collision energy and the characteristics of fatty acyl moieties; whereas the ratios of $[M\text{-}(Sn2\text{-}H_2O)]^-/[M\text{-}(Sn1\text{-}H_2O)]^-$ and $[M\text{-}Sn2]^-/[M\text{-}Sn1]^-$ are always higher than unity (Figures 5.7 (a-c)). Thus for diacyl glycerophosphoinositols the regiospecificity can only be determined through the differential abundance of these lyso-form fragment ions.

5.4 Characterization of diacyl glycerophospholipids in lipid extracts from rat hepatoma cells.

We next tested the present methodology for the characterization of phospholipids in realistic complex samples. Briefly, lipids were extracted from rat hepatoma cells over

expressing lipin-1α, as described in the Experimental section, and analyzed by our methodology. Lipin-1α functions as phosphatidate phosphatase enzyme in lipid metabolism (*30-31*). The identical fatty acyl compositions of glycerophospholipids in different subclasses (with different polar head groups) could possibly link them together into a specific metabolic pathway. Testing this hypothesis necessitated a reliable mass spectrometric technique capable of determining the stereospecificity of diacyl glycerophospholipids. Under negative ion mode, precursor ion scans for *m/*z -153 and -196 were first performed on the lipid extracts isolated from the lipin-1α overexpressing cell line to highlight PA/PS/PG/PI and PE, respectively (Figure 5.8). Molecular anions of diacyl glycerophospholipids were then subjected to fragmentation.

Clearly, in some instances isobaric species will be combined as precursor ions. However, the power of this methodology is that it can differentiate the different isobaric lipid species. For example, Figure 5.9 shows the superimposed product ion spectra of the isobaric precursor ions at *m/z* -834.6. The fragment ions at *m/z* -153 ([glycerophosphate-H_2O]$^-$) and those at *m/z* -747.5 (neutral loss of 87 Da, the serine head group) indicated these lipid species were glycerophosphoserines. The fragment ions at *m/z* -281.3, -283.3, -327.2, and -329.2, corresponding to fatty acyl anions [FA18:1]$^-$, [FA18:0]$^-$, [FA22:6]$^-$, and [FA22:5]$^-$, respectively, suggested the compositions of these lipids to be PS(18:0-22:6) and PS(18:1-22:5) (The stereospecificity is yet to be determined). For diacyl PS the abundance of acyl anions [FA2]$^-$ is lower than that of [FA1]$^-$ (*12*). The higher intensities of [FA18:1]$^-$ and [FA18:0]$^-$ compared with those of [FA22:5]$^-$ and [FA22:6]$^-$, respectively, allowed the two lipid species to be identified as PS(18:0/22:6) and PS(18:1/22:5) (with the stereospecificity determined), respectively. Abundant fragment ions are also observed at *m/z* -419.3, -437.3, -463.3, and -481.3, corresponding to [M-Serine-FA22:6]$^-$, [M-Serine-(FA22:6-H_2O)]$^-$, [M-Serine-FA18:0]$^-$, and [M-Serine-(FA18:0-H_2O)]$^-$, respectively. The ions corresponding to [M-Serine-FA22:6]$^-$ (*m/z* -419.3) and [M-Serine-(FA22:6-H_2O)]$^-$ (*m/z* -437.3) exhibited higher abundances than [M-Serine-FA18:0]$^-$ (*m/z* -463.3) and [M-Serine-(FA18:0-H_2O)]$^-$ (*m/z* -481.3), respectively, thus allowing definitive identification of PS(18:0/22:6). Similarly, PS(18:1/22:5) can be identified on the basis that the lyso-form fragment ions at *m/z* -417.3 and -435.3 were observed at higher abundances than their respective counterpart ions. In this

case the structural information based on either the fatty acyl anions or the lyso-form fragment ions allowed the lipid species of interest to be exclusively determined.

Figure 5.10 shows a second example of a mixed product ion spectrum of molecular anions of isobaric lipid species at *m/z* -885.5. The fragment ions at *m/z* -153 ([glycerophosphate-H_2O]$^-$), -223 ([inositolphosphate-$2H_2O$]$^-$), -241 ([inositolphosphate-H_2O]$^-$), and -259 ([inositolphosphate]) indicated that these lipid species were glycerophosphoinositols. The fragment ions at *m/z* -281.3, -283.3, -303.2, and -305.2, corresponding to fatty acyl anions [FA18:1]$^-$, [FA18:0]$^-$, [FA20:4]$^-$, and [FA20:3]$^-$, respectively, suggested the compositions of these lipids were PI(18:0-20:4) and PI(18:1-20:3), respectively. The relative abundance of the two fatty acyl anions of diacyl glycerophosphoinositols depends on the collision energy and the length of the fatty acyl moieties, therefore the stereospecific positions of the two fatty acyl chain have to be determined via the relative abundances of their lyso-form fragments (*15*). For PI(18:0-20:4), the lyso-form fragment ions can be found at m/z 601.3, 619.3, 581.3, and 599.3, corresponding to [M-FA18:0]$^-$, [M-(FA18:0-H_2O)]$^-$, [M-FA20:4]$^-$, and [M-(FA20:4-H_2O)]$^-$, respectively. The intensities of peak at *m/z* -581.3 ([M-FA20:4]$^-$) and -599.3 ([M-(FA20:4-H_2O)]$^-$) are higher than those at *m/z* -601.3 ([M-FA18:0]$^-$) and -619.3 ([M-(FA18:0-H_2O)]$^-$), respectively, thus allowing the assignment of FA20:4 to *sn2* and FA18:0 to *sn1*. It followed that the complete structure of the lipid species of interest was PI(18:0/20:4). Similarly, PI(18:1/20:3) was determined on the basis that the lyso-form fragment ions at *m/z* -579.3 and -597.3 exhibited higher intensities than those at *m/z* -603.3 and -621,3, respectively. The assignment of the stereospecific structure of PI(18:0/20:4) and PI(18:1/20:3) can also be achieved on the basis of higher peak intensities at *m/z* -417.3 ([M-Inositol-FA20:3]$^-$) and -419.3 ([M-Inositol-FA20:4]$^-$) than those of their respective counterpart ions. To the best of our knowledge this is the first time that the stereospecificities of diacyl glycerophosphoinositols from lipid extracts of biological samples are determined based on their tandem mass spectra.

Shotgun lipidomic approaches usually analyze lipid extracts without or with very little pre-purification (*1, 25-26*). Most lipid species are identified under conditions subject to interferences from other isobaric species (or lipid species with molecular ion mass included

within the isolation window for precursor ions) of the same class or other classes. As a result, the peak intensities of some fatty acyl anions recorded in a tandem mass spectrum often include contributions from different lipid species. Figure 5.11 demonstrates that even isobaric lipids from different subclasses can be successfully identified using the present methodology. The product ion spectrum for the precursor at *m/z* -762.5 shows fragment ions at *m/z* -153 ([glycerophosphate-H_2O]$^-$), -196 ([ethanolaminephosphate-H_2O]$^-$), and -675.5 (neutral loss of 87 Da, the serine head group), indicating that the precursor at a nominal *m/z* value of -762.5 is a mixture of several isobaric PE and PS lipid species. Following the methodology discussed above, PE(18:1/20:5), PE(18:2/20:4), PE(16:0/22:6), and PE(16:1/22:5) can be identified on the basis of structural information associated with both the fatty acyl anions and the lyso-form fragment ions. (For diacyl PE species the fragment anion [FA2]$^-$ exhibited higher abundance than [FA1]$^-$) (*14*). In addition PS(16:0-18:0) can also be confirmed to be present in the mixture. Unfortunately, its stereospecific information could not be determined on the basis of the relative abundance of the two fatty acyl anions [FA16:0]$^-$ (*m/z* -255.2) and [FA18:0]$^-$ (*m/z* -283.2), which were virtually equal. However, the stereospecificity can be established based on the lyso-form fragment ion [M-Serine-FA16:0]$^-$ (*m/z* -419.3), which exhibited higher intensity than [M-Serine-FA18:0]$^-$ (*m/z* -391.3), and confirmed the presence of PS(18:0/16:0). The fragmentation of PS(18:0/16:0) by itself would result in a noticeable lower intensity of [FA16:0]$^-$ (*m/z* -255.2) than that of [FA18:0]$^-$ (*m/z* -283.2), as the fatty acyl anion [FA2]$^-$ of a diacyl PS should exhibit lower abundance than [FA1]$^-$(*12*). However, in this case the intensity of [FA16:0]$^-$ (*m/z* -255.2) also contained partial contributions from PE(16:0/22:6). The overlapping of [FA16:0]$^-$ from two different lipid species compromised the abundance ratio between [FA16:0]$^-$ (*m/z* -255.2) and [FA18:0]$^-$ (*m/z* -283.2) and thus prevented the determination of fatty acyl chain positions of PS(18:0/16:0) on the basis of this abundance ratio. The lyso-form fragment ions allowed the stereospecific information to be unambiguously determined. Also there is no overlap between the lyso-form fragment ions of PE and PS. The lyso-form fragment ions of PE have even nominal *m/z* values while those of PS have odd nominal values.

Table 5.1 lists the identified diacyl glycerophospholipids from the cell extracts of lipin 1α over expressing cells, including PS, PE, PI, PA, and PG species. This result demonstrates that the novel methodology reported in this work can be employed to determine

the stereospecificity of all glycerophospholipids that are preferentially ionized under negative ion mode. The stereospecificity of the vast majority of the lipid species can be consistently elucidated based on the structural information obtained from either the fatty acyl anions or the lyso-form ions (in black). Around 30% of the listed diacyl glycerophospholipids were identified primarily based on the lyso-form ions (in red). These lipids included the diacyl glycerophosphoinositols, for which the stereospecificity cannot be identified on the basis of their fatty acyl anions (~10%), and other diacyl glycerophospholipids, for which the relative abundances of the fatty acyl anions of interest were either too close to call or lead to opposite positional isomers (~20%). As mentioned previously these fatty acyl anions were most likely overlapped with those from other lipid species. The determination of the fatty acyl positions for diacyl PE species represented the most challenging task, owing to the relatively lower abundance of the lyso-form ions and possible interferences from PC species. As a result, the fatty acyl chain positions of several diacyl PE species were proposed only based on the relative abundance of their acyl anions (in blue).

The ultimate solution for comprehensive determination of the stereospecific information of diacyl glycerophospholipids would likely necessitate the integration of front-end chromatographic separation. Nevertheless, diacyl PE species were identified in this work primarily based on the structural information from the lyso-form fragment ions without any chromatographic separation. Furthermore, the lipid species primarily identified on the basis of lyso-form fragment ions, such as PA(18:0/20:3), PG(18:0/16:1), PI(18:0/18:2), PI(16:0/20:2), PI(18:0/20:4), PI(18:0/20:3), PE(16:0/20:2), PE(16:0/22:4), and PE(16:0/22:3) have stereospecificities in agreement with the biochemistry convention, that assigns the saturated fatty acyl to the *sn1* position and the poly-unsaturated fatty acyl to the *sn2* position. It is interesting to note that stereospecificity of PE (18:1/16:1), which was determined primarily based on the lyso-form fragment ions, was consistent with PS (18:1/16:1), which was identified based on the structural information of both acyl anions and lyso-form ions. Similarly PE (18:1/20:2) and PI (18:1/20:2) were consistent with PA (18:1/20:2), where the former two were identified primarily based on the lyso-form fragment ions and the latter was identified based on the structural information of both acyl anions and lyso-form ions. It is also interesting to note that the stereospecificities of some diacyl glycerophospholipids,

identified primarily based on the lyso-form fragment ions, were consistent across different subclasses taking PS(18:1/18:3) and PE(18:1/18:3), and PS(18:1/20:3), PE(18:1/20:3), and PI(18:1/20:3), as examples. These results suggested that lyso-form fragment ions provided reliable structural information for the determination of stereospecificity of diacyl glycerophospholipids. Conveniently, this structural information was readily available from MS^2 mass spectra recorded on a hybrid quadrupole time-of-flight mass spectrometer.

5.5 Conclusions

In this work, we developed a novel approach for the determination of fatty acyl positions of diacyl glycerophospholipids, including PA, PS, PG, PI, and PE, for which all the structural information was obtained from MS^2 mass spectra recorded using a hybrid quadrupole time-of-flight mass spectrometer. We first fully examined the fragmentation patterns of a variety of diacyl glycerophospholipid standards over a wide range of collision energy. For all the diacyl glycerophospholipid standards examined it was found that the lyso-form fragment ions corresponding to the neutral loss of fatty acids from *sn2* position consistently exhibited higher abundance than those corresponding to the neutral loss from *sn1* position on the glycerol backbone. We then demonstrated the feasibility of determining the stereospecific information for diacyl glycerophospholipids in a lipid extract from rat hepatoma cell line, primarily on the basis of lyso-form fragment ions. We demonstrated that this new methodology is capable of accurately determining the stereospecific information for diacyl glycerophospholipids even with the interferences from isobaric lipid species and without chromatographic pre-separation. In addition, the approach is capable of locating the fatty acyl moieties of diacyl glycerophosphoinositols, which is impossible for methodologies that examine only structural information provided by the fatty acyl anions. Combining the novel methodology reported in this work with the currently widely practiced mass spectrometric techniques such as MPIS, FAS, and MDMS-SL, should enable a reliable and convenient platform for comprehensive glycerophospholipid profiling.

Figure Captions

Figure 5.1 Product ion spectrum of PA (17:0/14:1) recorded on a hybrid quadrupole time-of-flight mass spectrometer (QSTAR Pulsar) at collision energy of 20, 30, 40, and 50 eV, respectively. Reprinted with permission from Rapid Communication in Mass Spectrometry. Copyright © 2010 John Willey & Sons, Ltd.

Figure 5.2 (a). Absolute intensities (ion counts) of molecular ions, polar head group (*m/*z -153.0), and fatty acyl anions (*m/z* -225.2 and -269.3) of PA (17:0/14:1) plotted vs. collision energy. (b) Absolute intensities of lyso-form fragment ions $[M\text{-}Sn1]^-$, $[M\text{-}Sn2]^-$, $[M\text{-}(Sn1\text{-}H_2O)]^-$, and $[M\text{-}(Sn2\text{-}H_2O)]^-$ of PA (17:0/14:1) plotted vs. collision energy. (c) Ratios of the signal intensities of $[FA2]^-$ vs. $[FA1]^-$, $[M\text{-}(Sn2\text{-}H_2O)]^-$ vs. $[M\text{-}(Sn1\text{-}H_2O)]^-$, and $[M\text{-}Sn2]^-$ vs. $[M\text{-}Sn1]^-$ of PA (17:0/14:1). Reprinted with permission from Rapid Communication in Mass Spectrometry. Copyright © 2010 John Willey & Sons, Ltd.

Figure 5.3 (a). Absolute intensities (ion counts) of lyso-form fragment ions $[M\text{-}Sn1]^-$, $[M\text{-}Sn2]^-$, $[M\text{-}(Sn1\text{-}H_2O)]^-$, and $[M\text{-}(Sn2\text{-}H_2O)]^-$ of PA (12:0/13:0) plotted vs. collision energy. (b). Absolute intensities of lyso-form fragment ions $[M\text{-}Sn1]^-$, $[M\text{-}Sn2]^-$, $[M\text{-}(Sn1\text{-}H_2O)]^-$, and $[M\text{-}(Sn2\text{-}H_2O)]^-$ of PA (17:0/20:4) plotted vs. collision energy. Reprinted with permission from Rapid Communication in Mass Spectrometry. Copyright © 2010 John Willey & Sons, Ltd.

Figure 5.4 Fragmentation patterns of PA (17:0/14:1), PS (17:0/14:1), PG (17:0/14:1), PI (17:0/14:1), and PE (17:0/14:1). The diagrams exhibit the structure of these lipids and the bond cleavages of major fragments. The spectrum of PI (17:0/14:1) was recorded at 50 eV; all the other spectra were recorded at recorded at 40 eV. The PA, PS, PG, and PI species exhibited identical fragment ions in the region between the two red lines. Adapted with permission from Rapid Communication in Mass Spectrometry. Copyright © 2010 John Willey & Sons, Ltd.

Figure 5.5 Absolute intensities (ion counts) of lyso-form fragment ions of molecular anions of (17:0/14.1) diacylglycerophospholipids, plotted with respect to collision energy. (a). $[M\text{-Serine-Sn1}]^-$, $[M\text{- Serine-Sn2}]^-$, $[M\text{-Serine-(Sn1-}H_2O)]^-$, and $[M\text{-Serine-(Sn2-}H_2O)]^-$ of PS (b). $[M\text{-Sn1}]^-$, $[M\text{-Sn2}]^-$, $[M\text{-(Sn1-}H_2O)]^-$, and $[M\text{-(Sn2-}H_2O)]^-$ of PG (c). $[M\text{-Glycerol-Sn1}]^-$ and $[M\text{-Glycerol-Sn2}]^-$ of PG. Intensities corresponding to $[M\text{-Glycerol-(Sn1-}H_2O)]^-$ and $[M\text{-Glycerol-(Sn2-}H_2O)]^-$ are too low to be measured reliably (d). $[M\text{-Sn1}]^-$, $[M\text{-Sn2}]^-$, $[M\text{-(Sn1-}H_2O)]^-$, and $[M\text{-(Sn2-}H_2O)]^-$ of PI (17:0/14:1). (e). $[M\text{-Inositol-Sn1}]^-$, $[M\text{- Inositol-Sn2}]^-$ and $[M\text{- Inositol-(Sn2-}H_2O)]^-$ of PI. Intensities of $[M\text{-Inositol-(Sn1-}H_2O)]^-$ was too low to be measured reliably (f) $[M\text{-Sn1}]^-$, $[M\text{-Sn2}]^-$, $[M\text{-(Sn1-}H_2O)]^-$, and $[M\text{-(Sn2-}H_2O)]^-$ of PE. Reprinted with permission from Rapid Communication in Mass Spectrometry. Copyright © 2010 John Willey & Sons, Ltd.

Figure 5.6 Absolute intensities (ion counts) of lyso-form fragment ions plotted as a function of collision energy. (a). $[M\text{-Sn1}]^-$, $[M\text{-Sn2}]^-$, $[M\text{-(Sn1-}H_2O)]^-$, and $[M\text{-(Sn2-}H_2O)]^-$ of PS (12:0/13:0). (b). $[M\text{-Sn1}]^-$, $[M\text{-Sn2}]^-$, $[M\text{-(Sn1-}H_2O)]^-$, and $[M\text{-(Sn2-}H_2O)]^-$ of PS (17:0/20:4). (c). $[M\text{-Sn1}]^-$, $[M\text{-Sn2}]^-$, $[M\text{-(Sn1-}H_2O)]^-$, and $[M\text{-(Sn2-}H_2O)]^-$ of PG (12:0/13:0). (d). $[M\text{-Sn1}]^-$, $[M\text{-Sn2}]^-$, $[M\text{-(Sn1-}H_2O)]^-$, and $[M\text{-(Sn2-}H_2O)]^-$ of PG (17:0/20:4). (e). $[M\text{-Sn1}]^-$, $[M\text{-Sn2}]^-$, $[M\text{-(Sn1-}H_2O)]^-$, and $[M\text{-(Sn2-}H_2O)]^-$ of PI (12:0/13:0). (f). $[M\text{-Sn1}]^-$, $[M\text{-Sn2}]^-$, $[M\text{-(Sn1-}H_2O)]^-$, and $[M\text{-(Sn2-}H_2O)]^-$ of PI (17:0/20:4). (g). $[M\text{-Sn1}]^-$, $[M\text{-Sn2}]^-$, $[M\text{-(Sn1-}H_2O)]^-$, and $[M\text{-(Sn2-}H_2O)]^-$ of PE (12:0/13:0). (h). $[M\text{-Sn1}]^-$, $[M\text{-Sn2}]^-$, $[M\text{-(Sn1-}H_2O)]^-$, and $[M\text{-(Sn2-}H_2O)]^-$ of PE (17:0/20:4). Reprinted with permission from Rapid Communication in Mass Spectrometry. Copyright © 2010 John Willey & Sons, Ltd.

Figure 5.7 (a). Ratios of the signal intensities of $[FA2]^-$ vs. $[FA1]^-$, $[M\text{-(Sn2-}H_2O)]^-$ vs. $[M\text{-(Sn1-}H_2O)]^-$, and $[M\text{-Sn2}]^-$ vs. $[M\text{-Sn1}]^-$ of PI (12:0/13:0) plotted vs. collision energy. (b). Ratios of the signal intensities of $[FA2]^-$ vs. $[FA1]^-$, $[M\text{-(Sn2-}H_2O)]^-$ vs. $[M\text{-(Sn1-}H_2O)]^-$, and $[M\text{-Sn2}]^-$ vs. $[M\text{-Sn1}]^-$ of PI (17:0/14:1) plotted vs. collision energy. (c). Ratios of the signal intensities of $[FA2]^-$ vs. $[FA1]^-$, $[M\text{-(Sn2-}H_2O)]^-$ vs. $[M\text{-(Sn1-}H_2O)]^-$, and $[M\text{-Sn2}]^-$ vs. $[M\text{-Sn1}]^-$ of PI (17:0/20:4) plotted vs. collision energy. Reprinted with permission from Rapid Communication in Mass Spectrometry. Copyright © 2010 John Willey & Sons, Ltd.

Figure 5.8 (a). Precursor ion spectrum for fragment ions at *m/z* -153 to identify molecular anions of PA, PS, PG, and PI species from lipin-1α overexpressing cell line lipid extract. (b). Precursor ion spectrum for fragment ions at *m/z* -196 to identify molecular anions of PE species from lipin-1α overexpressing cell line lipid extract. Reprinted with permission from Rapid Communication in Mass Spectrometry. Copyright © 2010 John Willey & Sons, Ltd.

Figure 5.9 The overlapped product ion spectrum of molecular anions of the isobaric lipid species PS(18:0/22:6) and PS(18:1/22:5) at *m/z* -834.6. Fragment ions at *m/z* -153 correspond to [Glycerophosphate-H_2O]$^-$ and those at *m/z* -747.5 to neural loss of 87 Da (the serine head group). Fragment ions at *m/z* -281.3, -283.3, -327.2, and -329.2, corresponding to fatty acyl anions [FA18:1]$^-$, [FA18:0]$^-$, [FA22:6]$^-$, and [FA22:5]$^-$, respectively. For PS(18:0/22:6), lyso-form fragment ions are observed at *m/z* -419.3, -437.3, -463.3, and -481.3, corresponding to [M-Serine-FA22:6]$^-$, [M-Serine-(FA22:6-H_2O)]$^-$, [M-Serine-FA18:0]$^-$, and [M-Serine-(FA18:0-H_2O)]$^-$, respectively. Fragment ions at *m/z* -417.3 and -435.3 are lyso-form fragment ions from PS(18:1/22:5). Reprinted with permission from Rapid Communication in Mass Spectrometry. Copyright © 2010 John Willey & Sons, Ltd.

Figure 5.10 The overlapped product ion spectrum of molecular anions of the isobaric lipid species PI(18:0/20:4) and PI(18:1/20:3) at *m/z* -885.5. Fragment ions at *m/z* -153, -223, -241, and -259 correspond to [Glycerophosphate-H_2O]$^-$, [Inositolphosphate-$2H_2O$]$^-$, [Inositolphosphate-H_2O]$^-$, and [Inositolphosphate]$^-$, respectively. Fragment ions at *m/z* -281.3, -283.3, -303.2, and -305.2, correspond to fatty acyl anions [FA18:1]$^-$, [FA18:0]$^-$, [FA20:4]$^-$, and [FA20:3]$^-$, respectively. For PI(18:0/20:4), the lyso-form fragment ions are observed at *m/z* -601.3, -619.3, -581.3, and -599.3, corresponding to [M-FA18:0]$^-$, [M-(FA18:0-H_2O)]$^-$, [M-FA20:4]$^-$, and [M-(FA20:4-H_2O)]$^-$, respectively. For PI(18:1/20:3), lyso-form fragment ions are at *m/z* -579.3, -597.3, -603.3, and -621.3. Peaks at *m/z* -417.3 and -419.3 correspond to lyso-form fragment ions [M-Inositol-FA20:3]$^-$ and [M-Inositol-FA20:4]$^-$, respectively. Reprinted with permission from Rapid Communication in Mass Spectrometry. Copyright © 2010 John Willey & Sons, Ltd.

Figure 5.11 The overlapped product ion spectrum of molecular anions of the isobaric lipid species PE(18:1/20:5), PE(18:2/20:4), PE(16:0/22:6), PE(16:1/22:5), and PS(18:0/16:0) at *m/z* -762.5. Fragment ions at *m/z* -153 ([Glycerophosphate-H_2O]$^-$), -196 ([Ethanolaminephosphate-H_2O]$^-$), and -675.5 (neutral loss of 87 Da, the serine head group) indicate the presence of a mixture of several isobaric PE and PS lipid species. Lyso-form fragment ions of PE(18:1/20:5), PE(18:2/20:4), PE(16:0/22:6), and PE(16:1/22:5) are observed at even nominal *m/z* values while lyso-form fragment ions of PS(18:0/16:0) are at odd nominal *m/z*. The intensity of [FA16:0]$^-$ (m/z 255.2) contained contributions from both PE(16:0/22:6) and PS(18:0/16:0). Reprinted with permission from Rapid Communication in Mass Spectrometry.

Table 5.1 List of diacyl glycerophospholipids identified and their relative abundance with respect to the base peak. Lipid species in black are those for which the stereospecificity is consistently elucidated based on the structural information obtained from either the fatty acyl anions or the lyso-form ions. Lipid species in red are those for which the stereospecificity is identified primarily based on the lyso-form ions, including the diacyl glycerophosphoinositols, for which the stereospecificity cannot be identified on the basis of their fatty acyl anions, and other diacyl glycerophospholipids, for which the relative abundances of the fatty acyl anions of interest were either too close to call or lead to opposite positional isomers. Lipid species in blue are those for which the stereospecificity is proposed only based on the relative abundance of their acyl anions.

Lipid classes	m/z	% of base peak	Lipid Species
PA	725.4	37.6	PA(18:1/20:2)
			PA(18:2/20:1)
			PA(18:0/20:3)
PG	747.9	16.8	PG(16:0/18:1)
			PG(18:0/16:1)
PI	861.6	28.8	PI(18:0/18:2)
			PI(18:1/18:1)
			PI(16:0/20:2)
	885.6	38.4	PI(18:0/20:4)
			PI(18:1/20:3)
	887.7	36	PI(18:0/20:3)
			PI(18:1/20:2)
PS	732.3	16	PS(16:0/16:1)
	758.4	23.2	PS(16:0/18:2)
			PS(18:1/16:1)
	760.5	46.4	PS(16:0/18:1)
			PS(18:0/16:1)
	762.5	17.6	PS(18:0/16:0)
	782.4	20.8	PS(16:0/20:4)
			PS(18:1/18:3)
			PS(18:2/18:2)
	784.5	26.4	PS(16:0/20:3)
			PS(18:0/18:3)
			PS(18:1/18:2)
	786.6	64	PS(18:0/18:2)
			PS(18:1/18:1)
			PS(16:0/20:2)
	788.4	42.4	PS(18:0/18:1)
	808.5	36.8	PS(18:0/20:5)
			PS(18:1/20:4)
	810.6	48.8	PS(18:0/20:4)
			PS(18:1/20:3)
	812.4	52.8	PS(18:0/20:3)
	834.6	100	PS(18:0/22:6)
			PS(18:1/22:5)
	836.4	62.4	PS(18:0/22:5)
	862.5	32	PS(20:0/22:6)
			PS(20:1/22:5)

Lipid classes	m/z	% of base peak	Lipid Species
PE	714.5	58.2	PE(16:0/18:2)
			PE(18:1/16:1)
	716.6	94.5	PE(16:0/18:1)
			PE(18:0/16:1)
	736.4	52.7	PE(16:0/20:5)
			PE(16:1/20:4)
	738.5	65.5	PE(16:0/20:4)
			PE(16:1/20:3)
			PE(18:2/18:2)
			PE(18:1/18:3)
	740.3	72.7	PE(16:0/20:3)
			PE(20:2/16:1)
			PE(18:0/18:3)
			PE(18:1/18:2)
	742.7	85.5	PE(16:0/20:2)
			PE(18:1/18:1)
			PE(18:0/18:2)
	744.8	43.6	PE(16:0/20:1)
			PE(18:0/18:1)
	762.2	60	PE(16:0/22:6)
			PE(18:1/20:5)
			PE(18:2/20:4)
	764.6	100	PE(18:0/20:5)
			PE(18:1/20:4)
	766.7	96.4	PE(18:0/20:4)
			PE(18:1/20:3)
			PE(16:0/22:4)
	768.5	40	PE(16:0/22:3)
			PE(18:0/20:3)
			PE(20:1/18:2)
			PE(18:1/20:2)
	788.3	18.2	PE(18:1/22:6)
	790.1	30.9	PE(18:0/22:6)
			PE(18:1/22:5)

Figure 5.1

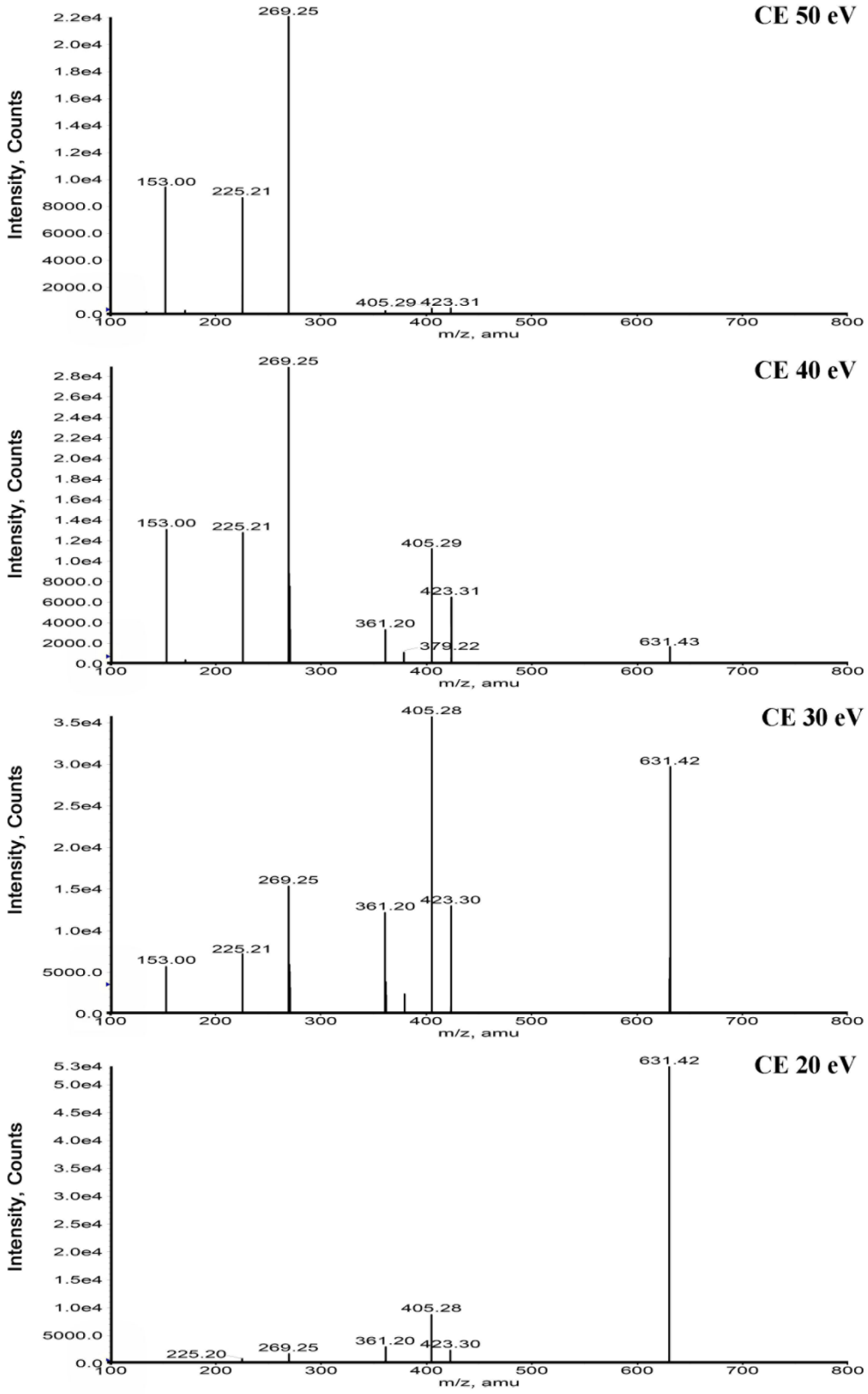
CE 50 eV
Intensity, Counts
m/z, amu
269.25
153.00
225.21
405.29
423.31
CE 40 eV
Intensity, Counts
m/z, amu
269.25
153.00
225.21
405.29
423.31
361.20
379.22
631.43
CE 30 eV
Intensity, Counts
m/z, amu
405.28
631.42
269.25
361.20
423.30
153.00
225.21
CE 20 eV
Intensity, Counts
m/z, amu
631.42
405.28
225.20
269.25
361.20
423.30

Figure 5.2

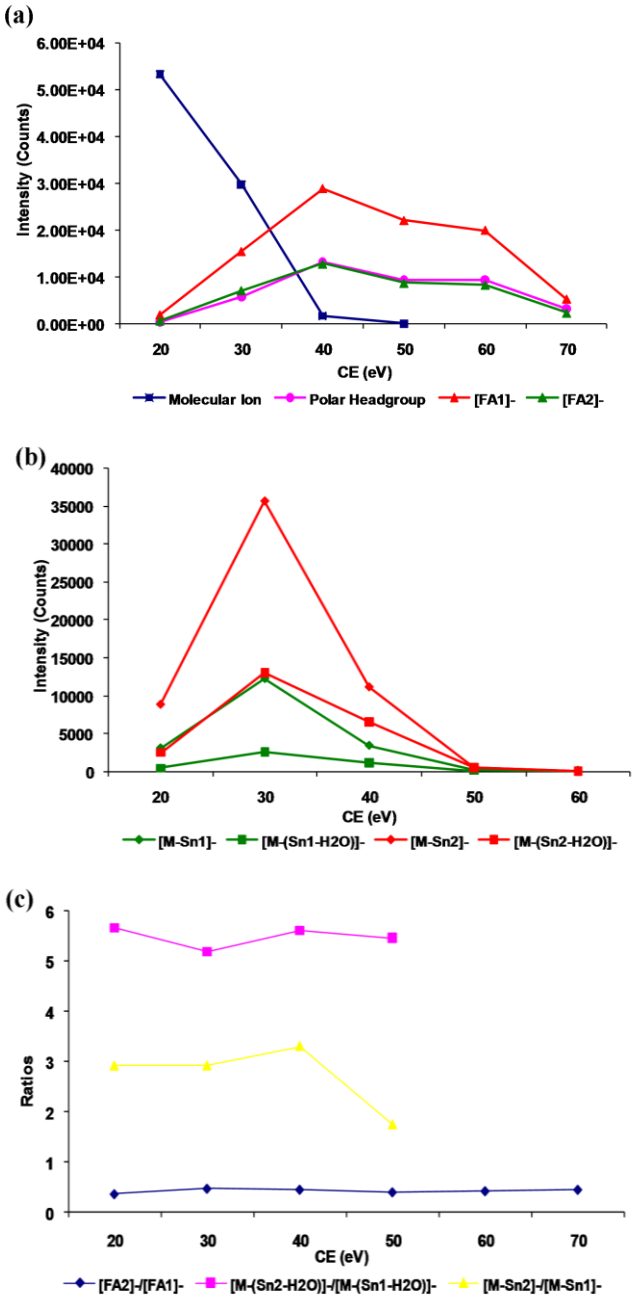
(a)
6.00E+04
5.00E+04
4.00E+04
3.00E+04
2.00E+04
1.00E+04
0.00E+00
Intensity (Counts)
20
30
40
50
60
70
CE (eV)
Molecular Ion
Polar Headgroup
[FA1]-
[FA2]-
(b)
40000
35000
30000
25000
20000
15000
10000
5000
0
Intensity (Counts)
20
30
40
50
60
CE (eV)
[M-Sn1]-
[M-(Sn1-H2O)]-
[M-Sn2]-
[M-(Sn2-H2O)]-
(c)
6
5
4
3
2
1
0
Ratios
20
30
40
50
60
70
CE (eV)
[FA2]-/[FA1]-
[M-(Sn2-H2O)]-/[M-(Sn1-H2O)]-
[M-Sn2]-/[M-Sn1]-

Figure 5.3

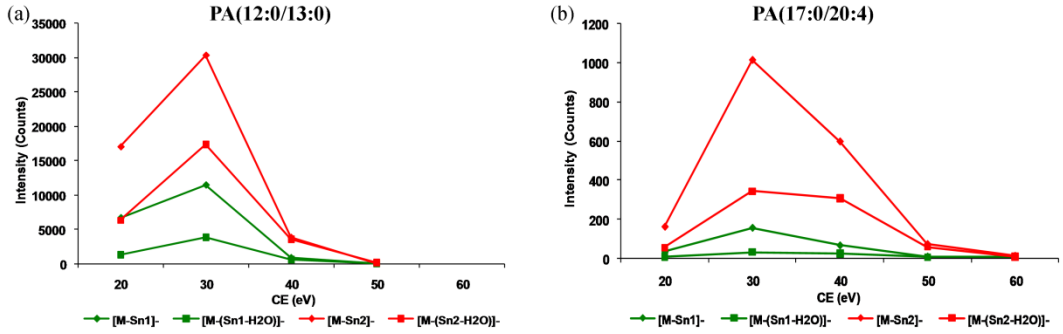
(a)
PA(12:0/13:0)
Intensity (Counts)
35000
30000
25000
20000
15000
10000
5000
0
20
30
40
50
60
CE (eV)
[M-Sn1]-
[M-(Sn1-H2O)]-
[M-Sn2]-
[M-(Sn2-H2O)]-
(b)
PA(17:0/20:4)
Intensity (Counts)
1200
1000
800
600
400
200
0
20
30
40
50
60
CE (eV)
[M-Sn1]-
[M-(Sn1-H2O)]-
[M-Sn2]-
[M-(Sn2-H2O)]-

Figure 5.4

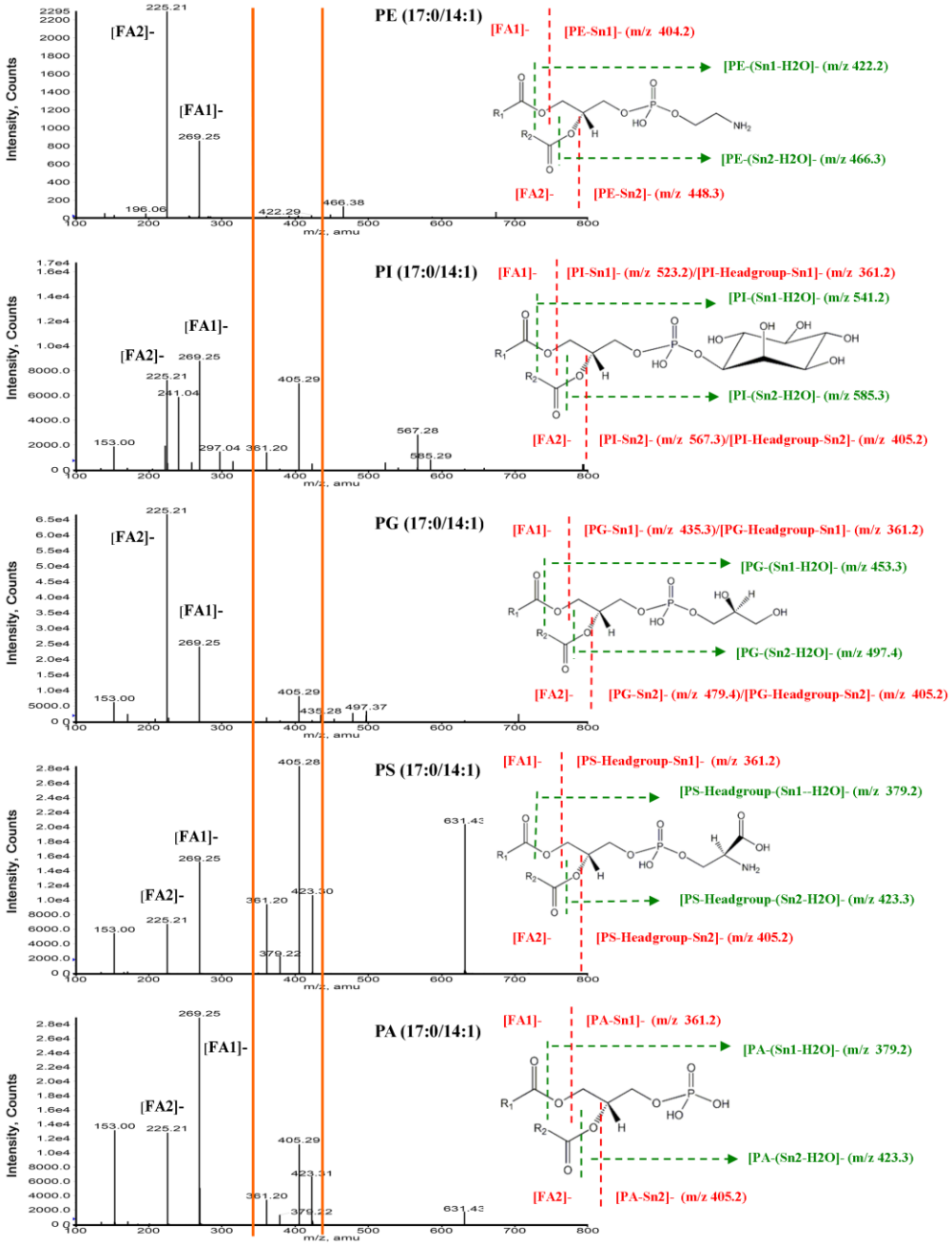
PE (17:0/14:1)
[FA1]-
[PE-Sn1]- (m/z 404.2)
[PE-(Sn1-H2O]- (m/z 422.2)
[PE-(Sn2-H2O]- (m/z 466.3)
[FA2]-
[PE-Sn2]- (m/z 448.3)
PI (17:0/14:1)
[PI-Sn1]- (m/z 523.2)/[PI-Headgroup-Sn1]- (m/z 361.2)
[PI-(Sn1-H2O]- (m/z 541.2)
[PI-(Sn2-H2O]- (m/z 585.3)
[PI-Sn2]- (m/z 567.3)/[PI-Headgroup-Sn2]- (m/z 405.2)
PG (17:0/14:1)
[PG-Sn1]- (m/z 435.3)/[PG-Headgroup-Sn1]- (m/z 361.2)
[PG-(Sn1-H2O]- (m/z 453.3)
[PG-(Sn2-H2O]- (m/z 497.4)
[PG-Sn2]- (m/z 479.4)/[PG-Headgroup-Sn2]- (m/z 405.2)
PS (17:0/14:1)
[PS-Headgroup-Sn1]- (m/z 361.2)
[PS-Headgroup-(Sn1--H2O]- (m/z 379.2)
[PS-Headgroup-(Sn2-H2O]- (m/z 423.3)
[PS-Headgroup-Sn2]- (m/z 405.2)
PA (17:0/14:1)
[PA-Sn1]- (m/z 361.2)
[PA-(Sn1-H2O]- (m/z 379.2)
[PA-(Sn2-H2O]- (m/z 423.3)
[PA-Sn2]- (m/z 405.2)
Intensity, Counts
m/z, amu

Figure 5.5

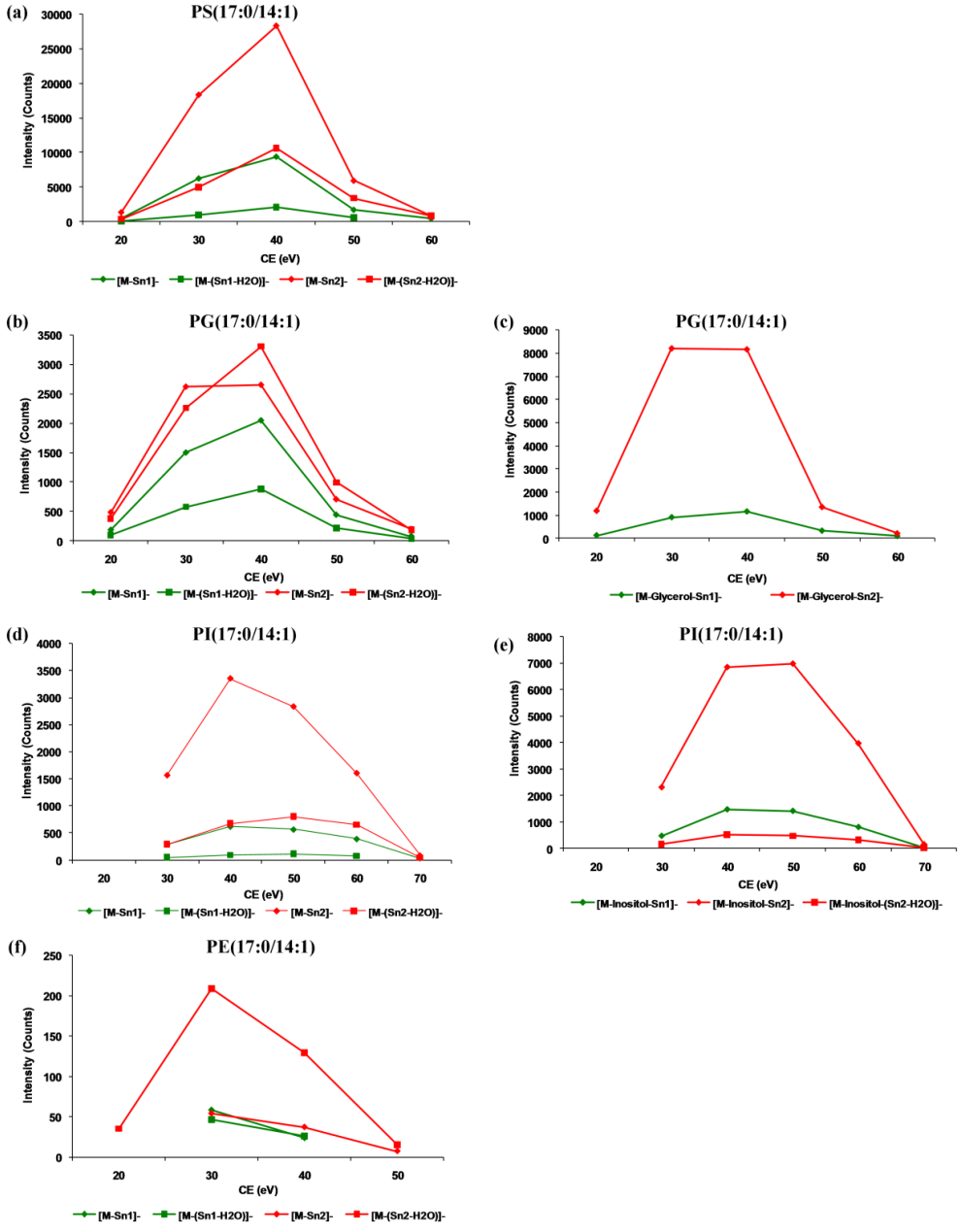
(a)
PS(17:0/14:1)
Intensity (Counts)
CE (eV)
[M-Sn1]-
[M-(Sn1-H2O)]-
[M-Sn2]-
[M-(Sn2-H2O)]-
(b)
PG(17:0/14:1)
Intensity (Counts)
CE (eV)
[M-Sn1]-
[M-(Sn1-H2O)]-
[M-Sn2]-
[M-(Sn2-H2O)]-
(c)
PG(17:0/14:1)
Intensity (Counts)
CE (eV)
[M-Glycerol-Sn1]-
[M-Glycerol-Sn2]-
(d)
PI(17:0/14:1)
Intensity (Counts)
CE (eV)
[M-Sn1]-
[M-(Sn1-H2O)]-
[M-Sn2]-
[M-(Sn2-H2O)]-
(e)
PI(17:0/14:1)
Intensity (Counts)
CE (eV)
[M-Inositol-Sn1]-
[M-Inositol-Sn2]-
[M-Inositol-(Sn2-H2O)]-
(f)
PE(17:0/14:1)
Intensity (Counts)
CE (eV)
[M-Sn1]-
[M-(Sn1-H2O)]-
[M-Sn2]-
[M-(Sn2-H2O)]-

Figure 5.6

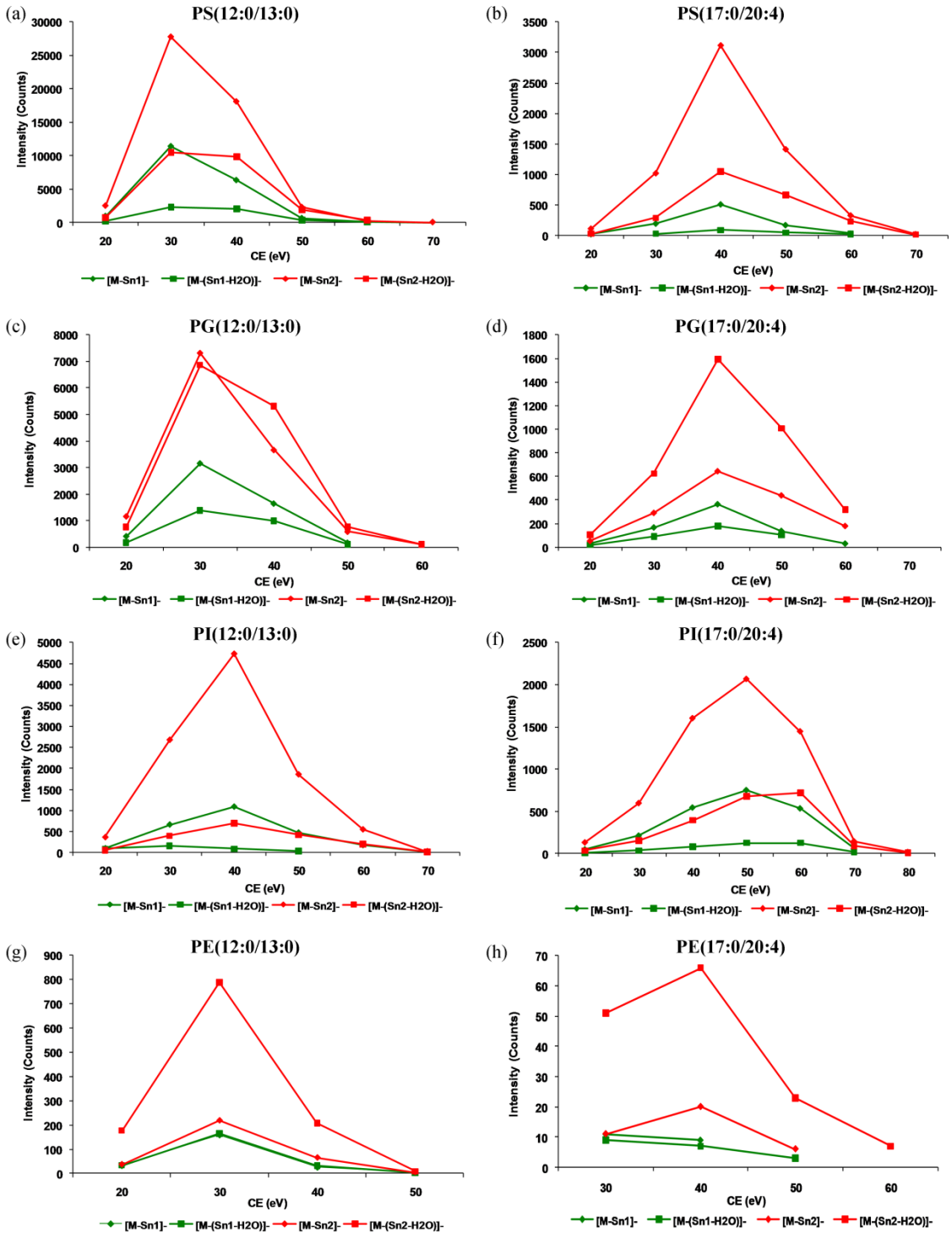
(a)
PS(12:0/13:0)
(b)
PS(17:0/20:4)
(c)
PG(12:0/13:0)
(d)
PG(17:0/20:4)
(e)
PI(12:0/13:0)
(f)
PI(17:0/20:4)
(g)
PE(12:0/13:0)
(h)
PE(17:0/20:4)
Intensity (Counts)
CE (eV)
[M-Sn1]-
[M-(Sn1-H2O)]-
[M-Sn2]-
[M-(Sn2-H2O)]-

Figure 5.7

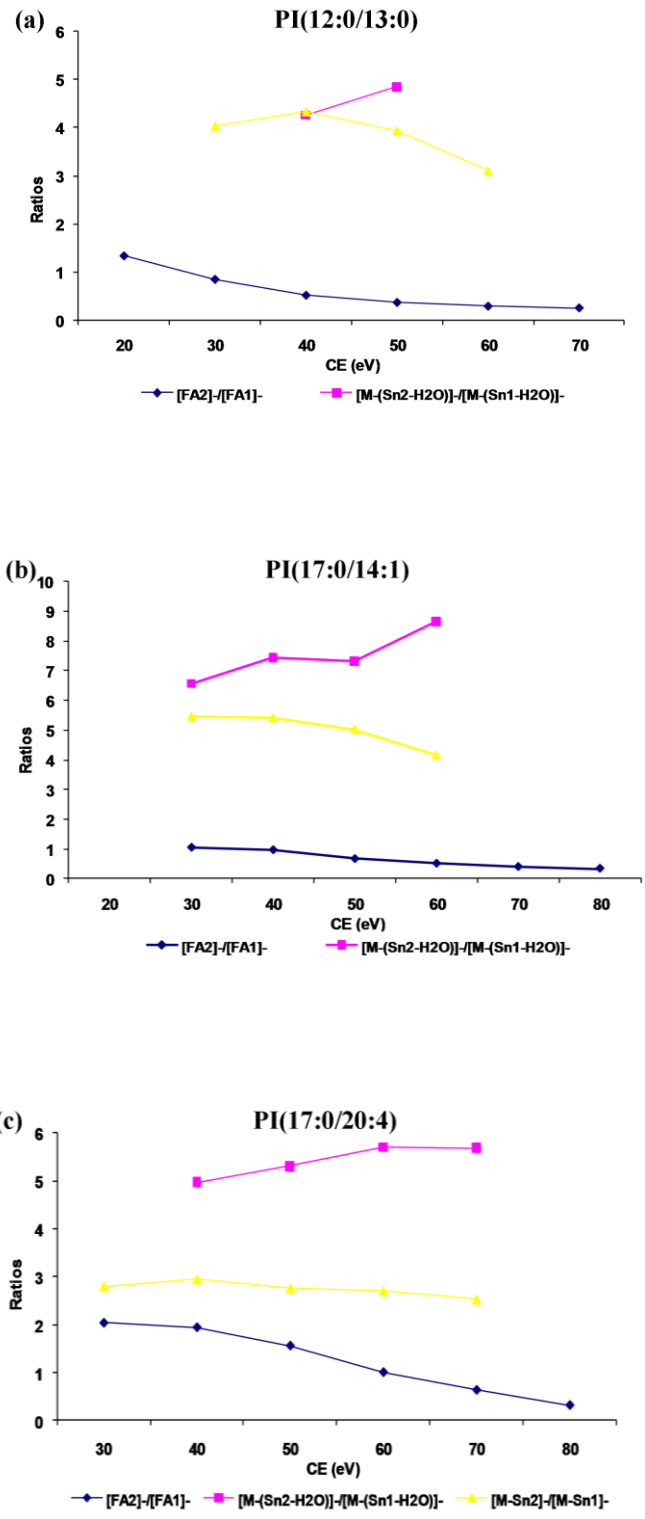
(a)
PI(12:0/13:0)
Ratios
CE (eV)
[FA2]-/[FA1]-
[M-(Sn2-H2O)]-/[M-(Sn1-H2O)]-
(b)
PI(17:0/14:1)
Ratios
CE (eV)
[FA2]-/[FA1]-
[M-(Sn2-H2O)]-/[M-(Sn1-H2O)]-
(c)
PI(17:0/20:4)
Ratios
CE (eV)
[FA2]-/[FA1]-
[M-(Sn2-H2O)]-/[M-(Sn1-H2O)]-
[M-Sn2]-/[M-Sn1]-

Figure 5.8

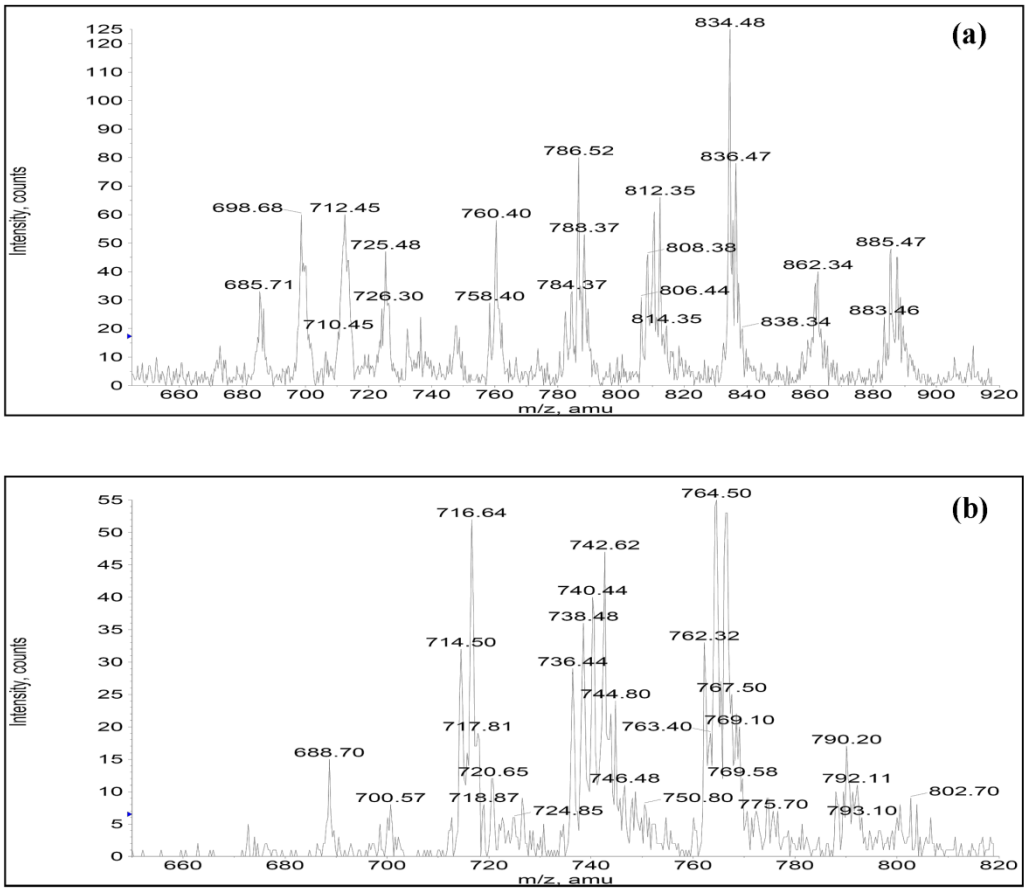
(a)
Intensity, counts
m/z, amu
834.48
786.52
836.47
812.35
698.68
712.45
760.40
788.37
725.48
808.38
885.47
862.34
685.71
726.30
758.40
784.37
806.44
883.46
710.45
814.35
838.34
(b)
Intensity, counts
m/z, amu
764.50
716.64
742.62
740.44
738.48
762.32
714.50
736.44
744.80
767.50
717.81
763.40
769.10
790.20
688.70
720.65
746.48
769.58
792.11
802.70
700.57
718.87
724.85
750.80
775.70
793.10

Figure 5.9

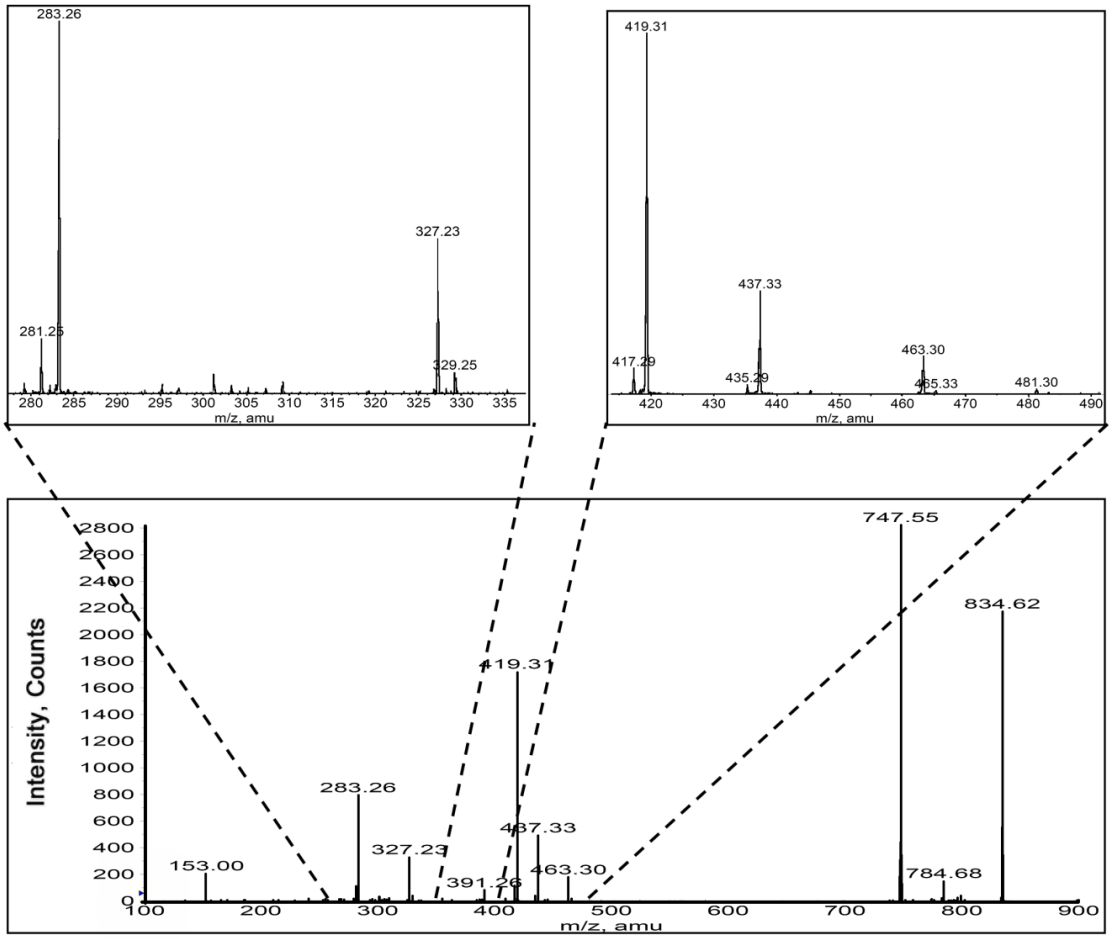
283.26
327.23
281.25
329.25
m/z, amu
419.31
437.33
417.29
435.29
463.30
481.30
m/z, amu
Intensity, Counts
747.55
834.62
419.31
283.26
437.33
327.23
153.00
391.26
463.30
784.68
m/z, amu

Figure 5.10

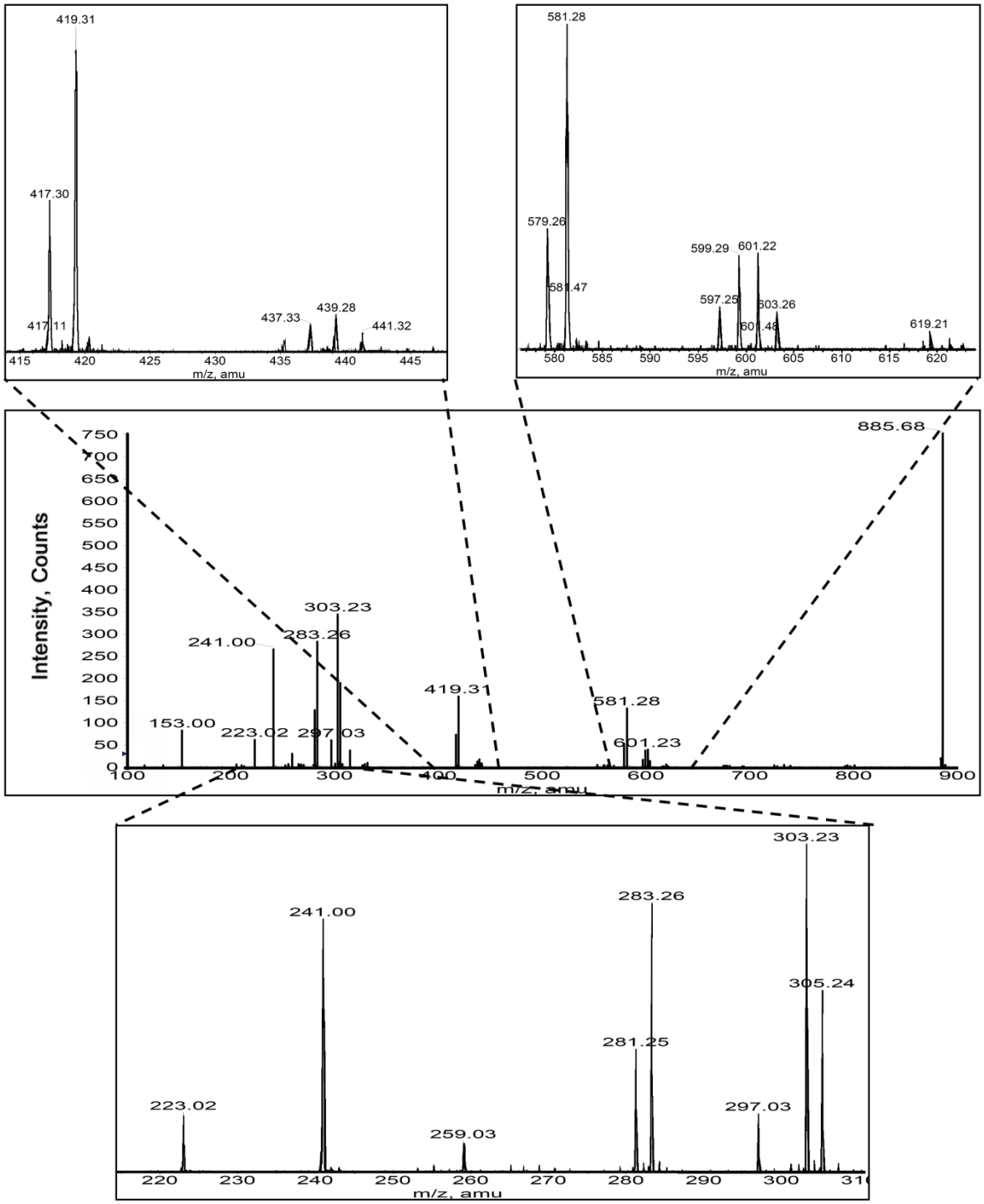
419.31
417.30
417.11
437.33
439.28
441.32
415
420
425
430
435
440
445
m/z, amu
581.28
579.26
581.47
599.29
601.22
597.25
603.26
601.48
619.21
580
585
590
595
600
605
610
615
620
m/z, amu
Intensity, Counts
750
700
650
600
550
500
450
400
350
300
250
200
150
100
50
0
885.68
303.23
283.26
241.00
419.31
581.28
153.00
223.02
297.03
601.23
100
200
300
400
500
600
700
800
900
m/z, amu
303.23
241.00
283.26
305.24
281.25
223.02
259.03
297.03
220
230
240
250
260
270
280
290
300
m/z, amu

Figure 5.11

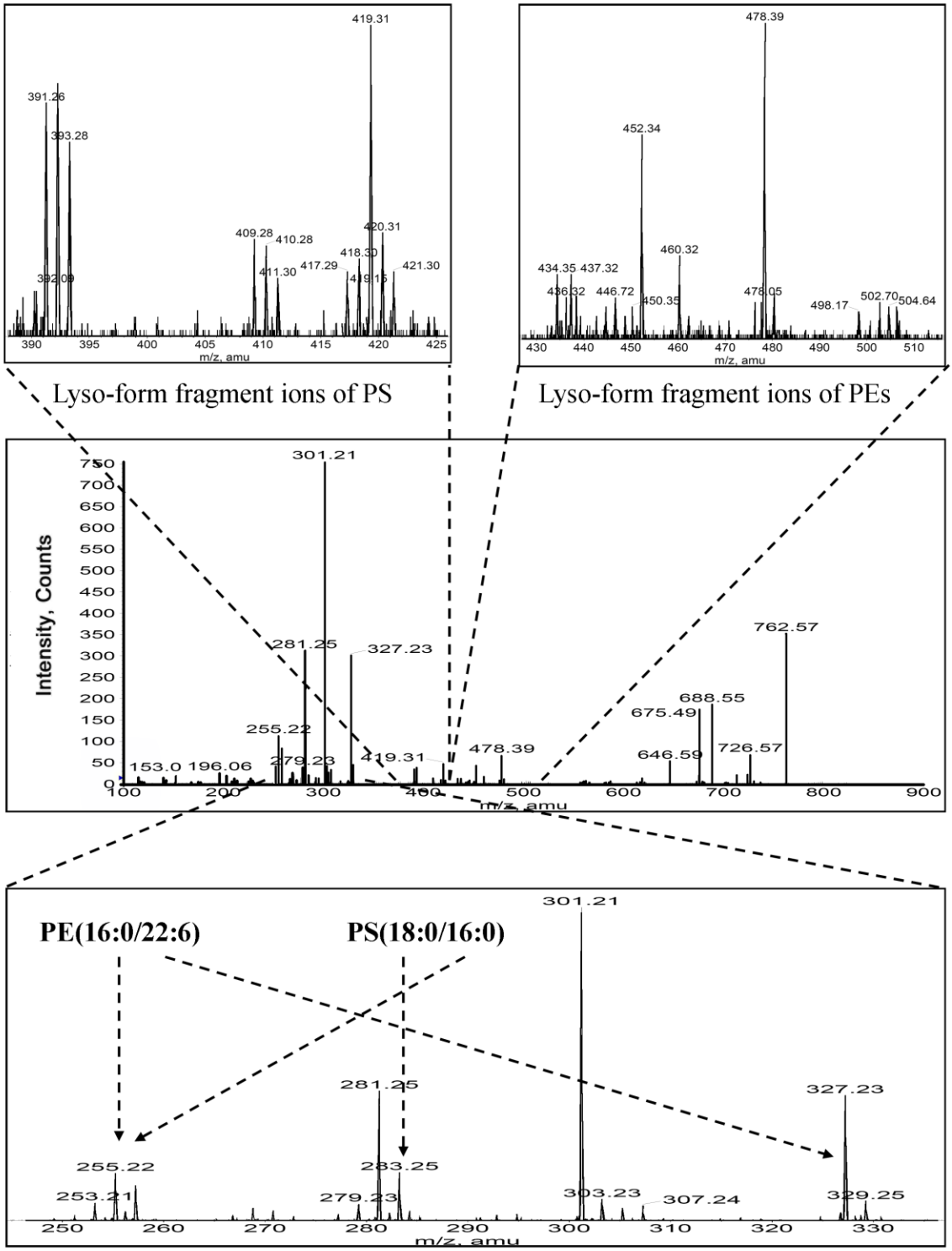
Lyso-form fragment ions of PS
Lyso-form fragment ions of PEs
Intensity, Counts
m/z, amu
PE(16:0/22:6)
PS(18:0/16:0)

References

1. Han, X., and Gross, R. W. (2005) Shotgun lipidomics: electrospray ionization mass spectrometric analysis and quantitation of cellular lipidomes directly from crude extracts of biological samples, *Mass Spectrom Rev 24*, 367-412.
2. Wenk, M. R. (2005) The emerging field of lipidomics, *Nat Rev Drug Discov 4*, 594-610.
3. Wenk, M. R., Lucast, L., Di Paolo, G., Romanelli, A. J., Suchy, S. F., Nussbaum, R. L., Cline, G. W., Shulman, G. I., McMurray, W., and De Camilli, P. (2003) Phosphoinositide profiling in complex lipid mixtures using electrospray ionization mass spectrometry, *Nat Biotechnol 21*, 813-817.
4. Pulfer, M., and Murphy, R. C. (2003) Electrospray mass spectrometry of phospholipids, *Mass Spectrom Rev 22*, 332-364.
5. Hou, W., Zhou, H., Elisma, F., Bennett, S. A., and Figeys, D. (2008) Technological developments in lipidomics, *Brief Funct Genomic Proteomic 7*, 395-409.
6. Milne, S., Ivanova, P., Forrester, J., and Alex Brown, H. (2006) Lipidomics: an analysis of cellular lipids by ESI-MS, *Methods 39*, 92-103.
7. Ejsing, C. S., Sampaio, J. L., Surendranath, V., Duchoslav, E., Ekroos, K., Klemm, R. W., Simons, K., and Shevchenko, A. (2009) Global analysis of the yeast lipidome by quantitative shotgun mass spectrometry, *Proc Natl Acad Sci U S A 106*, 2136-2141.
8. Aebersold, R., and Mann, M. (2003) Mass spectrometry-based proteomics, *Nature 422*, 198-207.
9. Yetukuri, L., Ekroos, K., Vidal-Puig, A., and Oresic, M. (2008) Informatics and computational strategies for the study of lipids, *Mol Biosyst 4*, 121-127.
10. Oresic, M., Hanninen, V. A., and Vidal-Puig, A. (2008) Lipidomics: a new window to biomedical frontiers, *Trends Biotechnol 26*, 647-652.
11. Hsu, F. F., and Turk, J. (2000) Charge-driven fragmentation processes in diacyl glycerophosphatidic acids upon low-energy collisional activation. A mechanistic proposal, *J Am Soc Mass Spectrom 11*, 797-803.
12. Hsu, F. F., and Turk, J. (2005) Studies on phosphatidylserine by tandem quadrupole

and multiple stage quadrupole ion-trap mass spectrometry with electrospray ionization: structural characterization and the fragmentation processes, *J Am Soc Mass Spectrom 16*, 1510-1522.

13. Hsu, F. F., and Turk, J. (2001) Studies on phosphatidylglycerol with triple quadrupole tandem mass spectrometry with electrospray ionization: fragmentation processes and structural characterization, *J Am Soc Mass Spectrom 12*, 1036-1043.
14. Hsu, F. F., and Turk, J. (2000) Charge-remote and charge-driven fragmentation processes in diacyl glycerophosphoethanolamine upon low-energy collisional activation: a mechanistic proposal, *J Am Soc Mass Spectrom 11*, 892-899.
15. Hsu, F. F., and Turk, J. (2000) Characterization of phosphatidylinositol, phosphatidylinositol-4-phosphate, and phosphatidylinositol-4,5-bisphosphate by electrospray ionization tandem mass spectrometry: a mechanistic study, *J Am Soc Mass Spectrom 11*, 986-999.
16. Hsu, F. F., and Turk, J. (2000) Characterization of phosphatidylethanolamine as a lithiated adduct by triple quadrupole tandem mass spectrometry with electrospray ionization, *J Mass Spectrom 35*, 595-606.
17. Han, X., and Gross, R. W. (1995) Structural Determination of Picomole Amounts of Phospholipids Via Electrospray Ionization Tandem Mass Spectrometry, *J Am Soc Mass Spectrom 6*, 1202-1210.
18. Hsu, F. F., Bohrer, A., and Turk, J. (1998) Formation of lithiated adducts of glycerophosphocholine lipids facilitates their identification by electrospray ionization tandem mass spectrometry, *J Am Soc Mass Spectrom 9*, 516-526.
19. Ho, Y. P., Huang, P. C., and Deng, K. H. (2003) Metal ion complexes in the structural analysis of phospholipids by electrospray ionization tandem mass spectrometry, *Rapid Commun Mass Spectrom 17*, 114-121.
20. Hsu, F. F., and Turk, J. (2003) Electrospray ionization/tandem quadrupole mass spectrometric studies on phosphatidylcholines: the fragmentation processes, *J Am Soc Mass Spectrom 14*, 352-363.
21. Yang, K., Cheng, H., Gross, R. W., and Han, X. (2009) Automated lipid identification and quantification by multidimensional mass spectrometry-based shotgun lipidomics, *Anal Chem 81*, 4356-4368.

22. Ejsing, C. S., Duchoslav, E., Sampaio, J., Simons, K., Bonner, R., Thiele, C., Ekroos, K., and Shevchenko, A. (2006) Automated identification and quantification of glycerophospholipid molecular species by multiple precursor ion scanning, *Anal Chem 78*, 6202-6214.
23. Ekroos, K., Chernushevich, I. V., Simons, K., and Shevchenko, A. (2002) Quantitative profiling of phospholipids by multiple precursor ion scanning on a hybrid quadrupole time-of-flight mass spectrometer, *Anal Chem 74*, 941-949.
24. Schwudke, D., Oegema, J., Burton, L., Entchev, E., Hannich, J. T., Ejsing, C. S., Kurzchalia, T., and Shevchenko, A. (2006) Lipid profiling by multiple precursor and neutral loss scanning driven by the data-dependent acquisition, *Anal Chem 78*, 585-595.
25. Han, X., Yang, J., Cheng, H., Ye, H., and Gross, R. W. (2004) Toward fingerprinting cellular lipidomes directly from biological samples by two-dimensional electrospray ionization mass spectrometry, *Anal Biochem 330*, 317-331.
26. Han, X., and Gross, R. W. (2003) Global analyses of cellular lipidomes directly from crude extracts of biological samples by ESI mass spectrometry: a bridge to lipidomics, *J Lipid Res 44*, 1071-1079.
27. Ekroos, K., Ejsing, C. S., Bahr, U., Karas, M., Simons, K., and Shevchenko, A. (2003) Charting molecular composition of phosphatidylcholines by fatty acid scanning and ion trap MS3 fragmentation, *J Lipid Res 44*, 2181-2192.
28. Larsen, A., Uran, S., Jacobsen, P. B., and Skotland, T. (2001) Collision-induced dissociation of glycero phospholipids using electrospray ion-trap mass spectrometry, *Rapid Commun Mass Spectrom 15*, 2393-2398.
29. Hvattum, E., Hagelin, G., and Larsen, A. (1998) Study of mechanisms involved in the collision-induced dissociation of carboxylate anions from glycerophospholipids using negative ion electrospray tandem quadrupole mass spectrometry, *Rapid Commun Mass Spectrom 12*, 1405-1409.
30. Reue, K., and Brindley, D. N. (2008) Thematic Review Series: Glycerolipids. Multiple roles for lipins/phosphatidate phosphatase enzymes in lipid metabolism, *J Lipid Res 49*, 2493-2503.
31. Bou Khalil, M., Sundaram, M., Zhang, H. Y., Links, P. H., Raven, J. F., Manmontri,

B., Sariahmetoglu, M., Tran, K., Reue, K., Brindley, D. N., and Yao, Z. (2009) The level and compartmentalization of phosphatidate phosphatase-1 (lipin-1) control the assembly and secretion of hepatic VLDL, *J Lipid Res 50*, 47-58.

Chapter 6 Conclusions

6.1 The development of proteomic reactors

In chapter 3, I described the development of different versions of microfluidic proteomic reactors, namely, the SCX proteomic reactor, the 96-well SCX plate reactor, and the SAX proteomic reactor, for processing complex protein samples. To the best of my knowledge, there are no reports indicating that other groups have developed similar proteomic reactor devices for processing protein samples.

These microfluidic proteomic reactors developed in the thesis have provided an integrated platform for efficiently and reliably processing minute amounts of protein samples. These reactors can perform protein sample clean-up, preconcentration, chemical reactions (e.g. protein reduction and alkylation of cysteines), and enzymatic digestion all in a single device and therefore sample loss can be minimized. Although the proteomic reactor can be used as a standalone device, the resulting peptides are eluted using a buffer readily compatible with HPLC-ESI-MS/MS.

As the total time to process protein samples using the proteomic reactor techniques is relatively shorter (~3 hours) in comparison to other protein digestion methodologies, the proteomic reactor approaches can also increase the throughput for processing complex biological samples, which is necessary for large scale analysis of proteomes.

Comparing the performance of both the SCX and SAX reactors for digesting the same amount of protein samples to that of the in-solution digestion, we have demonstrated that up to 10 times more protein and a significantly better sequence coverage for individual proteins can be obtained using the proteomic reactor techniques. The better performance of the proteomic reactor approaches is likely attributed to protein samples clean-up and preconcentration prior to enzymatic digestion, and the efficient protein digestion within an interstitial volume of nanoliters.

Comparing the performance of the SAX and SCX proteomic reactors with 2 μg of yeast lysates, we found that although the total number of unique peptides identified through the SCX or the SAX reactors are similar, only around 40% of the identified peptides overlapped. In addition, the overlap in proteins identified with SCX and SAX reactors is also low. Analysis of two proteins (YGR009C, YHR174W) identified with both SAX and SCX reactors, we found that the unique peptides identified with SAX and SCX reactor, respectively, were mapped to different sequence locations in these proteins. Further analysis of pI of these identified peptides/proteins revealed that the SAX reactor was biased for relatively acidic proteins/peptides and the SCX reactor for relatively basic protein/peptides. This suggests that more protein identification and extensive sequence coverage can be obtained by using both the SAX and SCX proteomic reactors in combination.

Integrating the 96-well plate SCX reactor with size exclusion chromatographic separation of MCF7 whole cell lysate, under stringent criteria, led to a total of 875 unique proteins identified. A more relaxed ion score cutoff level associated with a 1% false positive rate resulted in the identification of 2,683 unique proteins. This approach allows one protein to be identified per 3-10 ng of total protein lysate loaded on the reactor plate. The proteomic reactor techniques proved to be very efficient and sensitive in processing minute amounts of protein samples.

In summary, by minimizing sample loss and improving protein digestion efficiency, the proteomic reactor techniques can increase the depth and breadth of proteome coverage and identification confidence, and therefore increase the possibility to identify lower abundance proteins.

6.2 Specialized proteomic reactor techniques to address different biological problems

Based on the working principles described in chapter 3, it is possible to customize the proteomic reactor to address other biological problems. For example, a "glyco-proteomic reactor" has been developed, which allowed protein concentration/purification, disulfide bond reduction, peptide-N-glycosidase-mediated ^{18}O-labeling and deglycosylation,

alkylation, tryptic digestion and pH-based fractionation to be done on a single reactor (*1*). From as little as 5 μL of human plasma, a total of 82 unique glyco-peptides were identified, representing 41 unique glycoproteins. Multiplexed fractions of HuH7 cell lysates were processed with SCX proteomic reactors, followed by phosphopeptide enrichment using Ti-IMAC. This work identified a total of 1141 unique phosphopeptides from the subcellular fractions from HuH7 cells (*2*). We also customized the proteomic reactor techniques for membrane protein analysis (*3*). A total of 945 plasma membrane proteins and 955 microsomal membrane proteins were identified, where 63% and 47%, respectively, were predicted as *bona fide* membrane proteins. We also demonstrated that step pH gradients could be integrated with the SAX and SCX proteomic reactors, where a total of 1106 and 685 proteins, respectively, were identified from yeast lysate (*4*). These results demonstrate that the proteomic reactor techniques, as integrated with protein/peptide separation methodologies, are powerful and promising tools for the identification of low-abundance proteins from minute amount of samples.

6.3 Developing nano-HPLC-ESI-MS/MS for the analysis of platelet activating factor (PAF) and *lyso*-phosphocholine (LPC) lipid species

In chapter 4, methodology based on nano-HPLC-ESI-MS/MS for the analysis of PAF and LPC lipid species was described. In chapter 4.1, lipid extracts from non-differentiated and NGF-differentiated PC12 cells were separated with nano-flow HPLC prior to being introduced into a Q-TRAP 2000 mass spectrometer, where the lipid species of interest were highlighted with precursor ion scan at m/z 184. Absolute quantitation of PAF lipids in undifferentiated and differentiated PC12 cells were performed with the standard additions of PAF subspecies. Results indicated a 16-fold increase in C16:0 *lyso*-PAF, an 8-fold increase in C16:0 PAF, and a 3-fold increase in C18:0 *lyso*-PAF. C18:0 PAF levels remained below level of detection and were not identified in either PC12 cells or NGF-differentiated PC12 cells.

In chapter 4.2, an elevation in C16 PAF was identified in the posterior/entorhinal cortex of AD patients and TgCRND8 transgenic mice in comparison to the respective human

and mice controls. Over the course of 24 hour exposure of human hNT neurons to $A\beta_{42}$ treatment, the increases of endogenous C16:0 PAF levels were also identified. Further, the spiking of identical amount of non-endogenous C13:0 LPC at time of extraction in human samples allow the relative comparisons of PAF family and other LPC lipid species of interest between the AD and control human tissues.

In this thesis, absolute quantification of C16:0, C18:0 PAF and C16:0, C18:0 *lyso*-PAF were performed using standard addition approach, where 5 standard solutions containing 200, 400, 600, 800, and 1000 pg each of C16:0, C18:0 PAF and C16:0, C18:0 *lyso*-PAF were used in the experiment. At each standard addition concentration, samples were analyzed in triplicate. Therefore a total of 15 LC/MS runs were required for the quantification of the 4 PAF species of interest in each sample. As such, we took great effort to analyze all the lipid extracts from both the cells and tissue samples covered in the thesis. We introduced d4-C16:0 PAF for facilitating the identification of C16:0 PAF, as they exhibited the same retention time (Figure 4.2.2). As well, a quantification method based on stable isotope labelled lipid standard was developed for the analysis of specific PAF family lipid species. This should allow a faster analysis of the PAF family lipid species.

6.4 The development of shotgun lipidomic methodology for structure elucidation of diacyl glycerophospholipids

Chapter 5 described the development of a novel shotgun lipidomic methodology for the determination of stereospecificity of diacyl glycerophospholipids including glycerophosphatidic acids (PA), glycerophosphoserines (PS), glycerophosphoglycerols (PG), glycerophosphoinositols (PI), and glycerophosphoethanolamines (PE), which can be conventionally ionized under negative ion mode. The stereospecificity of diacyl glycerophospholipids was determined based on the relative abundance of the lyso-form fragment ions, attributed to the neutral loss of fatty acyl moieties. The fragmentation patterns of a variety of diacyl glycerophospholipid standards were first fully examined over a wide range of collision energy. We observed that lyso-form fragment ions corresponding to the neutral loss of fatty acyl moieties attached to the *sn2* position as free fatty acids ($[M-Sn2]^-$)

and as ketenes ($[M-(Sn2-H_2O)]^-$) exhibited consistently higher intensity than their counter part ions due to the neutral loss of fatty acyl moieties attached to the *sn1* position ($[M-Sn1]^-$ and $[M-(Sn1-H_2O)]^-$).

We then examined the product ion spectra of diacyl glycerophospholipids recorded from lipid extracts of rat hepatoma cells. We demonstrated that this new methodology is capable of accurately determining the stereospecific information for diacyl glycerophospholipids even with the interferences from isobaric lipid species and without chromatographic pre-separation. In addition, the approach is capable of locating the fatty acyl moieties of diacyl glycerophosphoinositols, which is impossible for methodologies that examine only structural information provided by the fatty acyl anions.

However, it should be noted that the developed methodology relies on manually inspecting the recorded MS/MS spectra, which are typically a mixture of fragmentation patterns of two or more lipid species. The annotation of the all the fragment ions in the recorded MS/MS spectra, particularly, the correct association of the lyso-form ions with the corresponding fatty acyl anions and the molecular ions is not an easy task. The next step is to incorporate the developed methodology with software for ease of use. Likely this can be done by customizing commercially available software for lipid analysis (e.g. LipidView Software). This should allow a quick and reliable identification of the fragment ions of interest, as well as the association of the lyso-form ions with the corresponding fatty acyl anions and molecular ions. This should allow a broader application of the developed methodology.

6.5 Future perspectives

In the human body, the levels of various lipid species are tightly regulated by different proteins, both spatially and temporally (*5*). It has been increasingly acknowledged that a variety of human diseases, including cancers (*6*-*8*), are associated with the deregulation of the lipid-protein interacting network. For example, the upregulation of phosphatidylinositol-3,4,5-trisphosphate (PtdIns(3,4,5)P3), a major regulator of cell

survival, cell proliferation and cell growth, was observed in many types of cancers (*7*). The phosphoinositide 3-kinase (PI3K) and 3-phosphatase (PTEN) stringently control PtdIns(3,4,5)P3 signaling (*5*) and play vital roles in cancer development and progression. Dysfunctions in the control of PtdIns(3,4,5)P3 signaling would result in its enhancement, often causing cancer (*7*). In future work, the MS-based analytical methodologies described in the thesis should be combined together as tools for the comprehensive probing the underlying biochemical mechanisms of various biological problems.

Proteomic reactor techniques have been used to address a variety of biological challenges, however, as pointed out by Figeys et al., "the widespread application of proteomic reactor techniques will likely require the development of commercial versions of these devices" and "the end goal is to develop systems in which the user only needs to introduce a cell/tissue lysate and all the steps for processing and analyzing the sample would be fully automated" (*9*). In this regard, the 96-well SCX plate format can be readily integrated with a robot for automated and programmed processing of multiplexed proteomic samples.

While working with quantitative lipidomics, lessons have been learned. The currently widely accepted MS-based lipidomics techniques can only provide a static portrait of molecular composition of a biological system, whereas the dynamic changes in lipid expression due to stimulations (such as inhibitions) are mostly concealed by the static background of lipid compositions of the biological system. This "metabolipidomics" approach is a promising technology for profiling metabolic dynamics of lipids in cells, organs/tissues, and whole animals (*10-11*). The principal tools for metabolipidomics are stable-isotope-labelled precursors and MS/MS. For example, Choline chloride-(*trimethyl*-d_9) (D9-choline chloride) and Ethanol-1,1,2,2-d_4-amine (D4-ethanolamine) can be added in cell culture media to selectively label PCs and PEs synthesized through the CDP-choline and CDP-ethanolamine pathway (Figure 6.1) for a short period of time (pulse labeling). Newly synthesized PCs and PEs, which are incorporated with head groups containing heavy isotopes during the pulse labelling, can then be distinguished from those of the static composition of molecular species as they are subject to mass spectrometric analysis. The so-called "metabolipidomics" approach should provide critical information for revealing the

biochemical processes of lipid regulation and metabolism, which is impossible to obtain with the conventional shotgun lipidomic approaches.

Figure Captions:

Figure 6.1 The two branches of the Kennedy pathway: the CDP-ethanolamine and the CDP-choline pathways. Enzymes: CK, choline kinase; CCT, phosphocholine cytidylyltransferase; CPT, cholinephosphotransferase; EK, ethanolamine kinase; ECT, phosphoethanolamine cytidylyltransferase; EPT, ethanolaminephosphotransferase; PEMT, glycerophosphoethanoamine-N- methyltransferase. Adapted with permission from IUBMB life. Copyright © 2010, International Union of Biochemistry and Molecular Biology, Inc.

Figure 6.1

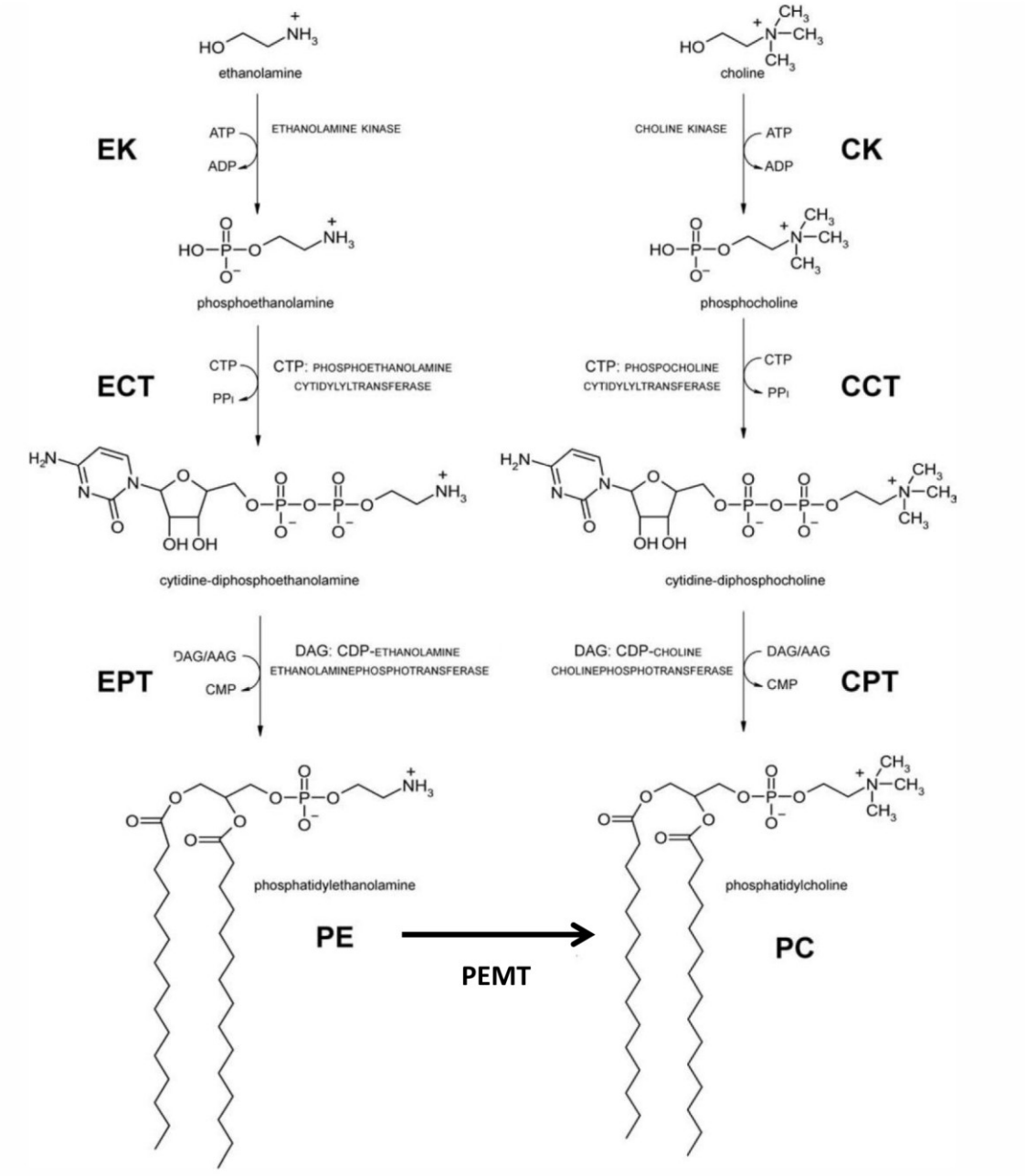
ethanolamine
EK
ATP
ADP
ETHANOLAMINE KINASE
phosphoethanolamine
ECT
CTP
PPi
CTP: PHOSPHOETHANOLAMINE CYTIDYLYLTRANSFERASE
cytidine-diphosphoethanolamine
EPT
DAG/AAG
CMP
DAG: CDP-ETHANOLAMINE ETHANOLAMINEPHOSPHOTRANSFERASE
phosphatidylethanolamine
PE
choline
CK
CHOLINE KINASE
ATP
ADP
phosphocholine
CCT
CTP: PHOSPOCHOLINE CYTIDYLYLTRANSFERASE
CTP
PPi
cytidine-diphosphocholine
CPT
DAG: CDP-CHOLINE CHOLINEPHOSPHOTRANSFERASE
DAG/AAG
CMP
phosphatidylcholine
PC
PEMT

References

1. Zhou, H., Hou, W., Denis, N. J., Vasilescu, J., Zou, H., and Figeys, D. (2009) Glycoproteomic reactor for human plasma, *J Proteome Res 8*, 556-566.
2. Zhou, H., Elisma, F., Denis, N. J., Wright, T. G., Tian, R., Hou, W., Zou, H., and Figeys, D. (2010) Analysis of the subcellular phosphoproteome using a novel phosphoproteomic reactor, *J Proteome Res 9*, 1279-1288.
3. Zhou, H., Wang, F., Wang, Y., Ning, Z., Hou, W., Wright, T. G., Sundaram, M., Zhong, S., Yao, Z., and Figeys, D. (2011) Improved recovery and identification of membrane proteins from rat hepatic cells using a centrifugal proteomic reactor, *Mol Cell Proteomics 10*, O111 008425.
4. Zhou, H., Hou, W., Lambert, J. P., Tian, R., and Figeys, D. (2010) Analysis of low-abundance proteins using the proteomic reactor with pH fractionation, *Talanta 80*, 1526-1531.
5. Wenk, M. R. (2005) The emerging field of lipidomics, *Nat Rev Drug Discov 4*, 594-610.
6. Wymann, M. P., and Schneiter, R. (2008) Lipid signalling in disease, *Nat Rev Mol Cell Biol 9*, 162-176.
7. Bunney, T. D., and Katan, M. Phosphoinositide signalling in cancer: beyond PI3K and PTEN, *Nat Rev Cancer 10*, 342-352.
8. Al-Saffar, N. M., Jackson, L. E., Raynaud, F. I., Clarke, P. A., Ramirez de Molina, A., Lacal, J. C., Workman, P., and Leach, M. O. The phosphoinositide 3-kinase inhibitor PI-103 downregulates choline kinase alpha leading to phosphocholine and total choline decrease detected by magnetic resonance spectroscopy, *Cancer Res 70*, 5507-5517.
9. Zhou, H., Ning, Z., Wang, F., Seebun, D., and Figeys, D. (2011) Proteomic reactors and their applications in biology, *FEBS J 278*, 3796-3806.
10. Bleijerveld, O. B., Houweling, M., Thomas, M. J., and Cui, Z. (2006) Metabolipidomics: profiling metabolism of glycerophospholipid species by stable isotopic precursors and tandem mass spectrometry, *Anal Biochem 352*, 1-14.

11. DeLong, C. J., Shen, Y. J., Thomas, M. J., and Cui, Z. (1999) Molecular distinction of phosphatidylcholine synthesis between the CDP-choline pathway and phosphatidylethanolamine methylation pathway, *J Biol Chem 274*, 29683-29688.

Statements of author contributions

Chapter 1.2 was modified based on part of the paper published in Brief Funct Genomic Proteomic: Hou, W., Zhou, H., Elisma, F., Bennett, S. A., and Figeys, D. *Technological developments in lipidomics, Brief Funct Genomic Proteomic,7, 395-409 (2008)*. WH, HZ, and FE wrote the manuscript. DF and SAB edited the manuscript. The thesis has not included the part of the manuscipt that HZ and FE contributed to the paper.

Chapter 2 was modified/rewritten based on the experimental section of the published papers that were included in chapters 3, 4 and 5 of the thesis.

Chapter 3.1 was rewritten based on part of the paper published in Journal of Proteome Research: *Ethier, M., Hou, W., Duewel, H. S., and Figeys, D. (2006) The proteomic reactor: a microfluidic device for processing minute amounts of protein prior to mass spectrometry analysis, J Proteome Res 5, 2754-2759.* ME and WH deisigned the experiments, WH performed the experiments except for the on-line cell lysis experiment. ME wroe the manuscript. DF edited the manuscript. The thesis has not included the on-line cell lysate experiment.

Chapter 3.2 was modified based on the full paper published in Analytical Chemistry: *Hou, W., Ethier, M., Smith, J. C., Sheng, Y., and Figeys, D. (2007) Multiplexed proteomic reactor for the processing of proteomic samples, Anal Chem 79, 39-44.* WH conceived, designed, and performed the experiments. ME and JCS assisted in MS experiments and data analysis. YS assisted in MCF7 cell lysates fractionation experiment and provided MCF7 cell lysates. WH wrote the manuscript. DF edited the manuscript.

Chapter 3.3 was rewritten based on part of the paper published in Analytical and Bioanalytical Chemistry: *Zhou, H., Hou, W., Lambert, J. P., and Figeys, D. (2010) New ammunition for the proteomic reactor: strong anion exchange beads and multiple enzymes enhance protein identification and sequence coverage, Anal Bioanal Chem 397, 3421-3430.* WH and HZ conceived, desined and performed the SAX proteomic reactor experiments

using trypsin as enzyme. HZ desinged and performed the experiments using chymotrypsin and Glu-C as enzymes. JPL provided the yearst samples. HZ and WH wrote the manuscript. DF edited the manuscript. The thesis has not included the the experiments using chymotrypsin and Glu-C as enzymes.

Chapter 4.1 was rewritten based on most part of paper published in Analytical Chemistry: *Whitehead, S. N., Hou, W., Ethier, M., Smith, J. C., Bourgeois, A., Denis, R., Bennett, S. A., and Figeys, D. (2007) Identification and quantitation of changes in the platelet activating factor family of glycerophospholipids over the course of neuronal differentiation by high-performance liquid chromatography electrospray ionization tandem mass spectrometry, Anal Chem 79, 8539-8548.(WH, SNW,and ME contibuted equally).* WH and ME designed the experiments. WH and ME performed the MS experiments. SAB Lab performed PC12 cell differentiation experiments and lipid extraction. WH and SNW wrote the manuscript. DF and SAB edited the manuscript. The thesis has not included table 1 of the paper, which listed the detected candidate lipid species. This work was performed by other authors of the paper.

Chapter 4.2 was rewritten based on part of the paper published in Proceedings of the National Academy of Sciences of the United States of America: *Ryan, S. D., Whitehead, S. N., Swayne, L. A., Moffat, T. C., Hou, W., Ethier, M., Bourgeois, A. J., Rashidian, J., Blanchard, A. P., Fraser, P. E., Park, D. S., Figeys, D., and Bennett, S. A. (2009) Amyloid-beta42 signals tau hyperphosphorylation and compromises neuronal viability by disrupting alkylacylglycerophosphocholine metabolism, Proc Natl Acad Sci USA 106, 20936-20941.* WH conceived, desinged and performed the HPLC-MS/MS experiments. SAB lab performed all the biological expriments and lipid extraction. WH wrote the HPLC-MS/MS experiments part of the manuscript and contributed to editng the manuscript. The thesis has not included the biological experiments that are not directly associated with the HPLC-MS/MS experiments.

Chapter 5 was modified based on the full paper published in Rapid Communications in Mass Spectrometry: *Hou, W., Zhou, H., Bou Khalil, M., Seebun, D., Bennett, S. A., and Figeys, D. (2011) Lyso-form fragment ions facilitate the determination of stereospecificity of diacyl glycerophospholipids, Rapid Commun Mass Spectrom 25, 205-217.* WH conceived,

designed and performed the experiments. HZ assisted in MS experiments. MBK performed the lipin-1α plasmid transfection experiment. DS performed cell culture. WH wrote the manuscript. DF edited the manuscript.

List of publications

1. Ethier, M., Hou, W., Duewel, H. S., and Figeys, D. (2006) The proteomic reactor: a microfluidic device for processing minute amounts of protein prior to mass spectrometry analysis, *J Proteome Res 5*, 2754-2759.

2. Hou, W., Ethier, M., Smith, J. C., Sheng, Y., and Figeys, D. (2007) Multiplexed proteomic reactor for the processing of proteomic samples, *Anal Chem 79*, 39-44.

3. Whitehead, S. N., Hou, W., Ethier, M., Smith, J. C., Bourgeois, A., Denis, R., Bennett, S. A., and Figeys, D. (2007) Identification and quantitation of changes in the platelet activating factor family of glycerophospholipids over the course of neuronal differentiation by high-performance liquid chromatography electrospray ionization tandem mass spectrometry, *Anal Chem 79*, 8539-8548.

4. Hou, W., Zhou, H., Elisma, F., Bennett, S. A., and Figeys, D. (2008) Technological developments in lipidomics, *Brief Funct Genomic Proteomic 7*, 395-409.

5. Smith, J. C., Hou, W., Whitehead, S. N., Ethier, M., Bennett, S. A., and Figeys, D. (2008) Identification of lysophosphatidylcholine (LPC) and platelet activating factor (PAF) from PC12 cells and mouse cortex using liquid chromatography/multi-stage mass spectrometry (LC/MS3), *Rapid Commun Mass Spectrom 22*, 3579-3587.

6. Wislet-Gendebien, S., Visanji, N. P., Whitehead, S. N., Marsilio, D., Hou, W., Figeys, D., Fraser, P. E., Bennett, S. A., and Tandon, A. (2008) Differential regulation of wild-type and mutant alpha-synuclein binding to synaptic membranes by cytosolic factors, *BMC Neurosci 9*, 92.

7. Ryan, S. D., Whitehead, S. N., Swayne, L. A., Moffat, T. C., Hou, W., Ethier, M., Bourgeois, A. J., Rashidian, J., Blanchard, A. P., Fraser, P. E., Park, D. S., Figeys, D., and Bennett, S. A. (2009) Amyloid-beta42 signals tau hyperphosphorylation and compromises neuronal viability by disrupting alkylacylglycerophosphocholine metabolism, *Proc Natl Acad Sci U S A 106*, 20936-20941.

8. Zhou, H., Hou, W., Denis, N. J., Vasilescu, J., Zou, H., and Figeys, D. (2009) Glycoproteomic reactor for human plasma, *J Proteome Res 8*, 556-566.

9. Bou Khalil, M., Hou, W., Zhou, H., Elisma, F., Swayne, L. A., Blanchard, A. P., Yao, Z., Bennett, S. A., and Figeys, D. (2010) Lipidomics era: accomplishments and challenges, *Mass Spectrom Rev 29*, 877-929.

10. Zhou, H., Elisma, F., Denis, N. J., Wright, T. G., Tian, R., Hou, W., Zou, H., and Figeys, D. (2010) Analysis of the subcellular phosphoproteome using a novel phosphoproteomic reactor, *J Proteome Res 9*, 1279-1288.

11. Zhou, H., Hou, W., Lambert, J. P., and Figeys, D. (2010) New ammunition for the proteomic reactor: strong anion exchange beads and multiple enzymes enhance protein identification and sequence coverage, *Anal Bioanal Chem 397*, 3421-3430.

12. Zhou, H., Hou, W., Lambert, J. P., Tian, R., and Figeys, D. (2010) Analysis of low-abundance proteins using the proteomic reactor with pH fractionation, *Talanta 80*, 1526-1531.

13. Hou, W., Zhou, H., Bou Khalil, M., Seebun, D., Bennett, S. A., and Figeys, D. (2011) Lyso-form fragment ions facilitate the determination of stereospecificity of diacyl glycerophospholipids, *Rapid Commun Mass Spectrom 25*, 205-217.

14. Zhou, H., Wang, F., Wang, Y., Ning, Z., Hou, W., Wright, T. G., Sundaram, M., Zhong, S., Yao, Z., and Figeys, D. (2011) Improved recovery and identification of membrane proteins from rat hepatic cells using a centrifugal proteomic reactor, *Mol Cell Proteomics 10*, O111 008425.